

ABSORPTION AND DESORPTION OF CO₂ AND CO IN ALKANOLAMINE SYSTEMS

by

AQIL JAMAL

M.Sc., King Fahd University of Petroleum and Minerals, Dhahran, Saudi Arabia, 1992

M.Tech., Indian Institute of Technology, Madras, India, 1986

B. Tech., Harcourt Butler Technological Institute, Kanpur, India, 1984

A THESIS SUBMITTED IN PARTIAL FULFILLMENT OF THE
REQUIREMENTS FOR THE DEGREE OF

DOCTOR OF PHILOSOPHY

in

THE FACULTY OF GRADUATE STUDIES

Department of Chemical and Biological Engineering

We accept this thesis, as conforming to the required standard

THE UNIVERSITY OF BRITISH COLUMBIA

July 2002

© Aqil Jamal, 2002

In presenting this thesis in partial fulfillment of the requirements for an advanced degree at the University of British Columbia, I agree that the Library shall make it freely available for reference and study. I further agree that permission for extensive copying of this thesis for scholarly purposes may be granted by the head of my department or by his or her representatives. It is understood that copying or publication of this thesis for financial gain shall not be allowed without my written permission.

Department of Chemical and Biological Engineering

The University of British Columbia
Vancouver, Canada

Date August 7, 2002

ABSTRACT

Absorption and desorption of carbon dioxide (CO₂) and carbon monoxide (CO) in aqueous alkanolamine solutions are modeled and important kinetic and physical property data are obtained using novel experimental methods. The model is based on the principle of diffusional mass transfer accompanied with fast to very slow chemical reactions in the liquid phase. Fast reactions are represented by CO₂ absorption/desorption in aqueous alkanolamines and slow reactions are represented by CO absorption in aqueous diethanolamine (DEA).

The experiments for CO₂ absorption and desorption were conducted in a novel hemispherical contactor designed and developed in this work. The absorption experiments were conducted at near atmospheric pressure using pure CO₂ saturated with water at 293 to 323 K with initially unloaded solutions. The desorption experiments were performed at 333 to 383 K for CO₂ loadings between 0.02 to 0.7 moles of CO₂ per mole of amine using humidified N₂ gas as a stripping medium.

The experiments for CO absorption were carried out in a 660 mL batch autoclave reactor at 313 to 413 K with amine concentration between 5 to 50-wt% in distilled water. The partial pressure of CO in the reactor was varied from 800 to 1100 kPa.

The data for CO₂ absorption and desorption in aqueous amine systems were analyzed using a new, rigorous mathematical model. The model predicts the experimental results well for all amine systems studied. The results indicate

that the theory of absorption with reversible chemical reaction could be used to predict desorption rates. The kinetic data obtained show that desorption experiments could be used to determine both forward and backward rate constants accurately. The absorption experiments on the other hand could only be used to determine forward rate constants.

The data for CO absorption in aqueous diethanolamine (DEA) solutions were analyzed using the model for mass transfer with extremely slow reactions. The data are consistent with a mechanism by which formyl-diethanolamine (DEAF) is predominantly formed by direct insertion of CO into DEA. The data also confirm that DEAF formation via the DEA-formate reaction is relatively slow and reversible.

TABLE OF CONTENTS

ABSTRACT.....	ii
LIST OF TABLES.....	x
LIST OF FIGURES.....	xviii
ACKNOWLEDGEMENT.....	xxix
CHAPTER 1. INTRODUCTION.....	1
1.1 Background.....	1
1.1.1 Commercially Important Amines.....	2
1.1.2 Acid Gas Treating Process.....	5
1.2 Importance of Kinetic and Physical Property data in Design and Simulation of Gas Treating Systems.....	8
1.2.1 Kinetic Data on CO ₂ -Amine Systems.....	9
1.2.2 Kinetic Data on CO-Amine systems.....	10
1.3 Objectives and Scope of This Work.....	11
1.3.1 Organization of the Thesis.....	12
PART I. CO₂ ABSORPTION AND DESORPTION IN AMINE SYSTEMS	
CHAPTER 2. LITERATURE REVIEW.....	14
2.1 Mass Transfer with Chemical Reaction.....	15
2.2 Reaction Mechanisms of CO ₂ -Amine-Water Systems.....	20
2.2.1 CO ₂ Reactions with Water.....	20
2.2.2 CO ₂ Reactions with Amines.....	21
2.2.3 CO ₂ Reactions with Aqueous Amine Blends.....	26
2.3 Kinetic Data for CO ₂ Absorption/Desorption in Aqueous Amines.....	27
2.3.1 Kinetic Data for CO ₂ -MEA-Water System.....	27
2.3.2 Kinetic Data for CO ₂ -DEA-Water System.....	30

2.3.3	Kinetic Data for CO ₂ -MDEA-Water System.....	34
2.3.4	Kinetic Data for CO ₂ -AMP-Water System.....	37
2.3.5	Kinetic Data for Amine Blends.....	42
2.4	Research Needs.....	46

CHAPTER 3. EXPERIMENTAL APPARATUS AND METHODS.....48

3.1	Overview.....	48
3.2	Hemispherical Contactor.....	49
3.3	Experimental Setup and Procedure.....	52
3.4	Data Acquisition and Calibration.....	57
3.5	Chemicals.....	60

CHAPTER 4. MATHEMATICAL MODEL.....61

4.1	Reaction Mechanism.....	62
4.1.1	Reactions for CO ₂ +AMP+H ₂ O (Base Case).....	62
4.1.2	Reactions for O ₂ +MEA+H ₂ O.....	64
4.1.3	Reactions for CO ₂ +DEA+H ₂ O.....	64
4.1.4	Reactions for CO ₂ +MDEA+H ₂ O.....	65
4.1.5	Reactions for CO ₂ +MEA+MDEA+H ₂ O.....	66
4.1.6	Reactions for CO ₂ +MEA+AMP+H ₂ O.....	66
4.1.7	Reactions for CO ₂ +DEA+MDEA+H ₂ O.....	66
4.1.8	Reactions for CO ₂ +DEA+AMP+H ₂ O.....	67
4.2	Reaction Rates.....	67
4.2.1	Reaction Rates for CO ₂ +AMP+H ₂ O System (Base Case).....	67
4.2.2	Reaction Rates for CO ₂ +MEA+H ₂ O System.....	68
4.2.3	Reaction Rates for CO ₂ +DEA+H ₂ O System.....	69
4.2.4	Reaction Rates for CO ₂ +MDEA+H ₂ O System.....	69
4.2.5	Reaction Rates for CO ₂ +MEA+MDEA+H ₂ O System.....	70

4.2.6	Reaction Rates for CO ₂ +MEA+AMP+H ₂ O System.....	70
4.2.7	Reaction Rates for CO ₂ +DEA+MDEA+H ₂ O System.....	72
4.2.8	Reaction Rates for CO ₂ +DEA+AMP+H ₂ O System.....	72
4.3	Reactive Gas Absorption/Desorption Model.....	73
4.3.1	Hydrodynamics of Liquid Film.....	73
4.3.2	Model Equations.....	76
4.3.3	Liquid Bulk Concentrations.....	81
4.3.4	Rate of Absorption or Desorption with Chemical Reaction.....	83
4.3.5	Rate of Absorption or Desorption without Chemical Reaction.....	83
4.3.6	Enhancement Factor.....	85
4.3.7	Overall Reaction Rate (r_{total}).....	85
4.4	Model Parameters.....	86
4.5	Numerical Implementation.....	87
4.6	Parameter Estimation.....	89
 CHAPTER 5. RESULTS AND DISCUSSION.....		93
5.1	Model Verification.....	93
5.1.1	CO ₂ Absorption/Desorption in Aqueous Amines	93
5.1.2	Detailed Profiles in the Hemispherical Film	97
5.1.3	Numerical versus Analytical Solutions	102
5.2	Parametric Sensitivity Analysis.....	104
5.2.1	Effect of Operating Parameters.....	104
5.2.2	Effect of Physical Property Parameters.....	109
5.2.3	Effect of Kinetic Parameters.....	111
5.3	Henry's Constant and CO ₂ Diffusivity in Amine Solutions.....	115
5.3.1	Correlation for Henry's Constant of CO ₂ in Amine Solutions.. ..	115
5.3.2	Correlation for CO ₂ Diffusivity in Amine Solutions.....	116
5.4	CO ₂ Absorption and Desorption in Aqueous Amine Solutions.....	118
5.4.1	CO ₂ Absorption/Desorption in Aqueous Solutions of MEA, DEA and AMP Solutions.....	120

5.4.2	CO ₂ Absorption/Desorption in Aqueous MDEA Solutions	134
5.4.3	CO ₂ Absorption/Desorption in Aqueous Amine Blends.....	138
5.4.4	Comparison of the Parameter Estimates with Literature Data....	142
5.4.5	Predicted Absorption/Desorption Rates Based on Correlations Developed in This Work.....	147
5.5	Conclusions	155

PART II CO ABSORPTION AND CO INDUCED DEGRADATION IN AMINE SYSTEMS

CHAPTER 6. INTRODUCTION AND LITERATURE REVIEW.....157

6.1	Background.....	157
6.2	Literature Review.....	158
6.3	Objectives.....	161

CHAPTER 7. EXPERIMENTAL APPARATUS AND EXPLORATORY EXPERIMENTS.....163

7.1	Experimental Apparatus.....	163
7.2	Exploratory Experiments.....	166
7.2.1	CO Absorption in Aqueous DEA Solutions.....	166
7.2.2	Material Balance.....	168
7.2.3	CO Absorption in Pure DEA.....	170
7.3	Proposed Reaction Mechanism.....	170

CHAPTER 8. MATHEMATICALMODEL.....172

8.1	Reaction mechanism.....	172
8.2	Reaction Rates.....	173
8.3	Mathematical Model.....	173
8.4	Model Parameters.....	177
8.5	Parameter Estimation.....	178

CHAPTER 9. RESULTS AND DISCUSSION.....	180
9.1 Absorption and Degradation in CO-DEA System.....	180
9.1.1 Determination of k_{La}	180
9.1.2 Determination of H_{CO-D} by Nitrogen Analogy.....	184
9.1.3 Determination of k_3 and k_{-3}	188
9.1.4 Determination of k_1 , k_2 and H_{CO-DEA}	195
9.2 Absorption and Degradation in CO-MDEA System... ..	200
9.3 Absorption and Degradation in CO-DEA+DEAF System.....	202
9.4 Model Predictions.....	203
9.5 Process Implications.....	206
9.6 Conclusions.....	208
CHAPTER 10. OVERALL CONCLUSIONS AND	
RECOMMENDATIONS.....	210
10.1 Conclusions on CO ₂ Absorption and Desorption in Amine Systems Kinetics.....	210
10.2 Conclusions on CO Absorption and CO Induced Degradation in Amine Systems.....	214
10.3 Recommendations for Future Work.....	216
NOMENCLATURE.....	218
REFERENCES.....	222
APPENDICES.....	235
A. Determination of CO ₂ Loading in Amine Solutions.....	235
B. Calibration of Measuring Instruments.....	240
C. Analytical Solution for Physical Absorption/Desorption Model.....	252
D. Derivation of Rate Expression for Zwitterion Mechanism.....	259
E. Density and Viscosity of Aqueous Amine Solutions.....	262

F. Henry's Constant of CO ₂ and N ₂ O in Aqueous Amine Solutions.....	272
G. Diffusivity of CO ₂ and N ₂ O in Aqueous Amine Solutions.....	293
H. Equilibrium constants.....	313
I. Determination of Gas-Side of Gas-Side Mass Transfer Coefficient.....	319
J. Determination of Formate and DEAF.....	324
K. Experimental Data.....	327

LIST OF TABLES

Table 1.1:	Molecular structure of commonly used alkanolamines.....	3
Table 2.1:	Summary of the results reported on the CO ₂ -MEA-Water system.....	28
Table 2.2:	Summary of the results reported on the CO ₂ -MEA-Water system.....	31
Table 2.3:	Summary of results reported on the CO ₂ -MDEA-Water system.....	36
Table 2.4:	Carbamate stability constants for MEA, DEA and AMP by C ¹³ -NMR (Sartori and Savage, 1983).....	39
Table 2.5:	Summary of results reported on the CO ₂ -AMP+Water system.....	40
Table 2.6:	Summary of results reported on CO ₂ -MEA+MDEA+Water and CO ₂ -DEA+MDEA+Water systems.....	44
Table 4.1:	Overall reaction rate (r_{total}).....	86
Table 4.2:	Parameters for absorption/desorption model.....	88
Table 5.1:	Base case operating conditions for parametric sensitivity analysis.....	105
Table 5.2:	Effect of deviation in physical property parameters on CO ₂ absorption and desorption rates in aqueous systems of MEA, DEA, MDEA and AMP.....	110

Table 5.3:	Kinetic parameters for CO ₂ -aqueous amine systems studied in this work.....	112
Table 5.4:	Effect of reactions involving zwitterion deprotonation to water and hydroxyl ions on the rate of absorption (see rxns 4.3, 4.4, 4.12, 4.13, 4.18, 4.19).....	113
Table 5.5:	Kinetic parameters for CO ₂ -aqueous amine systems studied in this work (excluding reactions for zwitterion deprotonation to water and hydroxyl ions).....	114
Table 5.6:	Experimental conditions for CO ₂ absorption/desorption in aqueous amine solutions	119
Table 5.7:	Estimates of rate constants in eq. (5.4) from absorption and desorption data	128
Table 5.8:	Estimates of rate constants in eq. (5.5) from absorption and desorption data	128
Table 5.9:	Estimates of rate constants in eq. (5.6) from absorption and desorption data	129
Table 5.10:	Estimates of rate constants in eq. (5.7) from absorption and desorption data	136
Table 5.11:	Estimates of the combined rate constants for amine blends from desorption data	138
Table 5.12:	Comparison of the activation energies of k ₁ , k ₁₀ , k ₁₆ and k ₂₂	146
Table 7.1:	Overall CO balance as a function of temperature for CO absorption in 30 wt% aqueous DEA solutions.....	169

Table 7.2:	Formate and DEAF concentrations of solutions resulting from exposing pure DEA to CO for 5 hours at $p_{CO}^{\circ} = 690$ kPa.....	169
Table 8.1:	Model parameters.....	178
Table 9.1:	Henry's constant of CO in 30 wt% aqueous DEA solution from N ₂ -Analogy.....	186
Table 9.2:	Henry's constants of CO and N ₂ in water and organic solvents (Fogg and Gerrad, 1991).....	187
Table 9.3:	Estimates of the rate and equilibrium constants for reaction (6.3).....	193
Table 9.4:	Estimates of k_1 , k_2 and H_{CO-DEA}	196
Table 9.5:	CO reaction with aqueous DEA and MDEA.....	202
Table 9.6:	Measured and predicted Formate and DEAF concentrations for CO absorption in 30 wt% aqueous DEA solution.....	204
Table 9.7:	Effect of amine concentration on CO reaction with aqueous DEA solution at 393 K.....	205
Table 9.8:	CO absorption in aqueous solution of 30 wt% DEA and 18.4 wt% DEAF.....	205
Table 9.9:	CO absorption in 30 wt% aqueous MDEA solution.....	205
Table A.1:	Calibration Data for Gastec Detector Tubes No. 2HH (Standard Solution: 10, 000 ppm (by weight) Na ₂ CO ₃ , N ₂ Flow = 120 ml/min, Sparge Time = 40 min).....	239

Table B.1:	GC operating conditions for gas phase N ₂ O/CO ₂ measurement	248
Table B.2:	Calibration Data for N ₂ O measurement using GC.....	249
Table B.3:	Calibration Data for CO ₂ measurement using GC.....	250
Table E.1:	Binary Parameters of the Redlich-Kister Equation of the Excess Volume (eq. E.4 and E.5).....	264
Table E.2:	Parameters of the Density Equation for Pure Fluids (eq. E.6)....	265
Table E.3:	Density of Aqueous Amine Blends at 303 K and 323 K (Total Amine = 25 wt%, Water = 75 wt%).....	266
Table E.4:	Binary Parameters of the Redlich-Kister Equation for the Viscosity Deviation (eqs. E.8 and E.9).....	269
Table E.5:	Parameters of the Viscosity Equation for Pure Fluids (eq. E.10).	270
Table E.6:	Viscosity of Aqueous Amine Blends at 303 K (Total Amine = 25 wt%, Water = 75 wt%).....	271
Table F.1:	Henry's constant of CO ₂ in water.....	278
Table F.2:	Henry's constant of N ₂ O in water.....	279
Table F.3:	Henry's constant of N ₂ O in aqueous MEA solutions.....	280
Table F.4:	Henry's constant of N ₂ O in aqueous DEA solutions.....	281

Table F.5:	Henry's constant of N ₂ O in aqueous MDEA solutions.....	283
Table F.6:	Henry's constant of N ₂ O in aqueous AMP solutions.....	285
Table F.7:	Henry's constant of N ₂ O in MEA+MDEA+H ₂ O.....	286
Table F.8:	Henry's constant of N ₂ O in MEA+AMP+H ₂ O.....	287
Table F.9:	Henry's constant of N ₂ O in DEA+MDEA+H ₂ O.....	288
Table F.10:	Henry's constant of N ₂ O in DEA+AMP+H ₂ O.....	289
Table F.11:	Parameters in eq. (F.6) for Henry's constant of N ₂ O in pure amines (Wang et al., 1992).....	290
Table F.12:	Parameters in excess Henry's constant of N ₂ O in binary and ternary solvent systems (this work).....	290
Table G.1:	Diffusivity of CO ₂ in water.....	301
Table G.2:	Diffusivity of N ₂ O in water.....	302
Table G.3:	Diffusivity of N ₂ O in aqueous MEA solutions.....	303
Table G.4:	Diffusivity of N ₂ O in aqueous DEA solutions.....	304
Table G.5:	Diffusivity of N ₂ O in aqueous MDEA solutions.....	305
Table G.6:	Diffusivity of N ₂ O in aqueous AMP solutions.....	307

Table G.7:	Diffusivity of N ₂ O in MEA+MDEA+H ₂ O.....	308
Table G.8:	Diffusivity of N ₂ O in MEA+AMP+H ₂ O.....	309
Table G.9:	Diffusivity of N ₂ O in DEA+MDEA+H ₂ O.....	310
Table G.10:	Diffusivity of N ₂ O in DEA+AMP+H ₂ O.....	311
Table G.11:	Constants in eq. (G.7) for interaction parameter B ₁₂ (this work).....	311
Table G.12:	Constants in eqs. (G.7) for interaction parameters A _{i1} and A _{i2} (this work).....	312
Table I.1:	Estimates of k _g from experiments and correlation (C _{DEA} = 25 wt%).....	323
Table J.1:	IC operating conditions for formate analysis.....	326
Table J.2:	GC operating conditions for DEAF analysis.....	326
Table K.1:	CO ₂ absorption in pure water.....	327
Table K.2:	N ₂ O absorption in pure water.....	328
Table K.3:	N ₂ O absorption in 25 wt% aqueous MEA solution.....	329
Table K.4:	N ₂ O absorption in 25 wt% aqueous DEA solution.....	330
Table K.5:	N ₂ O absorption in 25 wt% aqueous MDEA solution.....	331

Table K.6:	N ₂ O absorption in 25 wt% aqueous AMP solution.....	332
Table K.7:	N ₂ O absorption in aqueous solutions of 12.5 wt% MEA plus 12.5 wt% MDEA.....	333
Table K.8:	N ₂ O absorption in aqueous solutions of 12.5 wt% MEA plus 12.5 wt% AMP.....	334
Table K.9:	N ₂ O absorption in aqueous solutions of 12.5 wt% DEA plus 12.5 wt% MDEA.....	335
Table K.10:	N ₂ O absorption in aqueous solutions of 12.5 wt% DEA plus 12.5 wt% AMP.....	336
Table K.11:	CO ₂ absorption in aqueous MEA solutions.....	337
Table K.12:	CO ₂ absorption in aqueous DEA solutions.....	337
Table K.13:	CO ₂ absorption in aqueous DEA solutions for estimation of k _g ...	338
Table K.14:	CO ₂ absorption in aqueous MDEA solutions.....	339
Table K.15:	CO ₂ absorption in aqueous AMP solutions.....	340
Table K.16:	CO ₂ absorption in aqueous blends of MEA+MDEA.....	342
Table K.17:	CO ₂ absorption in aqueous blends of MEA+AMP.....	342
Table K.18:	CO ₂ absorption in aqueous blends of DEA+MDEA.....	343

Table K.19: CO ₂ absorption in aqueous blends of DEA+AMP.....	343
Table K.20: CO ₂ desorption from aqueous MEA solutions.....	344
Table K.21: CO ₂ desorption from aqueous DEA solutions.....	345
Table K.22: CO ₂ desorption from aqueous MDEA solutions.....	346
Table K.23: CO ₂ desorption from aqueous AMP Solutions.....	347
Table K.24: CO ₂ desorption from aqueous blends of MEA+MDEA.....	348
Table K.25: CO ₂ desorption from aqueous blends of MEA+AMP.....	348
Table K.26: CO ₂ desorption from aqueous blends of DEA+MDEA.....	349
Table K.27: CO ₂ desorption from aqueous blends of DEA+AMP.....	349

LIST OF FIGURES

Figure 1.1:	Typical absorber/stripper system for acid gas removal.....	7
Figure 2.1:	Comparison of second-order rate constant for CO ₂ -AMP reaction.....	39
Figure 3.1:	Schematic Drawing of the Absorption/Desorption with the Hemispherical Contactor.....	50
Figure 3.2:	Experimental setup.....	53
Figure 3.3:	Typical computer output from an absorption experiment (MEA = 14.3 wt%, T = 303 K, P _T = 101.2 kPa, Q _L = 2.1 mL/s).....	59
Figure 3.4:	Typical computer output from a desorption experiment:(MEA = 20 wt%, α = 0.279 mol/mol, T = 378 K, P _T = 202 kPa, Q _L = 2.2 mL/s).....	59
Figure 4.1:	Schematic of the Liquid Film.....	74
Figure 4.2:	Numerical scheme for model solution.....	91
Figure 4.3:	Numerical scheme for parameter estimation.....	92
Figure 5.1:	Predicted and experimental absorption rates of CO ₂ in aqueous solutions of MEA, DEA and MDEA at 303 K (p _{CO₂} = 97.0 kPa).....	94
Figure 5.2:	Predicted and experimental desorption rates of CO ₂ from aqueous solutions of MEA, DEA and MDEA at 373 K.....	95

Figure 5.3:	Predicted and experimental desorption rates for CO ₂ desorption from aqueous MEA solution at 373 K.....	96
Figure 5.4:	Predicted CO ₂ profiles at different latitudes for CO ₂ absorption in pure water (T = 313 K, Q _L = 2.0 mL/s, p _{CO₂} = 92.7 kPa).....	98
Figure 5.5:	Predicted CO ₂ profiles at different latitudes for CO ₂ desorption from aqueous AMP solution (T = 383 K, Q _L = 2.0 mL/s, C _{AMP} = 2.11 kmol/m ³ , P _{total} = 220 kPa, α = 0.2 mole of CO ₂ /mole of amine).....	98
Figure 5.6:	Effect of amine concentration on CO ₂ profile at θ = 90° for CO ₂ absorption in aqueous AMP solution (T = 313 K, Q _L = 2.0 mL/s, p _{CO₂} = 92.7 kPa).....	99
Figure 5.7:	Predicted concentration profiles for CO ₂ absorption in aqueous AMP solution at θ = 45° (T = 313 K, Q _L = 2.0 mL/s, C _{AMP} = 0.223 kmol/m ³ , p _{CO₂} = 92.7 kPa).....	100
Figure 5.8:	Predicted concentration profiles for CO ₂ absorption in aqueous AMP solution at θ = 90° (T = 313 K, Q _L = 2.0 mL/s, C _{AMP} = 0.223 kmol/m ³ , p _{CO₂} = 92.7 kPa).....	100
Figure 5.9:	Predicted concentration profiles for CO ₂ desorption in aqueous AMP solution at θ = 45° (T = 383 K, Q _L = 2.0 mL/s, C _{AMP} = 2.11 kmol/m ³ , P _{total} = 220 kPa, α = 0.2 mole of CO ₂ /mole of amine)...	101
Figure 5.10:	Predicted concentration profiles for CO ₂ desorption in aqueous AMP solution at θ = 90° (T = 383 K, Q _L = 2.0 mL/s, C _{AMP} = 2.11 kmol/m ³ , P _{total} = 220 kPa, α = 0.2 mole of CO ₂ /mole of amine).....	101
Figure 5.11:	Absorption rates of CO ₂ in pure water predicted from analytical and numerical solutions (Q _L = 2.0 mL/s, p _{CO₂} = 87-97 kPa).....	103

Figure 5.12: Effect of amine concentration on CO ₂ absorption and desorption rates in aqueous AMP system.....	106
Figure 5.13: Effect of CO ₂ loading on CO ₂ absorption and desorption rates in aqueous AMP system	107
Figure 5.14: Effect of temperature on CO ₂ absorption and desorption rates in aqueous AMP system.....	107
Figure 5.15: Effect of CO ₂ partial pressure on CO ₂ absorption and desorption rates in aqueous AMP system	108
Figure 5.16: Effect of total pressure on CO ₂ absorption and desorption rates in aqueous AMP system	108
Figure 5.17: Effect of liquid flow rate on CO ₂ absorption and desorption rates in aqueous AMP system.....	109
Figure 5.18: Predicted and experimental absorption rates for CO ₂ absorption in aqueous MEA solution at 303 K.....	122
Figure 5.19: Predicted and experimental absorption rates for CO ₂ absorption in aqueous DEA solution at 303 K.....	123
Figure 5.20: Predicted and experimental absorption rates for CO ₂ absorption in aqueous AMP solution at 303 K.....	123
Figure 5.21: Predicted and experimental desorption rates for CO ₂ desorption from aqueous MEA solution at 378 K.....	124
Figure 5.22: Predicted and experimental desorption rates for CO ₂ desorption from aqueous DEA solution at 382 K.....	124

Figure 5.23: Predicted and experimental desorption rates for CO ₂ desorption from aqueous AMP solution at 378 K.....	125
Figure 5.24: Predicted and experimental desorption rates for CO ₂ desorption in aqueous MEA solution at 333 to 378 K using literature correlations	125
Figure 5.25: Predicted and experimental desorption rates for CO ₂ desorption in aqueous DEA solution at 343 to 382 K using literature correlations	126
Figure 5.26: Predicted and experimental desorption rates for CO ₂ desorption in aqueous AMP solution at 343 to 378 K using literature correlations	126
Figure 5.27: Arrhenius plot of the estimates for k_{10} from absorption and desorption data.....	129
Figure 5.28: Arrhenius plot of the estimates for $k_{10} / K_{10} K_{11}$ from absorption and desorption data.....	130
Figure 5.29: Arrhenius plot of the estimates for k_{-10} / k_{11} from absorption and desorption data.....	130
Figure 5.30: Arrhenius plot of the estimates for k_{16} from absorption and desorption data	131
Figure 5.31: Arrhenius plot of the estimates for $k_{16} / K_{16} K_{17}$ from absorption and desorption data.....	131
Figure 5.32: Arrhenius plot of the estimates for k_{-16} / k_{17} from absorption and desorption data.....	132

Figure 5.33: Arrhenius plot of the estimates for k_1 from absorption and desorption data.....	132
Figure 5.34: Arrhenius plot of the estimates for k_1/K_1K_2 from absorption and desorption data	133
Figure 5.35: Arrhenius plot of the estimates for k_{-1}/k_2 from absorption and desorption data.....	133
Figure 5.36: Predicted and experimental absorption rates for CO ₂ absorption in aqueous MDEA solution at 303 K.....	135
Figure 5.37: Predicted and experimental desorption rates for CO ₂ desorption from aqueous MDEA solution at 378 K.....	135
Figure 5.38: Predicted and experimental desorption rates for CO ₂ desorption in aqueous MDEA solution at 343 to 378 K using literature correlations.....	136
Figure 5.39: Arrhenius plot of the estimates for k_{22} from absorption and desorption data.....	137
Figure 5.40: Arrhenius plot of the estimates for k_{-22} from absorption and desorption data	137
Figure 5.41: Arrhenius plot of the estimates for k_{-10}/k_{24} from desorption data	139
Figure 5.42: Arrhenius plot of the estimates for k_{-1}/k_{25} from desorption data.....	139
Figure 5.43: Arrhenius plot of the estimates for k_{-10}/k_{26} from desorption data	140

Figure 5.44: Arrhenius plot of the estimates for k_{-16}/k_{27} from desorption data	140
Figure 5.45: Arrhenius plot of the estimates for k_{-1}/k_{28} from desorption data	141
Figure 5.46: Arrhenius plot of the estimates for k_{-16}/k_{29} from desorption data	141
Figure 5.47: Comparison of the second-order rate constant (k_{10}) for CO ₂ -MEA reaction determined in this work with those reported in the literature.....	143
Figure 5.48: Comparison of the second-order rate constant (k_{16}) for CO ₂ -DEA reaction determined in this work with those reported in the literature.....	144
Figure 5.49: Comparison of the second-order rate constant (k_1) for CO ₂ -AMP reaction determined in this work with those reported in the literature	145
Figure 5.50: Comparison of the second-order rate constant (k_{22}) for CO ₂ -MDEA reaction determined in this work with those reported in the literature	146
Figure 5.51: Predicted and experimental desorption rates CO ₂ -MEA as a function of temperature and CO ₂ loading.....	148
Figure 5.52: Predicted versus experimental desorption rates CO ₂ -MEA calculated from the correlation developed in this work	148
Figure 5.53: Predicted and experimental desorption rates for CO ₂ -DEA system as a function of temperature and CO ₂ loading.....	149

Figure 5.54: Predicted versus experimental desorption rates CO ₂ -DEA system calculated from the correlation developed in this work	149
Figure 5.55: Predicted and experimental desorption rates for CO ₂ -AMP system as a function of temperature and CO ₂ loading	150
Figure 5.56: Predicted versus experimental desorption rates CO ₂ -AMP system calculated from the correlation developed in this work.....	150
Figure 5.57: Predicted and experimental desorption rates for CO ₂ -MDEA system as a function of temperature and CO ₂ loading	151
Figure 5.58: Predicted versus experimental desorption rates CO ₂ -MDEA system calculated from the correlation developed in this work	151
Figure 5.59: Predicted versus experimental absorption rates for CO ₂ -MEA+MDEA system at 303 K based on the correlation developed in this work (p_{CO_2} =97 kPa).....	153
Figure 5.60: Predicted versus experimental absorption rates for CO ₂ -DEA+MDEA system at 303 K based on the correlation developed in this work (p_{CO_2} =97 kPa).....	153
Figure 5.61: Predicted versus experimental absorption rates for CO ₂ -MEA+AMP system at 303 K based on the correlation developed in this work (p_{CO_2} =97 kPa).....	154
Figure 5.62: Predicted versus experimental absorption rates for CO ₂ -DEA+AMP system at 303 K based on the correlation developed in this work (p_{CO_2} =97 kPa).....	154
Figure 7.1: Schematic diagram of the experimental setup.....	164

Figure 7.2:	CO loading as a function of time and temperature (DEA= 30 wt%, $p_{CO}^o = 760-990$ kPa).....	167
Figure 8.1:	Schematic diagram of chemical reaction autoclave.....	174
Figure 9.1:	Nitrogen absorption in 30 wt% aqueous DEA solution at 1050 rpm and 284-333 K.....	182
Figure 9.2:	Nitrogen absorption in 30 wt% aqueous DEA solution at 1050 rpm and 353-413 K.....	182
Figure 9.3:	Measured and predicted volumetric mass transfer coefficient.....	184
Figure 9.4:	Measured and predicted formate ions and DEAF concentration..	191
Figure 9.5:	Arrhenius plot of the estimates for the forward rate constant of reaction (6.3).....	193
Figure 9.6:	Arrhenius plot of the estimates for the reverse rate constant of reaction (6.3).....	194
Figure 9.7:	Arrhenius plot of the estimates for the equilibrium constant of reaction (6.3).....	195
Figure 9.8:	Measured and predicted partial pressures for CO absorption in 30 wt% aqueous DEA solution.....	197
Figure 9.9:	Arrhenius plot of the estimates for the second order rate constant of reaction (6.1).....	198
Figure 9.10:	Arrhenius plot of the estimates for the second order rate constant of reaction (6.2).....	198

Figure 9.11: Effect of reaction (6.3) on the formation of formate and DEAF at T = 393 K , $p_{CO}^o = 1000$ kPa and $C_{DEA} = 30$ wt%.....	200
Figure 9.12: Measured and predicted concentration and partial pressure profiles for CO absorption in aqueous solution of 30 wt% DEA and 18.4 wt% DEAF at 393 K.....	203
Figure 9.13: Predicted concentration profiles for CO absorption in 30 wt% aqueous DEA solution at T = 313 K and $p_{CO}^o = 1000$ kPa.....	207
Figure 9.14: Predicted concentration profiles for CO absorption in 30 wt% aqueous DEA solution at T = 393 K and $p_{CO}^o = 1,000$ kPa.....	207
Figure A.1: Experimental setup for CO ₂ measurement in Liquid Samples.....	236
Figure A.2: Calibration Curve for Gastec Detector Tube No. 2HH for CO ₂ Measurement in Liquid Samples.....	238
Figure B.1: Calibration Curve for Pressure Transducer on Absorption/Desorption Chamber (Omega Model PX202-030GV)	241
Figure B.2: Calibration Curve for Pressure Transducer on Heating Tank (Omega Model PX202-030GV).....	241
Figure B.3: Setup for Mass Flow Meter Calibration using a Soap Film Meter	242
Figure B.4: Calibration Curve for Measuring Dilution N ₂ Flow Rate using Mass Flow Meter (Brooks Model 5700).....	242
Figure B.5: Calibration Curve for Measuring Stripping N ₂ Flow Rate using Mass Flow Meter (Colepalmer Model GFM171).....	243

Figure B.6:	Calibration Curve for Measuring CO ₂ Flow Rate using Mass Flow Meter (Colepalmer Model GFM171).....	243
Figure B.7:	Calibration Curve for Measuring N ₂ O Flow Rate Using Mass Flow Meter (Colepalmer Model GFM 171).....	244
Figure B.8:	Setup for CO ₂ Analyzer Calibration.....	245
Figure B.9:	Calibration Curve for Gas-Phase CO ₂ Measurement using Infrared Analyzer (Model NOVA-300).....	246
Figure B.10:	Calibration Curve for Gas Phase N ₂ O measurement using GC (Shimadzu Model GC 8A, Column: Chromosorb 102).....	247
Figure B.11:	Calibration Curve for Gas-Phase CO ₂ Measurement using GC (Shimadzu Model GC 8A, Column: Chromosorb 102).....	248
Figure E.1:	Measured and calculated densities at 303 and 323 K.....	265
Figure E.2:	Measured and calculated viscosities at 303 K.....	270
Figure F.1:	Henry's constant of CO ₂ in water.....	291
Figure F.2:	Henry's constant of N ₂ O in water.....	291
Figure F.3:	Measured and calculated values of Henry's constant of N ₂ O in aqueous amine solutions between 288 to 393 K.....	292
Figure F.4:	Measured and calculated values of Henry's constant of N ₂ O in aqueous amine blends between 288 to 393 K.....	292

Figure G.1: Diffusivity of CO ₂ in water as a function of temperature.....	298
Figure G.2: Diffusivity of N ₂ O in water as a function of temperature.....	298
Figure G.3: Stokes-Einstein plot for diffusivity of N ₂ O in aqueous alkanolamine solutions.....	299
Figure G.4: Stokes-Einstein plot for diffusivity of N ₂ O in aqueous alkanolamine blends.....	299
Figure G.5: Measured and calculated diffusivities of N ₂ O in aqueous amine solutions.....	300
Figure G.6: Measured and calculated diffusivities of N ₂ O in aqueous amine blends.....	300
Figure I.1: Measured and calculated gas-side mass-transfer coefficients....	322

ACKNOWLEDGEMENT

I wish to express my sincere gratitude and admiration to my thesis supervisors, Dr. Axel Meisen and Dr. C. Jim Lim for their guidance and encouragement over the entire course of this work without which this work would not have been possible. I would also like to thank my thesis committee members Dr. Alfred Guenkel, and Dr. Bruce Bowen for their guidance and support.

I am indebted to Mr. Peter Roberts in the workshop for his professional work in the construction of the experimental apparatus. Thanks to Mr. Horace Lam and Ms Qi Chen in the stores who were always very helpful and friendly.

The financial support provided by the Natural Science and Engineering Research Council of Canada is gratefully acknowledged.

Finally, I want to thank my parents, my wife and my son Cengiz for their love and understanding during the course of this work.

CHAPTER 1

INTRODUCTION

1.1 Background

The separation of acid gas impurities such as carbon dioxide (CO₂) and hydrogen sulfide (H₂S) from gas mixtures is an important operation in natural gas processing, petroleum refining, coal gasification and ammonia manufacture. The amount of CO₂ and H₂S in these gas streams may vary from a few hundred parts per million to more than 30 percent by volume. In most cases, the H₂S is almost completely removed from the gas mixtures because it is highly toxic to humans and extremely corrosive to gas pipelines and other equipment. In natural gas, the CO₂ is removed to meet pipeline specifications, to enhance heating value and to reduce transportation costs. In ammonia plants, on the other hand, the CO₂ is removed from the synthesis gas mainly to prevent catalyst deactivation. Since CO₂ is widely regarded as a major greenhouse gas, potentially contributing to global warming, there has recently been considerable interest in developing technologies for capturing and sequestering the large quantities of CO₂ produced from industrial sources such as fossil-fuel electric power generation facilities.

Various technologies have been developed for CO₂ and H₂S removal from gas streams. These include absorption by chemical and physical solvents, cryogenic separation and membrane separation. Among these methods, gas absorption by chemical solvents is one of the most popular and effective

methods. In general, aqueous solutions of alkanolamines are the most commonly used chemical solvents for the removal of acid gases. The basic idea in this type of process is to remove the acid component (e.g., CO₂ and/or H₂S) from the gas-phase by using a basic species (i.e., aqueous amines) with which it reacts in a reversible manner. The reversibility of these reactions is extremely important as it enables continuous use of amine solution over extended periods.

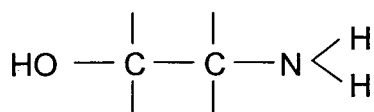
1.1.1 Commercially Important Amines

Table 1.1 lists some of the common alkanolamines used in gas treating applications. These solvents can be thought of as substituted ammonia molecules. The number of substitutions on the nitrogen atom determines the type of alkanolamine. In primary amines, one hydrogen atom on the nitrogen is replaced with a functional group, in secondary amines two hydrogen atoms are replaced and in tertiary amines all three hydrogen atoms are replaced. The chemical structure of alkanolamines is ideally suited for acid gas removal. The amine group provides the required basicity that allows it to react with acid gases reversibly and the hydroxyl group makes the amine more water-soluble thereby reducing its vapor pressure, so that less amine is lost at the top of the absorber and stripper.

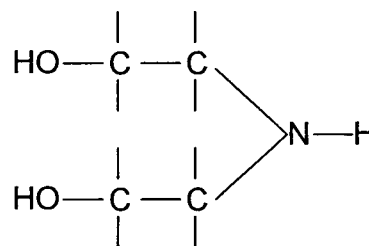
The reaction rates of H₂S and CO₂ differ greatly in alkanolamine solutions because of the difference in their structure. As a Bronsted acid, H₂S reacts directly with the amine function in the acid-base neutralization step. This neutralization is much faster than the time it takes for H₂S to diffuse into the bulk liquids. Consequently, H₂S can be considered in chemical equilibrium in the

liquid at all points in the contactor including the interfacial film and actual kinetic data are not generally required to model H₂S transport.

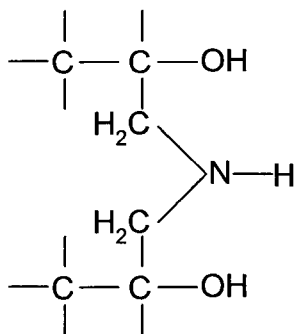
Table 1.1 Molecular structure of commonly used alkanolamines



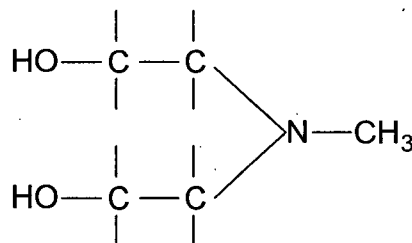
Monoethanolamine (MEA)



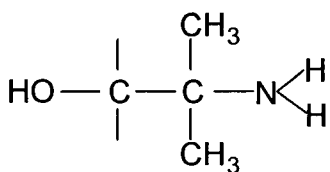
Diethanolamine (DEA)



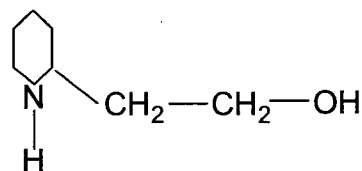
Diisopropanolamine (DIPA)



Methyldiethanolamine (MDEA)



2-amino-2-methyl-1-propanol (AMP)



2-piperidine ethanol (PE)

The reaction of CO_2 with a basic solvent is much slower than that of H_2S . The slower reaction rate of CO_2 is due to its nature as a Lewis acid, which must hydrate before it can react by acid-base neutralization. It may also react directly with the amine to form a carbamate. The rate of hydration and carbamation are both slow and can be comparable to the rate of diffusion of CO_2 . The reaction rate may therefore limit the overall absorption for CO_2 . It is this fact which creates a need for reliable reaction rate data so that the acid gas contactor can be modeled accurately.

Aqueous MEA and DEA solutions are generally used for bulk CO_2 removal when the partial pressure of CO_2 is relatively low and the product purity requirement is high. DIPA is used primarily in special applications where it is necessary to preferentially absorb H_2S over CO_2 . Both primary and secondary amines react fairly strongly with CO_2 to form stable carbamates and their heats of reactions are substantial. Consequently, these amines require substantial energy for regeneration. The energy is supplied in a stripper at elevated temperatures thereby making the amine susceptible to degradation.

MDEA is the most commonly used tertiary amine and it is mostly used for the selective removal of H_2S from natural gases. The most important difference between primary and secondary amines on the one hand and tertiary amines on the other is that tertiary amines do not directly react with CO_2 to form carbamate. Instead, they are believed to catalyze the hydrolysis of CO_2 to carbonate and bicarbonate ions. This also means that regeneration of CO_2 rich MDEA solution requires less energy in comparison to primary and secondary amines.

In many gas-treating applications one finds that MDEA is too selective towards H₂S (i.e., it allows too much CO₂ to slip through the absorber), while DEA and MEA are not selective enough. In MEA and DEA based plants, this lack of sufficient selectivity towards H₂S causes too much CO₂ to be removed and pushes up solvent regeneration cost. Therefore, in recent years there has been considerable interest in using blends of MDEA and DEA or MDEA and MEA. The benefit of using such amine blends is that they combine the advantages of higher absorption rates of MEA and DEA and the better stripping characteristics of MDEA. Moreover, they provide an additional degree of freedom in the form of amine composition that can be manipulated to exercise some control on the selectivity of MDEA towards H₂S over CO₂ by adjusting the gas-liquid contact time.

Recently a new class of amines referred to as sterically hindered amines, has been introduced as a commercially attractive alternative to MEA, DEA and DIPA. Examples are 2-amino-2-methyl-1-propanol (AMP), which is the hindered form of MEA, and 2-piperidine ethanol (PE), which is the hindered form of DEA. In comparison to primary and secondary amines, hindered amines form less stable carbamate and have good selectivity for H₂S. Exxon Research and Engineering Company have already commercialized a hindered amine based H₂S-selective gas treating process (Goldstein et al., 1986).

1.1.2 Acid Gas Treating Process

A typical process schematic for removing acid gases is shown in Figure 1.1. A feed gas containing typical hydrocarbons (CH₄, C₂H₆, C₃H₈, etc.) along

with acid gases is contacted countercurrently with the descending amine solution in a packed or plate column to provide favorable conditions for mass transfer and chemical reactions. The absorber operates at high pressure and low temperature (≤ 40 °C). The purified gas leaves the top of the absorber. The solution discharging from the bottom of the absorber is rich in acid gases and is heated in an exchanger after pressure reduction in a flash drum. The purpose of the flash is to liberate dissolved hydrocarbons. The rich solution is then fed to the stripper (or desorber) where acid gases are removed from the solution by steam stripping. The stripper operates at slightly above ambient pressure and high temperature (≥ 120 °C). The acid gases in the overhead accumulator are either incinerated or sent to a sulfur plant. The lean amine solution leaving the reboiler is cooled in the lean-rich heat exchanger, before being returned to the absorber.

The major energy consumption in this process is in the stripper. The energy supplied to the reboiler is used for two reasons: (1) to produce enough water vapor so that the vapor phase partial pressure of acid gases is reduced to provide a driving force for desorption, and (2) to provide enough energy to reverse the reactions which occur in the absorber. In fact the reactions of CO₂ with aqueous alkanolamine solutions are highly exothermic, releasing energy in the absorber and requiring energy in the stripper.

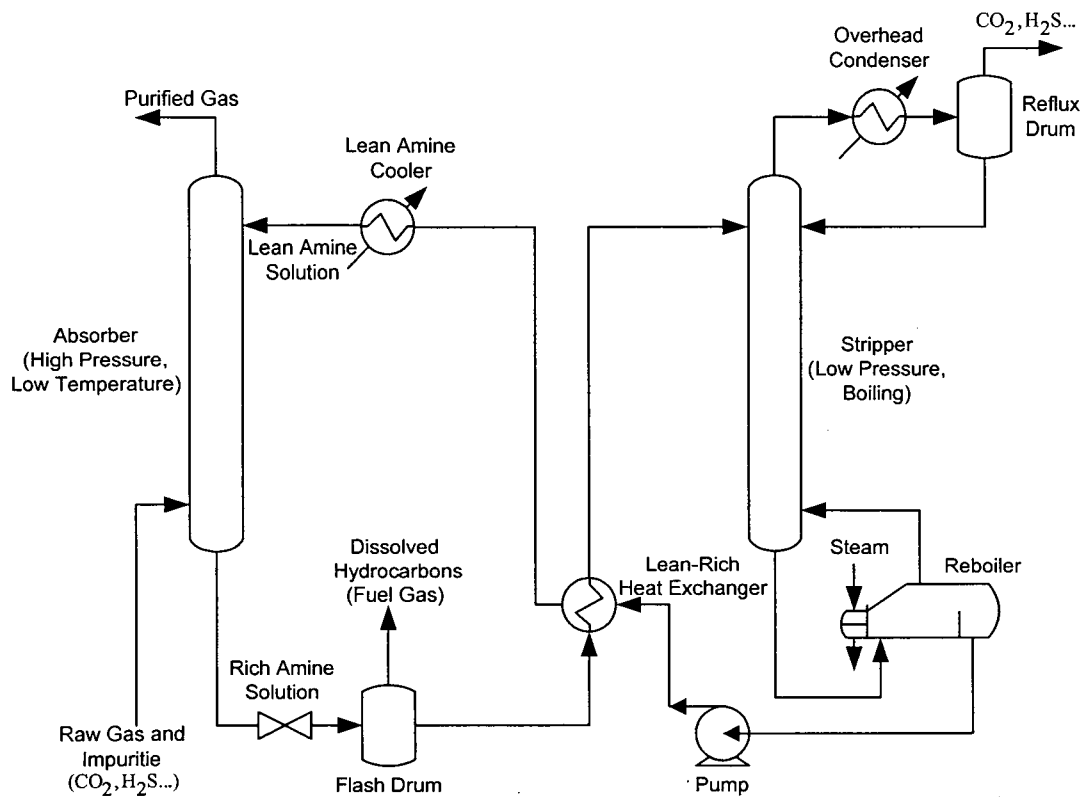


Figure 1.1: Typical absorber/stripper system for acid gas removal

The reboiler heat duty is the most significant operating cost of this type of system (Blauwhoff et al., 1985). It is, therefore, desirable to gain a better understanding of the underlying principles behind the absorption/desorption process and to find solvents and/or operating modes, which reduce the reboiler heat duty. Stripping is also an area where amine solutions are exposed to high temperatures (~ 120 °C). This may accelerate certain undesirable irreversible reactions between amine and acid gases resulting in products from which the amine cannot be regenerated under typical operating conditions. As a result, significant amounts of valuable amine may be lost or rendered ineffective. Recently, amine degradation has been the subject of considerable research, but

it is still not much fully understood. In fact, amine degradation due to the presence of CO is one of the topics covered in this dissertation.

1.2 Importance of Kinetic and Physical Property Data in Design and Simulation of Gas Treating Systems

Gas treating using alkanolamines has been practiced in industry for over half a century. However, it is only recently that substantial progress has been made in developing a fundamental understanding of these seemingly simple processes. Modern computer technology has made it possible to use sophisticated mass transfer rate-based models to design and simulate almost any type of gas treating systems (Katti, 1995; Katti and McDougal, 1986; Yu and Astarita, 1987; Krishnamurthy and Taylor, 1985; Sardar, 1985). These models have been particularly useful in the development and commercialization of mixed solvents, the composition of which can be tailored to specific applications (Katti, 1995).

Comprehensive models require calculations of component and energy balances around each phase on every tray or section of packing. This in turn, involves determining the driving forces, mass and heat transfer coefficients, interfacial area, and interaction between mass transfer and chemical reaction. Thus a rate-based model consists of a vapor-liquid equilibrium (VLE) model, reaction kinetics model, hydrodynamic model and a model to describe the effect of reaction on mass transfer. Although these models are robust enough to treat gas-liquid contacting from fundamental principles and therefore have the potential of accurately predicting the performance of chemical absorbers and

strippers, the models are ultimately as accurate as the experimental data upon which they are based. While great advances have been made in developing increasingly complex models to simulate gas-treating units, similar advances are lacking for the basic kinetic and physical property data.

1.2.1 Kinetic Data for CO₂-Amine Systems

A comprehensive literature review of basic kinetic data for commercially important amines is given in Chapter 2. Several general observations about the existing literature data are noted here. First, the great majority of data are gathered under absorption conditions. However, in designing and simulating real amine processes, data under stripping conditions are equally important. Second, the studies on absorption and desorption have been performed in isolation and there has never been a major attempt to investigate if data collected under absorber conditions can be utilized to predict desorption rates. Finally and most importantly, the experimental data on reaction kinetics have been mostly analyzed assuming highly simplified pseudo-first-order kinetics and pseudo-first-order or corresponding second-order rate coefficients have been reported. Whereas, this assumption greatly simplifies the mathematics, it does not adequately represent the parallel and reversible reactions that occur in typical acid gas-amine systems. In addition, the simplified approach provides no insight into the actual reactive mass transfer phenomena and the kinetic data have limited reliability for design and optimization and scale-up of industrial units. In real situations, rarely if ever is there a single mass transfer regime throughout column.

Therefore, it is highly desirable to develop a comprehensive model that includes all relevant possible reactions in an acid gas-amine system and that can be used to predict both absorption and desorption rates. The development of such a model is the primary objective of this thesis.

1.2.2 Kinetic Data on CO-Amine Systems

In gas treating plants, amine solutions are continuously regenerated and reused for extended periods. Thus, maintaining the quality of amine solution is absolutely critical for efficient and economic operation. Although acid gas-amine reactions are reversible, irreversible reactions may also occur resulting in products from which the amine cannot be regenerated under typical operating conditions. This phenomenon is called amine degradation. Numerous studies have been published on this subject (Dawodu and Meisen, 1991; Kim, 1988; Chakma, 1987; Chakma and Meisen, 1988; Kennard and Meisen, 1985; Kim and Sartori, 1984). However, all these studies are mainly concerned with amine degradation due to CO₂, carbon disulfide (CS₂), carbonyl sulfide (COS) and H₂S/CO₂ mixtures. However, some sour gas mixtures (e.g., gas mixtures in hydrogen plants and FCC units) may also contain significant concentrations of carbon monoxide that could also contribute to amine degradation.

A literature review on this subject (see Chapter 6) reveals that no detailed scientific study has ever been done to investigate the kinetics of CO-induced degradation of alkanolamines. This problem is of considerable commercial importance because in many refinery gas-treating units, where CO partial pressures are high, large quantities of DEA can be lost or rendered ineffective.

Therefore, it could be considerable economic benefit to investigate the mechanism by which CO reacts with aqueous DEA solution and estimate relevant solubility and kinetic parameters. These data are essential for estimating DEA losses. Therefore, the second part of this thesis is devoted to investigating the kinetics of the CO-induced degradation of DEA.

1.3 Objectives and Scope of this Work

The work presented in this thesis can be divided into two parts. Part 1 deals with the kinetics of CO₂ absorption/desorption in aqueous amines and Part 2 deals with the kinetics of CO-induced degradation of aqueous DEA.

The main objectives of Part 1 were to obtain kinetic and physical properties data that are needed to predict CO₂ absorption/desorption rates in aqueous amine solutions and to investigate if the theory of absorption with reversible chemical reactions can be applied to predict desorption rates. To accomplish these objectives, a new hemispherical gas-liquid contactor was designed and absorption/desorption rates of CO₂ into aqueous solutions of MEA, DEA, MDEA, AMP and their mixtures were measured at various temperatures, amine concentrations and CO₂ loadings. The experimental data were interpreted by developing a comprehensive reactive mass transfer model. This model takes into account the reversibility of the chemical reactions, the effect of the diffusion of reactants and reaction products through reaction zone, and the gas-phase mass transfer resistance. The model is capable of predicting both absorption and desorption rates.

In Part 2, the knowledge acquired in studying CO₂-amine kinetics (i.e., very fast reacting systems) was applied to investigate the kinetics of CO-induced degradation of aqueous DEA (i.e., very slow reacting system). This is the first detailed study ever done on this subject and the project grew out of discussion with Equilon Enterprises LLC, Westhollow Technology Center, Houston Texas and Shell Global Solutions International, Amsterdam, The Netherlands. The specific objectives of this study were to: (a) investigate the mechanism by which CO reacts with aqueous DEA, (b) identify major degradation products and (c) estimate the corresponding solubility and kinetic parameters over a range of temperatures and CO partial pressures so that DEA losses could be quantified and managed. To accomplish these objectives, a novel reaction mechanism was proposed and a mathematical model was developed. The model consists of a set of differential and algebraic equations that describes gas absorption with slow chemical reactions in a well-mixed batch reactor. The parameter estimation procedure presented in this work is based on a novel experimental approach that is fast, accurate and suitable for any gas-liquid reaction system.

1.3.1 Organization of the Thesis

The thesis is divided into two parts. The first part (Chapters 2 to 5) covers experimental and modeling study of CO₂ absorption/desorption in aqueous alkanolamine solutions using a novel hemispherical contactor. The second part (Chapters 6 to 9) deals with the kinetics of CO induced degradation of DEA.

Chapter 2 presents a comprehensive review of the literature on the kinetics of CO₂ absorption and desorption in aqueous solutions of MEA, DEA,

MDEA, AMP and their blends. In this chapter, the theory of mass transfer with chemical reactions is presented to highlight the importance of the kinetics of these systems. Major gaps in knowledge are identified and future research needs that form the basis of most of the work presented are recommended. Chapter 3 describes the novel hemispherical contactor and experimental procedures to measure absorption and desorption rates of CO₂ in aqueous amine solutions. Chapter 4 presents the development of a comprehensive model for gas absorption and desorption over a hemispherical liquid film. This chapter also includes the algorithms for solving the model equations and for parameter estimation. Chapter 5 presents the results of the CO₂ absorptions/desorption studies.

Chapters 6 to 9 present a comprehensive account of the work on CO-induced degradation of aqueous DEA. These chapters also present a novel technique (patterned on the so called "Nitrogen Analogy") to measure the physical solubility of CO in aqueous DEA solutions.

Major conclusions and recommendations for future work arising from Parts 1 and 2 are summarized in Chapter 10.

CHAPTER 2

LITERATURE REVIEW

CO₂ absorption/desorption in aqueous amines involves mass transfer with multiple reversible chemical reactions. Under typical operating conditions, the rates of these reactions (particularly those involving molecular CO₂) are of the same order of magnitude as rate of diffusion in the solution. Therefore, to model the CO₂ removal process, an understanding of the mechanism and kinetics of these reactions is essential.

A number of studies on the kinetics of CO₂-amine reactions in aqueous solutions have been reported in the literature. The experimental procedures in these studies typically involve measurements of CO₂ absorption rates in aqueous amines using laboratory apparatus with known hydrodynamics and interfacial areas. These rates are then interpreted using kinetic models to estimate rate constants. The purpose of this chapter is to emphasize the importance of kinetic data in predicting CO₂ absorption and desorption rates and review the results and methods reported in literature. The kinetic data for four important amines (MEA, DEA, MDEA and AMP) and their blends (MEA+MDEA, MEA+AMP, DEA+MDEA, DEA+AMP) have been compiled and research needs that are later studied in this work are identified. The discussion in this chapter is limited to reaction mechanisms and kinetics only. A review of important physical property data that are also needed for the process modeling of these systems is given in Appendices E to H.

2.1 Mass Transfer with Chemical Reaction

From two-film theory (Lewis and Whitman, 1924) the rate of CO₂ absorption or desorption in aqueous amines can be represented by:

$$N_A = -N_D = \frac{p_{\text{CO}_2}^b - p_{\text{CO}_2}^o}{\frac{1}{k_g a} + \frac{H_{\text{CO}_2}}{Ek_L^o a}} \quad (2.1)$$

The term $(p_{\text{CO}_2}^b - p_{\text{CO}_2}^o)$ in equation (2.1) represents the driving force for mass transfer, $p_{\text{CO}_2}^b$ denotes the partial pressure of CO₂ in the bulk gas and $p_{\text{CO}_2}^o$ denotes the equilibrium partial pressure of CO₂ corresponding to its concentration in the bulk liquid. For absorption $p_{\text{CO}_2}^b > p_{\text{CO}_2}^o$ and for desorption $p_{\text{CO}_2}^b < p_{\text{CO}_2}^o$. The value of $p_{\text{CO}_2}^o$ depends on the solubility of CO₂ in the liquid at the prevailing temperature and pressure. It can be calculated by solving thermodynamic equilibrium models. At low temperatures and high CO₂ partial pressures, the equilibrium favors absorption because most of the CO₂ in the liquid phase is chemically combined with the amine and water and the value of $p_{\text{CO}_2}^o$ is much lower than $p_{\text{CO}_2}^b$. At high temperatures and low CO₂ partial pressures, the equilibrium favors desorption because most of the CO₂ in the liquid is in molecular form and the value of $p_{\text{CO}_2}^o$ is much higher than $p_{\text{CO}_2}^b$.

The equilibrium chemistry that governs the CO₂-Water-Amine system is therefore important in determining the mass transfer driving forces. The most commonly used models for calculating $p_{\text{CO}_2}^o$ are those of Kent and Eisenberg

(1976), Deshmukh and Mather (1981) and Austgen (1989). The main difference among these models is in their description of liquid phase non-idealities. The model of Kent and Eisenberg (1976) does not account for liquid phase non-ideality and is therefore the simplest. The models of Deshmukh and Mather (1981) and Austgen (1989) properly account for thermodynamic non-idealities and, while more accurate, they are also mathematically complex and computationally time consuming. All three models have been used extensively, and comprehensive reviews have been provided by Weiland et al. (1993) and Austgen et al. (1991).

The denominator in equation (2.1) represents the resistance to mass transfer and it consists of two terms: the gas-phase resistance ($1/k_g a$) and the liquid-phase resistance ($H_{CO_2} / Ek_L^o a$). Depending on the operating condition, one or both of these resistances are significant. The gas-side resistance to mass transfer is usually important for systems containing highly reactive amines such as MEA and piperazine or when the CO_2 partial pressure in the gas phase is low. Fortunately, the gas-side resistance to mass transfer can be easily estimated because the only major unknown parameters in evaluating the gas-film coefficient are the gas diffusivities, which are readily available in the literature (Reid et al., 1987).

In CO_2 removal processes, the liquid-side resistance to mass transfer is generally dominant. The estimation of this resistance requires knowledge of the effect of chemical reaction on mass transfer. The effect is usually expressed in terms of the enhancement factor (E), which is defined as the ratio of the rate of

absorption or desorption with chemical reaction to the rate without chemical reaction. In most cases of practical importance, the enhancement factor is a complex function of a dimensionless parameter commonly referred to as the Hatta number (DeCoursey, 1982, 1992) given by:

$$M = \frac{\sqrt{k_{2^{nd}} C_{AM} D_{CO_2}}}{k_L^o} \quad (2.2)$$

Under the assumption that the amine concentration at the gas-liquid interface is not significantly different from that in the bulk solution, Danckwerts, (1970) derived the following expression:

$$E = \sqrt{1 + M^2} \quad (2.3)$$

When the gas-side resistance to mass transfer is negligible because of the low gas solubility (i.e., Large H_{CO_2}), then substitution of equations (2.2) and (2.3) into equation (2.1) gives:

$$N_A = -N_D = \sqrt{1 + \left(\frac{k_{2^{nd}} C_{AM} D_{CO_2}}{k_L^{o2}} \right)} \frac{k_L^o a}{H_{CO_2}} (p_{CO_2}^b - p_{CO_2}^o) \quad (2.4)$$

Equation (2.4) demonstrates that the kinetic coefficient, $k_{2^{nd}}$, is important in determining absorption/desorption rates. The effect of $k_{2^{nd}}$ on the mass transfer rate can be examined with respect to the Hatta number (M). When $M \ll 1$, the rate of reaction is slow and it does not affect the mass transfer rate; consequently $E \approx 1$. This regime is called "slow reaction regime". In this regime the reaction kinetics have no significant effect on mass transfer, corresponding to the case of physical absorption or desorption. When $M \gg 1$, the enhancement factor is

approximately M and the mass transfer rate becomes independent of the liquid-film coefficient; i.e.,

$$N_A = -N_D = \frac{\sqrt{k_{2^{nd}} C_{AM} D_{CO_2}}}{H_{CO_2}} a (p_{CO_2}^b - p_{CO_2}^o) \quad (2.5)$$

This regime is called the “fast” or “pseudo-first-order regime” (Levenspiel, 1972). In this regime the reaction is fast enough that it enhances the mass transfer but not so fast that it depletes the amine concentration in the boundary layer significantly. Therefore, in this regime, C_{AM} can be considered constant throughout in the boundary layer and can be taken as equal to the bulk liquid concentration, and an apparent or pseudo-first-order rate constant ($k_{app} = k_{2^{nd}} C_{AM}$) can be defined.

The pseudo-first-order approximation is usually used in the literature to estimate k_{app} from absorption rate data (see Tables 2.1 to 2.6). In these studies, the experimental conditions are set so that $3 < M \ll E_\infty$, where E_∞ is the maximum possible enhancement factor. For a CO_2 -amine reaction, Danckwerts (1970) has derived the following expression for E_∞ :

$$E_\infty = \sqrt{\frac{D_{CO_2}}{D_{AM}}} + \frac{1}{v_{AM}} \frac{C_{AM}}{C_{CO_2}^i} \sqrt{\frac{D_{AM}}{D_{CO_2}}}$$

where v_{AM} is the amine stoichiometric coefficient.

As $M \rightarrow \infty$, the implication is that the reactions are so fast that chemical equilibrium prevails everywhere. The transport rate becomes independent of the reaction rate and is limited by the diffusion of the liquid reactant to the interface.

This regime is called the “instantaneous reaction regime” (Levenspiel, 1972). The enhancement factor in this regime represents an upper bound on the potential enhancement of mass transfer. In this regime the interface concentrations of liquid reactants and products may be calculated by solving the chemical equilibrium model.

In the transition from the “fast” to “instantaneous regime” ($1 \ll M \leq E_{\infty}$), the reactions occur largely near the interface and the amine concentration within the boundary layer may become significantly depleted. Consequently, the pseudo-first-order approximation given by equation (2.5) is no longer valid and the reaction rates at any point in the boundary layer must be calculated using the actual amine concentration at that point. This requires solving the mass balances (including chemical reaction terms) for each species throughout the liquid film. Analytical solutions for the enhancement factor (like eq. 2.3) are not possible and the equations must be solved numerically.

An important objective of this thesis is to determine mass transfer rates in mixed solvents where the components may react at different rates. Therefore, the transition regime cannot be ignored. A set of conditions that gives the pseudo-first-order regime for one component may well give a transition regime for the other. For this reason we have developed a model that covers all reaction regimes and can be applied to interpret both absorption and desorption rate data.

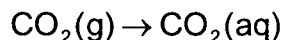
It is clear from the above observations that kinetics plays an important role in the CO₂ absorption/desorption process using aqueous amines. A thorough understanding of the reaction mechanism and determination of reliable kinetic

data are essential for effective design and simulation of such systems. The remainder of this chapter is therefore devoted to developing an understanding of the mechanism of CO₂ reactions with aqueous amines and a review of the literature data on absorption and desorption kinetics. Physical properties such as Henry's constant of CO₂ in amine solution, diffusivities of CO₂ and other chemical species in the aqueous solution and density and viscosity of amine solutions are equally important for process modeling. An extensive literature review of each physical property is given in Appendices E to H.

2.2 Reaction Mechanisms of CO₂-Amine-Water Systems

2.2.1 CO₂ Reactions with Water

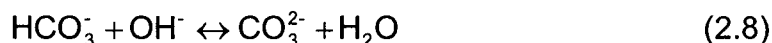
In aqueous solution, CO₂ exists in several forms. First it dissolves:



and then it reacts with water and hydroxyl ions:



The bicarbonate ions quickly establish equilibrium with carbonate ions:



The direct reaction of CO₂ with water (reaction 2.6) is very slow ($k = 0.026 \text{ s}^{-1}$ at 298 K, Pinsent et al., 1956) and usually neglected in interpreting absorption rate data, as its contribution to mass transfer is insignificant (Rinker et al., 1996;

Danckwerts, 1979). This is appropriate because the absorption experiments are generally conducted in equipment with short contact time ($\tau_c < 1$ s).

The CO₂ reaction with hydroxyl ions (reaction 2.7) is fast and can enhance mass transfer even when the concentration of OH⁻ ions is low. Pinsent et al. (1956) and Read (1975) have reported correlations for the forward rate constant and equilibrium constant of reaction (2.7). Reaction (2.8) is an equilibrium reaction and Read (1975) has reported a correlation for its equilibrium constant. These correlations are presented in Appendix H.

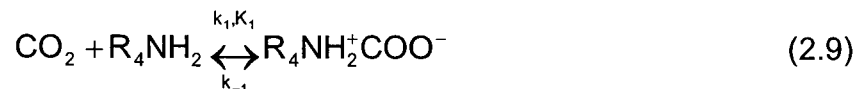
2.2.2 CO₂ Reactions with Amines

Data for CO₂ reactions with aqueous amines have been interpreted either by the zwitterion mechanism, which was first proposed by Caplow (1968) and later reintroduced by Danckwerts (1979), or by the base-catalyzed hydration reaction mechanism proposed by Donaldson and Nguyen (1980).

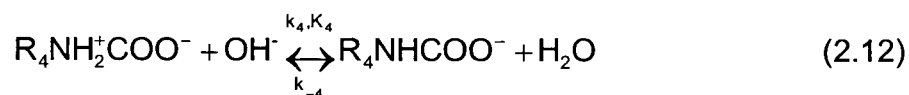
2.2.2.1 Zwitterion Mechanism

According to this mechanism, CO₂ in the liquid phase reacts with amine to form a zwitterion intermediate that is subsequently deprotonated by any base in the solution (Danckwerts, 1979; Blauwhoff et al., 1984). Most of the published kinetic data for MEA, DEA and AMP have been analyzed using this mechanism. For the CO₂-AMP system, the zwitterion mechanism is described by the following reactions:

Zwitterion Formation:



Zwitterion Deprotonation:



Similar reactions have been reported for MEA and DEA.

Danckwerts (1979) combined reactions (2.9) to (2.12) and derived the following expression for the CO₂ amine reaction:

$$r_{\text{CO}_2} = \frac{-k_1[\text{R}_4\text{NH}_2]([\text{CO}_2] - [\text{CO}_2]_e)}{1 + \frac{k_{-1}}{k_2[\text{R}_4\text{NH}_2] + k_3[\text{H}_2\text{O}] + k_4[\text{OH}^-]}} \quad (2.13)$$

where [CO₂]_e is the concentration of molecular CO₂ that is in equilibrium with the other ionic and non-ionic species present in the solution. Equation (2.13) suggests two limiting cases (Versteeg and van Swaaij, 1988):

(a) when the term $k_{-1}/(k_2[\text{RNH}_2] + k_3[\text{H}_2\text{O}] + k_4[\text{OH}^-]) \ll 1$ (i.e., the zwitterion deprotonation is much faster than its formation), then the rate of CO₂ reaction with amine can be expressed in terms of simple second-order kinetics:

$$r_{\text{CO}_2} = -k_1[\text{R}_4\text{NH}_2]\{[\text{CO}_2] - [\text{CO}_2]_e\} \quad (2.14)$$

(b) when $k_2[\text{RNH}_2] \gg k_3[\text{H}_2\text{O}]$ and $k_4[\text{OH}^-]$ and the term $k_{-1}/k_2[\text{RNH}_2] \gg 1$ (i.e., the zwitterion deprotonates only with the amine and the zwitterion deprotonation is much slower than its formation), then the overall kinetics are third order:

$$r_{\text{CO}_2} = -\frac{k_1 k_2}{k_{-1}} [\text{R}_4\text{NH}_2]^2 ([\text{CO}_2] - [\text{CO}_2]_e) \quad (2.15)$$

The above analysis indicates that the zwitterion mechanism is able to cover the transition region where the reaction order with respect to amine lies between 1 and 2.

It may be noted that equation (2.13) is applicable to both absorption and desorption. However, since the majority of research reported in the literature has been focused on absorption into CO_2 -free amine solutions, $[\text{CO}_2]_e$ is generally taken as zero. Furthermore, in most cases it was assumed that during the absorption experiments the amine concentration did not change appreciably and the forward reaction dominated (Danckwerts and Sharma, 1966; Sada et al., 1976; Hikita et al., 1977a). As a result, equation (2.14) can be simplified further and the following pseudo-first-order rate expression results (Little et al., 1992a,b):

$$r_{\text{CO}_2} = -k_{\text{app}} \text{CO}_2 \quad (2.16)$$

where $k_{\text{app}} = k_2^{\text{nd}}[\text{Amine}]$.

In the studies where the full zwitterion mechanism rate expression represented by equation (2.13) was used and combined rate constants (k_1 , $k_1 k_2 / k_{-1}$, $k_1 k_3 / k_{-1}$ and $k_1 k_4 / k_{-1}$) were reported, the methodology used in estimating

rate constants was essentially the same as for the pseudo-first-order approach. Again, $[\text{CO}_2]_e$ was set to zero and equation (2.13) could be simplified to:

$$r_{\text{CO}_2} = -k_{\text{app}} [\text{R}_4\text{NH}_2][\text{CO}_2] \quad (2.17)$$

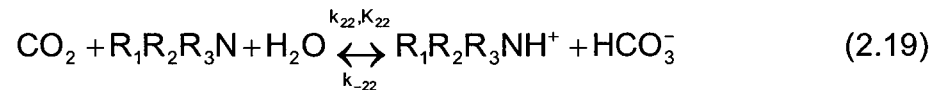
where:

$$k_{\text{app}} = \frac{1}{k_1} + \frac{1}{\frac{k_1 k_2}{k_{-1}} [\text{R}_4\text{NH}_2] + \frac{k_1 k_3}{k_{-1}} [\text{H}_2\text{O}] + \frac{k_1 k_4}{k_{-1}} [\text{OH}^-]} \quad (2.18)$$

In this approach, k_{app} is estimated by using equation (2.17) for various amine concentrations and, from equation (2.18), the individual and combined rate constants are estimated by non-linear regression (Blauwhoff et al., 1984; Versteeg and van Swaaij, 1988; Xu et al., 1996; Xiao et al., 2000; Ko and Li, 2000). The concentrations of amine and water are generally taken as their initial values whereas the concentration of hydroxyl ions is calculated from the dissociation constants of water and amine. In any given experiment, these concentrations were assumed constant. As shown in the next section, most of the recent studies on the kinetics of CO_2 with MEA, DEA and AMP have used this approach. For aqueous solutions, the contribution of OH^- ions in the deprotonation of zwitterion is generally neglected (Blauwhoff et al., 1984; Versteeg and van Swaaij, 1988; Versteeg and Oyevaar, 1989; Bosch et al., 1990b; Rinker et al., 1996; Xu et al., 1996; and Xiao et al., 2000). This is justified because the concentration of hydroxyl ions in aqueous amine solutions is 2 to 3 orders of magnitude lower than that of water or amine. Furthermore, it falls significantly as a result of CO_2 absorption.

2.2.2.2 Base-Catalyzed Hydration Reaction Mechanism

Donaldson and Nguyen (1980) proposed this mechanism for CO₂ reaction with tertiary alkanolamines. According to these authors, the tertiary alkanolamines, such as TEA and MDEA, do not react directly with CO₂ to form carbamate. Instead they catalyze the CO₂ hydration reaction:



The important point to note in this mechanism is that water must be present for the reaction to occur. Most of the data on CO₂-MDEA systems have been analyzed based on this mechanism. There is general agreement in the literature (see Table 2.3) that the reaction rate is first order with respect to amine and CO₂. Therefore, the rate expression for reaction (2.19) can be written as:

$$r_{\text{CO}_2} = -k_{22}[\text{R}_1\text{R}_2\text{R}_3\text{N}][\text{CO}_2] + \frac{k_{22}}{K_{22}}[\text{R}_1\text{R}_2\text{R}_3\text{NH}^+][\text{HCO}_3^-] \quad (2.20)$$

Except for Rinker et al. (1995), almost all studies on the kinetics of the CO₂-MDEA system have assumed that the forward reaction is the dominant one and that the amine concentration does not change appreciably during the experiment. Consequently, equation (2.20) can be simplified as:

$$r_{\text{CO}_2} = -k_{22}[\text{R}_1\text{R}_2\text{R}_3\text{N}][\text{CO}_2] = -k_{\text{app}}[\text{CO}_2] \quad (2.21)$$

Equation (2.21) is identical to equation (2.16) and represents a pseudo-first-order rate expression similar to that for MEA, DEA and AMP. Therefore, the methodology described above was also used to estimate the rate constants for

the CO₂-MDEA system (Barth et al., 1984; Little et al., 1990a; Ko and Li, 2000). Since the CO₂ reaction with MDEA is much slower compared to its reaction with MEA, DEA and AMP, the pseudo-first-order approximation may well be justified.

To analyze desorption data, the rate expression given by equation (2.20) must be used. Furthermore, the CO₂-MDEA reaction is slow, and reaction (2.7), therefore, must also be considered for interpreting absorption/desorption rate data. Recently, Rinker et al. (1995) have shown that the effect of reaction (2.7) on the mass transfer enhancement of the CO₂-MDEA system is quite significant.

2.2.3 CO₂ Reactions with Aqueous Amine Blends

When more than one amine is present (e.g., AMP+MEA or MDEA+AMP), the zwitterion of carbamate-forming amines (such as MEA, DEA and AMP) will also be deprotonated by the second amine present in the solution. For the CO₂+AMP+MEA system, the reaction is:



In the literature (Glasscock et al., 1991, Xiao et al., 2000) the kinetic data for blended amines are treated in the same way as those for single amines and the approximate rate expression given by equation (2.17) is used. The only difference in this case is that the apparent rate constant (k_{app}) is modified to include reaction (2.22):

$$k_{app} = \frac{1}{k_1} + \frac{1}{\frac{k_1k_2}{k_{-1}}[R_4NH_2] + \frac{k_1k_3}{k_{-1}}[H_2O] + \frac{k_1k_4}{k_{-1}}[OH^-] + \frac{k_1k_{25}}{k_{-1}}[R_1NH_2]} \quad (2.23)$$

As before, the term involving hydroxyl ions is usually neglected since it is negligible compared to other terms (Xiao et al., 2000)

2.3 Kinetic Data for CO₂ Absorption/Desorption in Aqueous Amines

2.3.1 Kinetic Data for CO₂-MEA-Water System

MEA is the most commonly used alkanolamine in the gas treating industry and has been studied widely. The literature sources with kinetic data on the CO₂-MEA reaction are summarized in Table 2.1. Even though different experimental conditions have been used, the agreement between the published data is fairly good. As concluded by Blauwhoff et al. (1984) and later confirmed by Barth et al. (1986), the correlation of Hikita et al. (1977a) fits the data quite well over the temperature range of 288 to 353 K:

$$\log_{10}(k_{2,MEA}) = 10.99 - 2152/T$$

where $k_{2,MEA}$ is the second-order rate constant in units of $\text{m}^3 \text{kmol}^{-1} \text{s}^{-1}$ and T is the temperature in Kelvins. The activation energy from this correlation is 41.2 kJ/mol, which agrees well with the values reported by other investigators. Without exception, an overall second-order reaction (first-order with respect to MEA and first-order with respect to CO₂) was found regardless of experimental techniques and conditions (Blauwhoff et al., 1984).

Table 2.1: Summary of the results reported on the CO₂-MEA-Water system

Reference	T (K)	C _{AM} (kmol/ m ³)	k ₂ nd @ 298 K (m ³ / kmol s)	E _a (kJ/mol)	Model ⁺	Apparatus & Method
Little et al. (1992b)	318, 333	1.0	(3703) ⁺⁺	-	g-z	stirred cell (A) ⁺⁺⁺
Alper (1990)	278- 298	0.01- 1.5	5545	46.7	ps-1	stopped flow (A)
Bosch et al. (1990a)	313- 323	1.0	-	-	ps-1	stirred cell (D)
Penny & Ritter (1983)	278- 303	0.01- 0.06	4990	42.2	ps-1	stopped flow (A)
Laddha & Danckwerts (1981)	298	0.5- 1.7	5720	-	ps-1	stirred cell (A)
Donaldson & Nguyen (1980)	298	0.03- 0.08	6000	-	ps-1	aq. amine membrane (A)
Alvarez- Fuster et al. (1980)	293	0.2- 2.0	(5750)	-	ps-1	wetted wall column (A)
Hikita et al. (1977a)	278- 315	0.02- 0.18	5868	41.2	ps-1	rapid mixng (A)
Sada et al. (1976)	298	0.2- 1.9	8400, 7140	-	ps-1	laminar jet (A)
Leder et al. (1971)	353		7194	39.7	ps-1	Stirred cell (A)
Groothius (1966)	298	2.0	6500,5720	-	ps-1	Stirred cell (A)

Contd.

Table 2.1: Summary of the results reported on the CO₂-MEA-Water system
(Contd.)

Reference	T (K)	C _{AM} (kmol/ m ³)	k ₂ nd @ 298 K (m ³ / kmol s)	E _a (kJ/mol)	Model	Apparatus & Method
Danckwerts & Sharma (1966)	291- 308	1.0	7600, 6970	41.8	ps-1	laminar jet (A)
Clarke (1964)	298	1.6- 4.8	7500	-	ps-1	laminar jet (A)
Astarita (1961)	295	0.25- 2.0	(6443)	-	ps-1	laminar jet (A)
Jensen et al. (1954a)	291	0.1, 0.2	(6103)	-	-	competition method with 0.1 and 0.2 M NaOH (A)

+ ps-1 = pseudo-first-order, ps-1-z = pseudo-first-order with zwitterion mechanism, g-z = general model with zwitterion mechanism

++ Values in the bracket indicate that k₂nd was estimated using E_a = 41 kJ/mole

+++ A = absorption, D = desorption

Although the data generally agree well with regard to reaction order and activation energy, it should be noted that most data were acquired under absorption conditions in the temperature range of 293 to 308 K. These data were mostly interpreted using simplified pseudo-first-order models. The more recent data of Little et al. (1992b) were analyzed using a rigorous model based on the zwitterion mechanism but their study was again limited to absorption. An important conclusion from this study was that, for fast reversible reactions like

those in the CO₂-MEA system, rigorous modeling is the only way to estimate the reaction rate constants from absorption experiments.

There has been no significant work on the kinetics of the CO₂-MEA reaction under desorption conditions. Bosch et al. (1990a) provided the only published data for CO₂ desorption rates from rich MEA solutions. However, their data were taken at low temperatures in the range of 313 to 323 K. These authors used pseudo-first-order kinetics with a simplified equilibrium model to predict their CO₂ desorption rates. However, they were unsuccessful in interpreting their data.

2.3.2 Kinetic Data for CO₂-DEA-Water System

DEA is the second most common alkanolamine used for bulk CO₂ removal. Because of its wide use, the literature on CO₂-absorption is extensive. The principal results, mostly from Blauwhoff et al. (1984) and Rinker et al. (1996), are summarized in Table 2.2. There is general disagreement on the order and rate of reaction with respect to DEA. The reaction order for CO₂ is generally accepted to be one but the order for the amine varies between 1 and 2. Blauwhoff et al. (1984) explained some of the discrepancies in the reported results by means of the zwitterion mechanism that includes all bases (i.e., [Amine], [H₂O] and [OH⁻¹]) for zwitterion deprotonation. However, recently Rinker et al. (1996) using a rigorous approach for data interpretation were unable to find any significant contribution of hydroxyl ions and water in zwitterion deprotonation.

Table 2.2: Summary of results reported on the CO₂-DEA+Water system

Reference	T (K)	C _{AM} (kmol/m ³)	k ₂ nd @ 298 K (m ³ /kmol s)	Order w.r.t. Amine	E _a (kJ/mol)	Model ⁺	Apparatus & Method
Rinker et al. (1996)	293-343	0.25-2.8	4089	1-2	14.1	g-z	laminar jet (A) ⁺⁺⁺
Davis & Sandall (1993)	293-313	0.25-2.0	351 (no water)	1-2	-	ps-1-z	Wetted sphere (A)
Little et al. (1992b)	303-318	0.2-4.0	(1454) ⁺⁺	1-2	-	g-z	stirred cell (A)
Crooks & Donellan (1989)	298	0.1-1.0	2250	2	-	-	stopped flow (A)
Versteeg & Oyevaar (1989)	298	0.09-4.40	3170	1-2	-	ps-1-z	stirred cell (A)
Versteeg & van Swaij (1988)	298	-	5790	1-2	-	ps-1-z	stirred cell (A)
Barth et al. (1986)	298	0.02	275	1	-	ps-1	stopped flow (A)
Blauwhoff et al. (1984)	298	0.5-2.3	5800	1-2	-	ps-1-z	stirred cell (A)
Blanc & Demarais (1984)	293-333	0.01-4.0	656	1	43.5	ps-1	wetted wall column (A)

Contd.

Table 2.2: Summary of results reported on the CO₂-DEA+Water system
(Contd.)

Reference	T (K)	C _{AM} (kmol/m ³)	k ₂ nd @298 K (m ³ /kmol s)	Order w.r.t. Amine	E _a (kJ/mol)	Model	Apparatus & Method
Laddha & Danckwerts (1982)	284	0.5-2.0	(1492)	1-2	-	ps-1-z	stirred cell (A)
Laddha & Danckwerts (1981)	298	0.46-2.88	1410	1-2	-	ps-1-z	stirred cell (A)
Donaldson & Nguyen (1980)	298	0.03-0.09	1400	1	-	ps-1	aq. Amine membrane (A)
Alvarez-Fuster et al. (1980)	293	0.25 - 0.82	(3006)	2	-	ps-1	Wetted wall column (A)
Hikita et al. (1977a)	278-313	0.17-0.72	3132	2	-	ps-1	rapid mixing (A)
Coldrey & Harris (1976)	292	0.1-1.0	(1636)	1	-	ps-1	rapid mixing with 0.002- 0.005 M NaOH (A)
Sada et al. (1976)	298	0.25-1.92	1340	1	-	ps-1	laminar jet (A)
Leder (1971)	353	-	(7870)	1	-	ps-1	stirred cell (A)
Groothuis (1966)	298	2.0	1300	1	-	-	stirred cell (A)

Contd.

Table 2.2: Summary of results reported on the CO₂-DEA+Water system
(Contd.)

Reference	T (K)	C _{AM} (kmol/m ³)	k ₂ nd @298 K (m ³ /kmol s)	Order w.r.t. Amine	E _a (kJ/mol)	Model	Apparatus & Method
Danckwerts &Sharma (1966)	308	1.0	(1317)	1	-	ps-1	laminar jet (A)
Sharma (1964)	291	1.0	(1648)	1	-	ps-1	laminar jet (A)
Jorgensen (1956)	273	0.1- 0.3	(3381)	2	-	-	competitive reaction with 0.1, 0.2, 0.3 M NaOH (A)
Jorgensen (1956)	291	0.2- 0.3	(6595)	1	-	-	competitive reaction with 0.2, 0.3 M NaOH (A)
Jensen et al. (1954a)	291	0.1- 0.2	(8360)	1	-	-	competitive reaction with 0.1, 0.2 M NaOH (A)
van Krevelen & Hoftizer (1948)	292- 329	0.05- 3.0	650	2	-	-	packed column (A)

* ps-1 = pseudo-first-order, ps-1-z = pseudo-first-order with zwitterion
mechanism, g-z = general model with zwitterion mechanism

** Values in the bracket indicate that k₂nd was estimated using E_a = 14.1 kJ/mole

*** A = absorption, D = desorption

Crooks and Donnellan (1989) suggested a different mechanism for the reaction of CO₂ with DEA by proposing a single step termolecular reaction. In this mechanism, DEA is postulated to react simultaneously with one molecule of CO₂ and one molecule of base. Their mechanism leads to an overall reaction rate, which has the same form as, that of the second limiting case of the zwitterion mechanism discussed above. However, as pointed by Little et al. (1992b) and Rinker et al. (1996), this mechanism does not explain the fractional orders with respect to DEA concentration observed in non-aqueous solvents (Sada et al., 1985; Versteeg and van Swaaij, 1988; Davis and Sandall, 1993). Nevertheless, there is no plausible explanation in the literature as to why a proton transfer step such as base proton extraction would be rate limiting.

Since the zwitterion mechanism adequately covers the varying reaction order, it is fairly universally used in the literature (see Table 2.2) to interpret CO₂ absorption data. Perhaps a different way of confirming the applicability of this mechanism would be to conduct experiments under desorption conditions and see if the kinetic data acquired under absorption conditions and using a zwitterion mechanism, could be used to predict desorption rates. No such study has been reported in the literature. Critchfield and Rochelle (1988) provided the only study that reports CO₂ desorption rates from rich DEA solutions but their experiments were performed only at 298 K.

2.3.3 Kinetic Data for CO₂-MDEA-Water System

MDEA is the most widely used tertiary amine with major applications in the selective removal of H₂S from gases containing both CO₂ and H₂S. The kinetics

of the CO₂ reaction with MDEA must be known to estimate CO₂ pickup in the absorber and in designing systems with mixed solvents where MDEA is blended with a fast reacting primary or secondary amine. Many studies dealing with the kinetics of CO₂-MDEA reactions have been reported in the literature. Important results from these studies are given in Table 2.3. All these studies confirm the base catalyzed CO₂ hydration reaction mechanism proposed by Donaldson and Nguyen (1980) for the CO₂-tertiary amine reaction. The reaction order with respect to both amine and CO₂ has always been found as one. There are some discrepancies regarding the activation energy and the reported values of second order rate constants. The second-order rate constants at 298 K vary by a factor of 2 depending on the authors (see Table 2.3). In most cases, pseudo-first order models were used to interpret the absorption rate data. Recently, Rinker et al. (1996) used the rigorous model to estimate kinetic coefficients and pointed out that in this system, the CO₂ reaction with hydroxyl ions must be taken into account.

CO₂ desorption from rich MDEA solutions has been studied by Critchfield and Rochelle (1987), Bosch et al. (1990a) and Xu et al. (1995) in the temperature range of 303 to 343 K. In all these studies, the experimental desorption rates are in good agreement with those predicted by simple models for mass transfer with fast pseudo-first-order reaction. These results are important as they indicate that CO₂ desorption from MDEA solutions is controlled by mass transfer with fast reaction and the rate of desorption could be predicted based on absorption kinetic data.

Table 2.3: Summary of results reported on the CO₂-MDEA-Water system

Reference	T (K)	C _{AM} (kmol/ m ³)	k ₂ nd @298 K (m ³ /kmol s)	E _a (kJ/mol)	Model ⁺	Apparatus & Method
Ko & Li (2000)	303- 313	1.0 - 2.5	5.41	44.9	ps-1	wetted wall column (A) ⁺⁺
Pacheco et al. (2000)	298- 373	2.9- 4.3	2.5	49.0	ps-1	wetted wall column (A)
Pani et al. (1997)	296- 343	0.8- 4.4	5.2	44.0	ps-1	stirred cell (A)
Rinker et al. (1995)	293- 342	0.8- 2.5	6.2	38.0	g	wetted sphere (A)
Xu et al. (1995)	313- 343	2.6- 3.9	-	-	ps-1	Packed column (D)
Rangwala et al. (1992)	298- 333	0.8 - 2.5	4.4	48.0	ps-1	stirred cell (A)
Bosch et al. (1990)	298- 323	1.0	-	-	ps-1	stirred cell (D)
Little et al. (1990a)	298	0.2- 2.7	5.5	-	ps-1	stirred cell (A)
Toman & Rochelle (1989)	298- 308	4.3	5.5	-	ps-1	stirred cell (A)
Tomcej & Otto (1989)	298- 348	1.7- 3.5	5.4	42	ps-1	wetted sphere (A)

Contd.

Table 2.3: Summary of results reported on the CO₂-MDEA-Water system
(Contd.)

Reference	T (K)	C _{AM} (kmol/ m ³)	k ₂ nd @298 K (m ³ /kmol s)	E _a (kJ/mol)	Model	Apparatus & Method
Versteeg &van Swaaij (1988)	293- 333	0.2- 2.4	4.4	42	ps-1	stirred cell (A)
Haimour et al. (1987)	288- 308	0.9- 1.7	2.4	72	ps-1	stirred cell (A)
Critchfield & Rochelle (1987)	282- 350	1.7	2.5	56	ps-1	stirred cell (A)
Yu et al. (1985)	313- 333	0.2- 2.5	4.8	39	ps-1	stirred cell (A)
Blauwoff et al. (1984)	298	0.5- 1.6	4.8	-	ps-1	stirred cell (A)
Barth et al. (1984)	298	0.02- 0.2	3.2	-	ps-1	stopped flow (A)

⁺ ps-1 = pseudo-first-order, g = general model

⁺⁺ A = absorption, D = desorption

2.3.4 Kinetic Data for CO₂-AMP-Water System

AMP, a relatively new amine, is primarily used for the selective removal of H₂S from natural gas (Goldstein, 1986). It is a primary amine in which the amino group is attached to the tertiary carbon atom. The reaction rates of CO₂ with AMP are significantly higher than those with MDEA and considerably less than those with MEA. Like MEA and DEA, AMP reacts directly with CO₂ to form carbamate, but its carbamate is highly unstable and quickly hydrolyzes to give free amine

and bicarbonate as evident from the value of its carbamate stability constant (K_c) given in Table 2.4 (Sartori et al., 1983). As a result, AMP can absorb up to 1 mole of CO_2 /mole of amine as opposed to 0.5 mole of CO_2 /mole of amine for MEA and DEA. Moreover, the heat of reaction for CO_2 -AMP is less than those of CO_2 -MEA and CO_2 -DEA. It, therefore, requires less energy for regeneration.

A number of studies on the kinetics of the CO_2 -AMP reactions have been reported in the literature. Important results and experimental conditions from these studies are summarized in Table 2.5. A plot of the second-order rate constant of the CO_2 -AMP reaction as a function of temperature as reported by various investigators is shown in Figure 2.1. Excluding, the data of Chakraborty (1986), who reported a k_2^{nd} value of $100 \text{ m}^3/\text{kmol s}$ at 313 K and Bosch et al. (1990b), who reported this value to be $10,000 \text{ m}^3/\text{kmol s}$ at 298 K, the agreement among the reported data is satisfactory. However, the values of k_2^{nd} at 298 K reported by various authors differ quite significantly (see Table 2.5). The activation energy obtained by regressing the reported data is 36.13 kJ/mole. It is interesting to note that the activation energy of 41.7 kJ/mole calculated from recently published data of Saha et al. (1995) is exactly the same as that reported by Alper (1990) even though the latter author used a different experimental technique. Recently, Xu et al. (1996) and Messaudi and Sada (1996) have reported significantly different activation energies, which are 24.6 and 51.5 kJ/mole, respectively.

Table 2.4: Carbamate stability constants for MEA, DEA and AMP by C¹³-NMR (Sartori and Savage, 1983)

Amine	K_c (m ³ /kmol) at 313 K
MEA	12.5
DEA	2.0
AMP	< 0.1

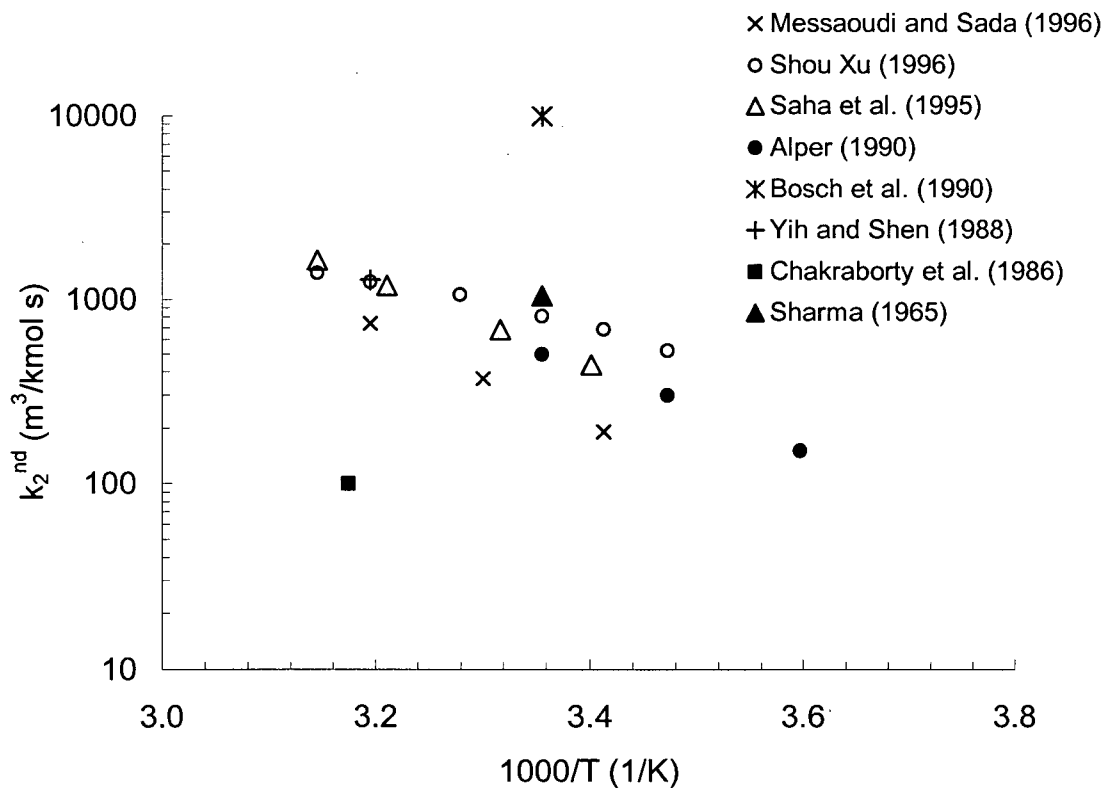


Figure 2.1: Comparison of second-order rate constant for CO₂-AMP reaction.

Table 2.5: Summary of results reported on the CO₂-AMP-Water system

Reference	T (K)	C _{AM} (kmol/ m ³)	k ₂ nd @298 K (m ³ / kmol s)	Order w.r.t. Amine	E _a (kJ/mol)	Model ⁺	Apparatus & Method
Messaoui and Sada (1996)	293- 313	0.5- 2.0	271.8	1	51.5	ps-1	stirred cell (A) ⁺⁺
Xu et al. (1996)	288- 318	0.25- 3.5	810.4	1.32- 1.50	24.3	ps-1-z	stirred cell (A)
Saha et al. (1995)	294- 318	0.5- 0.2	563.5	1	41.7	ps-1	wetted wall column (A)
Alper (1990)	278- 298	0.5- 2.0	502.0	1.14- 1.15	41.7	ps-1	stopped flow (A)
Bosch et al. (1990b)	298	0.2- 2.4	10,000	1	-	g-z	stirred cell (A)
Yih & Shen (1988)	313	0.26- 3.0	1270.0 (at 313 K)	1	-	ps-1	wetted wall column (A)
Chakraborty et al. (1986)	313	0.5- 1.0	100.0 (at 313 K)	1	-	ps-1	PD cell (A)
Sharma (1965)	298	0.2- 2.0	1048.0	1	-	ps-1	stirred cell (A)

⁺ ps-1 = pseudo-first-order, ps-1-z = pseudo-first-order with zwitterion mechanism, g-z = general model with zwitterion mechanism

⁺⁺ A = absorption, D = desorption

The reaction order with respect to CO₂ was generally found to be one (Alper, 1990; Saha et al. 1995; Xu et al., 1996). However, the order with respect to amine has been reported to be slightly more than one (Alper, 1990; Xu et al., 1996). This suggests that the zwitterion mechanism should describe the data better. There is some disagreement amongst the researchers about the right mechanism. The majority (Sartori and Savage, 1983; Alper, 1990; Bosch et al., 1990b; Xu et al., 1996) is of the view that CO₂ reacts with AMP to form carbamate by the zwitterion mechanism and that the carbamate is highly unstable, quickly hydrolyzing to bicarbonate. However, according to Yih and Shen (1988), the formation of carbamate in AMP is inhibited due to the bulkiness of the group attached to the tertiary carbon atom and the equilibrium favors bicarbonate formation via a zwitterion intermediate according to the following reaction:



Chakraborty et al. (1996) proposed yet another mechanism according to which AMP, like MDEA, does not participate directly in the reaction and acts only as a base catalyst for CO₂ hydration reaction.

Finally, the data are limited to temperatures typical of absorbers (i.e., 298 to 318 K). No desorption data have been reported. Except for Bosch et al. (1990b), the experimental data have been analyzed using simple pseudo-first-order models. More data are required so that discrepancies reported in the literature regarding the mechanism and the reaction order with respect to amine can be resolved. The data should be collected under both absorber and desorber

conditions. To analyze the data, a comprehensive model that involves all possible reactions should be developed so that other mechanisms proposed in the literature can be evaluated.

2.3.5 Kinetic Data for Amine Blends

Primary and secondary amines (such as MEA and DEA) are fast reacting amines that form stable carbamates by direct reaction with CO_2 . The tertiary amines, such as MDEA, on the other hand, are slow reacting amines and do not form carbamates. Hindered amines, such as AMP, have moderate reaction rates and can form carbamates, but the latter are highly unstable and quickly hydrolyze to give bicarbonate ions and free amine. Consequently, the regeneration energy requirements for MEA and DEA are quite high compared to those for MDEA and AMP. Blending of primary or secondary amines with tertiary or hindered amines is therefore an attractive option for designing less energy intensive processes for bulk CO_2 removal. An additional advantage of blended amines is that, by varying the composition of the amine blend, the selectivity towards H_2S can be adjusted. Although Chakraborty et al. (1986) introduced this concept over 15 years ago; little fundamental data are available for the rate of absorption/desorption of CO_2 in amine blends. Important kinetic studies involving blends of MDEA with MEA or DEA and blends of AMP with MEA or DEA are summarized in the next two sections.

2.3.5.1 Kinetic Data for Aqueous Blends of MEA+MDEA and DEA+MDEA

Previous work on CO₂ absorption/desorption in MEA+MDEA and DEA+MDEA systems is summarized in Table 2.6. Most of the data reported are for total amine concentrations between 1 and 3 kmol/m³ and temperatures between 298 and 313 K. Critchfield and Rochelle (1988,1987) and Glasscock et al. (1991) have reported both CO₂ absorption and desorption rate data but they are limited to low temperatures (i.e., 288-313 K). The effect of tertiary amines on the reaction rates of primary or secondary amines has generally been taken into account by including an additional reaction where the zwitterion is also deprotonated by the tertiary amine. The results of Glasscock et al. (1991) and Hagewiesche et al. (1995) are important, as they have used rigorous diffusion-reaction and equilibrium models to interpret their data. The available data on CO₂ absorption/desorption from these blends are sparse and more data, especially near stripper temperatures, are need.

2.3.5.2 Kinetic Data for Aqueous Blends of MEA+AMP and DEA+AMP

CO₂- MEA+AMP-Water System:

In recent years, there has been a considerable interest in capturing and sequestering CO₂ from industrial point sources such as flue gases from power plants. Because of its high reaction rates with CO₂, MEA is generally considered as the best solvent for this application. However, there are many technological problems associated with MEA-based process that require further

Table 2.6: Summary of results reported on CO₂-MEA+MDEA-Water and CO₂-DEA+MDEA-Water systems

Reference	Blend	T (K)	Total Amine Conc. (kmol/m ³)	Model ⁺	Apparatus & Method
Hagewiesche et al. (1995)	MEA+MDEA	313	2.6-3.0	g	laminar jet (A) ⁺⁺
Rangwala et al. (1992)	MEA+MDEA	293	2.0-3.5	ps-1	stirred cell (A)
Glasscock et al. (1991)	MEA+MDEA DEA+MDEA	288- 313	0.0-3.0	g-z	stirred cell (A/D)
Critchfield & Rochelle (1988)	DEA+MDEA	298	2.0	ps-1	stirred cell (A/D)
Critchfield & Rochelle (1987)	MEA+MDEA	304	2.0	ps-1	stirred cell (A/D)

⁺ ps-1 = pseudo-first-order, ps-1-z = pseudo-first-order with zwitterion mechanism, g=general model, g-z = general model with zwitterion mechanism

⁺⁺ A = absorption, D = desorption

considerations. MEA is highly corrosive to packing and other equipment and its concentration in the aqueous solution cannot exceed 15-17%. Consequently, very high circulation rates are required. Since MEA carbamate is highly stable, the energy requirements for regenerating the MEA are high. MEA is also highly susceptible to degradation, especially when gas streams contain small quantities of oxygen or fly ash as observed by our own research group and recently by Supap et al. (2001).

The above problems can be effectively addressed by designing a novel solvent blend containing MEA and AMP. The AMP has appreciable reactivity with CO₂, but adding small quantities of MEA can further enhance it. Being the major constituent of the blend, the higher cyclic capacity and lower heat of reaction of AMP may significantly reduce the regeneration heat requirement of the process.

Until the end of 1999, when the experimental work of this dissertation was being completed, no study on either absorption or desorption involving this system had been reported. Very recently, Xiao et al. (2000) have published absorption kinetic data for this system. They studied CO₂ absorption in aqueous mixtures of AMP and MEA in the temperature range of 303 and 313 K using a laboratory wetted wall column. The concentration of AMP was set at 1.7 and 1.5 kmol/m³ and the concentration of MEA was varied from 0.1 to 0.4 kmol/m³. A hybrid reaction rate model (consisting of a first-order reaction for MEA and a zwitterion mechanism for AMP) was used to model the data. Overall pseudo-first-order and corresponding second-order rate constants were reported. More theoretical and experimental work, especially under desorption conditions, is required.

CO₂-DEA+AMP-Water System:

No absorption or desorption studies on this system have been reported. This is probably because the reactivities of DEA and AMP with CO₂ are quite similar and apparently no advantage can be gained by blending these two amines. It will, however, be interesting to see if the capacity and desorption rates

of DEA can be increased by adding AMP as the latter does not form a stable carbamate.

2.4 Research Needs

The major areas needing further research on CO₂ absorption/desorption in the eight aqueous amine systems discussed above may be summarized as follows:

1. Most of the available data have been obtained under absorption conditions in the temperature range of 298 to 313 K using lean amine solutions representing typical conditions near the top of the absorption columns. The kinetic data that represent the absorber bottom and stripper conditions (high temperature and high loading) are needed as a function of CO₂ loading.
2. The studies on absorption and desorption have been done in isolation and there has never been an attempt to investigate if the data collected under absorber conditions can be utilized to predict desorption rates.
3. The experimental data on reaction kinetics have been mostly analyzed assuming simplified pseudo-first-order kinetic models with pseudo-first-order or corresponding second-order rate coefficients being reported. This assumption greatly simplifies the complex mathematics, which govern the reaction-diffusion process in the mass transfer boundary layer. However, the disadvantage of using this approach is that it does not represent the actual concentration profiles of different chemical species in the boundary

layer near the gas-liquid interface and the kinetic data obtained may not be reliable. In real situations, it is rare for a single reaction regime to exist throughout the column. Moreover, this approach does not provide any insight into which reactions enhance mass transfer and which reactions do not. A comprehensive model is therefore needed which describes the diffusion-reaction process in the boundary layer and that takes into account all possible reactions under absorption and desorption conditions.

4. The kinetic data for MEA and MDEA from various sources are in good agreement and no further data under absorption conditions are needed. However, it is important to investigate if these data can be used to predict desorption rates.
5. There are discrepancies in the literature regarding the reaction order with respect to amine for the CO₂-DEA and CO₂-AMP systems. More data, especially under stripping conditions, are needed to reconcile these differences.
6. The kinetic data on amine blends are scarce and more data under both absorption and desorption conditions are needed. Only a single study on CO₂ absorption in an MEA+AMP blend has been reported in the literature, and no absorption or desorption involving AMP+DEA have been published. It would be interesting to investigate (from both theoretical and experimental perspectives) if the addition of MEA or DEA can substantially enhance AMP reaction rates. If this occurs, such blends would become potential solvents for bulk CO₂ removal from flue gases.

CHAPTER 3

EXPERIMENTAL APPARATUS AND METHODS

3.1 *Overview*

In absorption/desorption studies on CO₂-alkanolamine systems, kinetic data are typically obtained by conducting experiments using special types of laboratory contactors. The most commonly used contactors are stirred cells, single sphere units, wetted wall columns and laminar jets. These contactors are designed in such a way that the interfacial area is accurately known and the hydrodynamics are well defined so that physical mass transfer coefficients can easily be obtained from first principles. The advantage of knowing the interfacial area and mass transfer coefficient in advance is that the reaction kinetics and the mass transfer can be decoupled and the measured rate data can be easily interpreted to study the kinetics of gas-liquid reactions.

In this chapter, a new laboratory gas-liquid contactor is described. The apparatus is, in principle, similar to the wetted sphere units used in many previous studies on CO₂-alkanolamine kinetics (Davidson and Cullen, 1957; Savage et al., 1980; Tseng et al., 1988; Al-Ghawas et al., 1989; Tomcej and Otto, 1989; Richard and Sandall, 1993; Tamimi et al., 1994a,b; Dehouche and Lieto, 1995; Rinker et al., 1995). However, in this work the conventional design has been improved by replacing the full sphere by a hemisphere and by designing a better liquid feed and receiver system.

3.2 Hemispherical Contactor

Figure 3.1 depicts the main features of the hemispherical contactor. All parts of the apparatus in contact with the amine solution were constructed from stainless steel, Teflon, or Pyrex glass. The hemispherical contacting surface was constructed from a 76-mm diameter solid, stainless steel sphere. The upper half of this sphere was machined to have shiny and smooth surface and the lower half was machined to fit into a 79-mm ID stainless steel funnel (included angle) leaving a uniform annular space of 1.5 mm. The hemisphere was centered by three equally spaced stainless steel inserts, which were fastened on the inside of the funnel by metal screws inserted from the outside.

The hemispherical assembly was enclosed in two concentric cylinders that formed the absorption/desorption chamber. The total height of the chamber was 457 mm. The inner cylinder was made from 19-mm thick Pyrex glass that had a conical shape, 152 mm ID at the bottom and 76 mm ID at the top. The outer cylinder was made from two cylindrical parts of 203 mm ID. The upper part was 152 mm long and constructed from 13-mm thick stainless steel pipe. The lower part was 305 mm long and was made from 13-mm thick QVF Corning glass. The purpose of using Corning glass in the lower part was to permit viewing the film during the experiment. To prevent heat losses, the upper part of the outer cylinder was wrapped in glass wool insulation and the lower part was wrapped in thermolyne electrical heating tape.

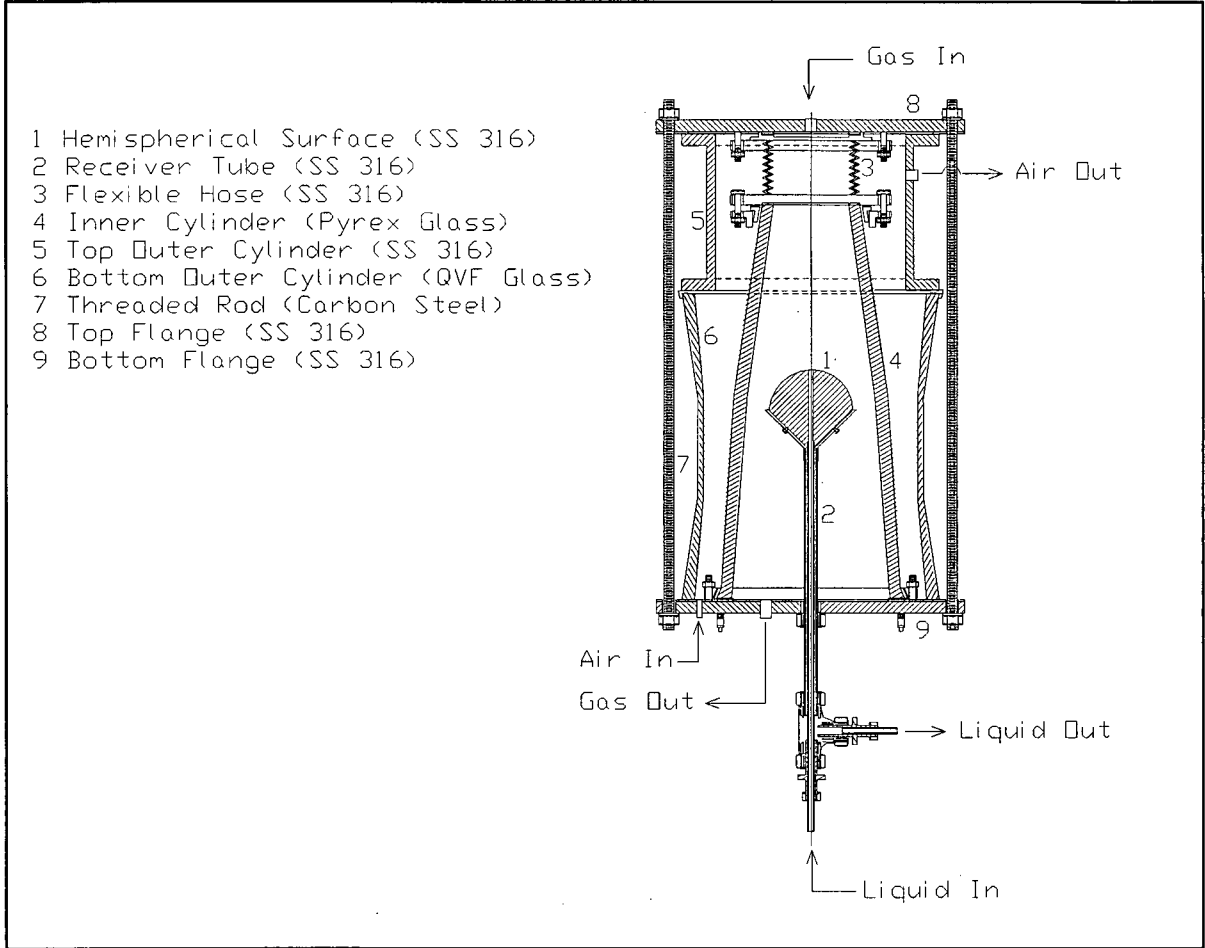


Figure 3.1 Schematic Drawing of the Absorption/Desorption with the Hemispherical Contactor

The seal on both ends of the absorption/desorption chamber was provided by two 12-mm thick and 305 mm diameter stainless steel flanges and Teflon O-rings between the flanges and the glass. The top flange was compressed on the glass cylinders by means of six equally spaced 10 mm diameter bolts attached to the bottom flange. To avoid breakage of the glass cylinders due to uneven thermal expansion of the glass and metal components, the inner cylinder was connected to the top flange by a flexible stainless steel hose. The hemispherical assembly with the attached receiver tube was installed at the center of the inner cylinder at 228 mm from the bottom flange. The receiver tube was sealed to the bottom flange by means of a compression fitting.

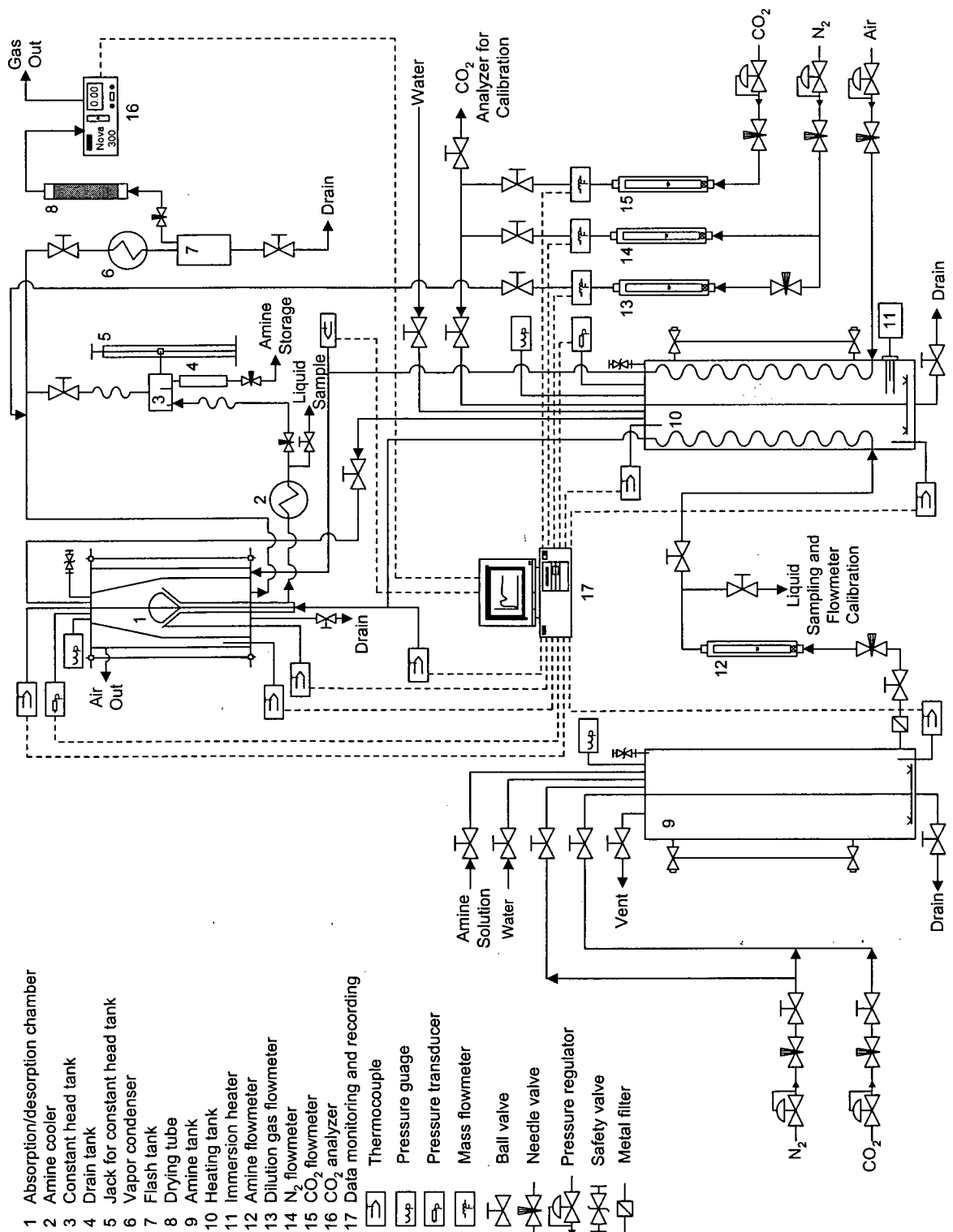
The feed liquid is passed through the stainless steel hemisphere by means of a 4-mm ID stainless steel tube and is discharged at the pole of the hemisphere (see Figure 3.1). It flows as a well-defined liquid film over the surface of the steel hemisphere and is collected by the stainless steel funnel at the base of the hemisphere. The effective mass transfer contact area provided by the hemisphere is 98.03 cm^2 . The liquid is discharged to the storage tank via a 10 mm ID stainless steel receiver tube soldered to the base of the funnel. The liquid level in the funnel is maintained by means of a stainless steel constant head tank (76 mm ID and 76 mm height). The constant head tank is moved vertically up or down on a finely threaded rod by means of a jacking mechanism. The receiver tube is connected to a constant head tank by a 4 mm ID stainless steel flexible Teflon tubing.

In Figure 3.1, the gas is shown to enter the top of the chamber and exit at the bottom. However, there are also provisions for the gas to enter at the bottom and exit at the top. The down flow of gas is generally preferred to prevent surface rippling due to opposite gas and liquid flow directions.

3.3 *Experimental Setup and Procedure*

Figure 3.2 shows the flow diagram of the experimental equipment. The amine solution was stored in a 40 L stainless steel tank (item number 9 in Figure 3.2) equipped with a stainless steel diffuser for mixing and loading the amine solution with CO₂ in case of desorption runs.

The amine solution and the gas stream were heated to the desired temperature in a carbon steel tank (item number 10 in Figure 3.2), which had the same dimensions as those of the amine tank. This tank was equipped with a diffuser, an immersion heater and two stainless steel heating coils, one for heating the amine solution and the other for heating the air that flowed through the annular space in the absorption/desorption chamber. Both coils were made from 12 m long, 4-mm ID stainless steel tubing. Inside the tank, these coils were immersed in the water that filled approximately half of the heating tank. The water temperature was raised to the experiment temperature by means of an immersion heater controlled using a PID type temperature controller (Omega CN76000).



- 1 Absorption/desorption chamber
 - 2 Amine cooler
 - 3 Constant head tank
 - 4 Drain tank
 - 5 Jack for constant head tank
 - 6 Vapor condenser
 - 7 Flash tank
 - 8 Drying tube
 - 9 Amine tank
 - 10 Heating tank
 - 11 Immersion heater
 - 12 Amine flowmeter
 - 13 Dilution gas flowmeter
 - 14 N₂ flowmeter
 - 15 CO₂ flowmeter
 - 16 CO₂ analyzer
 - 17 Data monitoring and recording
- Thermocouple
 - Pressure gauge
 - Pressure transducer
 - Mass flowmeter
 - Ball valve
 - Needle valve
 - Pressure regulator
 - Safety valve
 - Metal filter

Figure 3.2 Experimental Setup

The experimental setup shown in Figure 3.2 was used for both the absorption and desorption experiments. The procedure in both cases was essentially the same. In the absorption experiments, pure CO₂ or N₂O was used, whereas in the desorption experiments pure N₂ was used. All absorption experiments were done under atmospheric pressure. Desorption experiments below 343 K were performed at atmospheric pressure and those above 343 K were carried out at 203 kPa. Higher system pressure was required to prevent flashing of the feed solution due to boiling and excessive CO₂ desorption. The experimental setup was regularly tested for leaks by pressurizing it with N₂ up to 250 kPa and monitoring the system pressure for several hours. The apparatus always held the pressure extremely well.

In a typical absorption or desorption experiment, the amine tank was filled with approximately 20 L of freshly prepared solution and then sealed. The solution was circulated through the hemispherical unit kept under pressure by N₂ from a gas cylinder. The solution was initially fed at high flow rates to ensure complete wetting of the hemisphere. When the liquid film was stabilized, the flow rate was reduced to the desired value. The solution flow rate was measured using a Cole-Palmer variable area flow meter (model H03229-31) and controlled manually by a precision needle valve. For each run, the flow rate was checked using the bypass line. The bypass line was also used to withdraw liquid samples (10 mL) to determine CO₂ loadings as described in Appendix A. Typically, the liquid flow rate ranged between 1.5 to 3.5 mL/s and the exposure time varied between approximately 0.3 to 0.6 s. The solution temperature was measured

using a 1.5-mm diameter, K type thermocouple, installed at the center of the liquid feed point. The feed solution temperature was maintained at the desired value by regulating the power input to the immersion heater attached to the heating tank and the electrical tape wrapped around the liquid feed line.

After passing over the hemisphere, the liquid flowed into the receiving funnel where it was maintained at a desired level by means of a constant level device. Prior to entering the constant head tank (item 3 in Figure 3.2), the solution temperature was brought down to the ambient temperature by passing it through a water-cooled condenser (item 2). At this point, a liquid sample could also be withdrawn for analysis. From the constant head tank, the liquid ran down to a Pyrex glass drain tank (50 mm ID and 300 mm height). In the drain tank, the liquid level was maintained at a preset value by adjusting its outflow by means of a precision needle valve. The solution from the drain tank was collected in a storage tank for reuse. The CO₂ content (loading) in the amine solution was determined using Gastec tubes. The detailed procedure for this method is given in Appendix A.

The gas entering the absorption/desorption chamber was saturated with water vapor at the experiment temperature by bubbling it through the water in the heating tank (item 10). The stirring action of the bubbling gas also helped maintain a uniform water temperature in the heating tank. Saturating the gas feed with water vapor reduced water losses from the liquid film and heat imbalances in the chamber. At all times during an experiment, the water in the heating tank was kept saturated with the feed gas.

Gases were supplied from gas cylinders with a discharge pressure maintained at 35 kPa above the system pressure. The gas discharge pressure was controlled by means of low-pressure precision regulators (Skeans Model P-16-04-L00). Depending on the mode of operation, solution concentration and amine type, the flow rate of the gases ranged between 200-1200 mL/min. Typically, the gas stream entered the top of the chamber and exited at the bottom. After leaving the chamber the gas stream was diluted with a CO₂ free N₂ gas. The flow rate of dilution N₂ typically ranged between 200-1000 mL/min. The gas mixture was cooled to ambient temperature by passing it through a water-cooled condenser. The cooled gas was then flashed into a Pyrex glass tank (100 mm ID and 300 mm height), to separate the gas from the water condensate. The moisture in the gas stream was further lowered by passing it through an acrylic tube (50 mm ID and 30 mm height) filled with anhydrous calcium sulfate beads. The dry gas mixture was then analyzed using an infrared CO₂ analyzer (Model NOVA 300, NOVA Analytical Systems Inc., Hamilton, ON). In absorption experiments with N₂O, the gas samples were collected in 1 L Tedlar gas sampling bags and the gas composition analyzed using a GC (Shimadzu Model GC 8A). In some runs, the gas phase CO₂ concentration was also measured using the GC to double check the accuracy of the infrared analyzer. The calibrations and procedure for gas phase CO₂ and N₂O measurements using the infrared analyzer and GC are given in Appendix B.

The feed and dilution gas flow rates were measured using Cole-Palmer (Model GFM 171) and Brooks (Model 5700) mass flow meters, respectively. The

gas flow rates were maintained at the desired value by means of needle valves installed upstream of the mass flow meters. The mass flow meters were calibrated using a soap film meter (see Appendix B).

The temperatures of the gas stream in the heating tank and the absorption/desorption chamber were measured by type K thermocouples. In order to maintain the gas stream at the desired temperature, electrical heating tapes were wrapped around the gas feed line and the outer glass wall of the chamber. The power input to these tapes was regulated using two independent PID temperature controllers (Omega CN76000). All temperatures were controlled to within ± 0.5 °C.

The pressures in the chamber and heating tank were measured using Omega (Model PX-202-030GV) pressure transducers. In the desorption experiments, the system pressure was controlled manually by a precision needle valve installed on the gas line downstream of the flash tank. The transducers were precisely calibrated using a mercury manometer (see Appendix B).

3.4 Data Acquisition and Calibration

The signals from the thermocouples, pressure transducers, mass flow meters and CO₂ analyzer were read and recorded by means of an IBM 486 PC equipped with a CIO-DAS08 data acquisition board. The number of analog input channels in the A/D board were expanded using two externally mounted CIO-EXP16 signal-conditioning accessory boards, each with 16 input channels. The output signals from all sensors were calibrated as described in Appendix B. The

calibration equations were included in the data acquisition software written in Visual Basic specifically for this application. During data acquisition, the software also displayed (on a real time basis) all measurements as well as the absorption and desorption rates. The absorption or desorption rates at any given time were calculated by the program from the feed and dilution gas flow rates and the exit gas composition using the following mass balance equations:

$$N_A \text{ (mmol/s)} = F_{\text{CO}_2} - \frac{F_{\text{N}_2}^{\text{dil}} \times \% \text{ CO}_2 \text{ in Exit Gas}}{(100 - \% \text{ CO}_2 \text{ in Exit Gas})} \quad (3.1)$$

$$N_D \text{ (mmol/s)} = \frac{(F_{\text{N}_2}^{\text{feed}} + F_{\text{N}_2}^{\text{dil}}) \times \% \text{ CO}_2 \text{ in Exit Gas}}{(100 - \% \text{ CO}_2 \text{ in Exit Gas})} \quad (3.2)$$

where, N_A and N_D denote the absorption and desorption rates in units of mmol/s, and F_{CO_2} , $F_{\text{N}_2}^{\text{feed}}$ and $F_{\text{N}_2}^{\text{dil}}$ denote the flow rates of feed CO_2 , feed N_2 , and dilution N_2 respectively in units of mmol/s.

Figure 3.3 and 3.4 depict typical plots of exit gas compositions and mass transfer rates for CO_2 absorption and desorption for aqueous MEA. In the absorption experiments (Figure 3.3), the CO_2 concentration initially drops very rapidly and then increases to a steady value. This behavior results from the fact that the solution is fed initially at a high flow rate to ensure complete wetting of the hemisphere. This causes it to absorb more CO_2 and the exit CO_2 concentration consequently falls. However, when the liquid film stabilizes, its flow rate is

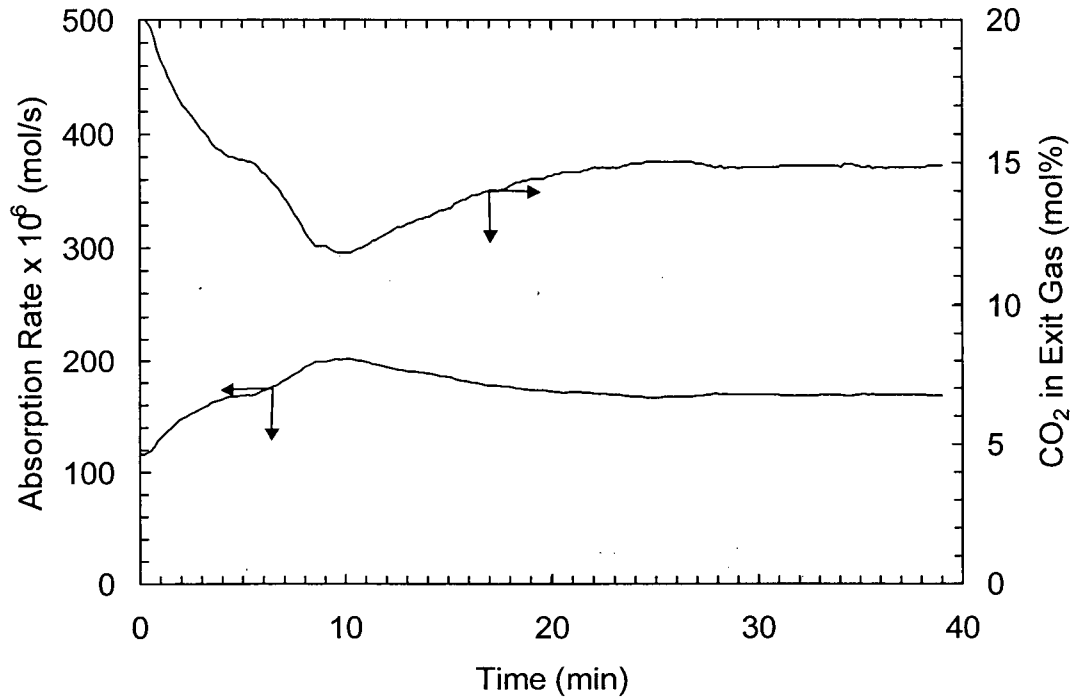


Figure 3.3: Typical computer output from an absorption experiment
 (MEA = 14.3 wt%, $T = 303 \text{ K}$, $P_T = 101.2 \text{ kPa}$, $Q_L = 2.1 \text{ mL/s}$)

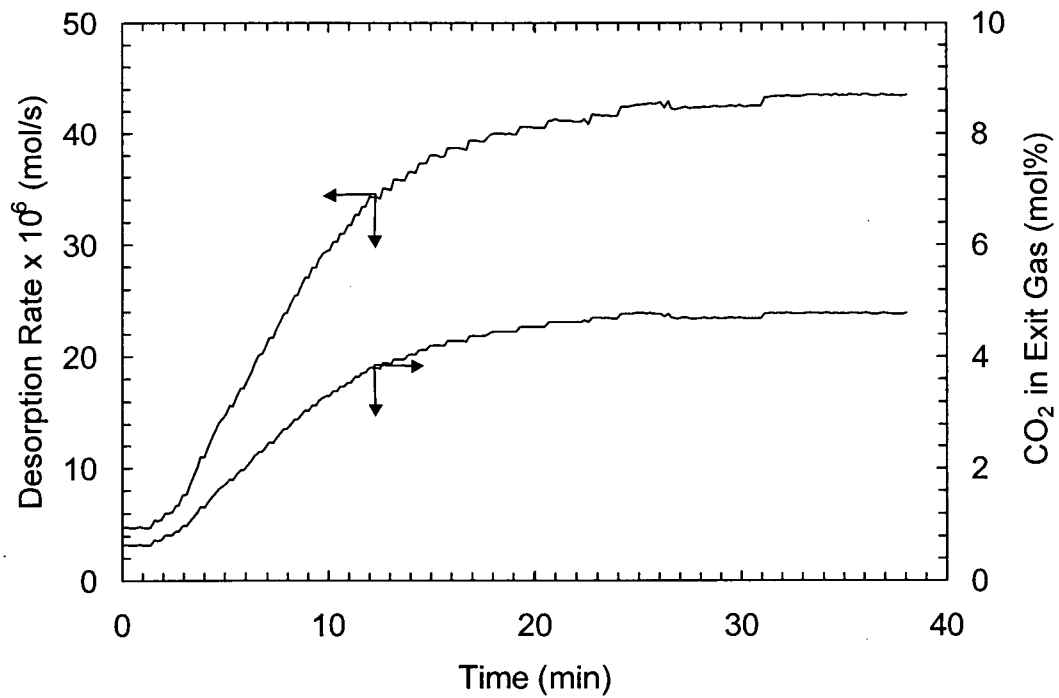


Figure 3.4: Typical computer output from a desorption experiment: (MEA = 20 wt%, $\alpha = 0.279 \text{ mol/mol}$, $T = 378 \text{ K}$, $P_T = 202 \text{ kPa}$, $Q_L = 2.2 \text{ mL/s}$)

reduced to the desired rate and the exit gas composition comes back to a steady value. An experiment was considered complete when the CO₂ concentration in the exit gas remained constant for at least 10 minutes.

In the desorption experiments (Figure 3.4), the concentration of CO₂ in the stripping gas steadily increases until it reaches a constant value. The gradual increase in CO₂ concentration in the stripping gas occurs because at the start of a desorption run all lines are purged with pure N₂ and it takes a while for the CO₂ to diffuse into N₂ gas filling the lines downstream of the absorption/desorption chamber. The reproducibility of the absorption and desorption experiments was always within 2%.

3.5 Chemicals

All gases had a purity of 99.9% and were supplied by Prax Air Company. The amines had a purity of more than 99% and were supplied by Sigma-Aldrich, van-Waters & Rogers and Travis Chemicals. The aqueous amine solutions were prepared using distilled water.

CHAPTER 4

MATHEMATICAL MODEL

This chapter presents a mathematical model for CO₂ absorption and desorption in aqueous amine solutions falling as a laminar liquid film over a hemispherical surface. The model was developed for the general case where the aqueous solution may contain a binary mixture of amines (e.g., MEA+AMP or MEA+MDEA) and where CO₂ undergoes a series of reversible reactions. This model can be readily modified to accommodate a single aqueous amine (e.g., MEA or AMP) or water by setting the initial concentration of one or both amines to zero. The model reduces to the well-known pseudo-first-order kinetics when all reactions are lumped into a single, overall reaction by setting the rates of all but one reaction to zero.

The important model parameters and physical property data needed to solve the model equations are identified. Correlations are presented for parameters for which data are available in the literature. For cases where data were deficient or not available in the literature (e.g., Henry's constant and diffusivity of CO₂ in aqueous amine blends), new data were obtained and new correlations were developed. A methodology to solve the model equations and to estimate unknown model parameters using the non-linear regression package GREG is also presented in this chapter.

4.1 Reaction Mechanism

The model for CO₂ absorption and desorption applies to the following aqueous amine systems:

- | | |
|---|---|
| 1. CO ₂ +MEA+H ₂ O | 5. CO ₂ +MEA+MDEA+H ₂ O |
| 2. CO ₂ +DEA+H ₂ O | 6. CO ₂ +MEA+AMP+H ₂ O |
| 3. CO ₂ +MDEA+H ₂ O | 7. CO ₂ +DEA+MDEA+H ₂ O |
| 4. CO ₂ +AMP+H ₂ O | 8. CO ₂ +DEA+AMP+H ₂ O |

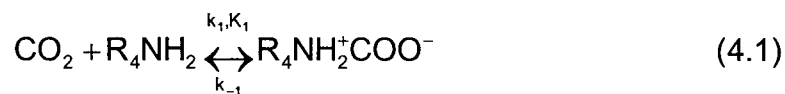
Since most of the data presented in this work refers to the CO₂+AMP+H₂O system, this system was chosen as the base case and the reactions governing this system are presented first. For systems involving other amines, the additional reactions are given subsequently.

In accordance with the convention used in the amine literature, MEA is represented as R₁NH₂, where R₁ denotes -CH₂CH₂OH. DEA is represented as R₁R₂NH, where R₁ = R₂ = -CH₂CH₂OH. MDEA is represented as R₁R₂R₃N, where R₁ = R₂ = -CH₂CH₂OH and R₃ = -CH₃. AMP is represented as R₄NH₂, where R₄ = -C(CH₃)₂CH₂OH.

4.1.1 Reactions for CO₂+AMP+H₂O (Base Case)

When CO₂ is absorbed or desorbed in aqueous AMP solutions, the following reactions may occur in the liquid phase:

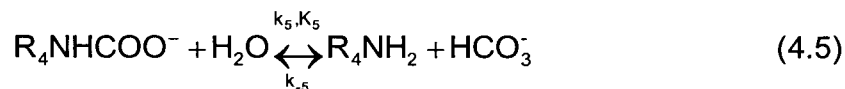
AMP- Zwitterion Formation:



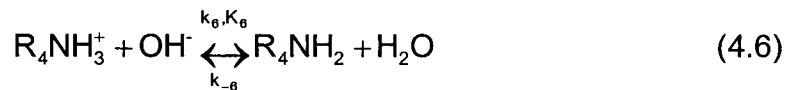
AMP-Zwitterion Deprotonation:



AMP-Carbamate Reversion:



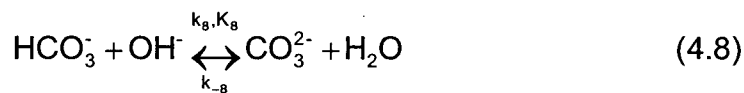
AMP Deprotonation:



Bicarbonate Formation:



Carbonate Formation:



Water Dissociation:

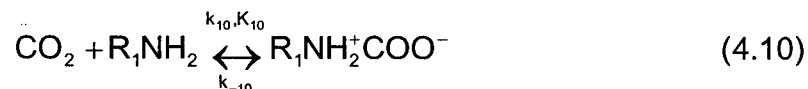


In the above reactions, the k's denote rate constants and the K's denote equilibrium constants.

4.1.2 Reactions for CO₂+MEA+H₂O

When CO₂ is absorbed or desorbed in aqueous MEA solutions, reactions (4.7) to (4.9) are the same as those in the base case, but reactions (4.1) to (4.6) are replaced by the following reactions:

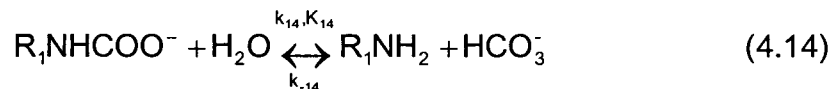
MEA-Zwitterion Formation:



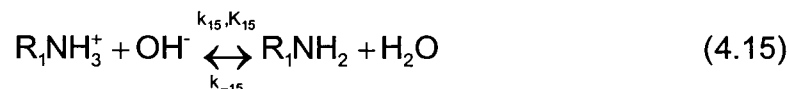
MEA-Zwitterion Deprotonation:



MEA-Carbamate Reversion:



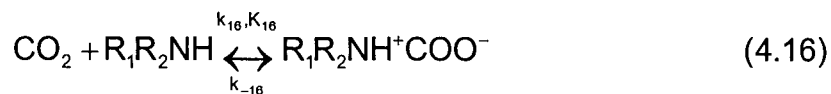
MEA Deprotonation:



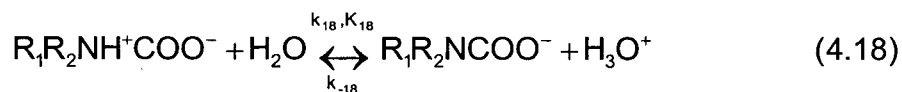
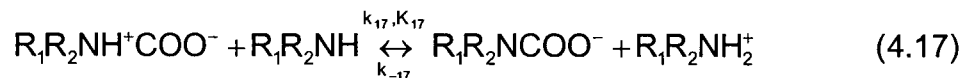
4.1.3 Reactions for CO₂+DEA+H₂O

When CO₂ is absorbed or desorbed in aqueous DEA solutions, reactions (4.7) to (4.9) are once again the same as those in the base case, but reactions (4.1) to (4.6) are replaced by the following reactions:

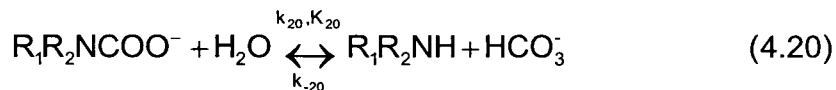
DEA- Zwitterion Formation:



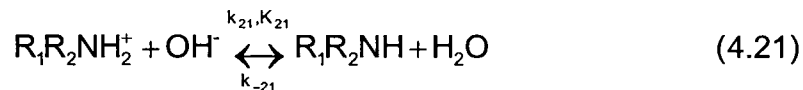
DEA-Zwitterion Deprotonation:



DEA-Carbamate Reversion:



DEA Deprotonation:



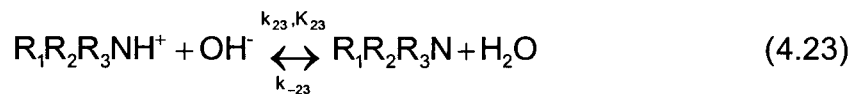
4.1.4 Reactions for CO₂+MDEA+H₂O

When CO₂ is absorbed or desorbed in aqueous MDEA solutions, reactions (4.7) to (4.9) are again unchanged, but reactions (4.1) to (4.6) are replaced by the following:

MDEA-CO₂ Reaction:



MDEA Deprotonation:



4.1.5 Reactions for CO₂+MEA+MDEA+H₂O

When CO₂ is absorbed or desorbed in aqueous blends of MEA and MDEA, in addition to reactions (4.7) to (4.15) and (4.22) to (4.23), the following reaction occurs:

Deprotonation of MEA-Zwitterion to MDEA:



4.1.6 Reactions for CO₂+MEA+AMP+H₂O

When CO₂ is absorbed or desorbed in aqueous blends of MEA and AMP, in addition to reactions (4.1) to (4.15), the following reactions must be included:

Deprotonation of AMP-Zwitterion to MEA:



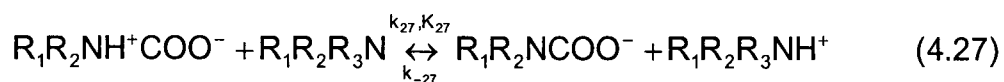
Deprotonation of MEA-Zwitterion to AMP:



4.1.7 Reactions for CO₂+DEA+MDEA+H₂O

When CO₂ is absorbed or desorbed in aqueous blends of DEA and MDEA, in addition to reactions (4.7) to (4.9) and (4.16) to (4.23), the following reaction occurs:

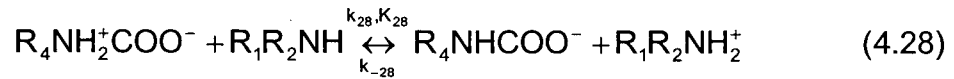
Deprotonation of DEA-Zwitterion to MDEA:



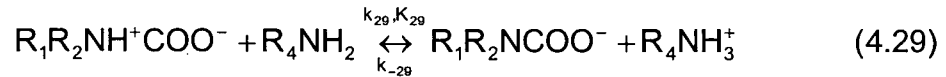
4.1.8 Reactions for CO₂+DEA+AMP+H₂O

When CO₂ is absorbed or desorbed in aqueous blends of DEA and AMP, the following reactions occur in addition to reactions (4.1) to (4.9) and (4.16) to (4.21):

Deprotonation of AMP-Zwitterion to DEA:



Deprotonation of DEA-Zwitterion to AMP:



4.2 Reaction Rates

In the above reaction schemes, all reactions are considered to be reversible. Some of these reactions proceed at finite rates while others (that involve only a proton transfer) occur almost instantaneously. This section presents the rate expressions for reactions with finite rates. For convenience, the chemical species in reactions (4.1) to (4.29) are renamed as follows:

$$\begin{aligned} C_1 &= CO_2, C_2 = R_4NH_2, C_3 = R_4NH_3^+, C_4 = R_4NHCOO^-, C_5 = HCO_3^-, C_6 = CO_3^{2-}, \\ C_7 &= OH^-, C_8 = H_3O^+, C_9 = H_2O, C_{10} = R_1NH_2, C_{11} = R_1NH_3^+, C_{12} = R_1NHCOO^-, \\ C_{13} &= R_1R_2NH, C_{14} = R_1R_2NH_2^+, C_{15} = R_1R_2NCOO^-, C_{16} = R_1R_2R_3N, C_{17} = R_1R_2R_3NH^+ \end{aligned} \quad (4.30)$$

4.2.1 Reaction Rates for CO₂+AMP+H₂O System (Base Case)

This case includes reactions (4.1) to (4.9). Among these, only reactions (4.1) to (4.4) and (4.7) have finite rates. The latter are expressed as follows:

$$r_{1-4} = \frac{-k_1 \left[C_1 C_2 - C_4 \left(\frac{A}{B} \right) \right]}{1 + \left(\frac{1}{B} \right)} \quad (4.31)$$

$$r_7 = -k_7 C_1 C_7 + \frac{k_7}{K_7} C_5 \quad (4.32)$$

where:

$$A = \left(\frac{k_2}{k_{-1}} \right) \frac{C_3}{K_1 K_2} + \left(\frac{k_3}{k_{-1}} \right) \frac{C_8}{K_1 K_3} + \left(\frac{k_4}{k_{-1}} \right) \frac{C_9}{K_1 K_4} \quad (4.33)$$

$$B = \left(\frac{k_2}{k_{-1}} \right) C_2 + \left(\frac{k_3}{k_{-1}} \right) C_9 + \left(\frac{k_4}{k_{-1}} \right) C_7 \quad (4.34)$$

Equation (4.31) is based on the assumption that pseudo-steady state is valid for the zwitterion. The detailed derivation of the base case equations is given in Appendix D. The derivations for other systems involving zwitterion mechanisms are similar and therefore not presented separately.

4.2.2 Reaction Rates for CO₂+MEA+H₂O System

This case includes reactions (4.7) to (4.15), with reactions (4.7) and (4.10) to (4.13) having finite rates. The rate expression for reaction (4.7) is given by equation (4.32). The rate for reactions (4.10) to (4.13) is given by:

$$r_{10-13} = \frac{-k_{10} \left[C_1 C_{10} - C_{12} \left(\frac{A}{B} \right) \right]}{1 + \left(\frac{1}{B} \right)} \quad (4.35)$$

where:

$$A = \left(\frac{k_{11}}{k_{-10}} \right) \frac{C_{11}}{K_{10}K_{11}} + \left(\frac{k_{12}}{k_{-10}} \right) \frac{C_8}{K_{10}K_{12}} + \left(\frac{k_{13}}{k_{-10}} \right) \frac{C_9}{K_{10}K_{13}} \quad (4.36)$$

$$B = \left(\frac{k_{11}}{k_{-10}} \right) C_{10} + \left(\frac{k_{12}}{k_{-10}} \right) C_9 + \left(\frac{k_{13}}{k_{-10}} \right) C_7 \quad (4.37)$$

4.2.3 Reaction Rates for CO₂+DEA+H₂O System

This case includes reactions (4.7) to (4.9) and (4.16) to (4.21), with reactions (4.7) and (4.16) to (4.19) having finite rates. The rate expression for reaction (4.7) is given by equation (4.32). The rate for reactions (4.16) to (4.19) is given by:

$$r_{16-19} = \frac{-k_{16} \left[C_1 C_{13} - C_{15} \left(\frac{A}{B} \right) \right]}{1 + \left(\frac{1}{B} \right)} \quad (4.38)$$

where:

$$A = \left(\frac{k_{17}}{k_{-16}} \right) \frac{C_{14}}{K_{16}K_{17}} + \left(\frac{k_{18}}{k_{-16}} \right) \frac{C_8}{K_{16}K_{18}} + \left(\frac{k_{19}}{k_{-16}} \right) \frac{C_9}{K_{16}K_{19}} \quad (4.39)$$

$$B = \left(\frac{k_{17}}{k_{-16}} \right) C_{13} + \left(\frac{k_{18}}{k_{-16}} \right) C_9 + \left(\frac{k_{19}}{k_{-16}} \right) C_7 \quad (4.40)$$

4.2.4 Reaction Rates for CO₂+MDEA+H₂O System

This case includes reactions (4.7) to (4.9) and (4.22) to (4.23), with reactions (4.7) and (4.22) having finite rates. The rate expression for reaction

(4.7) is given by equation (4.32) and the rate for reaction (4.22) can be obtained from:

$$r_{22} = -k_{22}C_1C_{16} + \frac{k_{22}}{K_{22}}C_5C_{17} \quad (4.41)$$

4.2.5 Reaction Rates for CO₂+MEA+MDEA+H₂O System

This case includes reactions (4.7) to (4.15) and (4.22) to (4.24), with reactions (4.7), (4.10) to (4.13), (4.22) and (4.24) having finite rates. The rate expressions for reactions (4.7) and (4.22) were already defined by equations (4.32) and (4.41), respectively. The rate of reactions (4.10) to (4.13) and (4.24) can be expressed as:

$$r_{10-13,24} = \frac{-k_{10} \left[C_1C_{10} - C_{12} \left(\frac{A}{B} \right) \right]}{1 + \left(\frac{1}{B} \right)} \quad (4.42)$$

where:

$$A = \left(\frac{k_{11}}{k_{-10}} \right) \frac{C_{11}}{K_{10}K_{11}} + \left(\frac{k_{12}}{k_{-10}} \right) \frac{C_8}{K_{10}K_{12}} + \left(\frac{k_{13}}{k_{-10}} \right) \frac{C_9}{K_{10}K_{13}} + \left(\frac{k_{24}}{k_{-10}} \right) \frac{C_{17}}{K_{10}K_{24}} \quad (4.43)$$

$$B = \left(\frac{k_{11}}{k_{-10}} \right) C_{10} + \left(\frac{k_{12}}{k_{-10}} \right) C_9 + \left(\frac{k_{13}}{k_{-10}} \right) C_7 + \left(\frac{k_{24}}{k_{-10}} \right) C_{16} \quad (4.44)$$

4.2.6 Reaction Rates for CO₂+MEA+AMP+H₂O System

This case includes reactions (4.1) to (4.15) and (4.25) to (4.26), with reactions (4.1) to (4.4), (4.7), (4.10) to (4.13) and (4.25) to (4.26) having finite

rates. The rate expression for reaction (4.7) is defined by equation (4.32). The rate of reactions (4.1) to (4.4), (4.25) and (4.10) to (4.13) and (4.26) are given by:

$$r_{1-4,25} = \frac{-k_1 \left[C_1 C_2 - C_4 \left(\frac{A}{B} \right) \right]}{1 + \left(\frac{1}{B} \right)} \quad (4.45)$$

where:

$$A = \left(\frac{k_2}{k_{-1}} \right) \frac{C_3}{K_1 K_2} + \left(\frac{k_3}{k_{-1}} \right) \frac{C_8}{K_1 K_3} + \left(\frac{k_4}{k_{-1}} \right) \frac{C_9}{K_1 K_4} + \left(\frac{k_{25}}{k_{-1}} \right) \frac{C_{11}}{K_1 K_{25}} \quad (4.46)$$

$$B = \left(\frac{k_2}{k_{-1}} \right) C_2 + \left(\frac{k_3}{k_{-1}} \right) C_9 + \left(\frac{k_4}{k_{-1}} \right) C_7 + \left(\frac{k_{25}}{k_{-1}} \right) C_{10} \quad (4.47)$$

and

$$r_{10-13,26} = \frac{-k_{10} \left[C_1 C_{10} - C_{12} \left(\frac{A}{B} \right) \right]}{1 + \left(\frac{1}{B} \right)} \quad (4.48)$$

where:

$$A = \left(\frac{k_{11}}{k_{-10}} \right) \frac{C_{11}}{K_{10} K_{11}} + \left(\frac{k_{12}}{k_{-10}} \right) \frac{C_8}{K_{10} K_{12}} + \left(\frac{k_{13}}{k_{-10}} \right) \frac{C_9}{K_{10} K_{13}} + \left(\frac{k_{26}}{k_{-10}} \right) \frac{C_3}{K_{10} K_{26}} \quad (4.49)$$

$$B = \left(\frac{k_{11}}{k_{-10}} \right) C_{10} + \left(\frac{k_{12}}{k_{-10}} \right) C_9 + \left(\frac{k_{13}}{k_{-10}} \right) C_7 + \left(\frac{k_{26}}{k_{-10}} \right) C_2 \quad (4.50)$$

4.2.7 Reaction Rates for CO₂+DEA+MDEA+H₂O System

This case includes reactions (4.7) to (4.9), (4.16) to (4.23) and (4.27), with reactions (4.7), (4.16) to (4.19), (4.22) and (4.27) having finite rates. The rate expressions for reactions (4.7) and (4.22) are defined by equations (4.32) and (4.41), respectively. The rate for reactions (4.16) to (4.19) and (4.27) is given by:

$$r_{16-19,27} = \frac{-k_{16} \left[C_1 C_{13} - C_{15} \left(\frac{A}{B} \right) \right]}{1 + \left(\frac{1}{B} \right)} \quad (4.51)$$

where:

$$A = \left(\frac{k_{17}}{k_{-16}} \right) \frac{C_{14}}{K_{16} K_{17}} + \left(\frac{k_{18}}{k_{-16}} \right) \frac{C_8}{K_{16} K_{18}} + \left(\frac{k_{19}}{k_{-16}} \right) \frac{C_9}{K_{16} K_{19}} + \left(\frac{k_{27}}{k_{-16}} \right) \frac{C_{17}}{K_{16} K_{27}} \quad (4.52)$$

$$B = \left(\frac{k_{17}}{k_{-16}} \right) C_{13} + \left(\frac{k_{18}}{k_{-16}} \right) C_9 + \left(\frac{k_{19}}{k_{-16}} \right) C_7 + \left(\frac{k_{27}}{k_{-16}} \right) C_{16} \quad (4.53)$$

4.2.8 Reaction Rates for CO₂+DEA+AMP+H₂O System

This case includes reactions (4.1) to (4.9), (4.16) to (4.21) and (4.28) to (4.29), with reactions (4.1) to (4.4), (4.7), (4.16) to (4.19) and (4.28) to (4.29) having finite rates. The rate expression for reaction (4.7) is defined by equation (4.32). The rates for reactions (4.1) to (4.4), (4.28), and (4.16) to (4.19) and (4.29) are given by:

$$r_{1-4,28} = \frac{-k_1 \left[C_1 C_2 - C_4 \left(\frac{A}{B} \right) \right]}{1 + \left(\frac{1}{B} \right)} \quad (4.54)$$

where:

$$A = \left(\frac{k_2}{k_{-1}} \right) \frac{C_3}{K_1 K_2} + \left(\frac{k_3}{k_{-1}} \right) \frac{C_8}{K_1 K_3} + \left(\frac{k_4}{k_{-1}} \right) \frac{C_9}{K_1 K_4} + \left(\frac{k_{28}}{k_{-1}} \right) \frac{C_{14}}{K_1 K_{28}} \quad (4.55)$$

$$B = \left(\frac{k_2}{k_{-1}} \right) C_2 + \left(\frac{k_3}{k_{-1}} \right) C_9 + \left(\frac{k_4}{k_{-1}} \right) C_7 + \left(\frac{k_{28}}{k_{-1}} \right) C_{13} \quad (4.56)$$

and

$$r_{16-19,29} = \frac{-k_{16} \left[C_1 C_{13} - C_{15} \left(\frac{A}{B} \right) \right]}{1 + \left(\frac{1}{B} \right)} \quad (4.57)$$

where:

$$A = \left(\frac{k_{17}}{k_{-16}} \right) \frac{C_{14}}{K_{16} K_{17}} + \left(\frac{k_{18}}{k_{-16}} \right) \frac{C_8}{K_{16} K_{18}} + \left(\frac{k_{19}}{k_{-16}} \right) \frac{C_9}{K_{16} K_{19}} + \left(\frac{k_{29}}{k_{-16}} \right) \frac{C_3}{K_{16} K_{29}} \quad (4.58)$$

$$B = \left(\frac{k_{17}}{k_{-16}} \right) C_{13} + \left(\frac{k_{18}}{k_{-16}} \right) C_9 + \left(\frac{k_{19}}{k_{-16}} \right) C_7 + \left(\frac{k_{29}}{k_{-16}} \right) C_2 \quad (4.59)$$

4.3 Reactive Gas Absorption/Desorption Model

4.3.1 Hydrodynamics of Liquid Film

Figure 4.1 is a schematic diagram of the hemispherical film described in Chapter 3. The liquid descends in the form of a laminar film from the pole of the

hemisphere towards its equator where it is collected in the funnel. The gas, depending on the operating conditions, is either absorbed into the liquid film or is desorbed from it.

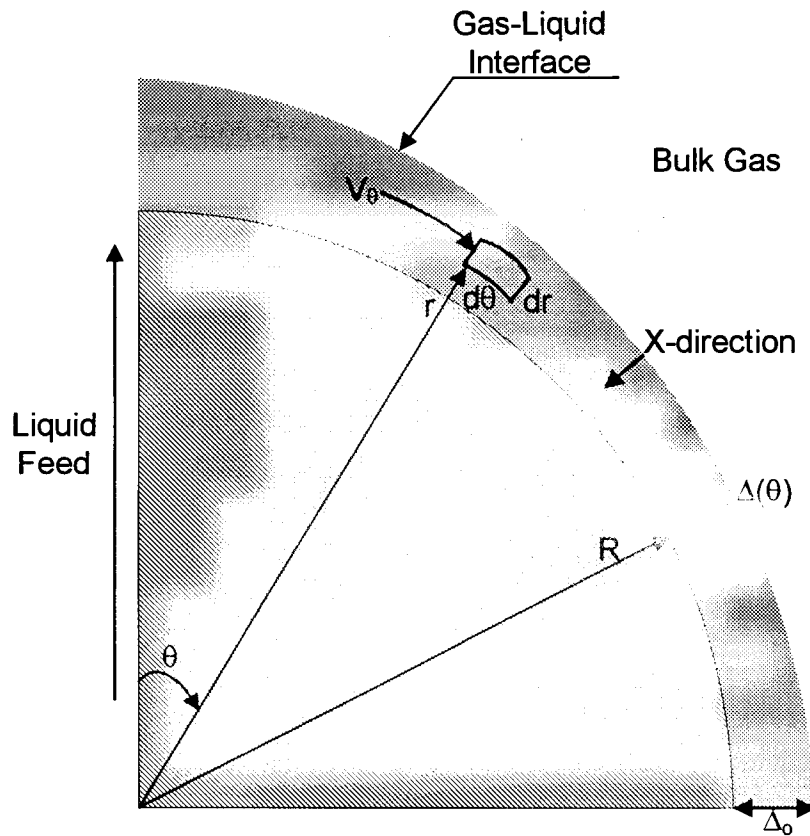


Figure 4.1: Schematic of the Liquid Film

This system can be mathematically modeled to calculate the rate of gas absorption or desorption over the exposed area of the film provided the film thickness and the velocity profile are known as a function of position (θ). Lynn et

hemisphere towards its equator where it is collected in the funnel. The gas, depending on the operating conditions, is either absorbed into the liquid film or is desorbed from it.

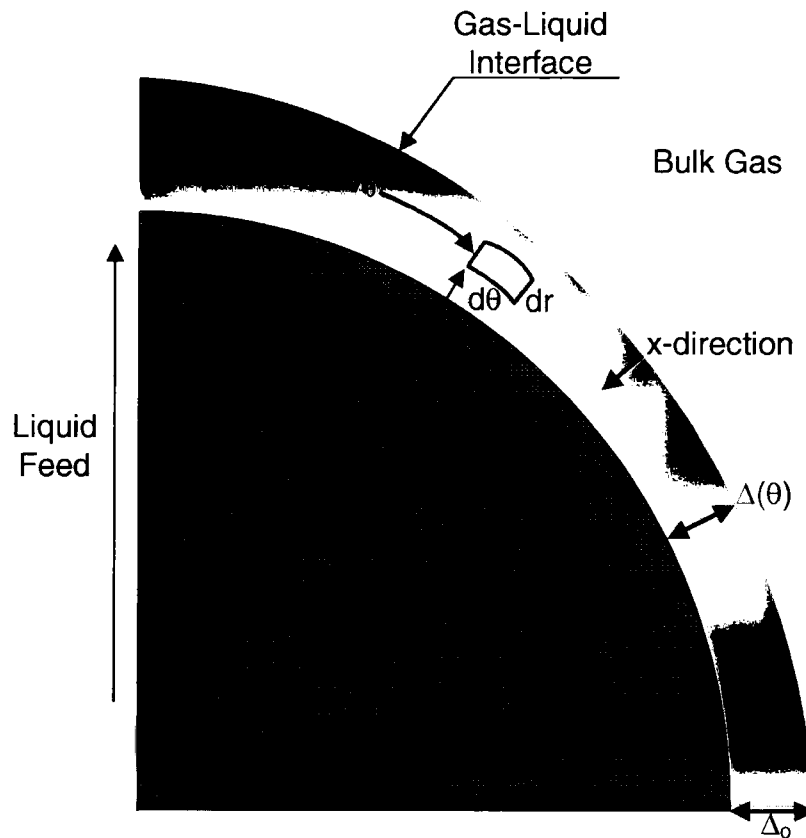


Figure 4.1: Schematic of the Liquid Film

This system can be mathematically modeled to calculate the rate of gas absorption or desorption over the exposed area of the film provided the film thickness and the velocity profile are known as a function of position (θ). Lynn et

al. (1955) have studied the hydrodynamics of laminar liquid films flowing over a sphere. They assumed that the thickness of the liquid film at any latitude on the sphere is the same as it would be for the same flow rate per unit length on a plane surface making the same angle with the vertical. Based on this assumption, the film thickness at latitude θ (Δ_θ) is given by:

$$\Delta_\theta = \Delta_o (\sin\theta)^{-2/3} \quad (4.60)$$

where Δ_o is the film thickness at the equator ($\theta = \pi/2$) of the sphere and is given by:

$$\Delta_o = \left(\frac{3\nu Q}{2\pi R g} \right)^{1/3} \quad (4.61)$$

It follows from the above assumption that a half parabolic velocity profile will exist at all latitude on the sphere so that the velocity distribution, V_θ , in the film can be approximated by the following equation:

$$V_\theta = V_o [1 - x^2] \quad (4.62)$$

where x is the dimensionless distance from the gas-liquid interface, i.e, $x = (R + \Delta_\theta - r) / \Delta_\theta$ (see Figure 4.1). V_o is the velocity at the film surface:

$$V_o = \left(\frac{3Q}{4\pi R \Delta_o} \right) (\sin\theta)^{-1/3} \quad (4.63)$$

Note that at $\theta = 0$ (i.e., at the pole of the hemisphere), equation (4.60) is not valid because at that point the thickness of the liquid film becomes infinite. However, this is a physical impossibility because only a finite amount of liquid

(about 2 mL/s) flows through the liquid feed tube of 3 mm I.D. We calculated the thickness of the liquid film at different θ values for water and amine solutions using equation (4.60) and we found that we get reasonable values at θ very close to the pole.

For numerical solution of the model equations, the liquid film in θ direction was divided into 200 points to integrate the absorption rate over the entire hemispherical surface. This means that the first point at which the concentration gradient was calculated lies at $\theta = 0.45^\circ$ (0.008 radian). For water at 298 K and liquid flow rates of 2, 3 and 4 mL/s, the film thickness at $\theta = 0.45^\circ$ (near the pole) calculated from equation (4.60) are 3.31, 3.80 and 4.17 mm respectively. The corresponding values at $\theta = 90^\circ$ (at the equator) are 0.13, 0.15 and 0.17 respectively. The thinning of the liquid film from the pole to the equator occurs because the same amounts of liquid flows through the increasing cross sectional area as it descends from the pole to the equator.

4.3.2 Model Equations

The mathematical model presented below is based on the concept of gas absorption or desorption accompanied by multiple reversible chemical reactions in a hemispherical liquid film. The main assumptions involved in the model derivation are:

- The interfacial concentration of dissolved (molecular) CO_2 corresponds to the physical solubility as determined by Henry's law (i.e., $p_1 = H_1 C_1^i$).

- Mass transfer in the direction of the liquid flow is dominated by bulk convection and diffusion in the θ direction is negligible.
- The flow field is uniform in the Φ direction ($V_{\Phi} = 0$). Hence, due to symmetry, bulk transfer and diffusion in the Φ direction are non-existent.
- The gas is saturated with water vapor at the system temperature and pressure and there is no transfer of amine or water from the liquid film into the gas phase.
- The diffusion coefficients of various ionic species are equal so that there are no electrostatic potential gradients present in the liquid film. Rinker et al. (1995) and Hagewiesche et al. (1995) have found that a more rigorous approach of taking into account the electrostatic gradient terms resulting from unequal diffusion coefficients requires much more computational effort and has little effect on the predicted rates of absorption. In addition, the parametric sensitivity analysis performed in this work show that a large deviation ($\pm 50\%$) in the values of the diffusivities of ionic species do not have any significant effect on the calculated absorption and desorption rates (see Table 5.2).
- The film is isothermal and the system is at steady state.

The following equations govern the diffusion and reaction processes for CO_2 absorption/desorption in an aqueous solution containing MEA and AMP. The equations are based on material balances for elements of the liquid film.

CO₂ Balance:

$$\frac{\partial C_1}{\partial \theta} = F_1(x, \theta) \sin \theta \frac{\partial^2 C_1}{\partial x^2} - 2 \frac{F_1(x, \theta) \sin \theta}{F_2(x, \theta)} \frac{\partial C_1}{\partial x} + F_1(x, \theta) (\sin \theta)^{-1/3} \frac{\Delta_o^2}{D_1} r_{\text{total}} \quad (4.64)$$

Total Carbon (CO₂) Balance:

$$\begin{aligned} \frac{\partial C_1}{\partial \theta} + \frac{\partial C_4}{\partial \theta} + \frac{\partial C_5}{\partial \theta} + \frac{\partial C_6}{\partial \theta} + \frac{\partial C_{12}}{\partial \theta} = \\ F_1(x, \theta) \sin \theta \left(\frac{\partial^2 C_1}{\partial x^2} + \frac{D_4}{D_1} \frac{\partial^2 C_4}{\partial x^2} + \frac{D_5}{D_1} \frac{\partial^2 C_5}{\partial x^2} + \frac{D_6}{D_1} \frac{\partial^2 C_6}{\partial x^2} + \frac{D_{12}}{D_1} \frac{\partial^2 C_{12}}{\partial x^2} \right) \\ - 2 \frac{F_1(x, \theta) \sin \theta}{F_2(x, \theta)} \left(\frac{\partial C_1}{\partial x} + \frac{D_4}{D_1} \frac{\partial C_4}{\partial x} + \frac{D_5}{D_1} \frac{\partial C_5}{\partial x} + \frac{D_6}{D_1} \frac{\partial C_6}{\partial x} + \frac{D_{12}}{D_1} \frac{\partial C_{12}}{\partial x} \right) \end{aligned} \quad (4.65)$$

Total AMP Balance:

$$\begin{aligned} \frac{\partial C_2}{\partial \theta} + \frac{\partial C_3}{\partial \theta} + \frac{\partial C_4}{\partial \theta} = F_1(x, \theta) \sin \theta \left(\frac{D_2}{D_1} \frac{\partial^2 C_2}{\partial x^2} + \frac{D_3}{D_1} \frac{\partial^2 C_3}{\partial x^2} + \frac{D_4}{D_1} \frac{\partial^2 C_4}{\partial x^2} \right) \\ - 2 \frac{F_1(x, \theta) \sin \theta}{F_2(x, \theta)} \left(\frac{D_2}{D_1} \frac{\partial C_2}{\partial x} + \frac{D_3}{D_1} \frac{\partial C_3}{\partial x} + \frac{D_4}{D_1} \frac{\partial C_4}{\partial x} \right) \end{aligned} \quad (4.66)$$

Total MEA Balance:

$$\begin{aligned} \frac{\partial C_{10}}{\partial \theta} + \frac{\partial C_{11}}{\partial \theta} + \frac{\partial C_{12}}{\partial \theta} = F_1(x, \theta) \sin \theta \left(\frac{D_{10}}{D_1} \frac{\partial^2 C_{10}}{\partial x^2} + \frac{D_{11}}{D_1} \frac{\partial^2 C_{11}}{\partial x^2} + \frac{D_{12}}{D_1} \frac{\partial^2 C_{12}}{\partial x^2} \right) \\ - 2 \frac{F_1(x, \theta) \sin \theta}{F_2(x, \theta)} \left(\frac{D_{10}}{D_1} \frac{\partial C_{10}}{\partial x} + \frac{D_{11}}{D_1} \frac{\partial C_{11}}{\partial x} + \frac{D_{12}}{D_1} \frac{\partial C_{12}}{\partial x} \right) \end{aligned} \quad (4.67)$$

Electron Neutrality Balance:

$$\begin{aligned}
 & \frac{\partial C_3}{\partial \theta} + \frac{\partial C_8}{\partial \theta} + \frac{\partial C_{11}}{\partial \theta} - \frac{\partial C_4}{\partial \theta} - \frac{\partial C_5}{\partial \theta} - 2 \frac{\partial C_6}{\partial \theta} - \frac{\partial C_7}{\partial \theta} - \frac{\partial C_{12}}{\partial \theta} = \\
 & F_1(x, \theta) \sin \theta \left(\frac{D_3}{D_1} \frac{\partial^2 C_3}{\partial x^2} + \frac{D_8}{D_1} \frac{\partial^2 C_8}{\partial x^2} + \frac{D_{11}}{D_1} \frac{\partial^2 C_{11}}{\partial x^2} - \frac{D_4}{D_1} \frac{\partial^2 C_4}{\partial x^2} - \right. \\
 & \quad \left. \frac{D_5}{D_1} \frac{\partial^2 C_5}{\partial x^2} - 2 \frac{D_6}{D_1} \frac{\partial^2 C_6}{\partial x^2} - \frac{D_7}{D_1} \frac{\partial^2 C_7}{\partial x^2} - \frac{D_{12}}{D_1} \frac{\partial^2 C_{12}}{\partial x^2} \right) \\
 & - 2 \frac{F_1(x, \theta) \sin \theta}{F_2(x, \theta)} \left(\frac{D_3}{D_1} \frac{\partial C_3}{\partial x} + \frac{D_8}{D_1} \frac{\partial C_8}{\partial x} + \frac{D_{11}}{D_1} \frac{\partial C_{11}}{\partial x} - \frac{D_4}{D_1} \frac{\partial C_4}{\partial x} - \right. \\
 & \quad \left. \frac{D_5}{D_1} \frac{\partial C_5}{\partial x} - 2 \frac{D_6}{D_1} \frac{\partial C_6}{\partial x} - \frac{D_7}{D_1} \frac{\partial C_7}{\partial x} - \frac{D_{12}}{D_1} \frac{\partial C_{12}}{\partial x} \right)
 \end{aligned} \tag{4.68}$$

Equilibrium Reactions:

$$K_5 = \frac{C_2 C_5}{C_4} \tag{4.69}$$

$$K_6 = \frac{C_2}{C_3 C_7} \tag{4.70}$$

$$K_8 = \frac{C_6}{C_5 C_7} \tag{4.71}$$

$$K_9 = C_7 C_8 \tag{4.72}$$

$$K_{14} = \frac{C_{10} C_5}{C_{12}} \tag{4.73}$$

$$K_{15} = \frac{C_{10}}{C_{11} C_7} \tag{4.74}$$

where:

$$\text{Re} = \frac{Q}{2\pi Rv} \quad (4.75)$$

$$\text{Sc} = \frac{v}{D_1} \quad (4.76)$$

$$\text{Ga} = \frac{R^3 g}{v^2} \quad (4.77)$$

$$G(\theta) = \left(\frac{\text{Ga}}{3\text{Re}} \right)^{1/3} (\sin \theta)^{2/3} \quad (4.78)$$

$$F_1(x, \theta) = \left[\frac{G(\theta) + (1-x)}{1-x^2} \right] \frac{2}{3\text{ReSc}} \quad (4.79)$$

$$F_2(x, \theta) = G(\theta) + (1-x) \quad (4.80)$$

The above model consists of eleven partial differential and algebraic equations (4.64 to 4.74) and eleven unknowns. The equations can be solved numerically subject to the following initial and boundary conditions:

Initial Conditions:

$$\text{At } \theta = 0, C_j = C_j^0 \text{ for } j=1-8,10-12 \quad (4.81)$$

Boundary Conditions:

$$\begin{aligned} \text{at } \theta > 0 \text{ and } x = 0, \quad & \left(C_1^i - \frac{p_1}{H_1} \right) = \left(\frac{D_1}{k_g H_1 \Delta_o} \right) (\sin \theta)^{2/3} \left(\frac{\partial C_1}{\partial x} \right) \\ \text{and } \left(\frac{\partial C_j}{\partial x} \right)_{j=2-8,10-12} &= 0 \end{aligned} \quad (4.82)$$

$$\text{at } \theta > 0 \text{ and } x = 1, \left(\frac{\partial C_j}{\partial x} \right)_{j=1-8,10-12} = 0 \quad (4.83)$$

For the case where the gas side resistance to mass transfer is negligible ($k_g \rightarrow \infty$), the boundary condition given by equation (4.82) reduces to:

$$\text{at } \theta > 0 \text{ and } x = 0, C_1^i = \frac{p_1}{H_1} \text{ and } \left(\frac{\partial C_j}{\partial x} \right)_{j=2-8,10-12} = 0 \quad (4.84)$$

Note that the model equations (4.64) to (4.74) are general and applicable to any of the aforementioned systems by substituting corresponding chemical species, reaction rates and diffusivities. The model equations were solved numerically using a commercial software package called Athena Visual Workbench (see Section 4.5).

4.3.3 Liquid Bulk Concentrations

In order to solve the model equations (4.64) to (4.74), the bulk concentrations (C_i^o), must be known. They can be obtained by writing the following balances:

Total CO₂ Balance:

$$C_1^o + C_4^o + C_5^o + C_6^o + C_{12}^o = \alpha_{\text{initial}} ([R_4NH_2]_{\text{initial}} + [R_1NH_2]_{\text{initial}}) \quad (4.85)$$

Total AMP Balance:

$$C_2^o + C_3^o + C_4^o = [R_4NH_2]_{\text{initial}} \quad (4.86)$$

Total MEA Balance:

$$C_{10}^{\circ} + C_{11}^{\circ} + C_{12}^{\circ} = [R_1NH_2]_{\text{initial}} \quad (4.87)$$

Electron Neutrality Balance:

$$C_3^{\circ} + C_8^{\circ} + C_{11}^{\circ} - C_4^{\circ} - C_5^{\circ} - 2C_6^{\circ} - C_7^{\circ} - C_{12}^{\circ} = 0 \quad (4.88)$$

Equilibrium Equations:

$$K_5 = \frac{C_2^{\circ}C_5^{\circ}}{C_4^{\circ}} \quad (4.89)$$

$$K_6 = \frac{C_2^{\circ}}{C_3^{\circ}C_7^{\circ}} \quad (4.90)$$

$$K_7 = \frac{C_5^{\circ}}{C_1^{\circ}C_7^{\circ}} \quad (4.91)$$

$$K_8 = \frac{C_6^{\circ}}{C_5^{\circ}C_7^{\circ}} \quad (4.92)$$

$$K_9 = C_7^{\circ}C_8^{\circ} \quad (4.93)$$

$$K_{14} = \frac{C_{10}^{\circ}C_5^{\circ}}{C_{12}^{\circ}} \quad (4.94)$$

$$K_{15} = \frac{C_{10}^{\circ}}{C_{11}^{\circ}C_7^{\circ}} \quad (4.95)$$

4.3.4 Rate of Absorption or Desorption with Chemical Reaction

The rate of gas absorption or desorption over the hemispherical film at any latitude θ can be calculated by invoking the Fick's law of diffusion:

$$N_A(\theta) = -N_D(\theta) = -\left[2\pi(R + \Delta_\theta)^2 \sin\theta\right] \frac{D_1}{\Delta_\theta} \left(\frac{\partial C_1}{\partial x}\right)_{(0,\theta)} \quad (4.96)$$

The total rate of absorption or desorption is obtained by integrating equation (4.96) over the entire hemisphere from $\theta = 0$ (at the pole) to $\theta = \pi/2$ (at the equator) as given by

$$\bar{N}_A = -\bar{N}_D = -2\pi D_1 \Delta_o \int_0^{\pi/2} [G(\theta) + 1]^2 (\sin\theta)^{1/3} \left(\frac{\partial C_1}{\partial x}\right)_{(0,\theta)} d\theta \quad (4.97)$$

Note that for absorption, the concentration gradient, $\left(\frac{\partial C_1}{\partial x}\right)_{(0,\theta)}$, is a negative quantity and for desorption it is a positive value. The procedure to calculate \bar{N}_A and \bar{N}_D using equation (4.97) is described in Section (4.6).

4.3.5 Rate of Absorption or Desorption without Chemical Reaction

When there is no reaction between the gas and liquid film, the general model reduces to a case of physical absorption or desorption. This situation is governed by a single partial differential equation, which under certain assumptions, can be solved analytically and an explicit expression for the mass transfer rate can be derived. The details of this derivation are given in Appendix C and the final results are reproduced below.

Rate of Physical Absorption or Desorption:

$$\bar{N}_A^o = -\bar{N}_B^o = 3.1774 \sqrt{\frac{QR^2D_1}{\Delta_o}} (C_1^i - C_1^o) \quad (4.98)$$

For absorption, the driving force $(C_1^i - C_1^o)$ is positive whereas for desorption it is negative.

Physical Mass Transfer Coefficient:

$$Sh = 1.26758 Re^{0.5} Sc^{0.5} \quad (4.99)$$

Contact Time:

$$\tau_c = 1.5848 \pi R^2 \left(\frac{\Delta_o}{Q} \right) \quad (4.100)$$

In equation (4.99), the Reynolds number (Re) and Schmidt number (Sc) are defined according to equations (4.75) and (4.76), respectively. The Sherwood number (Sh) is given by:

$$Sh = \frac{k_L^o \sqrt{R\Delta_o}}{D_1} \quad (4.101)$$

The analytical solution for physical absorption (i.e., equation 4.98) is very important because it can be used to calculate the diffusivity of a gas in a liquid from experimental absorption rate measurements. A comparison of the mass fluxes for physical absorption predicted by numerical methods and analytical solution is given in Chapter 5.

4.3.6 Enhancement Factor

Once the rate of absorption (or desorption) with and without chemical reaction is known, the enhancement factor can be determined from the following equation:

$$E_A = \frac{\bar{N}_A}{N_A^o} \quad \text{and} \quad E_D = \frac{\bar{N}_D}{N_D^o} \quad (4.102)$$

The enhancement factor is a measure of the effect of chemical reaction on the rate of mass transfer.

4.3.7 Overall Reaction Rate (r_{total})

In order to solve the model equations (4.64) to (4.74) to calculate the rate of absorption or desorption, an expression for overall reaction rate (r_{total}) is required (see equation 4.64). The term r_{total} is the sum of all rates of reactions that either consume or produce CO_2 in the solution. The relationships for r_{total} for the eight systems considered here are listed in Table 4.1.

Note that the reactions rates presented in Section 4.2 have been derived for the general case including all possible reactions that may occur when CO_2 reacts with aqueous amine solutions. However, for amines like MEA, DEA and AMP, where the zwitterion mechanism applies, it has been shown previously (Danckwerts, 1979; Versteeg and van Swaaij, 1988; Little et al., 1992a,b; Hagewiesche, et al., 1995; Rinker et al., 1996) and has been confirmed by our own data regression and parametric sensitivity analysis presented in Chapter 5 that the contribution to mass transfer rates of reactions involving the

deprotonation of amine-zwitterion to water and hydroxyl ions is negligible. Therefore, for AMP, reactions (4.3) and (4.4), for MEA, reactions (4.12) and (4.13) and for DEA, reactions (4.18) and (4.19) can be neglected without any loss of accuracy. This means that the rate expressions for systems involving AMP, MEA and DEA can be simplified by setting the rate constants k_3 , k_4 , k_{12} , k_{13} , k_{18} and k_{19} equal to zero.

Table 4.1: Overall reaction rate (r_{total})

System	r_{total}	Equation No.
CO ₂ +MEA+H ₂ O	$r_7 + r_{10-13}$	(4.32)+(4.35)
CO ₂ +DEA+H ₂ O	$r_7 + r_{16-19}$	(4.32)+(4.38)
CO ₂ +MDEA+H ₂ O	$r_7 + r_{22}$	(4.32)+(4.41)
CO ₂ +AMP+H ₂ O	$r_7 + r_{1-4}$	(4.32)+(4.31)
CO ₂ +MEA+MDEA+H ₂ O	$r_7 + r_{10-13,24} + r_{22}$	(4.32)+(4.42)+(4.41)
CO ₂ +MEA+AMP+H ₂ O	$r_7 + r_{10-13,26} + r_{1-4,25}$	(4.32)+(4.48)+(4.45)
CO ₂ +DEA+MDEA+H ₂ O	$r_7 + r_{16-19,27} + r_{22}$	(4.32)+(4.51)+(4.41)
CO ₂ +DEA+AMP+H ₂ O	$r_7 + r_{16-19,29} + r_{1-4,28}$	(4.32)+(4.57)+(4.54)

4.4 Model Parameters

The parameters needed to solve the mathematical model are listed in Table 4.2 and their determination is outlined below.

The density and viscosity of amine solutions were obtained using the correlations presented in Appendix E. The Henry's constant and the diffusion coefficient of CO₂ in aqueous amine solutions were obtained using the N₂O analogy and they are presented in Appendix F and Appendix G, respectively. The gas-side mass transfer coefficient was estimated by absorbing a mixture of CO₂ and N₂ in aqueous DEA solutions and its determination is presented in Appendix I. The equilibrium constants for fast reactions are presented in Appendix H.

4.5 Numerical Implementation

The model equations (4.64) to (4.97) were solved using a commercial software package called Athena Visual Workbench licensed from Stewart and Associate Engineering Software Inc., Madison, Wisconsin. Athena Visual Workbench is a Windows based fully integrated environment for process modeling and nonlinear parameter estimation. It consists of three mathematical solvers: DDAPLUS, PDAPLUS and GREGPLUS. DDAPLUS is used for the integration and sensitivity analysis of initial-value problems with mixed algebraic and differential equations, PDAPLUS is used for the integration and sensitivity analysis of initial-boundary value problems with mixed algebraic and differential equations and GREGPLUS is used for non-linear parameter estimation. DDAPLUS and PDAPLUS employ the method of lines with finite differences, global orthogonal collocation and collocation on finite elements and GREGPLUS uses weighted least squares and Bayesian estimators with single as well as

Table 4.2: Parameters for absorption/desorption model

Parameter	Definition	Source
ρ	Density of amine solutions	Appendix E
μ	Viscosity of amine solutions	Appendix E
H_{CO_2}	Henry's constant for CO_2 in amine solutions	Appendix F
D_1	Diffusivity of CO_2 in amine solution	Appendix G
D_2 - D_{17}	Diffusivities of amine and other ionic species in amine solutions	Appendix G
k_g	Gas-side mass transfer coefficient	Appendix I
K_5 to K_9 , K_{14} , K_{15} , K_{20} , K_{21} , K_{23} ,	Equilibrium constants for reaction (4.5) to (4.9), (4.14), (4.15), (4.20), (4.21) and (4.23)	Appendix H
k_7	Forward rate constant for CO_2 hydration reaction (Rxn. 4.7)	Appendix H
$k_1, k_{10}, k_{16}, k_{22}$	Forward rate constants for reactions (4.1), (4.10), (4.16) and (4.22)	Chapter 5
$\frac{k_2}{k_{-1}}, \frac{k_3}{k_{-1}}, \frac{k_4}{k_{-1}}$	Combined rate constants for CO_2 +AMP+ H_2O system	Chapter 5
$\frac{k_{11}}{k_{-10}}, \frac{k_{12}}{k_{-10}}, \frac{k_{13}}{k_{-10}}$	Combined rate constants for CO_2 +MEA+ H_2O system	Chapter 5
$\frac{k_{17}}{k_{-16}}, \frac{k_{18}}{k_{-16}}, \frac{k_{19}}{k_{-19}}$	Combined rate constants for CO_2 +DEA+ H_2O system	Chapter 5
$\frac{k_{24}}{k_{-10}}, \frac{k_{25}}{k_{-1}}, \frac{k_{26}}{k_{-10}},$ $\frac{k_{27}}{k_{-16}}, \frac{k_{28}}{k_{-16}}, \frac{k_{29}}{k_{-16}}$	Combined rate constants for mixed amine systems	Chapter 5

multi-response data. Further information about this package can be obtained from Caracotsios and Stewart (1985, 1995), Stewart et al. (1996) and Bain and Stewart (1990).

The present model is quite complex and cannot be solved directly using Athena. For a given set of operating conditions, the calculation of absorption and desorption rates involves: (a) calculation of physical-chemical properties, (b) solution of the equilibrium model (equations 4.84 to 4.95), (c) solution of the model equations (4.64) to (4.84) to calculate concentration gradients at different latitude θ , (d) calculation of the total absorption or desorption rate by integrating over the entire hemisphere. The Fortran code to perform tasks (a) and (d) were written as part of this study and that for tasks (b) and (c) were generated from Athena by implementing the model equations in the Athena Visual Workbench environment. All these subroutines were then combined according to the scheme shown in Figure 4.2 using the Compaq Visual-Fortran Developer Studio. For a typical run, an input data file consisting of identification flags and operating variables (see Figure 4.2) was generated in Excel and added to the Developer Studio's project files. The simulation was run using the fastest available desktop PC (Pentium 4, 1700 MHz, 256 RAM). The results were plotted using Microsoft Excel.

4.6 *Parameter Estimation*

The unknown parameters such as k_1 , k_{10} , k_{16} , k_{22} , etc. can be determined by minimizing the following objective function:

$$S(\mathbf{k}) = \sum_{i=1}^N [\hat{y}_i - y(\mathbf{k})]^T Q_i [\hat{y}_i - y(\mathbf{k})] \quad (4.103)$$

where $\mathbf{k} = (k_1, k_{10}, k_{16}, k_{22}, \text{etc.})^T$ is the unknown parameter vector, \hat{y}_i is the measured value of the state variable (in the present case, it is the absorption/desorption rate of CO_2) and $y(\mathbf{k})$ is the calculated value of the state variable which is obtained by solving the model equations (4.64) to (4.97) for a set of assumed values of the unknown parameters. N denotes the number of experimental data and Q is the weighting matrix. For least squares estimation, Q is taken as the identity matrix. Note that the parameters for each case were estimated separately. However, the same methodology was used in all cases. The optimization was carried out using Athena's GREGPLUS solver according to the scheme shown in Figure 4.3.

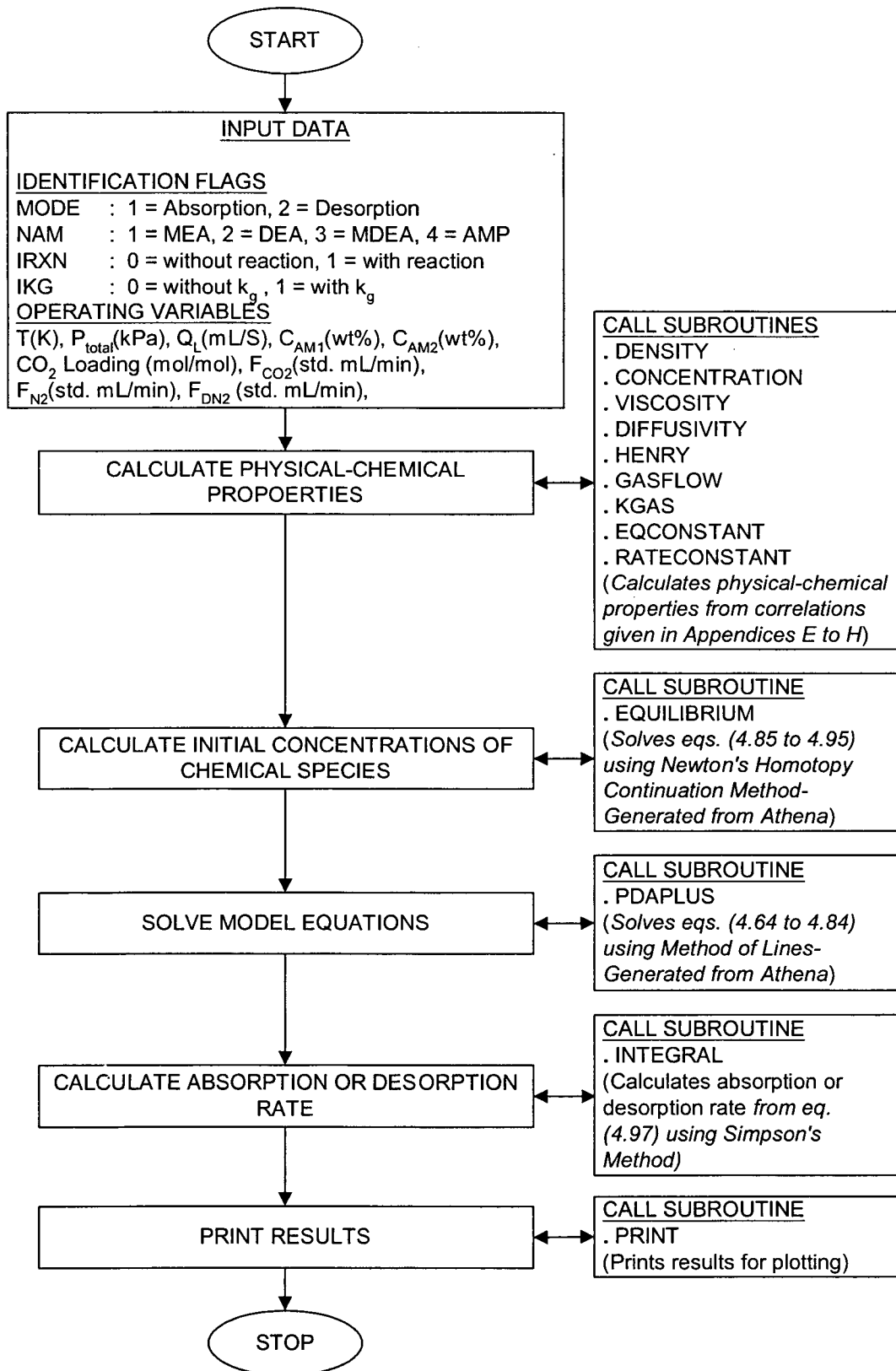


Figure 4.2: Numerical scheme for model solution

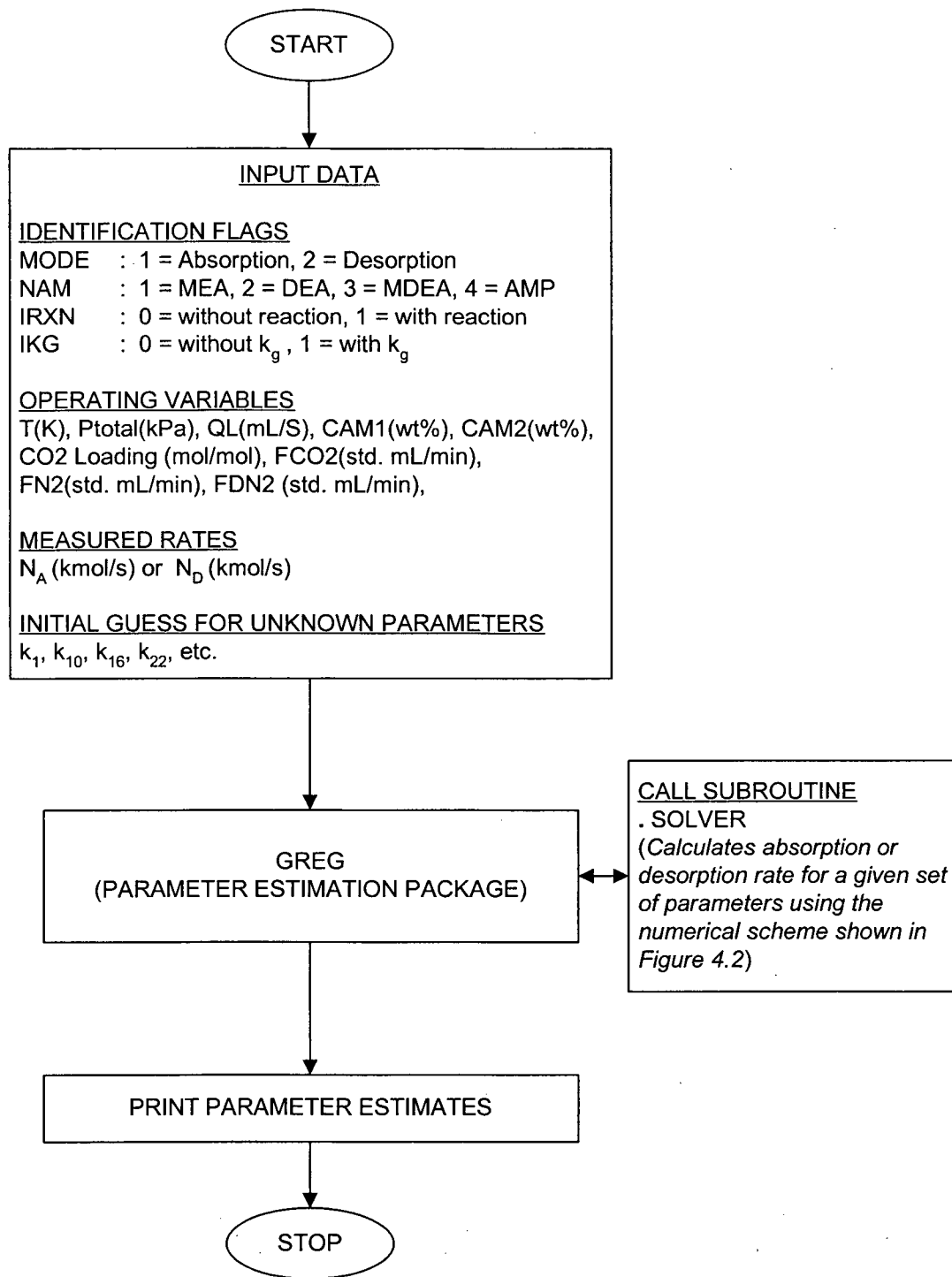


Figure 4.3: Numerical scheme for parameter estimation

CHAPTER 5

RESULTS AND DISCUSSION

This chapter presents the experimental and theoretical results and their interpretation for CO₂ absorption and desorption in aqueous amine solutions based on the novel hemispherical contactor and the comprehensive mathematical model discussed in Chapters 3 and 4 respectively. The results presented here pertain to the eight systems listed in Chapter 4. The bulk of the experimental work was focused on CO₂ desorption from aqueous amine systems. Some absorption experiments were also performed but the purpose of the absorption experiments was mainly to verify the experimental technique and the mathematical model because, for most amines, extensive absorption data are already available in the literature.

5.1 Model Verification

5.1.1 CO₂ Absorption/Desorption in Aqueous Amines

Figure 5.1 shows a comparison of the predicted and experimentally observed absorption rates for the three most commonly used alkanolamines namely MEA, DEA and MDEA at 303 K. Note that, unless otherwise stated, predicted results throughout this thesis were obtained based on best fit parameter estimates from this work. In Figure 5.1, MEA is a primary amine and has the highest reactivity, DEA is a secondary amine with intermediate reactivity

and MDEA is a tertiary amine with very low reactivity with CO₂ in aqueous solutions. This behavior is clearly demonstrated in Figure 5.1, where absorption rates decrease from MEA to DEA to MDEA.

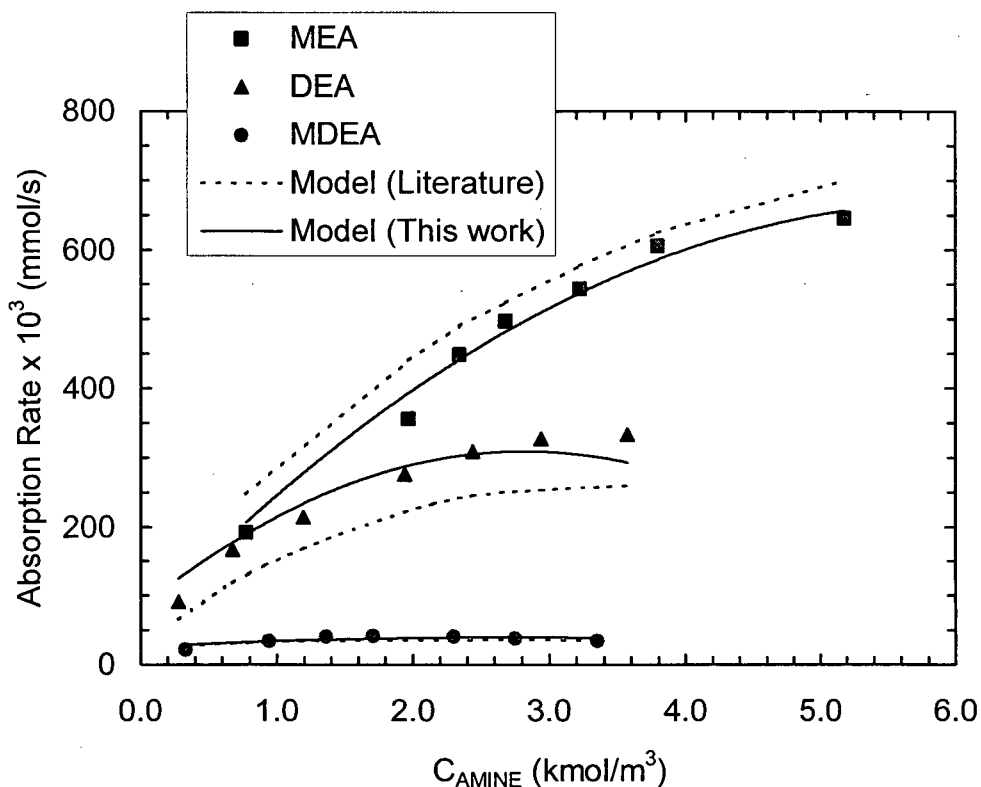


Figure 5.1: Predicted and experimental absorption rates of CO₂ in aqueous solutions of MEA, DEA and MDEA at 303 K ($p_{CO_2} = 97.0$ kPa, $Q_L \cong 2.0$ mL/s)

In Figure 5.1, the symbols represent the experimental data, the solid lines represent the model predictions based on the parameter estimates obtained in this work (described later in this chapter) and the dotted lines represents model predictions based on literature correlations (Hikita et al., 1977a; Rinker et al., 1996; Rinker et al., 1995) for the kinetic parameters. A slight deviation of the predicted trends using literature correlations is reasonable as different authors

have employed different experimental techniques (see Tables 2.1 to 2.3), different correlations to calculate physical properties and different ways to interpret their experimental data to estimate kinetic parameters. Furthermore, the presence of small amounts of impurities in the MEA and DEA solutions may cause significant variations in the measured absorption rates. Therefore, it can be safely said that the present model predicts absorption rates with fairly good accuracy.

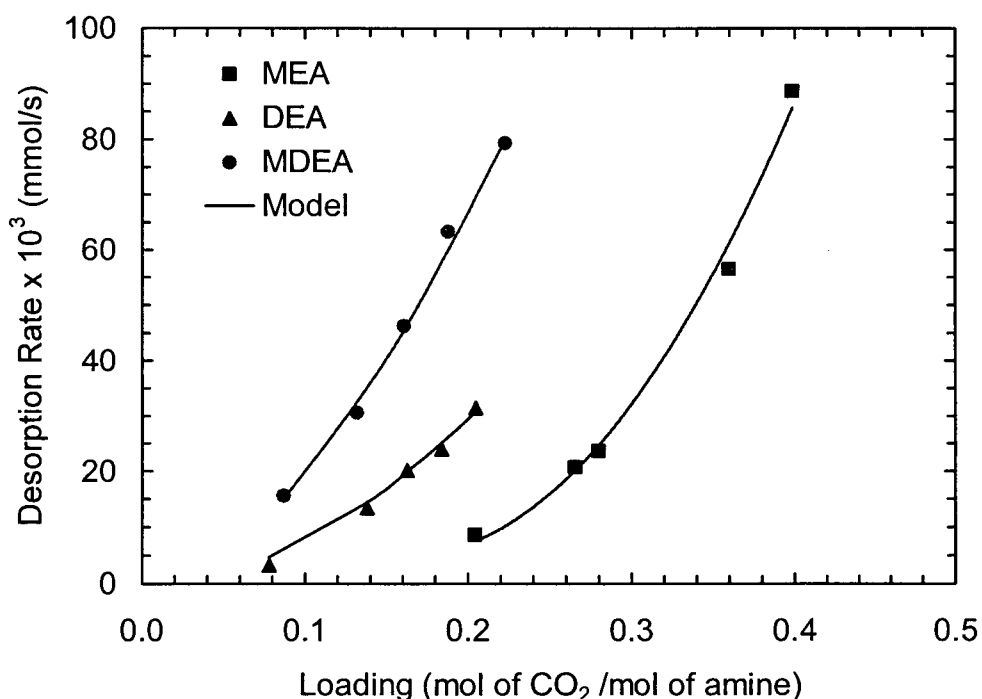


Figure 5.2: Predicted and experimental desorption rates of CO₂ from aqueous solutions of MEA, DEA and MDEA at 373 K ($p_{\text{CO}_2} < 5.0$ kPa, $Q_L \cong 2.0$ mL/s)

Figure 5.2 presents desorption rates of CO₂ from aqueous solutions of MEA, DEA and MDEA at 373 K. In this figure, the symbols represent the experimental data and the solid lines represent the model predictions based on

the parameter estimates obtained in this work. The agreement between experimental and predicted desorption rates is excellent. Figure 5.2 also shows that MDEA, which does not directly bond with CO₂, desorbs much faster compared to DEA and MEA, which react with CO₂ to form stable carbamate.

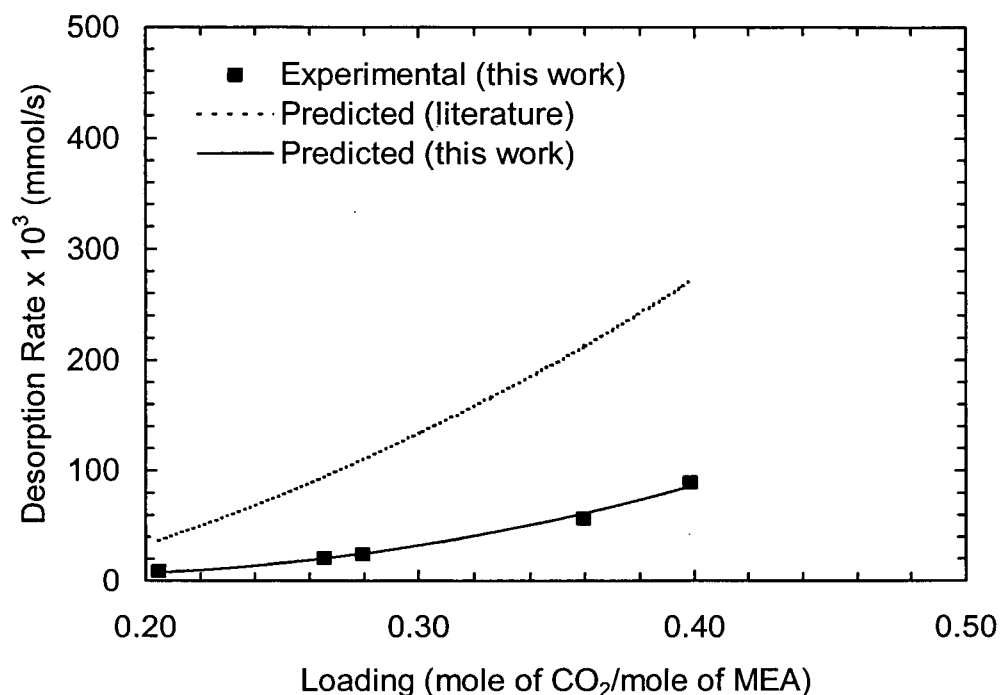


Figure 5.3: Predicted and experimental desorption rates for CO₂ desorption from aqueous MEA solution at 373 K ($p_{\text{CO}_2} < 5.0$ kPa, $Q_L \cong 2.0$ mL/s)

A comparison of the predicted and experimental desorption rates based on a literature correlation of Hikita et al. (1977) for the CO₂-MEA-H₂O system is shown in Figure 5.3. It can be seen from this figure that, although the predicted trend with respect to CO₂ loading is the same as that observed experimentally, the literature correlation over-predicts the desorption rates by a factor of 2 to 5. This is not surprising because most of these correlations were developed based

on absorption data only and (as discussed later in this chapter) cannot be reliably extrapolated to desorption conditions.

5.1.2 Detailed Profiles in the Hemispherical Film

In order to further validate the model and the numerical scheme to solve the model equations, in this section we analyze detailed concentration profiles within the hemispherical film generated from the numerical simulation results obtained for both absorption and desorption at various operating conditions. The profiles are plotted in Figures 5.4 to 5.10.

The plots for absorption were generated at 313 K with initially CO₂-free (unloaded) pure water and aqueous AMP solutions and the plots for desorption were generated at 383 K with partially loaded aqueous AMP solutions. These results were generated using the kinetic parameters obtained in this work as discussed later in this chapter. Other model parameters were calculated using the correlations given in Appendices E to H. The CO₂-AMP-H₂O is chosen just as an example. Similar results were obtained for other amines.

Figures 5.4 and 5.5 show the predicted concentration profiles at $\theta = 30^\circ$, 60° and 90° from the pole. As expected, for both absorption and desorption, the CO₂ profiles flatten with increasing distance from the pole. This is because the concentration driving force decreases from the pole to the equator.

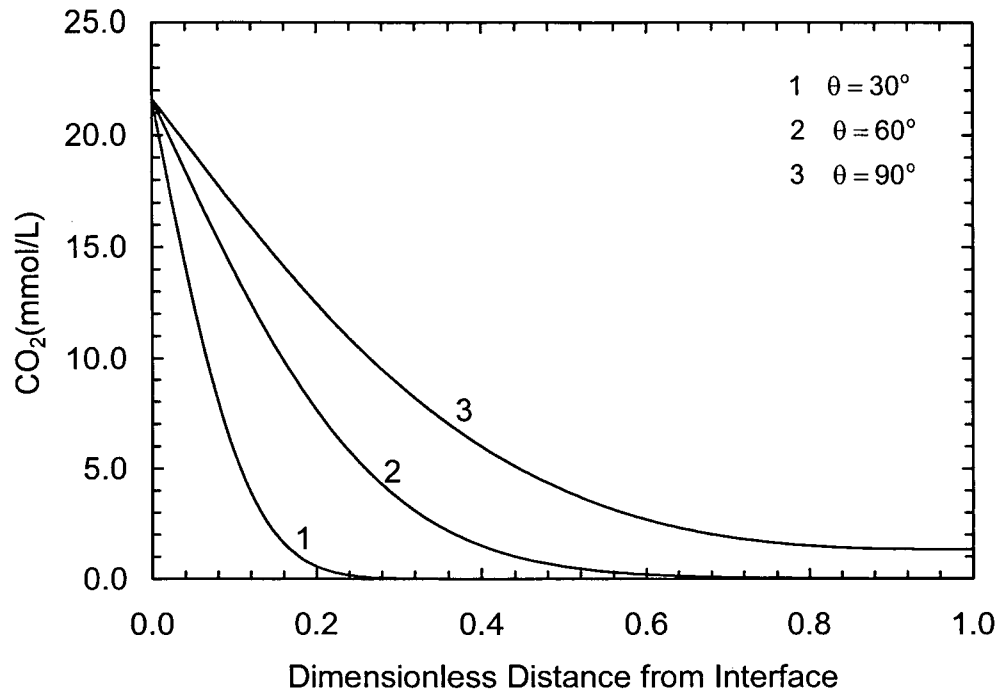


Figure 5.4: Predicted CO_2 profiles at different latitudes for CO_2 absorption in pure water ($T = 313 \text{ K}$, $Q_L = 2.0 \text{ mL/s}$, $p_{\text{CO}_2} = 92.7 \text{ kPa}$)

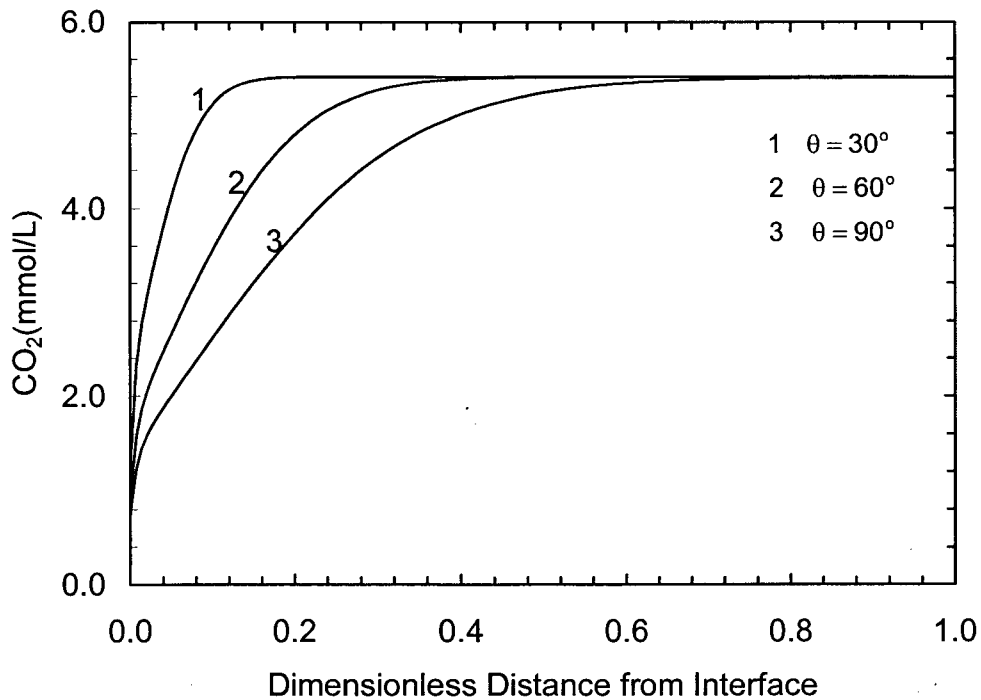


Figure 5.5: Predicted CO_2 profiles at different latitudes for CO_2 desorption from aqueous AMP solution ($T = 383 \text{ K}$, $Q_L = 2.0 \text{ mL/s}$, $C_{\text{AMP}} = 2.11 \text{ kmol/m}^3$, $P_{\text{total}} = 220 \text{ kPa}$, $\alpha = 0.2 \text{ mole of CO}_2/\text{mole of amine}$)

Figure 5.6 shows the effect of amine concentration on the CO_2 profile in the film under absorption conditions. Here again the results are as expected. When the AMP concentration is high, more CO_2 in the solution reacts with the amine and very little or no dissolved CO_2 is left in the solution thereby creating a higher driving force for mass transfer.

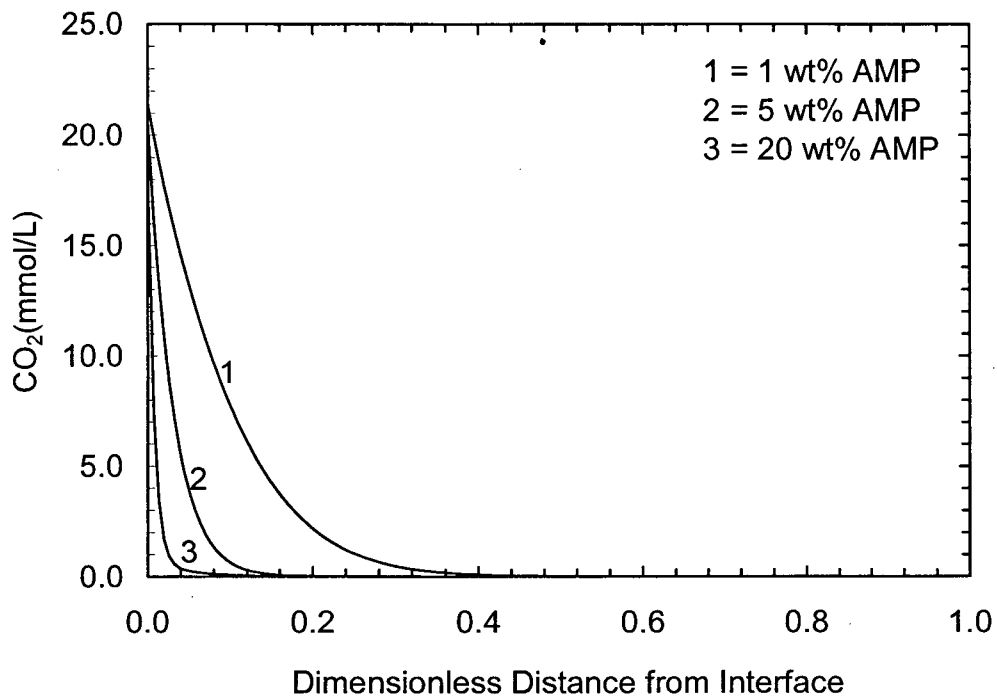


Figure 5.6: Effect of amine concentration on CO_2 profile at $\theta = 90^\circ$ for CO_2 absorption in aqueous AMP solution ($T = 313 \text{ K}$, $Q_L = 2.0 \text{ mL/s}$, $p_{\text{CO}_2} = 92.7 \text{ kPa}$)

Figures 5.7 to 5.10 show the predicted concentration profiles of all chemical species (ionic and non-ionic) that may be present when CO_2 is absorbed or desorbed in or from aqueous AMP solutions. Figures 5.7 and 5.9 are the profiles for absorption and desorption, respectively, at 45° from the pole and

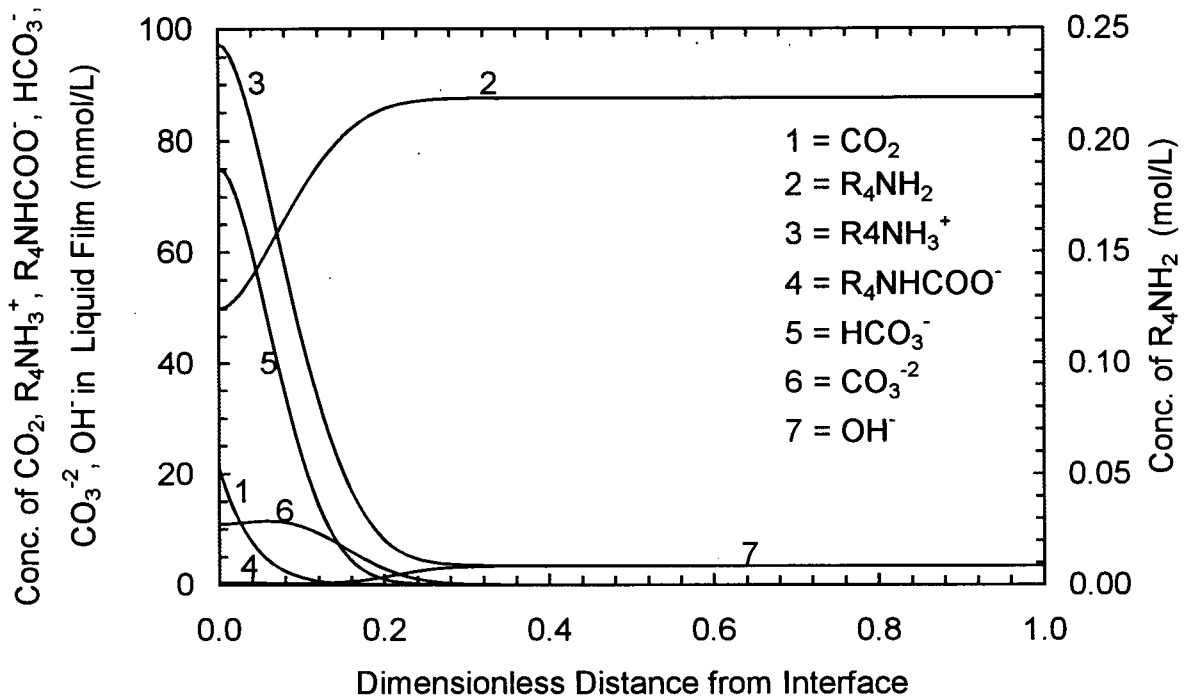


Figure 5.7: Predicted concentration profiles for CO_2 absorption in aqueous AMP solution at $\theta = 45^\circ$ ($T = 313 \text{ K}$, $Q_L = 2.0 \text{ mL/s}$, $C_{\text{AMP}} = 0.223 \text{ kmol/m}^3$, $p_{\text{CO}_2} = 92.7 \text{ kPa}$)

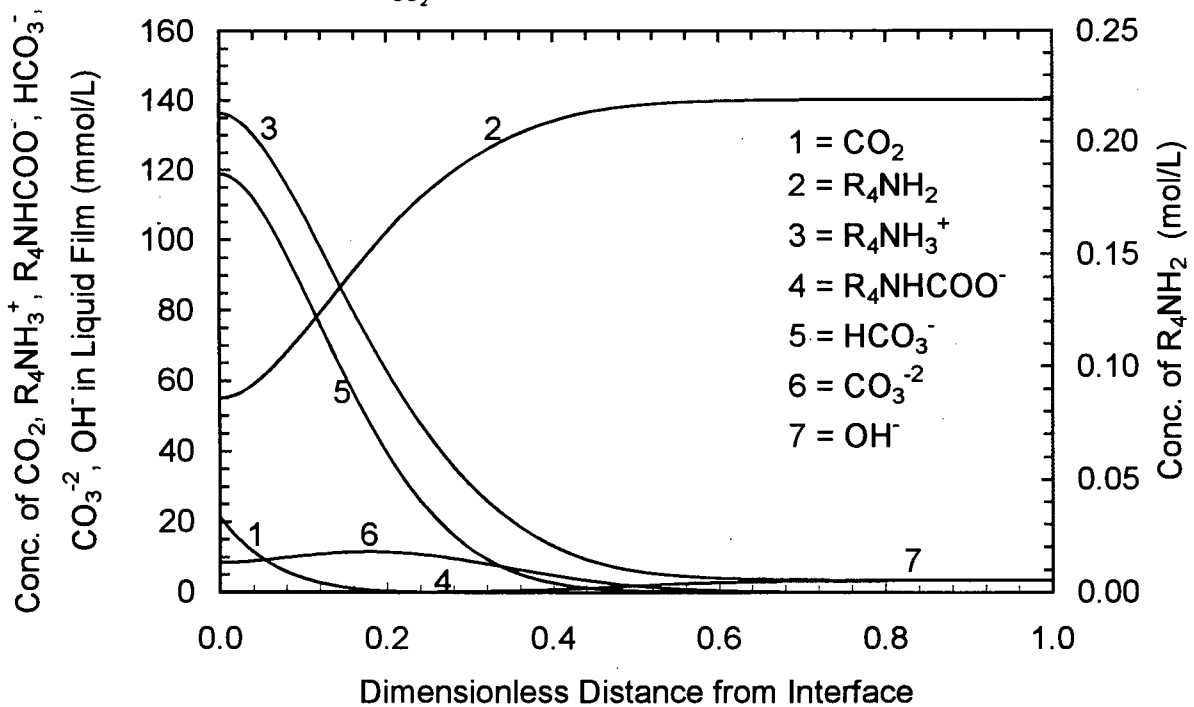


Figure 5.8: Predicted concentration profiles for CO_2 absorption in aqueous AMP solution at $\theta = 90^\circ$ ($T = 313 \text{ K}$, $Q_L = 2.0 \text{ mL/s}$, $C_{\text{AMP}} = 0.223 \text{ kmol/m}^3$, $p_{\text{CO}_2} = 92.7 \text{ kPa}$)

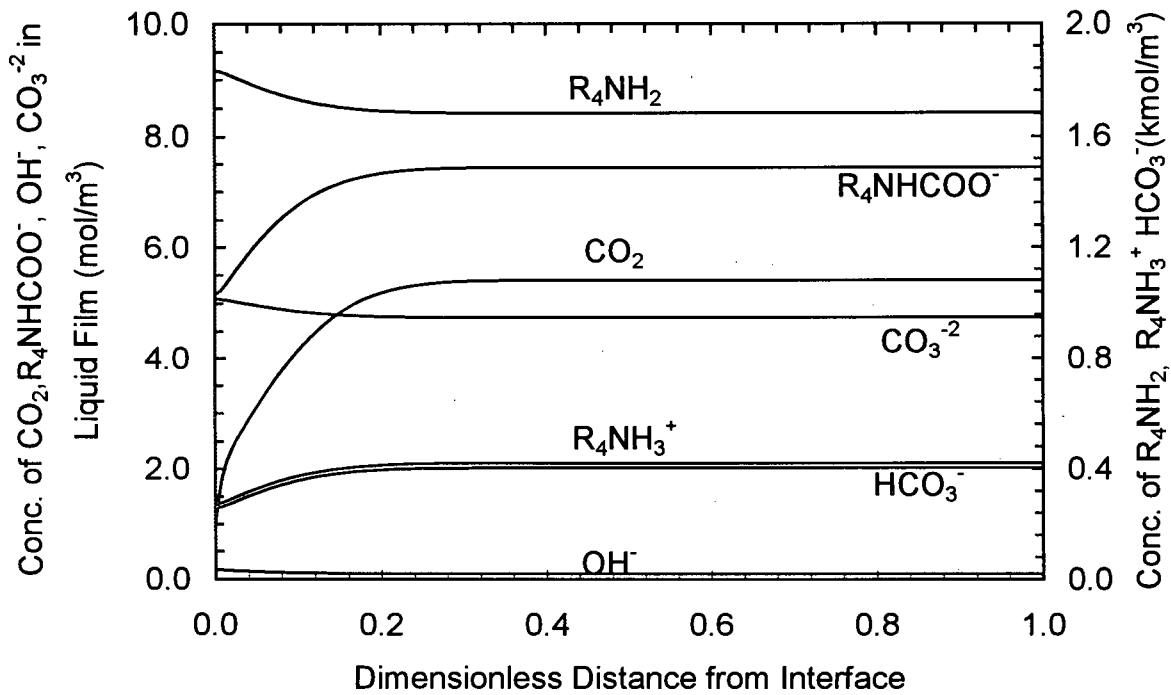


Figure 5.9: Predicted concentration profiles for CO_2 desorption in aqueous AMP solution at $\theta = 45^\circ$ ($T = 383 \text{ K}$, $Q_L = 2.0 \text{ mL/s}$, $C_{\text{AMP}} = 2.11 \text{ kmol/m}^3$, $P_{\text{total}} = 220 \text{ kPa}$, $\alpha = 0.2 \text{ mole of } \text{CO}_2/\text{mole of amine}$)

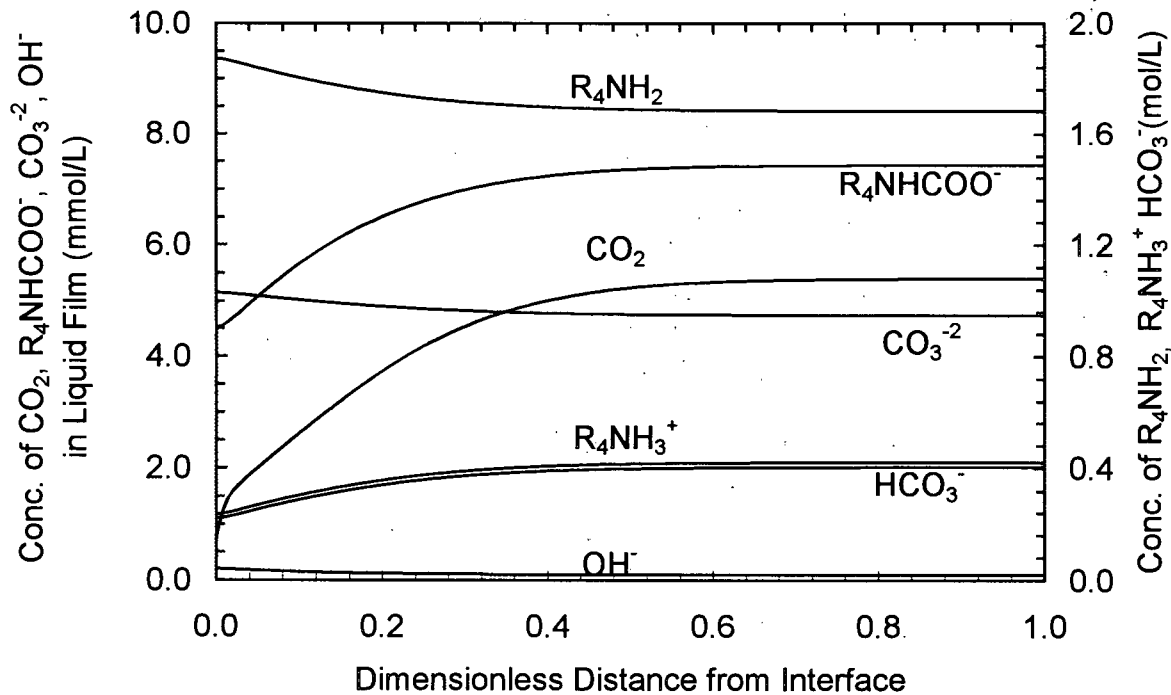


Figure 5.10: Predicted concentration profiles for CO_2 desorption in aqueous AMP solution at $\theta = 90^\circ$ ($T = 383 \text{ K}$, $Q_L = 2.0 \text{ mL/s}$, $C_{\text{AMP}} = 2.11 \text{ kmol/m}^3$, $P_{\text{total}} = 220 \text{ kPa}$, $\alpha = 0.2 \text{ mole of } \text{CO}_2/\text{mole of amine}$)

Figures 5.8 and 5.10 are the corresponding profiles at 90° from the pole. It can be seen from these figures that the concentrations of various species in the film vary both in the θ and x directions. As expected, for absorption, the concentrations of free amine and hydroxyl ions decreases from the bulk to the gas-liquid interface and from the pole to the equator, whereas the concentrations of protonated amine, carbamate, bicarbonate and carbonate ions at these locations increases with x . For desorption, exactly the opposite occurs. This is because during absorption the amine and hydroxyl ions are consumed and the other species (i.e., protonated amine, carbamate, bicarbonate and carbonate ions) are formed, whereas, during desorption, amine is regenerated and the concentrations of the other species are depleted.

5.1.3 Numerical versus Analytical Solutions

The general model (equations 4.64 to 4.97) cannot be solved analytically. However, when there is no reaction between the absorbing gas and liquid, the general model reduces to a case of physical absorption or desorption (e.g., CO_2 or N_2O in pure water). This situation is governed by a single partial differential equation, which using certain critical assumption can be solved analytically and an explicit expression for mass transfer rate can be derived (see Appendix C).

Figure 5.11 shows a comparison of the CO_2 absorption rates predicted from the analytical and numerical solutions of the model equations. The analytical result was calculated from equation (4.98) and the numerical solution was calculated from the general model by setting all the rate constants equal to

zero. Clearly, the agreement between the numerical and analytical solution is very good. The relative error is between -0.4 to +4.4 percent. Slight discrepancy may be due to analytical solution assumption that penetration depth is much smaller compared to the thickness of the liquid film.

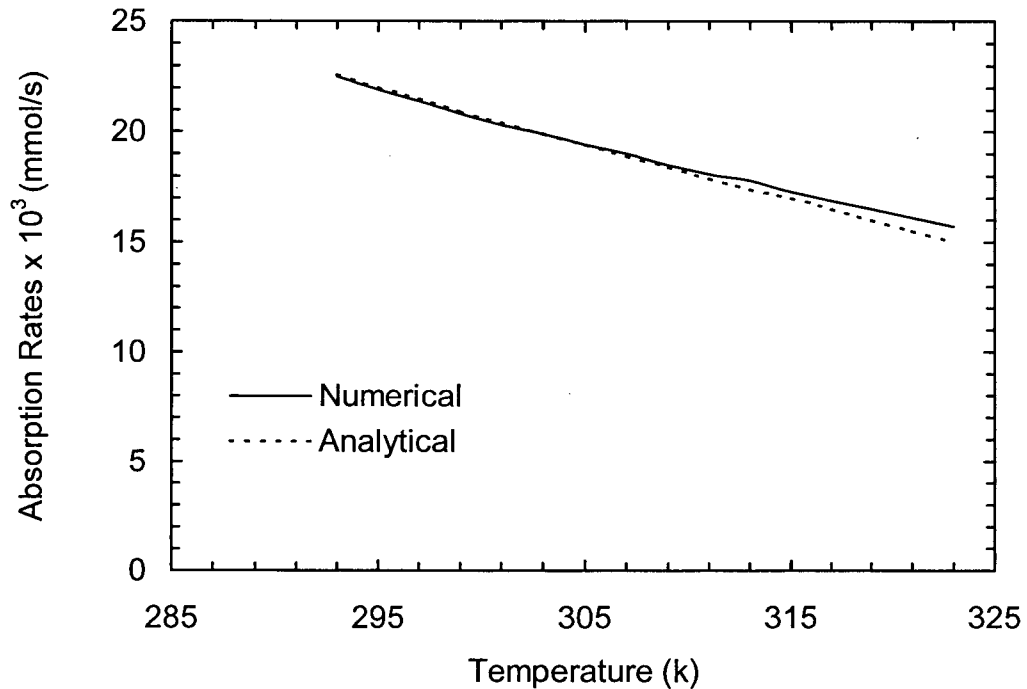


Figure 5.11: Absorption rates of CO_2 in pure water predicted from analytical and numerical solutions ($Q_L = 2.0 \text{ mL/s}$, $p_{\text{CO}_2} = 87\text{-}97 \text{ kPa}$)

The analysis presented above verifies that the present model accurately describes the absorption and desorption of a gas in and from the hemispherical film. It further confirms that the experimental technique and the numerical scheme used to solve the model equations are accurate and reliable.

5.2 Parametric Sensitivity Analysis

The present model consists of three types of parameters: (a) the operating parameters such as amine concentration, temperature, total pressure, CO₂ partial pressure, CO₂ loading and liquid and gas flow rates, (b) physical property parameters such as density, viscosity, gas-side mass transfer coefficient, liquid phase diffusivities and Henry's constants and (c) kinetic parameters such as rate constants and equilibrium constants. In this section we examine the effect of these parameters on the rate of absorption and desorption of CO₂ into and out of aqueous amine solutions.

5.2.1 Effect of Operating Parameters

In order to study the effect of operating parameters on CO₂ absorption and desorption rates, a series of simulation runs were carried out with CO₂-AMP as the example system. The simulation results are plotted in Figures 5.12 to 5.17. These results were obtained for the base case conditions listed in Table 5.1. To demonstrate the effect of each operating variable separately, only one of the operating parameters in Table 5.1 was varied while the others were fixed at their base value. The physical properties and the equilibrium constants were calculated from the correlations given in Appendices E to I and the rate constants were calculated from the correlations developed in this work.

Table 5.1: Base case operating conditions for parametric sensitivity analysis

Parameter	Value	
	Absorption	Desorption
T (K)	303	373
P ^{total} (kPa)	101.3	202.6
p _{CO₂} (kPa)	97.0	1.5
C _{AM} (wt%)	20.0	20.0
α _{initial} (mole/mole)	0.0	0.2
Q _L (mL/s)	2.0	2.0

The results presented in Figures 5.12 to 5.17 are plausible and self-explanatory with the exception of the effect of amine concentration given in Figure 5.12. This figure shows that both the absorption and desorption rates increase with increase in amine concentration. However, it should be noted that this increase in desorption rate is not because of the increase in amine concentration itself but because of the increase in total CO₂ present in the solution. As this plot was generated at a fixed CO₂ loading, which in our case is defined as moles of CO₂ (in all its forms) per mole of amine. Figure 5.12 also shows that the rate of increase in the absorption rate diminishes when the amine concentration exceeds 30-wt%. This is likely, because at higher amine concentrations, the kinetic effects are offset by the reduced water content, higher solution viscosity and lower physical solubility of CO₂ in the solution.

The results presented in Figures 5.12 to 5.17 clearly demonstrate that the absorption rate is most sensitive to changes in amine concentration, CO₂ partial pressure and temperature and the desorption rate is most sensitive to

temperature, CO₂ loading and CO₂ partial pressure in the stripping gas. Similar trends were observed for other systems studied in this work and for the sake of brevity those results are not included here. As will be discussed later in this chapter, the same trends were observed experimentally. Based on these observations, it was decided to conduct absorption experiments by varying mainly the amine concentration and temperature, and desorption experiments by varying the CO₂ loading and temperature.

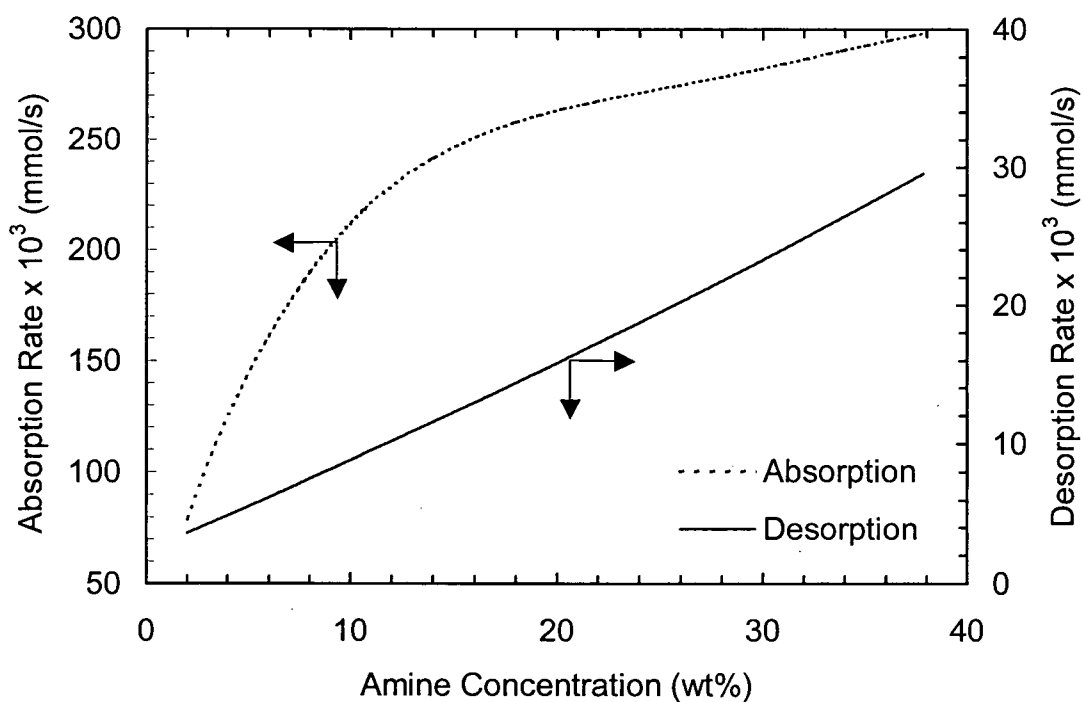


Figure 5.12: Effect of amine concentration on CO₂ absorption and desorption rates in aqueous AMP system

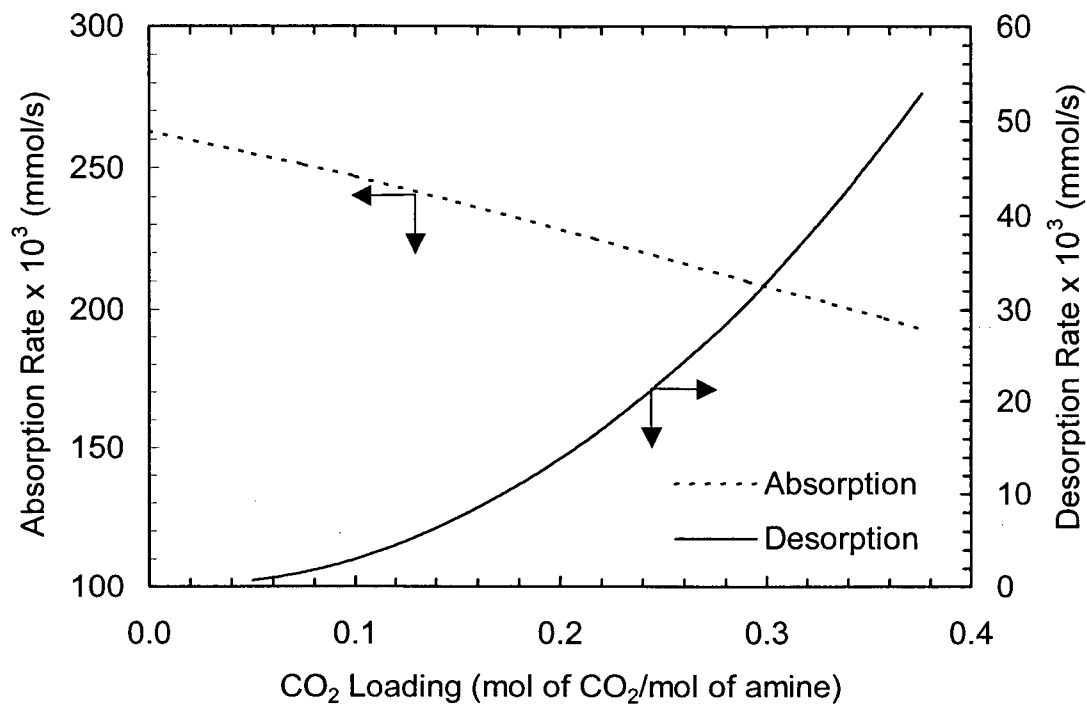


Figure 5.13: Effect of CO₂ loading on CO₂ absorption and desorption rates in aqueous AMP system

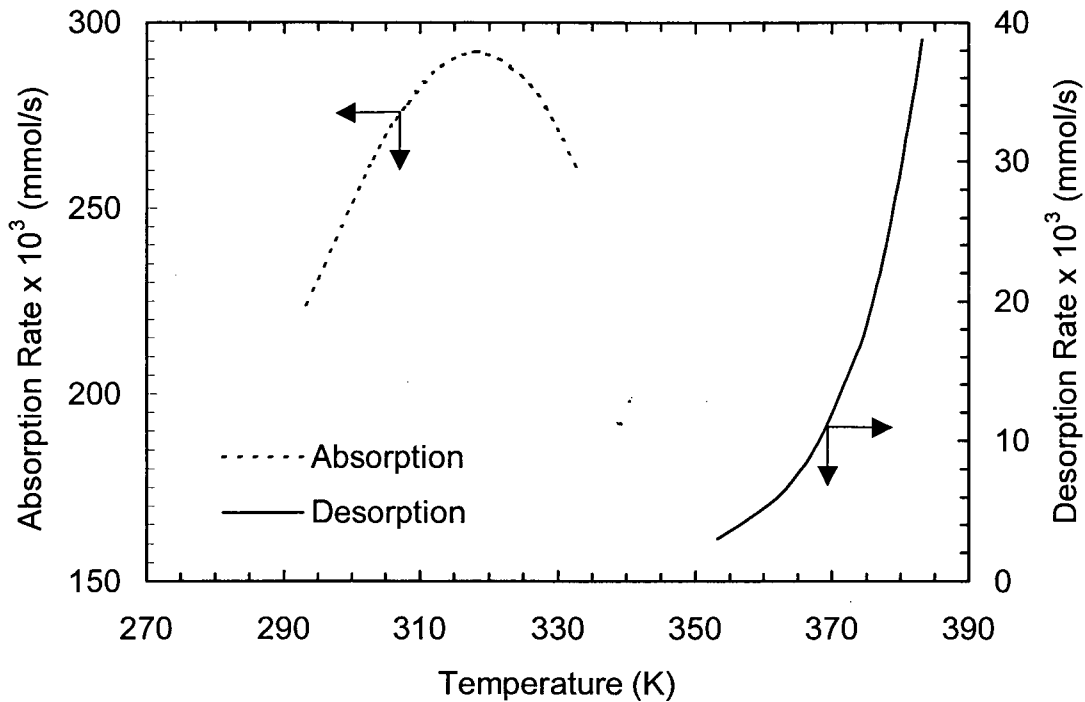


Figure 5.14: Effect of temperature on CO₂ absorption and desorption rates in aqueous AMP system

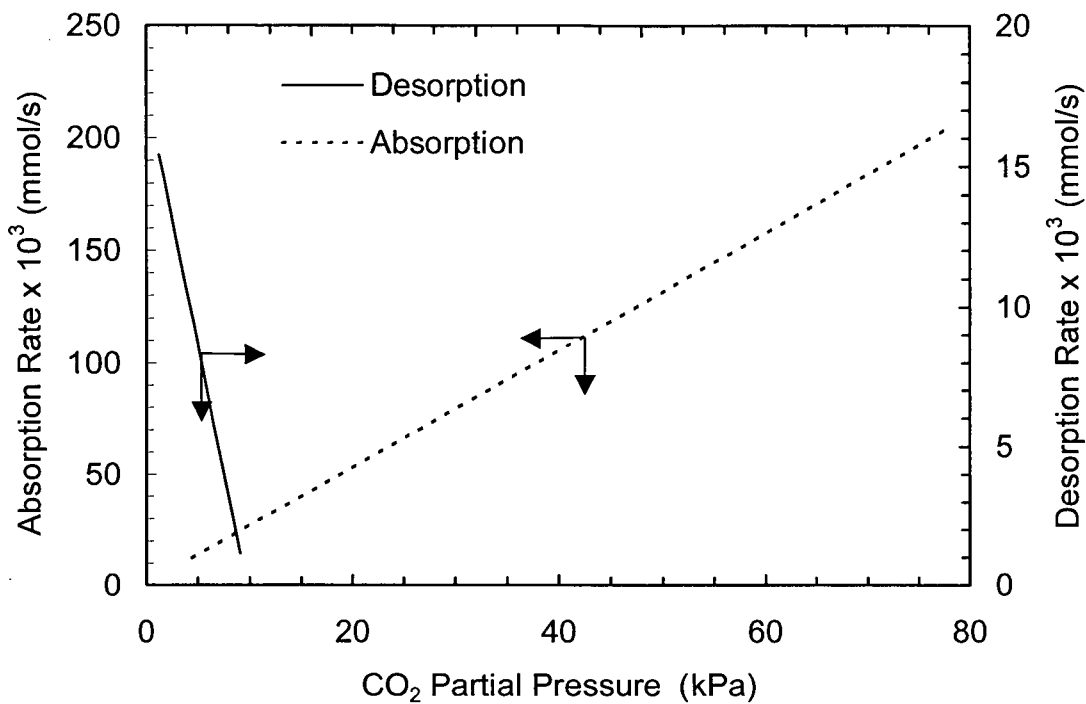


Figure 5.15: Effect of CO₂ partial pressure on CO₂ absorption and desorption rates in aqueous AMP system

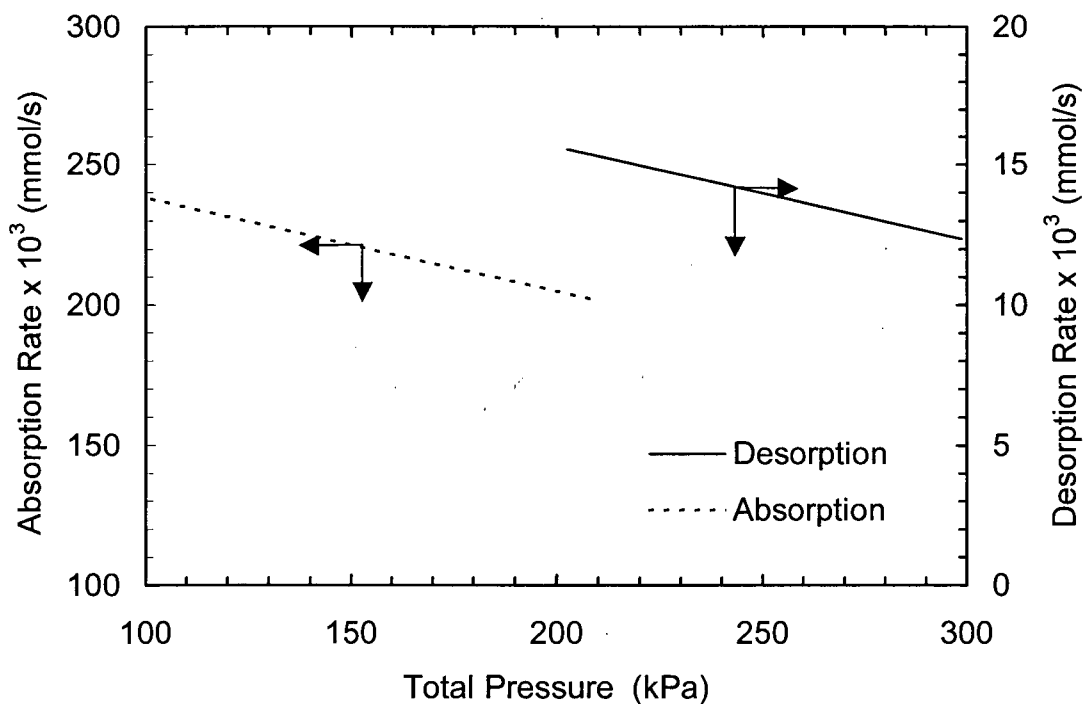


Figure 5.16: Effect of total pressure on CO₂ absorption and desorption rates in aqueous AMP system

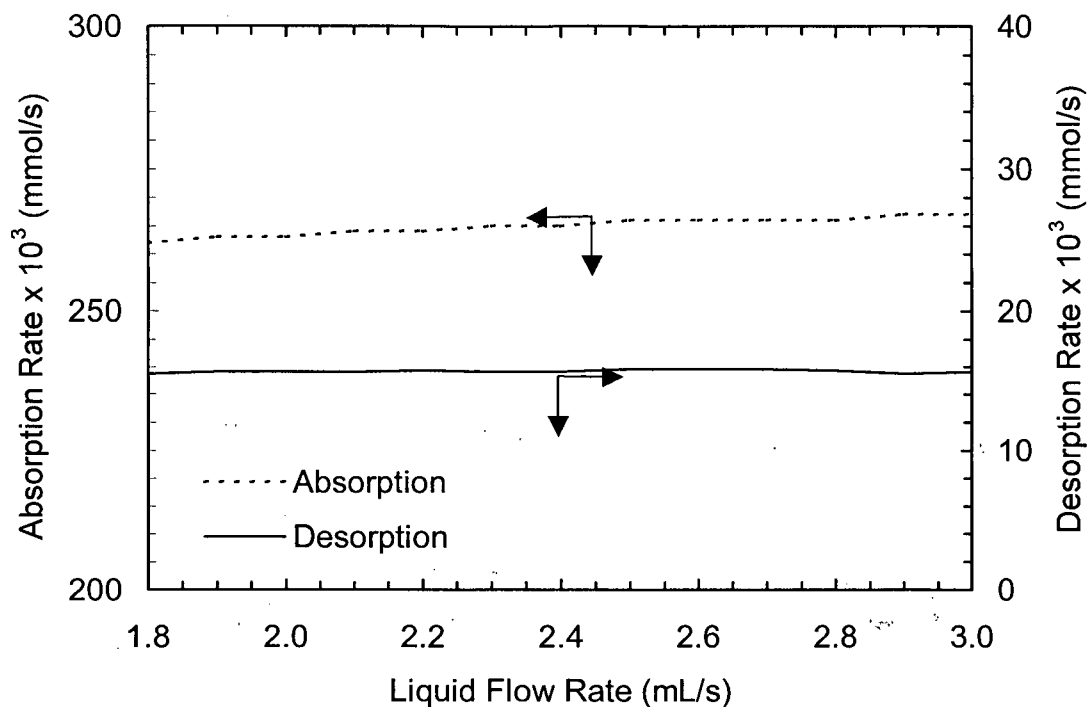


Figure 5.17: Effect of liquid flow rate on CO₂ absorption and desorption rates in aqueous AMP system

5.2.2 Effect of Physical Property Parameters

Table 5.2 shows the effect of errors in the values of physical property parameters on predicted absorption and desorption rates for MEA, DEA, MDEA and AMP systems. This table was produced by introducing ± 20 or $\pm 50\%$ deviations in the physical properties calculated from the correlations used in this work. For all systems the operating variables were kept the same as given in Table 5.1. The results clearly show that the predicted rates are most sensitive to CO₂ diffusivity in the amine solution, Henry's constant of CO₂ and to a lesser extent density of the solution. The effect of the diffusivities of amines and other ionic species on the absorption/desorption rates is not very significant.

Table 5.2: Effect of deviation in physical property parameters on CO₂ absorption and desorption rates in aqueous systems of MEA, DEA, MDEA and AMP

Param.	Param. Dev. (%)	Deviation in Calculated Rates (%)											
		Absorption					Desorption						
		MEA	DEA	MDEA	AMP	MEA	DEA	MDEA	AMP	MEA	DEA	MDEA	AMP
ρ_L	± 20	+11 to -12	+8 to -10	+3 to -5	+5 to -7	+9 to -14	+16 to -14	+19 to -21	+16 to -16	+9 to -14	+16 to -14	+19 to -21	+16 to -16
μ_L	± 20	-5 to +7	-4 to +6	-0.4 to +0.6	-2 to +3	-1 to +1	-1 to +2	-3 to +3	-1 to +1	-1 to +1	-1 to +2	-3 to +3	-1 to +1
D_{CO_2}	± 50	+10 to -21	+13 to -22	+23 to -30	+20 to -29	+14 to -22	+18 to -26	+16 to -23	+18 to -25	+14 to -22	+18 to -26	+16 to -23	+18 to -25
D_{AM}	± 50	11 to -19	+9 to -15	0.1 to -0.3	+4 to -7	+1 to -2	+2 to -3	+5 to -7	+2 to -2	+1 to -2	+2 to -3	+5 to -7	+2 to -2
$D_3 - D_{17}$	± 50	-0.1 to -0.2	-0.5 to +0.6	-0.1 to 0	0 to +0.2	+1 to -2	+2 to -2	+5 to -7	+2 to -2	+1 to -2	+2 to -2	+5 to -7	+2 to -2
H_{CO_2}	± 50	-18 to +24	-21 to +37	-33 to +97	-29 to +63	+22 to -45	+6 to -14	+4 to -12	+10 to -25	+22 to -45	+6 to -14	+4 to -12	+10 to -25
K_g	± 50	-	-	-	-	+11 to -23	+3 to -7	+2 to -5	+5 to -12	+11 to -23	+3 to -7	+2 to -5	+5 to -12

This table does not show a significant effect of the gas side mass transfer coefficient on the predicted desorption rates. This is because, in the case examined here, the CO₂ partial pressure in the stripping gas was less than 1 mol%. However, it can easily be shown that under certain operating conditions this effect may also become significant. As is discussed later in this chapter, in all our desorption experiments, we kept the CO₂ partial pressure in the stripping gas well below 5 mol%.

From the above analysis we find that, in order to predict absorption and desorption rates accurately, it is important that the values of the CO₂ diffusivities and Henry's constants in amine solutions are known fairly accurately. For this reason we developed new correlations for these parameters that are applicable for both single and blended amine systems and cover wider temperature ranges than the available literature data. These correlations are presented in Section 5.3 (see also Appendices F and G).

5.2.3 Effect of Kinetic Parameters

Table 5.3 lists all possible reactions with their associated kinetic parameters for the eight systems considered in this work. Most of these parameters are important to calculate absorption and desorption rates using our model. However, from our sensitivity analysis, we observed that, for carbamate-forming amines such as MEA, DEA and AMP, the contribution of reactions involving the deprotonation of amine-zwitterion to water and hydroxyl ions

Table 5.3: Kinetic parameters for CO₂-aqueous amine systems studied in this work

Systems	r_{total}	Reactions	Kinetic Parameters		
			Individual rate const.	Combined rate const.	Equilibrium const. (Individual & combined)
CO ₂ +MEA+H ₂ O	$r_7 + r_{10-13}$	(4.7) to (4.15)	k ₇ , k ₁₀	k ₁₁ /k ₋₁₀ , k ₁₂ /k ₋₁₀ , k ₁₃ /k ₋₁₀	K ₇ , K ₈ , K ₉ , K ₁₄ , K ₁₅ , K ₁₀ K ₁₁ , K ₁₀ K ₁₂ , K ₁₀ K ₁₃
CO ₂ +DEA+H ₂ O	$r_7 + r_{16-19}$	(4.7) to (4.9) & (4.16) to (4.21)	k ₇ , k ₁₆	k ₁₇ /k ₋₁₆ , k ₁₈ /k ₋₁₆ , k ₁₉ /k ₋₁₆	K ₇ , K ₈ , K ₉ , K ₂₀ , K ₂₁ , K ₁₆ K ₁₇ , K ₁₆ K ₁₈ , K ₁₆ K ₁₉
CO ₂ +MDEA+H ₂ O	$r_7 + r_{22}$	(4.7) to (4.9) & (4.22), (4.23)	k ₇ , k ₂₂ , k ₂₂		K ₇ , K ₈ , K ₉ , K ₂₂ , K ₂₃
CO ₂ +AMP+H ₂ O	$r_7 + r_{1-4}$	(4.1) to (4.9)	k ₇ , k ₁	k ₂ /k ₋₁ , k ₃ /k ₋₁ , k ₄ /k ₋₁	K ₅ , K ₆ , K ₇ , K ₈ , K ₉ , K ₁ K ₂ , K ₁ K ₃ , K ₁ K ₄
CO ₂ +MEA+MDEA+H ₂ O	$r_7 + r_{10-13,24} + r_{22}$	(4.7) to (4.15) & (4.22) to (4.24)	k ₇ , k ₁₀ , k ₂₂ , k ₂₂	k ₁₁ /k ₋₁₀ , k ₁₂ /k ₋₁₀ , k ₁₃ /k ₋₁₀ , k ₂₄ /k ₋₁₀	K ₇ , K ₈ , K ₉ , K ₁₄ , K ₁₅ , K ₁₀ K ₁₁ , K ₁₀ K ₁₂ , K ₁₀ K ₁₃ , K ₁₀ K ₂₄
CO ₂ +MEA+AMP+H ₂ O	$r_7 + r_{10-13,26} + r_{1-4,25}$	(4.1) to (4.15) & (4.25), (4.26)	k ₇ , k ₁ , k ₁₀	k ₂ /k ₋₁ , k ₃ /k ₋₁ , k ₄ /k ₋₁ , k ₂₅ /k ₋₁ , k ₁₁ /k ₋₁₀ , k ₁₂ /k ₋₁₀ , k ₁₃ /k ₋₁₀ , k ₂₆ /k ₋₁₀	K ₅ , K ₆ , K ₇ , K ₈ , K ₉ , K ₁₄ , K ₁₅ , K ₁ K ₂ , K ₁ K ₃ , K ₁ K ₄ , K ₁ K ₂₅ , K ₁₀ K ₁₁ , K ₁₀ K ₁₂ , K ₁₀ K ₁₃ , K ₁₀ K ₂₆
CO ₂ +DEA+MDEA+H ₂ O	$r_7 + r_{16-19,27} + r_{22}$	(4.7) to (4.9) & (4.16) to (4.24) & (4.27)	k ₇ , k ₁₆ , k ₂₂ , k ₂₂	k ₁₇ /k ₋₁₆ , k ₁₈ /k ₋₁₆ , k ₁₉ /k ₋₁₆ , k ₂₇ /k ₋₁₆	K ₇ , K ₈ , K ₉ , K ₂₀ , K ₂₁ , K ₁₆ K ₁₇ , K ₁₆ K ₁₈ , K ₁₆ K ₁₉ , K ₁₆ K ₂₇
CO ₂ +DEA+AMP+H ₂ O	$r_7 + r_{16-19,29} + r_{1-4,28}$	(4.1) to (4.9) & (4.16), (4.21) & (4.28), (4.29)	k ₇ , k ₁ , k ₁₆	k ₂ /k ₋₁ , k ₃ /k ₋₁ , k ₄ /k ₋₁ , k ₂₈ /k ₋₁ , k ₁₇ /k ₋₁₆ , k ₁₈ /k ₋₁₆ , k ₁₉ /k ₋₁₆ , k ₂₉ /k ₋₁₆	K ₅ , K ₆ , K ₇ , K ₈ , K ₉ , K ₂₀ , K ₂₁ , K ₁ K ₂ , K ₁ K ₃ , K ₁ K ₄ , K ₁ K ₂₈ , K ₁₆ K ₁₇ , K ₁₆ K ₁₈ , K ₁₆ K ₁₉ , K ₁₆ K ₂₉

(reactions 4.3 and 4.4 for AMP, 4.12 and 4.13 for MEA and 4.18 and 4.19 for DEA) to absorption and desorption rates is insignificant. As shown in Table 5.4, a change of four orders of magnitudes in the values of the rate constants associated with these reactions produce no significant change in the predicted rate of absorption. Therefore, these reactions can be ignored without significant loss of accuracy. Similar conclusions were arrived at previously by Rinker et al. (1996) in their work on the kinetics of CO₂ absorption in aqueous DEA solutions. This simplification greatly reduces the complexity of the kinetic rate expressions and cuts down the time required for parameter estimation by one third as the number of unknown parameters in each expression reduces from 5 to 3. With the present model, parameter estimation with 5 unknowns is extremely time consuming. It takes about 15 to 20 hours to obtain the estimates for a single data set even with the fastest PC (Pentium 4, 1700 Mhz, 256 RAM) available to us. This is because each function call to solve the model equations takes about 2 to 3 minutes and a typical parameter estimation run makes hundreds of such function calls. After this simplification is implemented, the reactions and kinetic parameters that remain are summarized in Table 5.5.

Table 5.4: Effect of reactions involving zwitterion deprotonation to water and hydroxyl ions on the rate of absorption (see reactions 4.3, 4.4, 4.12, 4.13, 4.18, 4.19)

Parameters Value	Calculated Absorption Rates x 10 ³ (mmol/s)		
	MEA k ₁₂ /k ₋₁₀ & k ₁₂ /k ₋₁₀	DEA k ₁₈ /k ₋₁₆ & k ₁₉ /k ₋₁₆	AMP k ₃ /k ₋₁ & k ₄ /k ₋₁
0-0	525.99	309.02	263.37
1-1	555.19	309.09	274.76
10-10	556.88	309.31	276.40
100-100	557.06	309.44	276.58
1000-1000	557.08	309.46	276.59

Table 5.5: Kinetic parameters for CO₂-aqueous amine systems studied in this work (excluding reactions for zwitterion deprotonation to water and hydroxyl ions)

Systems	r_{total}	Reactions	Kinetic Parameters		
			Individual rate const.	Combined rate const.	Equilibrium const. (Individual & combined)
CO ₂ +MEA+H ₂ O	$r_7 + r_{10-11}$	(4.7) to (4.11), (4.14), (4.15)	k_7, k_{10}	k_{11}/k_{-10}	$K_7, K_8, K_9, K_{14}, K_{15}, K_{10}K_{11}$
CO ₂ +DEA+H ₂ O	$r_7 + r_{16-17}$	(4.7) to (4.9), (4.16), (4.17), (4.20), (4.21)	k_7, k_{16}	k_{17}/k_{-16}	$K_7, K_8, K_9, K_{20}, K_{21}, K_{16}K_{17}$
CO ₂ +MDEA+H ₂ O	$r_7 + r_{22}$	(4.7) to (4.9), (4.22), (4.23)	k_7, k_{22}, k_{-22}		$K_7, K_8, K_9, K_{22}, K_{23}$
CO ₂ +AMP+H ₂ O	$r_7 + r_{1-2}$	(4.1), (4.2) & (4.5) to (4.9)	k_7, k_1	k_2/k_{-1}	$K_5, K_6, K_7, K_8, K_9, K_1K_2$
CO ₂ +MEA+MDEA+H ₂ O	$r_7 + r_{10-11,24} + r_{22}$	(4.7) to (4.11), (4.14), (4.15) & (4.22) to (4.24)	$k_7, k_{10}, k_{22}, k_{-22}$	$k_{11}/k_{-10}, k_{24}/k_{-10}$	$K_7, K_8, K_9, K_{14}, K_{15}, K_{10}K_{11}, K_{10}K_{24}$
CO ₂ +MEA+AMP+H ₂ O	$r_7 + r_{10-11,26} + r_{1-2,25}$	(4.1), (4.2), (4.5) to (4.11), (4.14), (4.15), (4.25), (4.26)	k_7, k_1, k_{10}	$k_2/k_{-1}, k_{25}/k_{-1}, k_{11}/k_{-10}, k_{26}/k_{-10}$	$K_5, K_6, K_7, K_8, K_9, K_{14}, K_{15}, K_1K_2, K_1K_{25}, K_{10}K_{11}, K_{10}K_{26}$
CO ₂ +DEA+MDEA+H ₂ O	$r_7 + r_{16-17,27} + r_{22}$	(4.7) to (4.9), (4.16), (4.17), (4.20), (4.21), (4.24) & (4.27)	$k_7, k_{16}, k_{22}, k_{-22}$	$k_{17}/k_{-16}, k_{27}/k_{-16}, k_{16}K_{27}$	$K_7, K_8, K_9, K_{20}, K_{21}, K_{16}K_{17}, K_{16}K_{27}$
CO ₂ +DEA+AMP+H ₂ O	$r_7 + r_{16-17,29} + r_{1-2,28}$	(4.1), (4.2), (4.5) to (4.9), (4.16), (4.17), (4.20), (4.21), (4.28), (4.29)	k_7, k_1, k_{16}	$k_2/k_{-1}, k_{28}/k_{-1}, k_{17}/k_{-16}, k_{29}/k_{-16}, k_{16}K_{29}$	$K_5, K_6, K_7, K_8, K_9, K_{20}, K_{21}, K_1K_2, K_1K_{28}, K_{16}K_{17}, K_{16}K_{29}$

5.3 Henry's Constant and CO₂ Diffusivity in Amine Solutions

With the help of Table 5.2, it was shown earlier that, in order to predict absorption and desorption rates accurately, fairly accurate values of CO₂ diffusivities and Henry's constants in amine solutions are required. In this section we examine existing literature data for these properties and present new data and new correlations that are applicable for both single and mixed amine systems and cover wider temperature ranges.

5.3.1 Correlations for Henry's Constants of CO₂ in Amine Solutions

Since CO₂ reacts with aqueous amine solutions, it is not possible to determine its physical solubility in these solutions by direct measurements and an indirect method based on the N₂O analogy is commonly used. According to this method, the ratio of the Henry's constants of CO₂ and N₂O in an aqueous amine solution is the same as that in water at the same temperature:

$$\frac{H_{\text{CO}_2}}{H_{\text{N}_2\text{O}}} = \frac{H_{\text{CO}_2}^{\circ}}{H_{\text{N}_2\text{O}}^{\circ}} \quad (5.1)$$

where H_{CO_2} and $H_{\text{N}_2\text{O}}$ denote the Henry's constants of CO₂ and N₂O in the aqueous amine solution, and $H_{\text{CO}_2}^{\circ}$ and $H_{\text{N}_2\text{O}}^{\circ}$ denote the Henry's constants of CO₂ and N₂O in water.

A large amount of data is available in the literature for the Henry's constant of CO₂ in water and N₂O in water and various amine solutions as a function of temperature. These data are summarized in Tables F.1 to F.10. It can be seen from these tables that most of the existing data are in the low

temperature range (293-323 K) typical of an absorber, and the data at stripper operating temperatures (373-393 K) simply do not exist.

In this work new data for the Henry's constant of CO₂ in water and N₂O in water and N₂O in aqueous amine solutions were obtained. These results are also listed in Tables F.1 to F.10. The details of the experimental apparatus and procedure are given in Appendix F.

The data for $H_{\text{CO}_2}^{\circ}$, $H_{\text{N}_2\text{O}}^{\circ}$ and $H_{\text{N}_2\text{O}}$ (from this work and from the literature) were correlated as a function of temperature. These correlations are given in Appendix F (see equations F.2 to F.4). The correlations represent the experimental data well. The absolute average percent deviation was within 7% (see Figures F.1 to F.4).

5.3.2 Correlations for CO₂ Diffusivities in Amine Solutions

Like Henry's constant, the diffusivity of CO₂ in amine solutions cannot be determined directly and an indirect method based on the N₂O analogy was used again. According to this method, the ratio of the diffusivities of CO₂ and N₂O in an aqueous amine solution is the same as that in water at the same temperature:

$$\frac{D_{\text{CO}_2}}{D_{\text{N}_2\text{O}}} = \frac{D_{\text{CO}_2}^{\circ}}{D_{\text{N}_2\text{O}}^{\circ}} \quad (5.2)$$

where D_{CO_2} and $D_{\text{N}_2\text{O}}$ denote the diffusivities of CO₂ and N₂O in the amine solution, and $D_{\text{CO}_2}^{\circ}$ and $D_{\text{N}_2\text{O}}^{\circ}$ denote the diffusivities of CO₂ and N₂O in water.

As shown in Appendix G, good quality data are available in the literature for $D_{\text{CO}_2}^{\circ}$, $D_{\text{N}_2\text{O}}^{\circ}$ and $D_{\text{N}_2\text{O}}$. Some correlations for these data as a function of

temperature and amine concentration also exist in the literature. However, most of these correlations, specifically for D_{N_2O} , are based on the data collected by individual authors valid only for narrow concentration and temperature ranges. Furthermore, in most of the published literature on CO₂-amine kinetics, D_{N_2O} at various temperatures and amine concentrations is calculated using the following modified Stokes-Einstein relation:

$$D_{N_2O}\mu_{sol}^{0.8} = D_{N_2O}^o\mu_{H_2O}^{0.8} \quad (5.3)$$

In order to check the validity of equation (5.3), we compiled all the available diffusivity data for pure water, and single and mixed amine systems from various sources (see Tables G.1 to G.10) and prepared Stokes-Einstein plots as shown in Figures G.3 and G.4. The data from our own diffusivity measurements using the hemispherical contactor were also included in these plots. It can be seen from these plots that the Stokes-Einstein type relationship does not represent the experimental data well. The average deviation (AAD%) for single amine systems is about 20% and that for mixed amine systems is about 30%. Therefore, in this work, new correlations were developed which are valid over a wider range of temperatures and amine concentrations. These correlations are discussed in detail in Appendix G (see equations G.5 and G.6).

Figures G.5 and G.6 show a comparison of the measured and calculated diffusion coefficients using new correlations. In general, the agreement is very good. The overall AAD% for single amine systems is about 13% and that for mixed amine systems is about 9%. In light of the fact that different sources have used different absorption apparatus to measure diffusivities, this much deviation

is expected and the correlations can be safely used. Note that for $C_{AM} = 0$, these correlations (equations G.5 and G.6) reduce to the correlation for N_2O-H_2O system (equations G.3). This unique and very important feature does not exist in other similar correlations proposed in the literature (Li and Lai, 1995; Li and Lee, 1996).

5.4 CO_2 Absorption and Desorption in Aqueous Amine Solutions

This section presents the experimental and theoretical results from the work on CO_2 absorption and desorption in aqueous amine solutions. The experimental data are given in Tables K.11 to K.27 and the experimental conditions for each system studied are summarized in Table 5.6. The bulk of the experiments were focused on desorption because the purpose of these experiments was to estimate kinetic parameters under desorption conditions. The absorption experiments were carried out mainly to verify experimental techniques, as for most amines, good quality absorption data already exist in the literature. The data were analyzed using the diffusion-reaction model presented in Chapter 4.

Based on the sensitivity analysis results presented above, it was assumed that for carbamate-forming amines (i.e., MEA, DEA, AMP), the contribution of reactions involving zwitterion deprotonation to water and hydroxyl ions is negligible. In all cases, the physical properties and equilibrium constants were calculated from correlations given in Appendices E to I. In all cases, the values of

Table 5.6: Experimental conditions for CO₂ absorption/desorption in aqueous amine solutions

Systems	Absorption (P ^{total} ≈ 102 kPa)				Desorption (for T < 353, P ^{total} ≈ 102 kPa for T > 353, P ^{total} ≈ 204 kPa)			
	T (K)	C _{AM} (wt%)	p _{CO₂} (kPa)	α _{initial} (mol/mol)	T (K)	C _{AM} (wt%)	p _{CO₂} (kPa)	α _{initial} (mol/mol)
CO ₂ +MEA+H ₂ O	303	4-31	96-97	0.0	333-378	20	0.5-4.0	0.20-0.49
CO ₂ +DEA+H ₂ O	303-323	3-36	4-97	0.0	343-382	20-25	0.2-5.0	0.04-0.48
CO ₂ +MDEA+H ₂ O	303	4-38	97	0.0	343-353	25	0.6-4.0	0.09-0.30
CO ₂ +AMP+H ₂ O	296-323	2-30	88-97	0.0	333-378	20	0.5-5.0	0.20-0.75
CO ₂ +MEA+MDEA+H ₂ O	303	25	97	0.0	353-373	12.5+12.5	0.6-5.0	0.19-0.34
CO ₂ +MEA+AMP+H ₂ O	303	25	97	0.0	353-373	12.5+12.5	0.7-5.0	0.22-0.36
CO ₂ +DEA+MDEA+H ₂ O	303	25	97	0.0	353-373	12.5+12.5	0.8-4.0	0.15-0.27
CO ₂ +DEA+AMP+H ₂ O	303	25	97	0.0	353-373	12.5+12.5	0.7-4.0	0.17-0.34

the forward rate constant for the CO₂ hydration reaction (k₇) were calculated from the correlation reported by Pinsent et al. (1956) and corrected for ionic strength using an equation developed by Astarita et al. (1983) (see equation H.2).

5.4.1 CO₂ Absorption/Desorption in Aqueous Solutions of MEA, DEA and AMP

The data interpretation for CO₂ absorption and desorption in aqueous solutions of MEA, DEA and AMP is discussed together as each of these amines forms carbamate and their reactions with CO₂ can be discussed based on the zwitterion mechanism. The major difference between AMP and MEA or DEA is that AMP-carbamate is not very stable and quickly hydrolyzes to give bicarbonate and free amine.

The experimental results for the CO₂-MEA system are reported in Tables K.11 and K.20, for the CO₂-DEA system in Tables K.12, K.13 and K.21 and for the CO₂-AMP in Tables K.15 and K.23. The simplified rate expressions for each of these systems are:

CO₂-MEA System:

$$r_{10-11} = \frac{-k_{10}C_1C_{10} + \left(\frac{k_{10}}{K_{10}K_{11}}\right)\frac{C_{11}C_{12}}{C_{10}}}{1 + \left(\frac{k_{-10}}{k_{11}}\right)\frac{1}{C_{10}}} \quad (5.4)$$

CO₂-DEA System:

$$r_{16-17} = \frac{-k_{16}C_1C_{13} + \left(\frac{k_{16}}{K_{16}K_{17}}\right)\frac{C_{14}C_{15}}{C_{13}}}{1 + \left(\frac{k_{-16}}{k_{17}}\right)\frac{1}{C_{13}}} \quad (5.5)$$

CO₂-AMP System:

$$r_{1-2} = \frac{-k_1 C_1 C_2 + \left(\frac{k_1}{K_1 K_2} \right) \frac{C_3 C_4}{C_2}}{1 + \left(\frac{k_{-1}}{k_2} \right) \frac{1}{C_2}} \quad (5.6)$$

Equations (5.4), (5.5) and (5.6) are essentially the same and therefore the procedure for parameter estimation is identical.

5.4.1.1 Predicted Rates using Literature Correlations

In order to see if the kinetic parameters obtained under absorption conditions could be used to predict desorption rates we first used literature correlations for the rate constants involved in equations (5.4) to (5.6). For the combined equilibrium constants (i.e., $K_1 K_2$, $K_{10} K_{11}$ and $K_{16} K_{17}$), the correlations given in Appendix H were used. For AMP, k_1 and k_{-1}/k_2 were calculated from the correlations given by Xu et al. (1996), for DEA, k_{16} and k_{-16}/k_{17} were calculated from the correlations given by Rinker et al. (1996) and for MEA, k_{10} was calculated from correlation of Hikita et al. (1977a) and k_{-10}/k_{11} was set equal to zero because no such correlation is available in the literature.

The results are plotted in Figures 5.18 to 5.26. These plots clearly demonstrate that the predictions based on literature correlations are fairly good for absorption rates (see Figures 5.18 to 5.20), but those for desorption rates are consistently higher than the experimental values by a factor of 2 to 6 (see

Figures 5.21-5.26). This was expected because the literature correlations have been developed based on the absorption data only. Also, desorption rates are very sensitive to the rate constants for the reverse reactions and accurate values of these constants are not available in the literature.

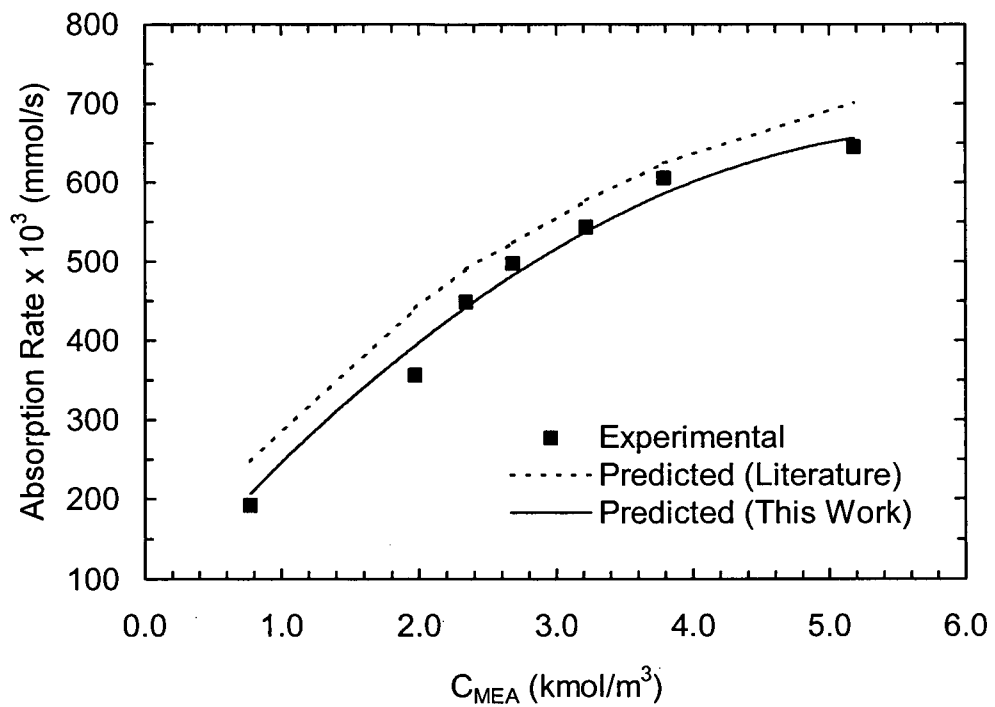


Figure 5.18: Predicted and experimental absorption rates for CO_2 absorption in aqueous MEA solution at 303 K.

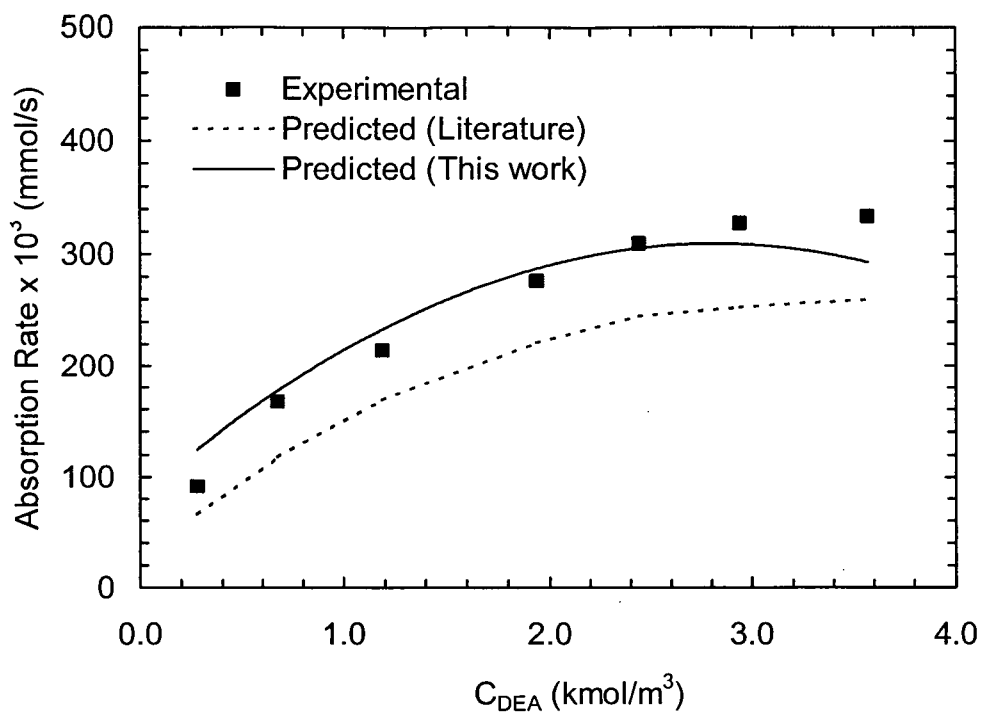


Figure 5.19: Predicted and experimental absorption rates for CO₂ absorption in aqueous DEA solution at 303 K.

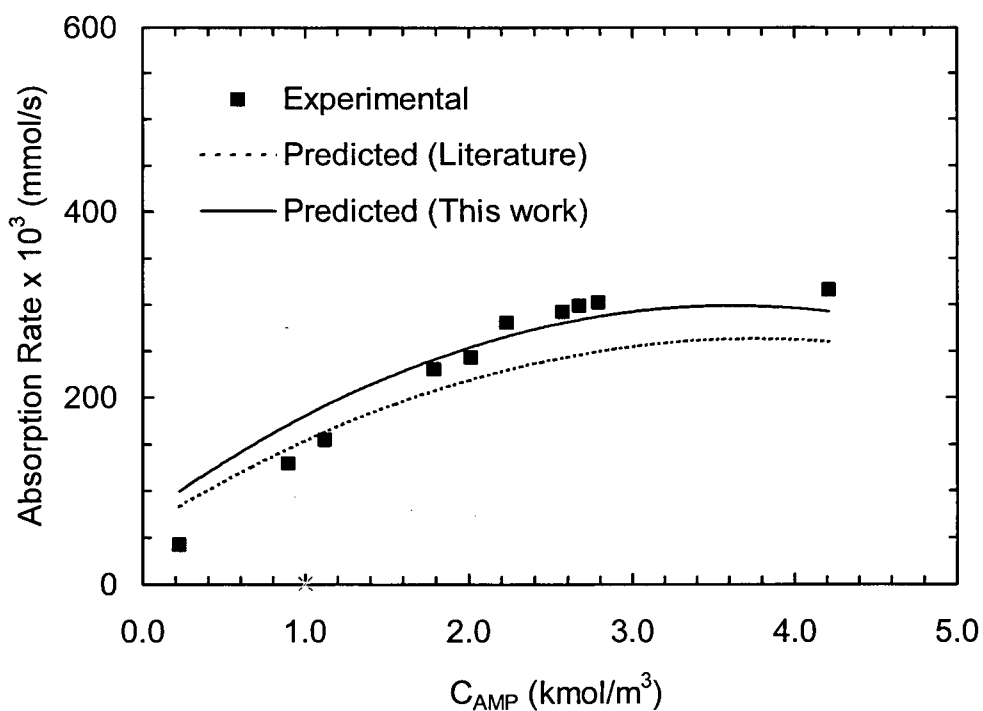


Figure 5.20: Predicted and experimental absorption rates for CO₂ absorption in aqueous AMP solution at 303 K.

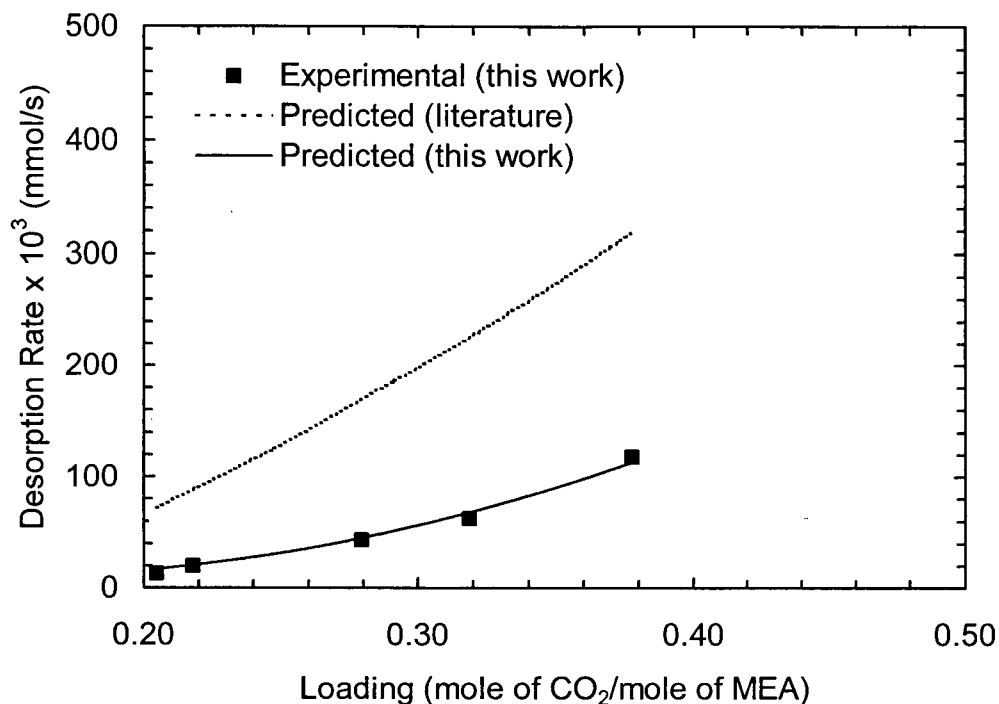


Figure 5.21: Predicted and experimental desorption rates for CO₂ desorption from aqueous MEA solution at 378 K.

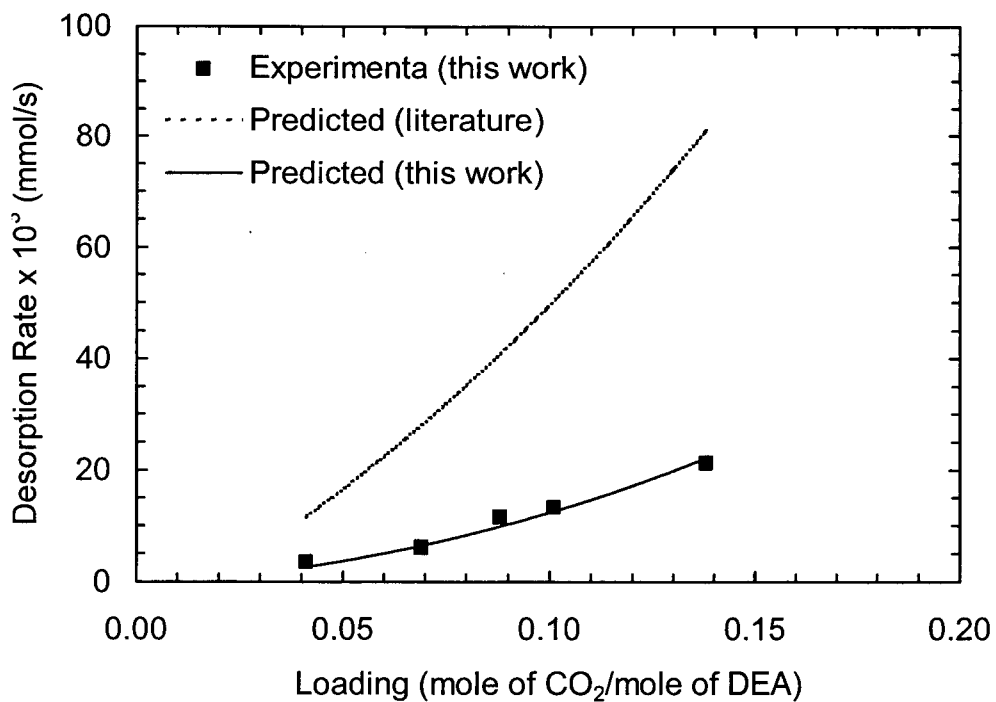


Figure 5.22: Predicted and experimental desorption rates for CO₂ desorption from aqueous DEA solution at 382 K.

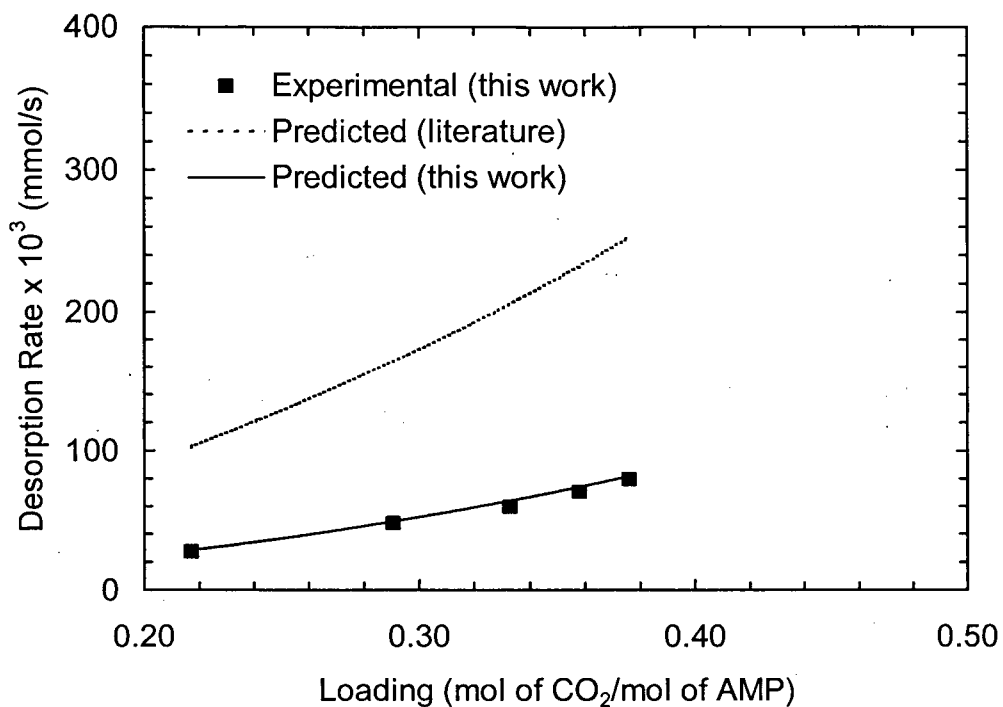


Figure 5.23: Predicted and experimental desorption rates for CO₂ desorption from aqueous AMP solution at 378 K.

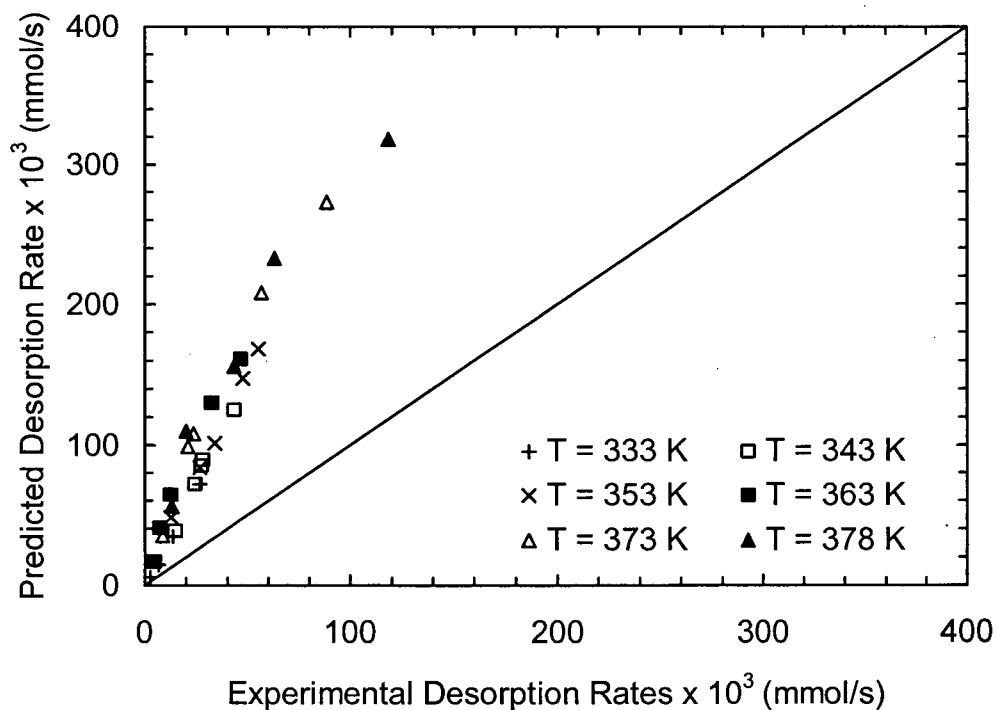


Figure 5.24: Predicted and experimental desorption rates for CO₂ desorption in aqueous MEA solution at 333 to 378 K using literature correlations

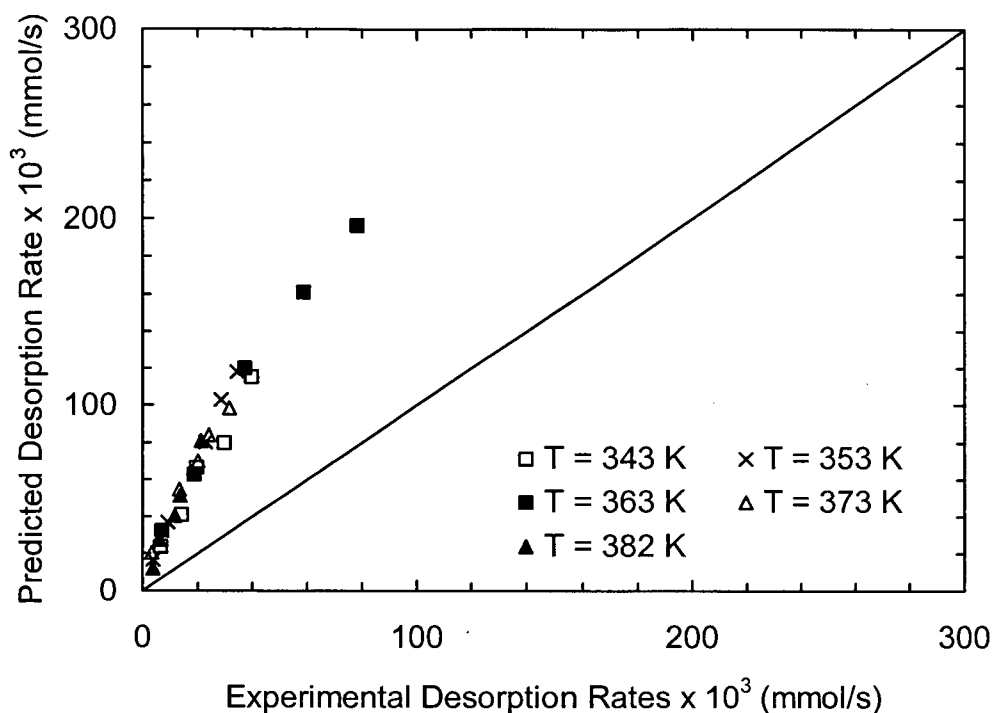


Figure 5.25: Predicted and experimental desorption rates for CO₂ desorption in aqueous DEA solution at 343 to 382 K using literature correlations

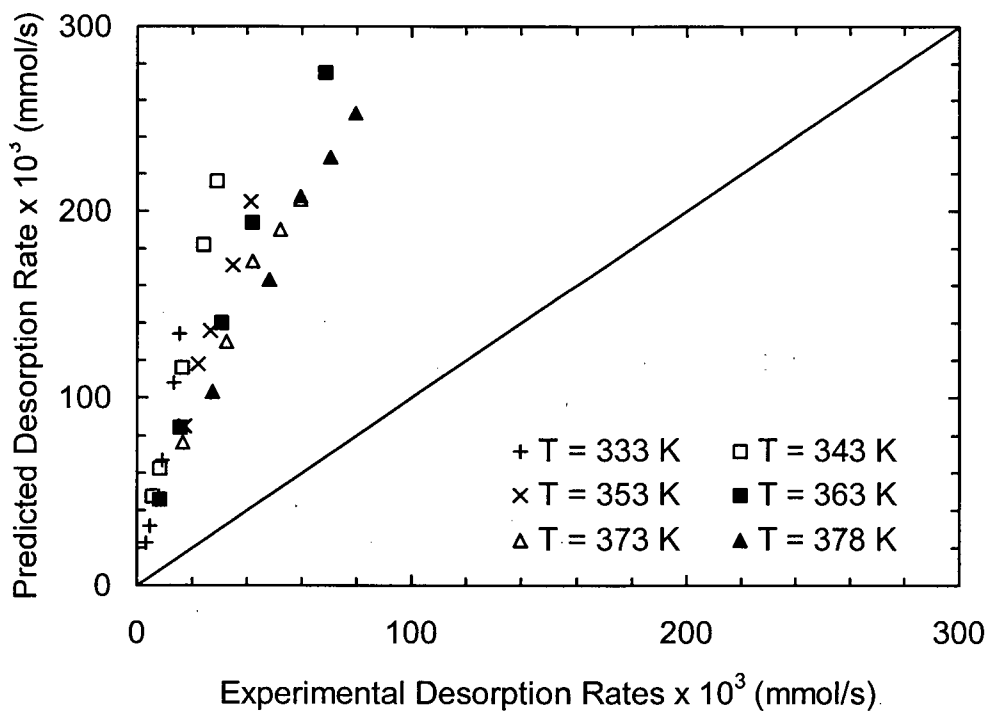


Figure 5.26: Predicted and experimental desorption rates for CO₂ desorption in aqueous AMP solution at 343 to 378 K using literature correlations

Minor deviations in the predicted absorption rates are understandable, as different authors have used different experimental techniques to measure absorption rates (see Tables 2.1 to 2.5). Note that, for MEA, the predicted absorption rates based on literature correlations are about 5 to 10% higher than the measured rates, for DEA they are about 20 to 25% less than the measured rates and for AMP, they vary from -10 to +20% of the measured rates (see Figures 5.18 to 5.20). This strongly suggests that the variation in predicted rates is due to the differences in experimental apparatus and the methods used for data interpretation and not due to some consistent error in our measurements. For example, Hikita et al. (1977a) used a pseudo-first-order model, Rinker et al (1996) used a rigorous model and Xu et al. (1996) used the zwitterion mechanism to analyze their data.

5.4.1.2 Parameter Estimates for MEA, DEA and AMP

The absorption and desorption rate data for MEA, DEA and AMP were regressed using our model and the kinetic parameters were estimated. These estimates are presented in Tables (5.7) to (5.9) and plotted as a function of temperature in Figures (5.27) to (5.35).

Note that all three parameters (e.g., k_1 , k_1/K_1K_2 and k_{-1}/k_2) were easily estimated from the desorption data. However, we were unable to obtain good estimates of combined rate constants (i.e., k_1/K_1K_2 and k_{-1}/k_2 ; $k_{10}/K_{10}K_{11}$ and k_{-10}/k_{11} ; $k_{16}/K_{16}K_{17}$ and k_{-16}/k_{17}), which represent the reverse reaction in the zwitterion mechanism, from absorption data. This is understandable, because for

initially unloaded solutions, the values of these parameters are so close to zero that it becomes impossible to obtain reliable estimates. Therefore, in this work, we first estimated all three parameters for each case using desorption data and then used the correlations for combined constants based on these estimates to obtain forward rate constants under absorption conditions (see Tables 5.7 to 5.9).

Table 5.7: Estimates of rate constants in eq. (5.4) from absorption and desorption data

T (K)	k_{10} ($\text{m}^3/\text{kmol s}$)	$k_{10}/K_{10}K_{11}$ (1/s)	k_{-10}/k_{11} (kmol/m^3)	Method
303.4	6,828.6	-	-	Absorption
333.2	45,108.0	14.6	23.0	Desorption
343.2	65,248.0	36.2	44.3	Desorption
353.4	149,720.0	198.1	148.9	Desorption
363.3	276,760.0	523.7	333.1	Desorption
373.2	364,820.0	1,512.8	776.4	Desorption
378.3	540,670.0	3,732.9	1,297.6	Desorption

Table 5.8: Estimates of rate constants in eq. (5.5) from absorption and desorption data

T (K)	k_{16} ($\text{m}^3/\text{kmol s}$)	$k_{16}/K_{16}K_{17}$ (1/s)	k_{-16}/k_{17} (kmol/m^3)	Method
303.2	3,055.8	-	-	Absorption
313.2	4,085.8	-	-	Absorption
323.2	7,290.7	-	-	Absorption
343.2	9,139.0	33.9	1.2	Desorption
353.4	12,271.0	122.4	8.7	Desorption
363.3	15,119.0	531.3	43.2	Desorption
373.2	17,058.0	1,515.6	110.0	Desorption
382.3	21,898.0	3,288.7	257.9	Desorption

Table 5.9: Estimates of rate constants in eq. (5.6) from absorption and desorption data

T (K)	k_1 ($\text{m}^3/\text{kmol s}$)	k_1/K_1K_2 (1/s)	k_{-1}/k_2 (kmol/m^3)	Method
296.1	924.3	-	-	Absorption
303.5	1,288.9	-	-	Absorption
308.3	1,368.1	-	-	Absorption
313.2	1,868.4	-	-	Absorption
318.2	2,427.2	-	-	Absorption
322.9	3,234.9	-	-	Absorption
333.4	4,264.2	108.5	4.5	Absorption
343.4	6,838.5	374.6	10.4	Desorption
353.5	8,561.9	1,480.6	22.5	Desorption
363.4	10,039.0	3,578.9	47.8	Desorption
373.3	15,386.0	9,651.1	94.4	Desorption
378.4	20,678.0	14,728.0	184.9	Desorption

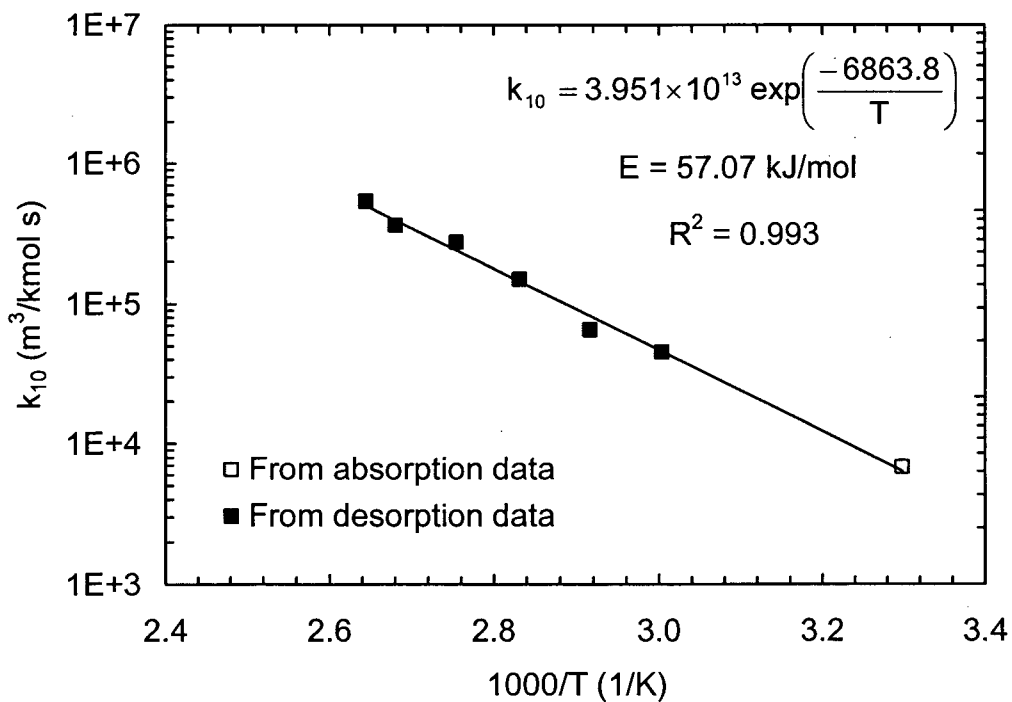


Figure 5.27: Arrhenius plot of the estimates for k_{10} from absorption and desorption data

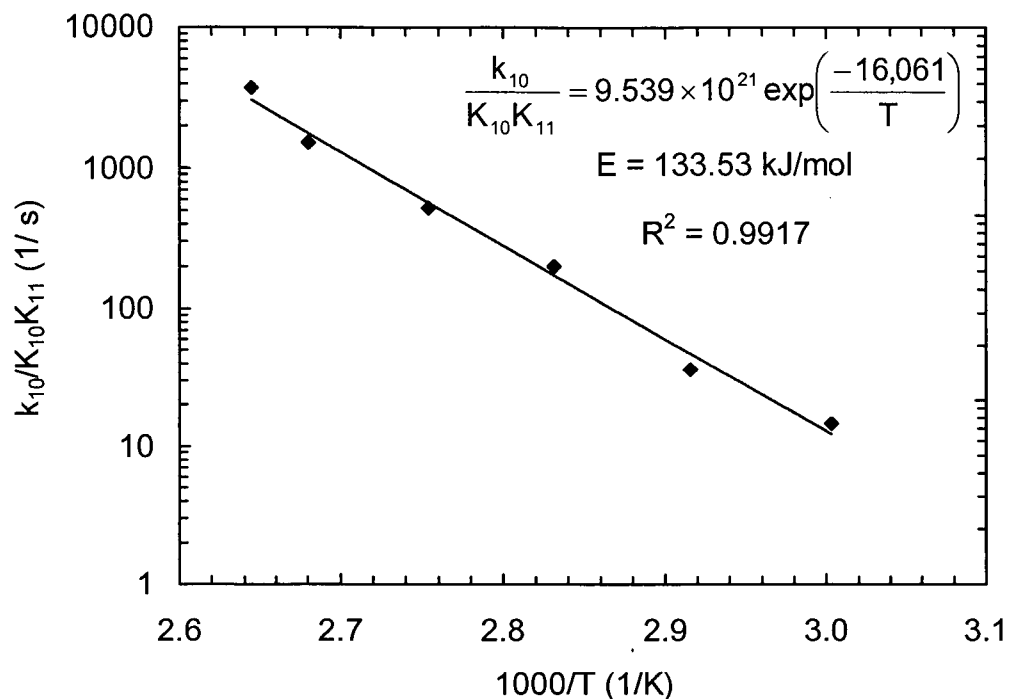


Figure 5.28: Arrhenius plot of the estimates for $k_{10}/K_{10}K_{11}$ from absorption and desorption data

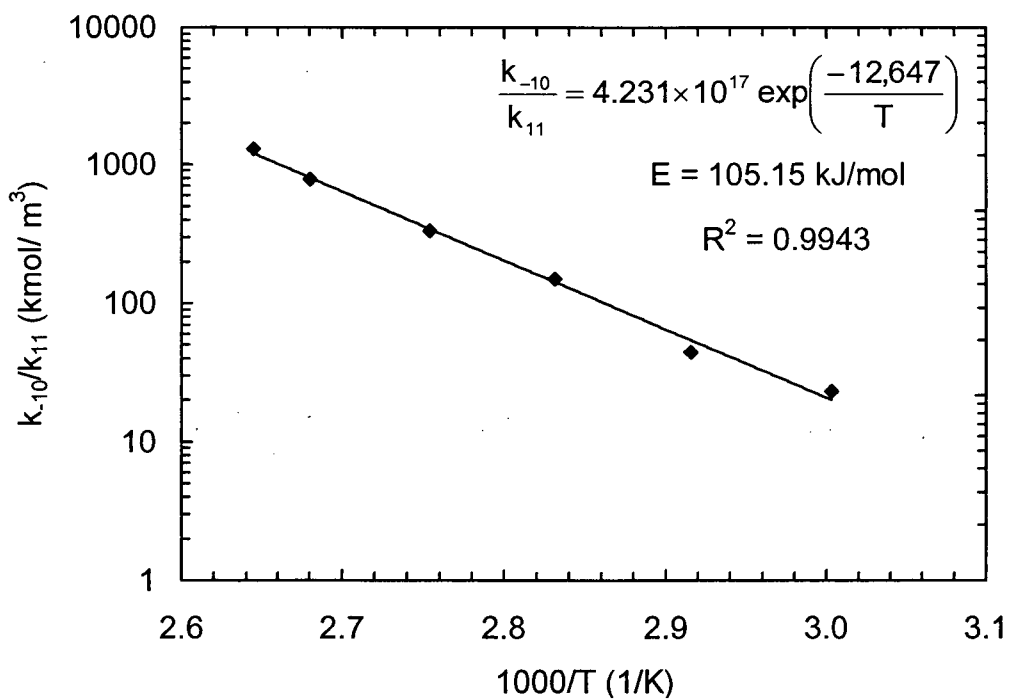


Figure 5.29: Arrhenius plot of the estimates for k_{-10}/k_{11} from absorption and desorption data

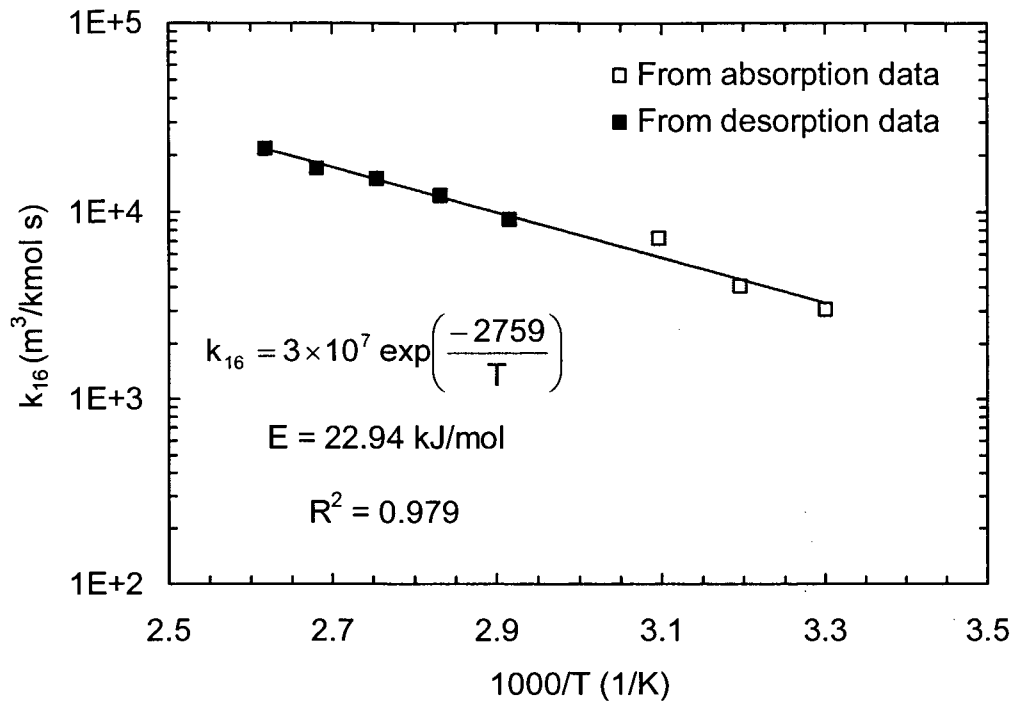


Figure 5.30: Arrhenius plot of the estimates for k_{16} from absorption and desorption data

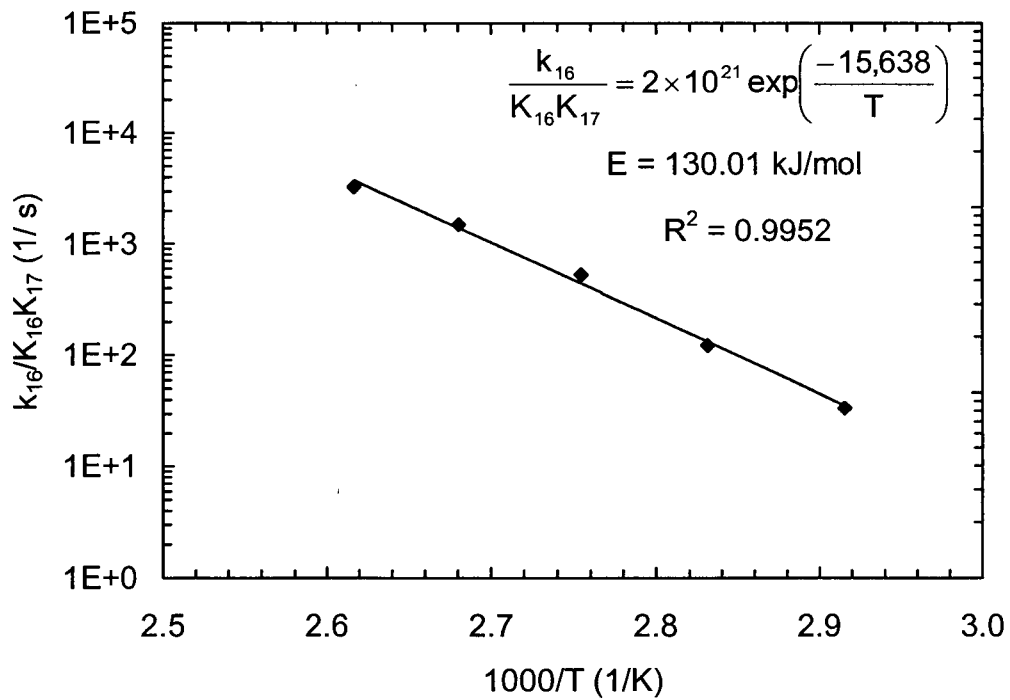


Figure 5.31: Arrhenius plot of the estimates for $k_{16}/K_{16}K_{17}$ from absorption and desorption data

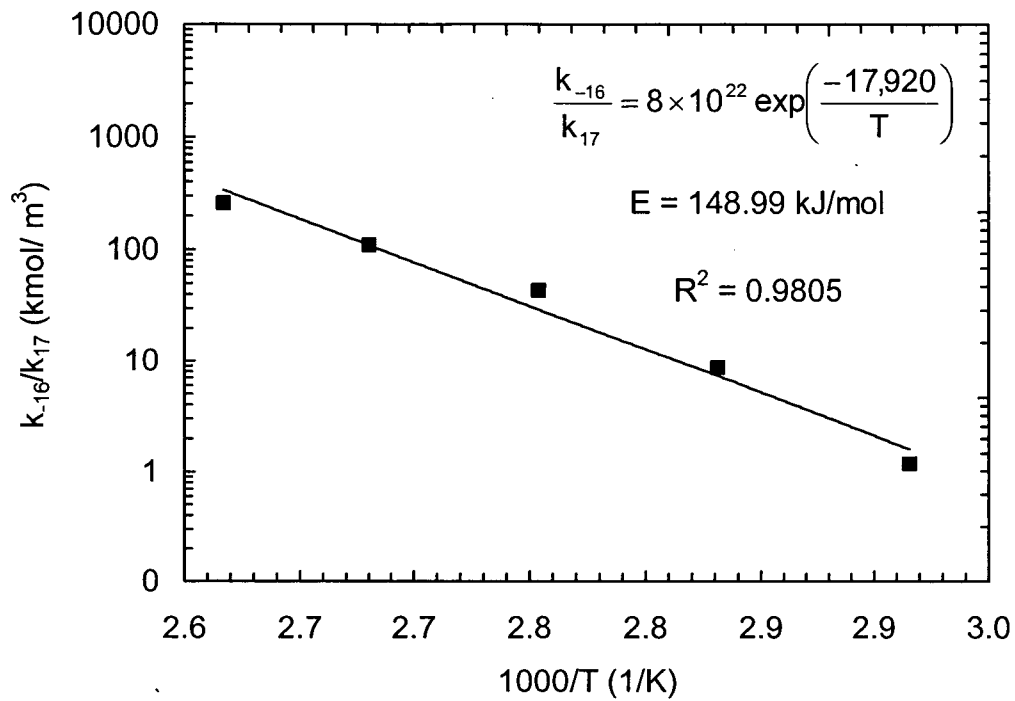


Figure 5.32: Arrhenius plot of the estimates for k_{-16}/k_{17} from absorption and desorption data

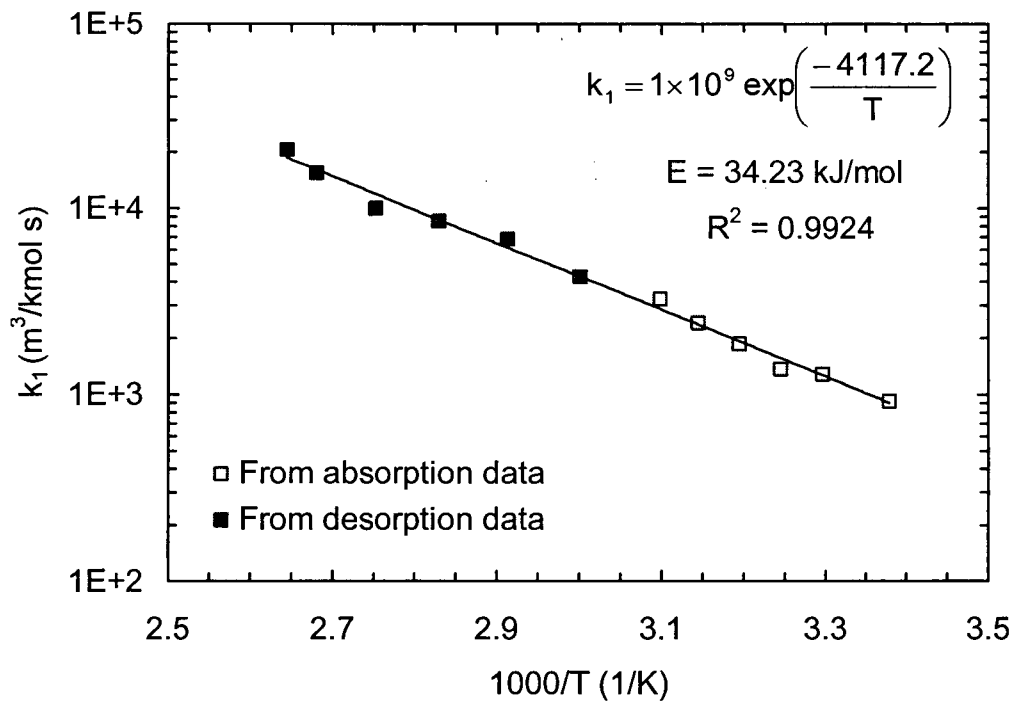


Figure 5.33: Arrhenius plot of the estimates for k_1 from absorption and desorption data

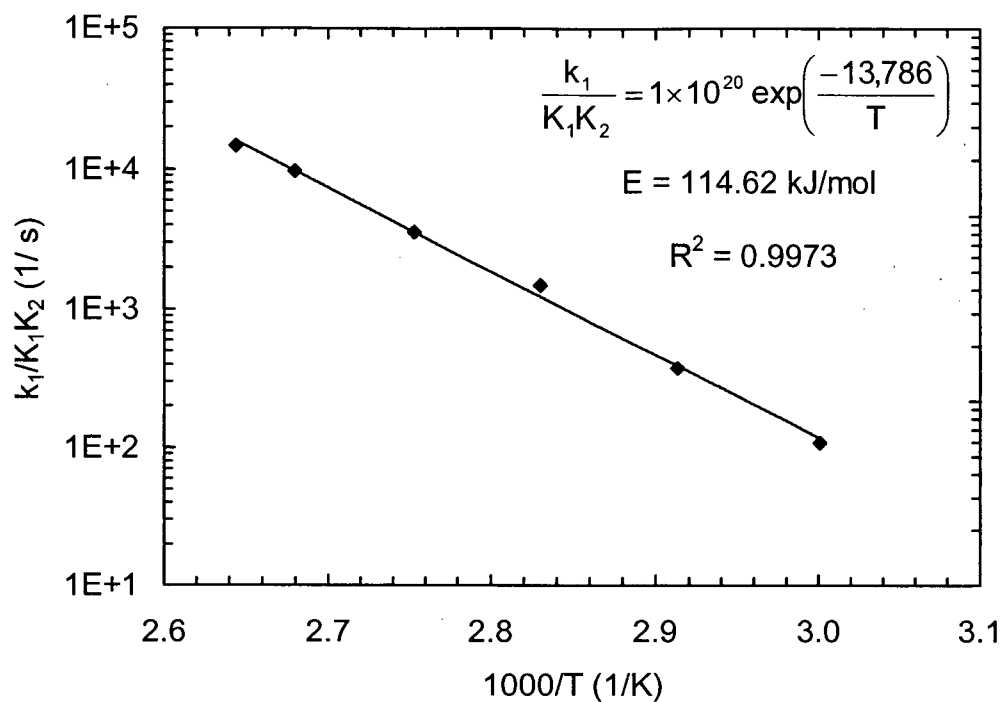


Figure 5.34: Arrhenius plot of the estimates for k_1/K_1K_2 from absorption and desorption data

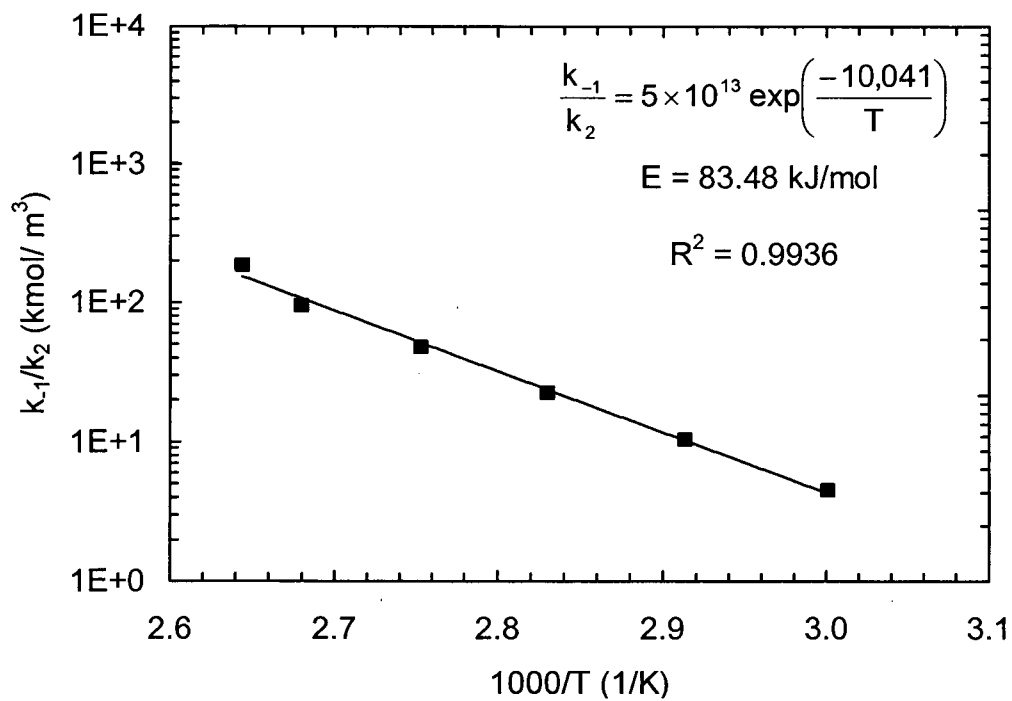


Figure 5.35: Arrhenius plot of the estimates for k_{-1}/k_2 from absorption and desorption data

5.4.2 CO₂ Absorption/Desorption in Aqueous MDEA Solutions

The experimental results for the CO₂-MDEA system are reported in Tables K.14 and K.22. As stated earlier in Chapter 4, MDEA does not react directly with CO₂ but catalyzes the CO₂ hydration reaction. The rate expression for this reaction is given by:

$$r_{22} = -k_{22}C_1C_{16} + \frac{k_{22}}{K_{22}}C_5C_{17} \quad (5.7)$$

Equation (5.7) has two unknown parameters (i.e., k_{22} , k_{-22} or k_{22}/K_{22}), which were determined from the absorption and desorption rate data given in Tables K.14 and K.22. Here again, first, the existing correlations for these parameters were used to compare the predicted absorption and desorption rates with our experimental data. The correlation to calculate K_{22} was taken from Appendix H and that for k_{22} was obtained from Rinker et al. (1995). The latter was developed based on absorption data only. These results are presented in Figures 5.36 to 5.38. In this case, the predictions based on the literature correlations are fairly good for both absorption and desorption rates. This is probably because the rate of the CO₂ reaction with MDEA is much slower compared to that MEA, DEA and AMP.

In the next step, we used our model to estimate k_{22} and k_{-22} by using the parameter estimation technique implemented earlier for MEA, DEA and AMP. These estimates from absorption and desorption data are listed in Table (5.10) and plotted as a function of temperature in Figures 5.39 and 5.40.

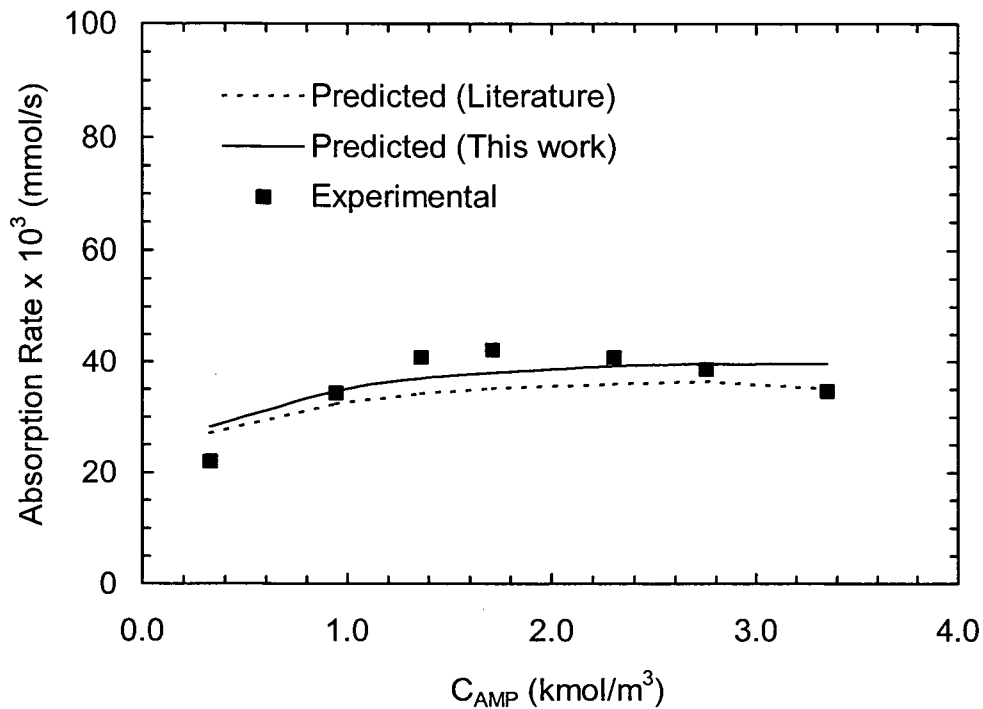


Figure 5.36: Predicted and experimental absorption rates for CO₂ absorption in aqueous MDEA solution at 303 K.

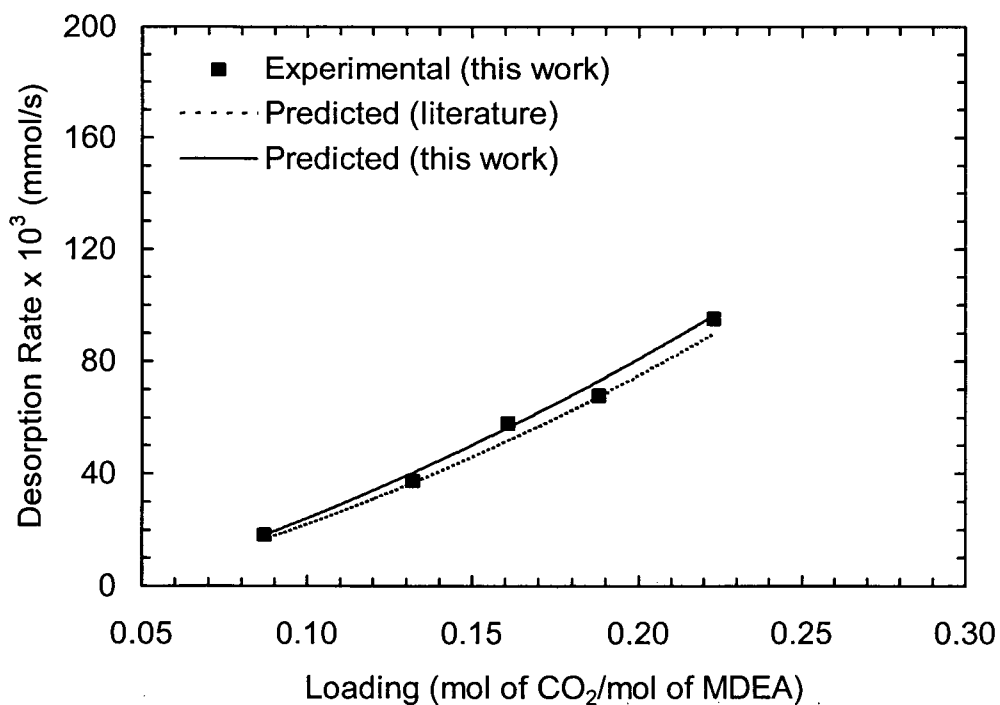


Figure 5.37: Predicted and experimental desorption rates for CO₂ desorption from aqueous MDEA solution at 378 K.

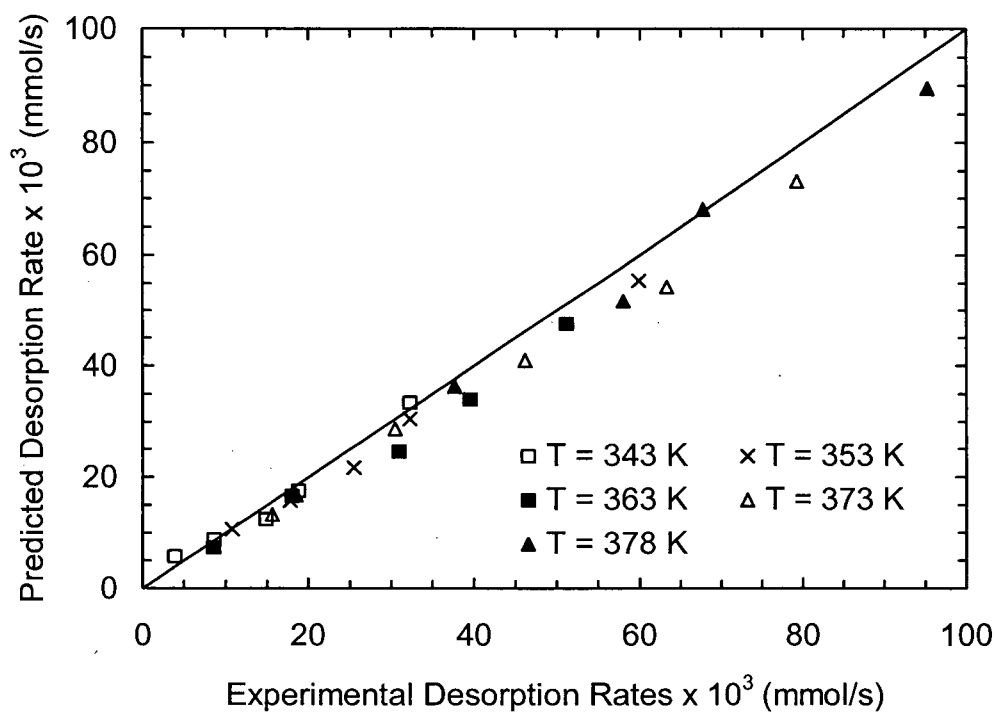


Figure 5.38: Predicted and experimental desorption rates for CO₂ desorption in aqueous MDEA solution at 343 to 378 K using literature correlations

Table 5.10: Estimates of rate constants in eq. (5.7) from absorption and desorption data

T (K)	k_{22} (m ³ /kmol s)	k_{-22} (m ³ /kmol s)	Method
303.2	9.9	-	Absorption
343.4	72.2	2.3	Desorption
353.2	123.3	6.1	Desorption
363.3	194.3	14.9	Desorption
373.3	357.6	35.9	Desorption
378.3	461.0	51.0	Desorption

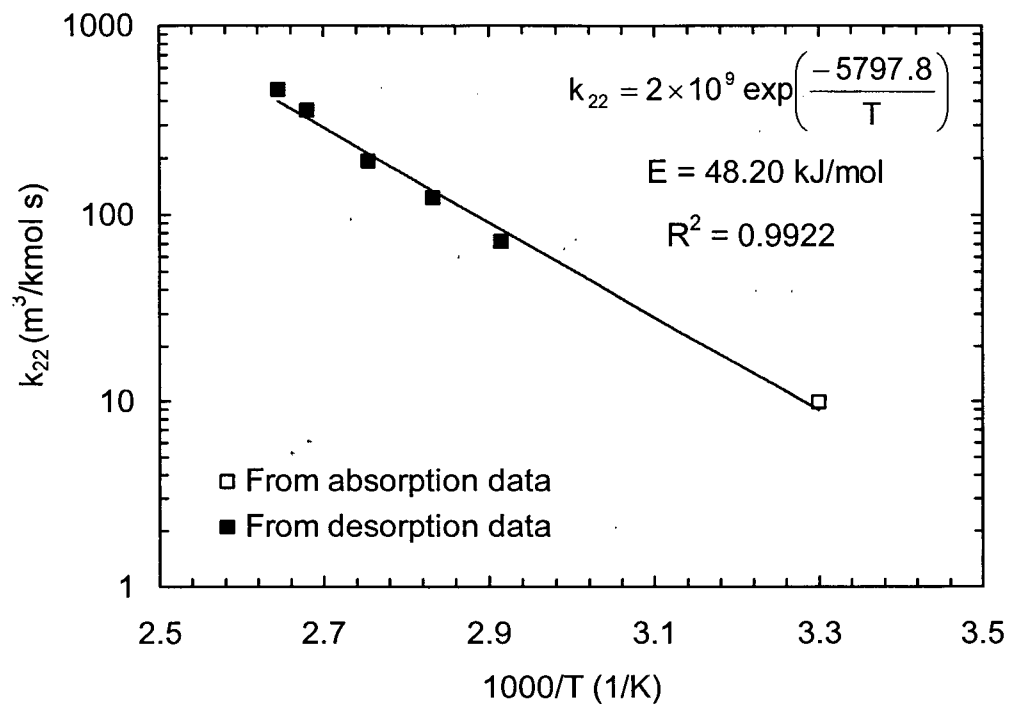


Figure 5.39: Arrhenius plot of the estimates for k_{22} from absorption and desorption data

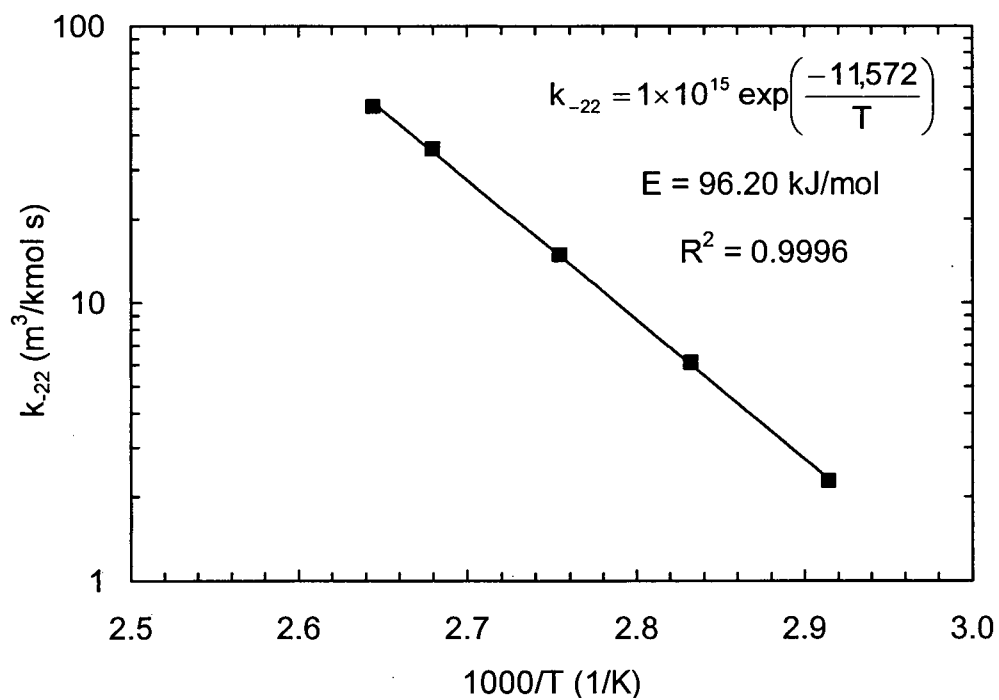


Figure 5.40: Arrhenius plot of the estimates for k_{-22} from absorption and desorption data

5.4.3 CO₂ Absorption/Desorption in Aqueous Amine Blends

The experimental data for CO₂ absorption and desorption in four amine blends (MEA+MDEA, MEA+AMP, DEA+MDEA and DEA+AMP) studied in this work are presented in Tables K.16 to K.19 and K.24 to K.27. These data were fitted to the overall rate expressions given in Table 5.5. It can be seen from this table that most of the unknown kinetic parameters have already been estimated using single amine systems. The only remaining unknowns in these expressions are: k_{24}/k_{-10} for MEA+MDEA blend; k_{25}/k_{-1} and k_{26}/k_{-10} for MEA+AMP blend; k_{27}/k_{-16} for DEA+MDEA blend and k_{28}/k_{-1} and k_{29}/k_{-16} for DEA+AMP blend. These parameters were estimated by regressing desorption data of corresponding blend at 353 to 373 K. The results are listed in Table (5.11) and plotted as a function of temperature in Figures (5.41) to (5.46).

Table 5.11: Estimates of the combined rate constants for amine blends from desorption data

T (K)	k_{-10}/k_{24} (kmol/m ³)	k_{-1}/k_{25} (kmol/m ³)	k_{-10}/k_{26} (kmol/m ³)	k_{-16}/k_{27} (kmol/m ³)	k_{-1}/k_{28} (kmol/m ³)	k_{-16}/k_{29} (kmol/m ³)
353.0	427.2	2,700.0	788.43	63.8	1,006.9	93.09
363.0	738.9	9,360.0	1,305.60	178.3	3,270.3	184.82
373.0	1,473.8	23,400.0	3,048.40	897.2	15,366.0	394.80

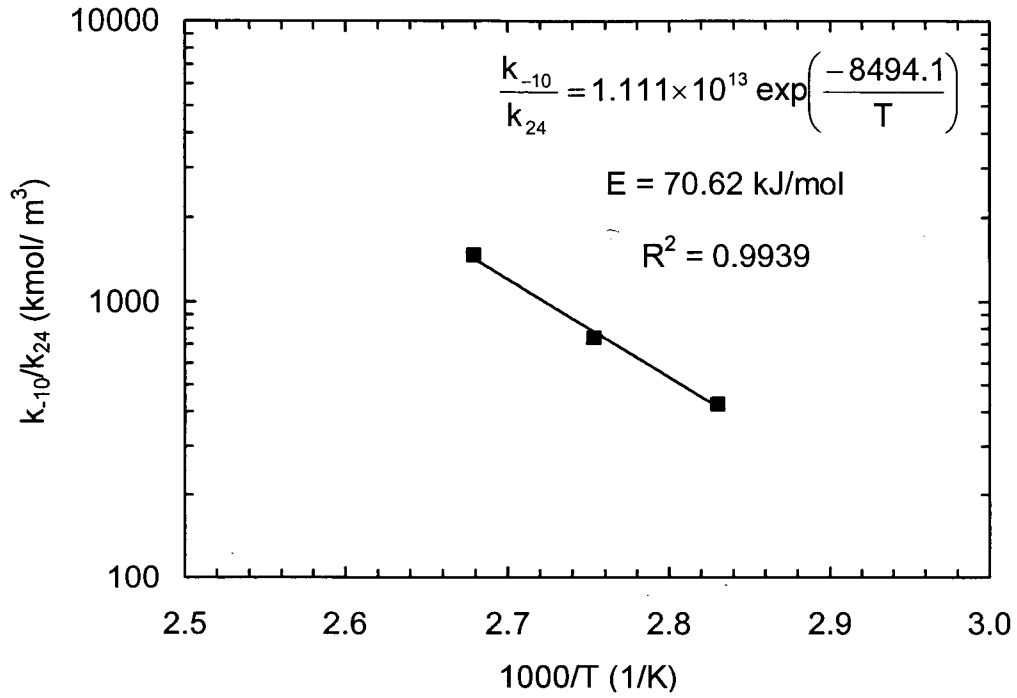


Figure 5.41: Arrhenius plot of the estimates for k_{-10}/k_{24} from desorption data

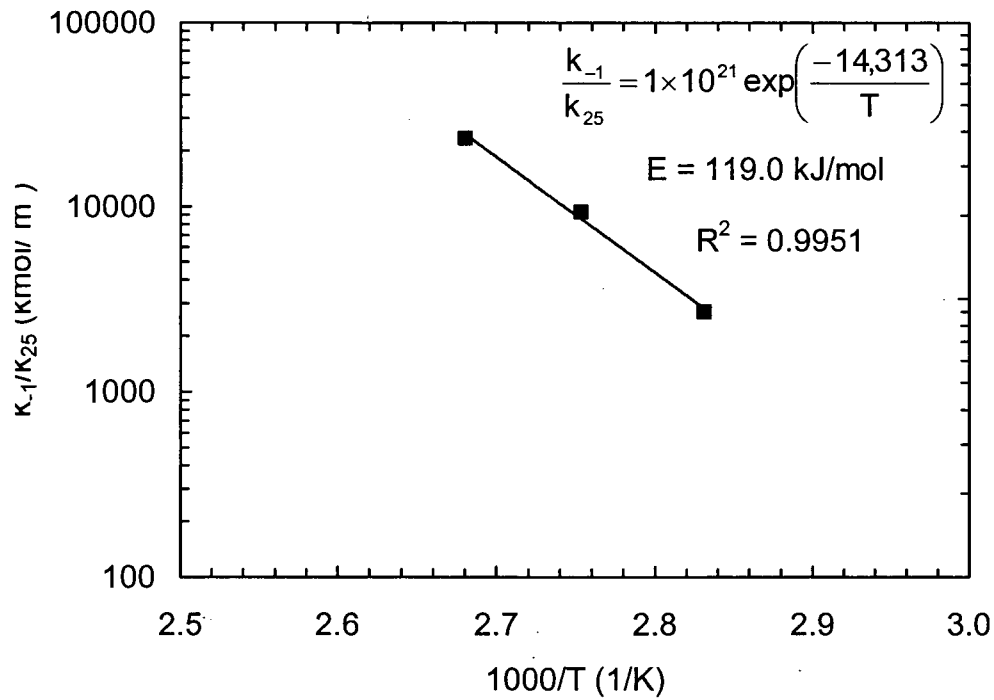


Figure 5.42: Arrhenius plot of the estimates for k_{-1}/k_{25} from desorption data

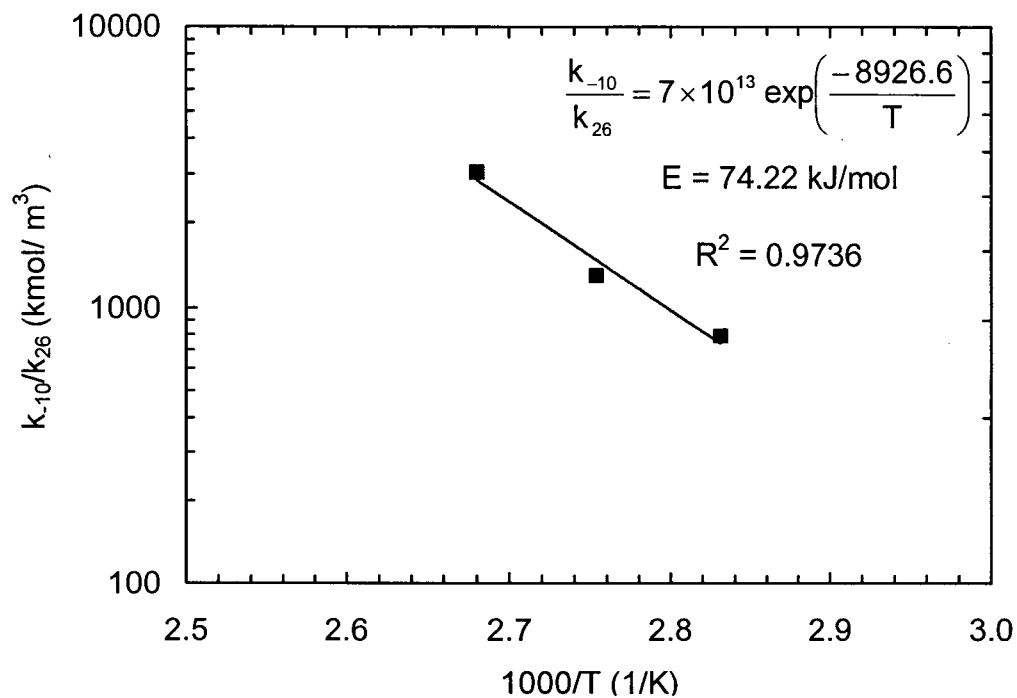


Figure 5.43: Arrhenius plot of the estimates for k_{-10}/k_{26} from desorption data

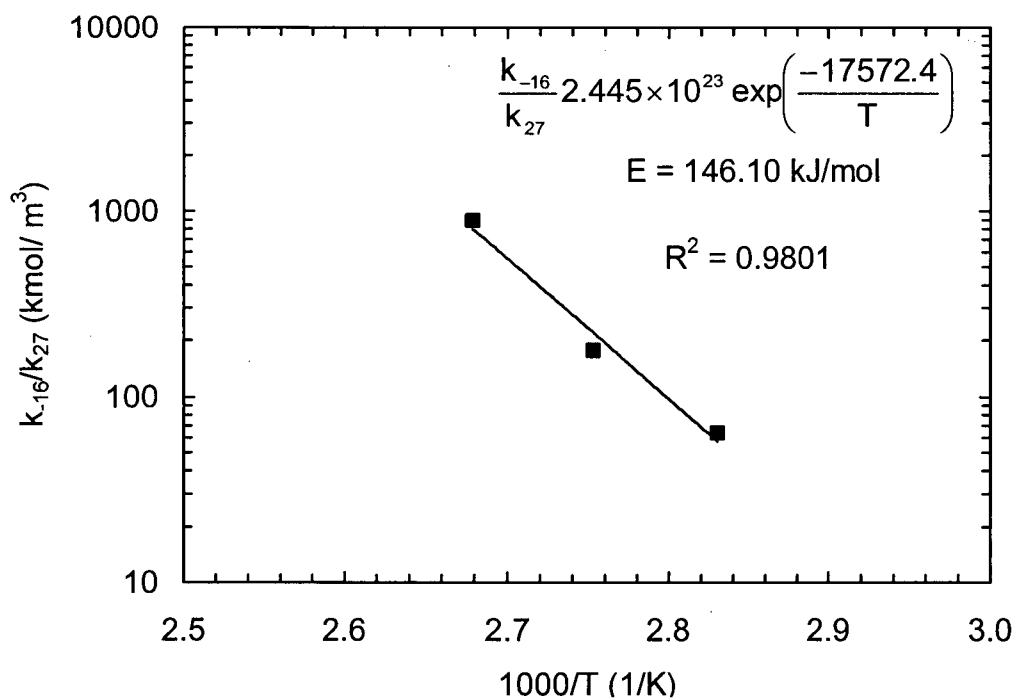


Figure 5.44: Arrhenius plot of the estimates for k_{-16}/k_{27} from desorption data

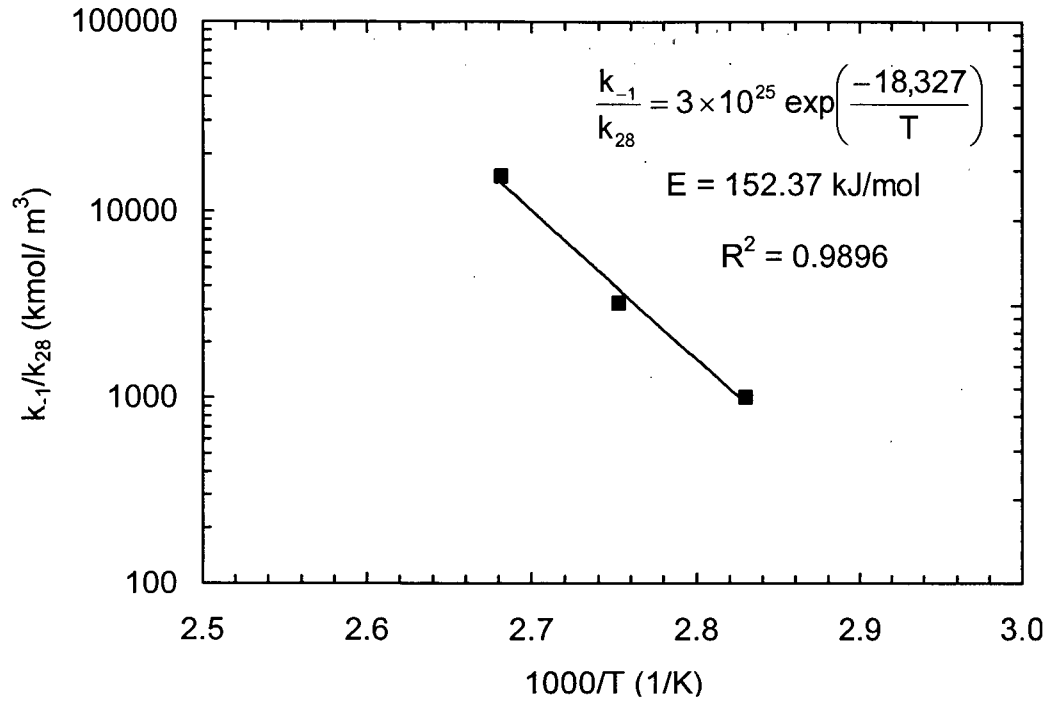


Figure 5.45: Arrhenius plot of the estimates for k_{-1}/k_{28} from desorption data

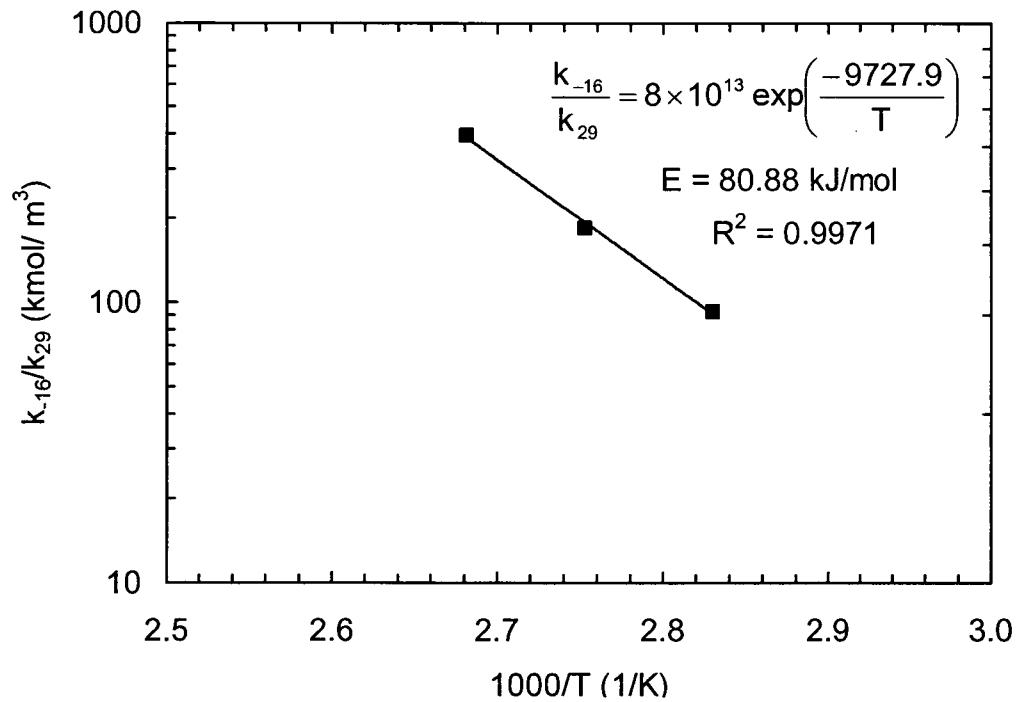


Figure 5.46: Arrhenius plot of the estimates for k_{-16}/k_{29} from desorption data

5.4.4 Comparison of the Parameter Estimates with Literature Data

Figures 5.47 to 5.50 compare the forward rate constants (i.e., k_{10} , k_{16} , k_1 and k_{22}) obtained in this work with those from the published literature. The estimates from this work are based on both absorption and desorption data whereas the literature values are from absorption data only. Clearly, our estimates from absorption data are in good agreement with those reported in the literature. These figures also show that in most cases the second-order rate constants obtained under absorption conditions cannot be extrapolated to desorption temperatures with good accuracy except for CO₂-MDEA-H₂O system (see Figure 5.50). The reason for much better extrapolation of kinetic data for CO₂-MDEA-H₂O system to desorption temperatures is because of very low reactivity of CO₂ in aqueous MDEA solution compared to MEA, DEA and AMP solutions. From these results, it can be concluded that to obtain good kinetic data, experiments must also be conducted under desorption conditions. In fact, the reverse rate constants can only be obtained accurately from desorption experiments.

Table 5.12 shows a comparison of the activation energies of k_1 , k_{10} , k_{16} and k_{22} determined in this work with those reported in the literature. It can be seen from this table that the activation energies determined in this work are slightly higher than the published values. This discrepancy could be because our correlations are based on both absorption and desorption measurements covering a much wider temperature range (from 303 to 382 K) as opposed to

293-323 K for the literature correlations that were developed based on absorption data only.

The higher activation energies of the combined rate constants indicate that the reverse reaction is a strong function of temperature and to regenerate the solution the amine solutions must first be heated to sufficiently high temperatures. As expected, the activation energy for the reverse reaction is highest for MEA and lowest for MDEA, indicating thereby that MDEA is lot easier to regenerate than MEA.

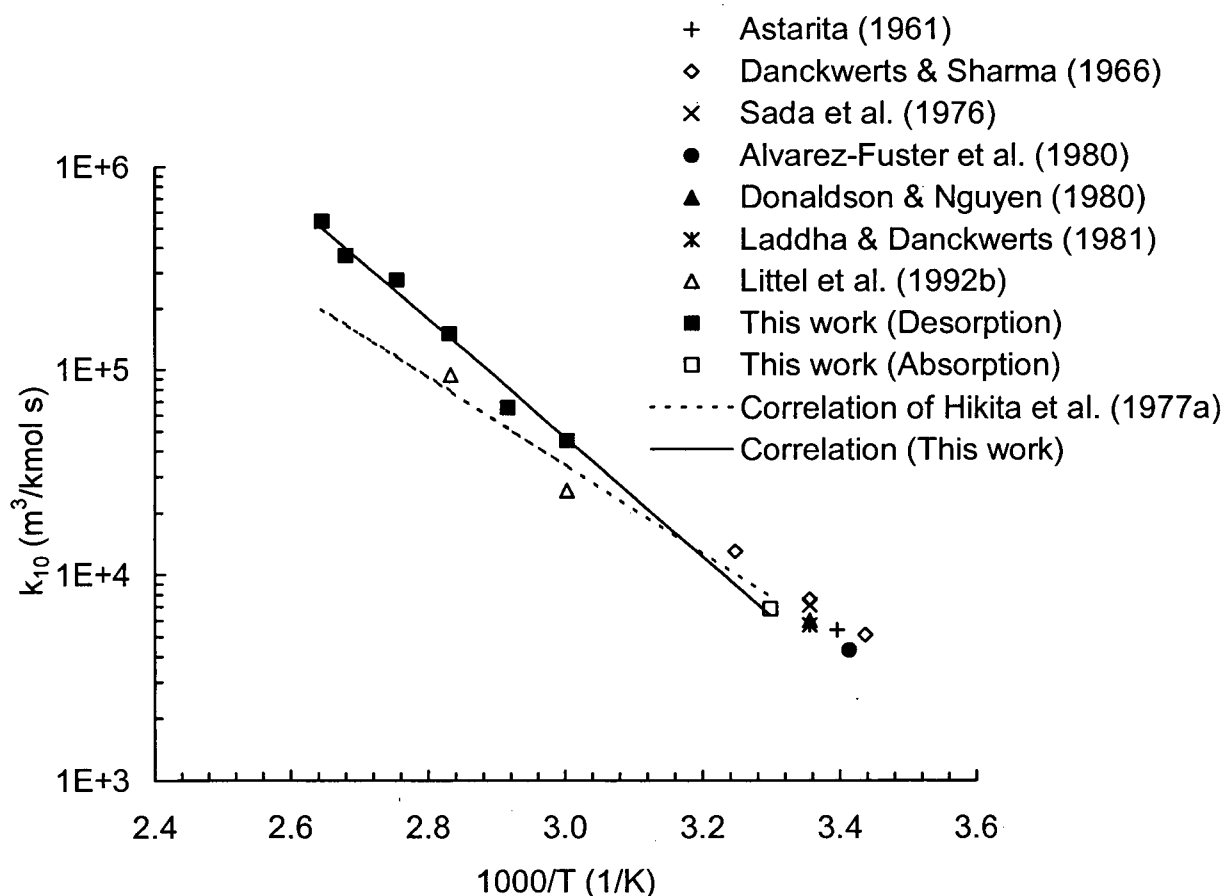


Figure 5.47: Comparison of the second-order rate constant (k_{10}) for CO_2 -MEA reaction determined in this work with those reported in the literature

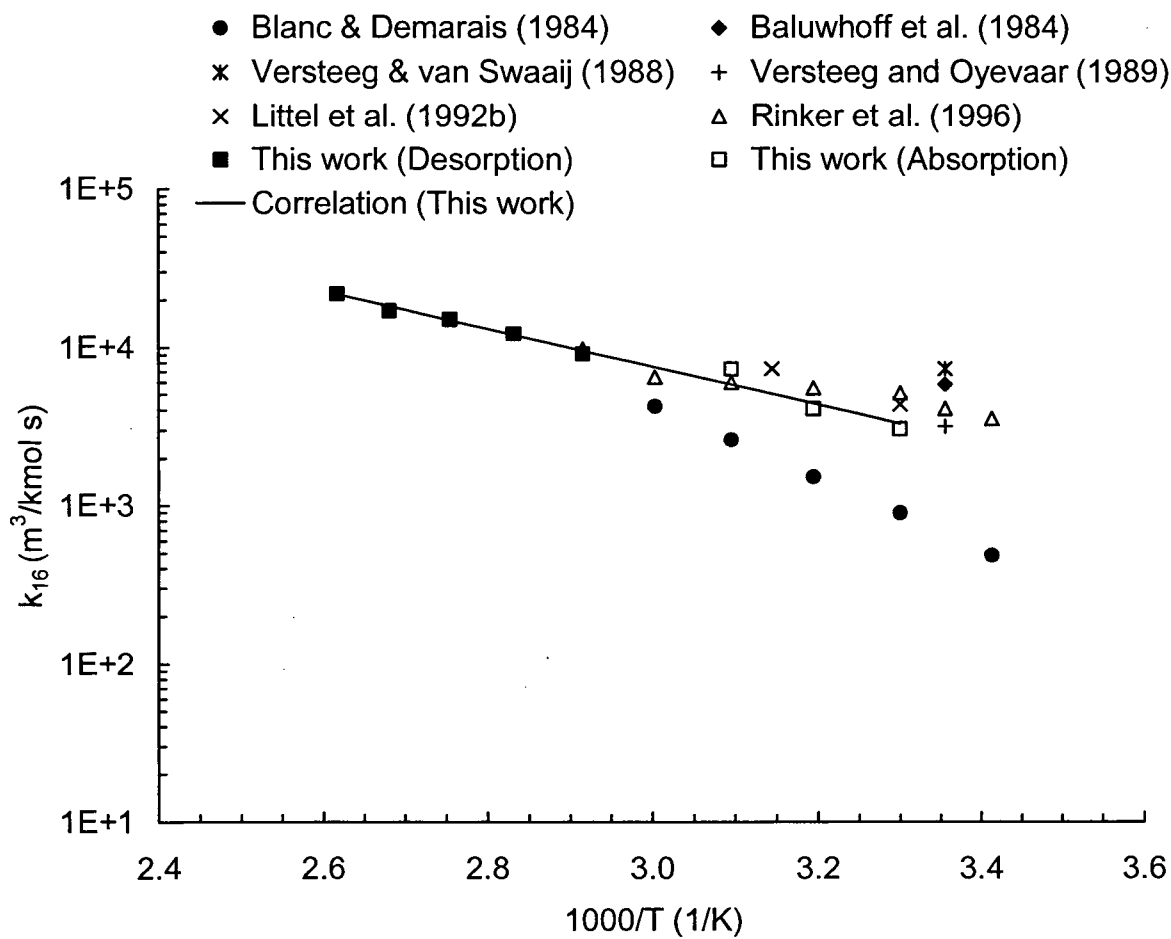


Figure 5.48: Comparison of the second-order rate constant (k_{16}) for CO_2 -DEA reaction determined in this work with those reported in the literature

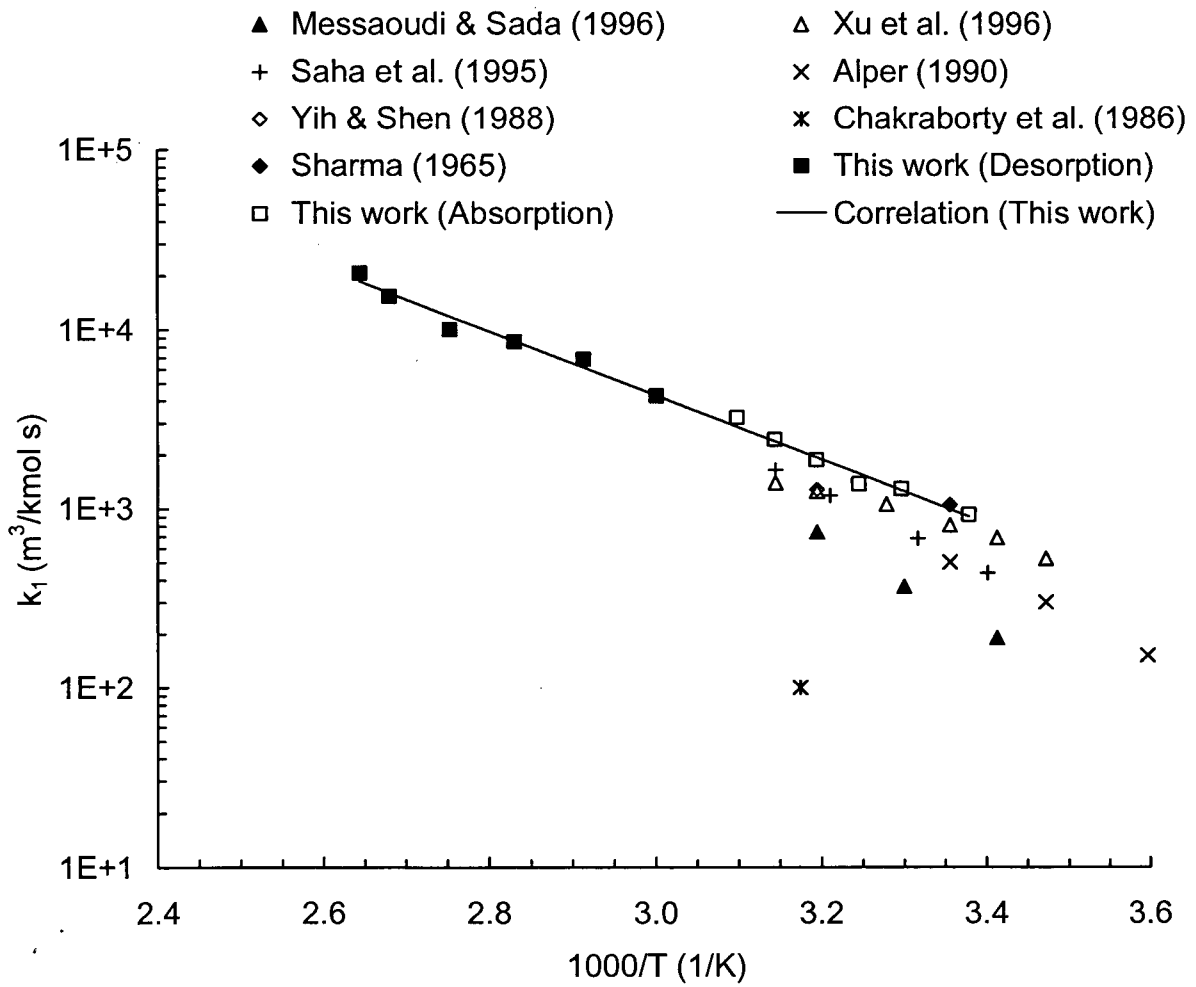


Figure 5.49: Comparison of the second-order rate constant (k_1) for CO_2 -AMP reaction determined in this work with those reported in the literature

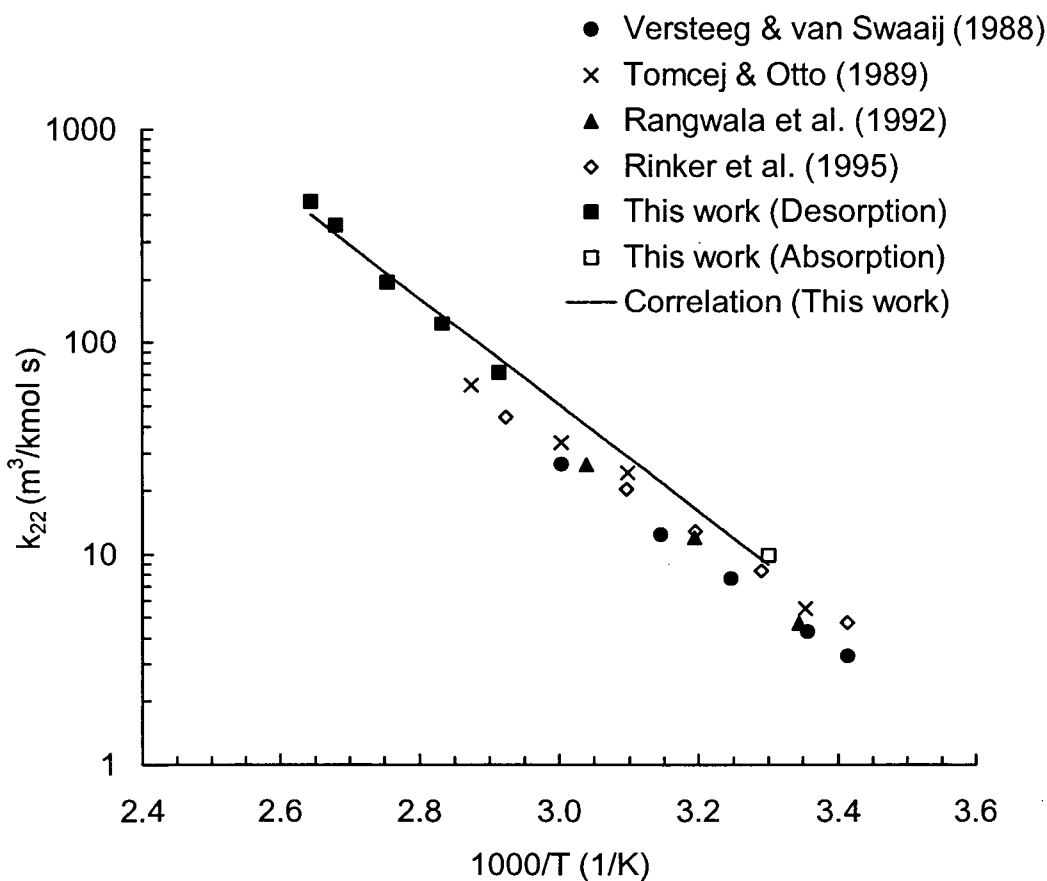


Figure 5.50: Comparison of the second-order rate constant (k_{22}) for CO_2 -MDEA reaction determined in this work with those reported in the literature

Table 5.12: Comparison of the activation energies of k_1 , k_{10} and k_{16}

Parameter	Activation Energy (kJ/mol)		
	This work	Literature	
		Values	Source
k_1	34.23	24.26	Xu et al. (1996)
k_{10}	57.07	41.20	Rinker et al. (1996)
k_{16}	22.94	14.14	Hikita et al. (1977a)
k_{22}	48.20	39.00	Rinker et al. (1995)

5.4.5 Predicted Absorption/Desorption Rates Based on Correlations Developed in this Work

Figures 5.51 to 5.58 compare the predicted and experimental desorption rates based on the correlations developed in this work. In general the agreement between the predicted and measured rates is very good. The percent absolute average deviations for MEA, DEA, AMP and MDEA are 8.71, 10.34%, 6.98% and 6.39% respectively. Similar agreement exists for mixed amine systems. The average deviation for the latter was less than 6%. This further validates the reaction mechanisms assumed and the experimental techniques used to estimate the kinetic parameters, and confirms that the theory for gas absorption with reversible chemical reactions can be applied to predict desorption rates.

A more rigorous error analysis based on 95% confidence interval of the parameters estimates could not be performed because of the limitation of the parameter estimation software used in this work.

In the next step, the model with the correlations developed in the previous section was used to predict the CO₂ absorption rates in 25 wt% amine blends namely: MEA+MDEA, DEA+MDEA, MEA+AMP, DEA+AMP. The purpose of this exercise was to investigate the effect of an addition of MEA and DEA on the absorption rates of MDEA and AMP. The predicted and experimental results are plotted in Figures 5.59 to 5.62. The agreement was satisfactory. However, more work is required to improve the capability of the model to handle mixed amine solutions. It can be seen from Figures 5.59 to 5.60, that small addition of MEA or DEA (< 5 wt%) can substantially enhance the rate of absorption of CO₂.

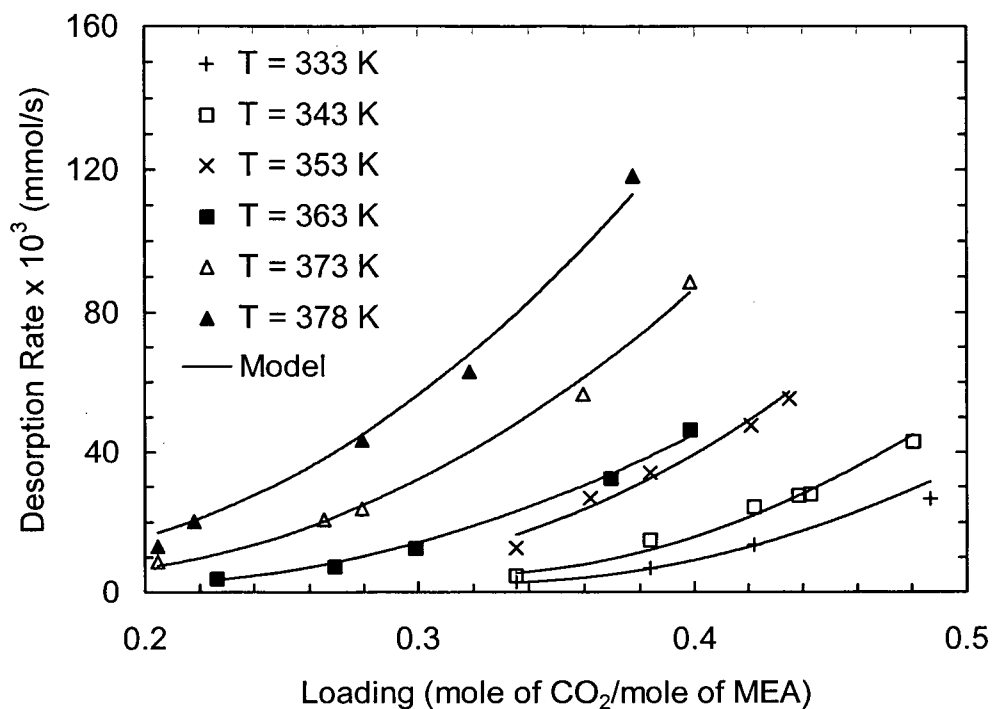


Figure 5.51: Predicted and experimental desorption rates CO₂-MEA as a function of temperature and CO₂ loading

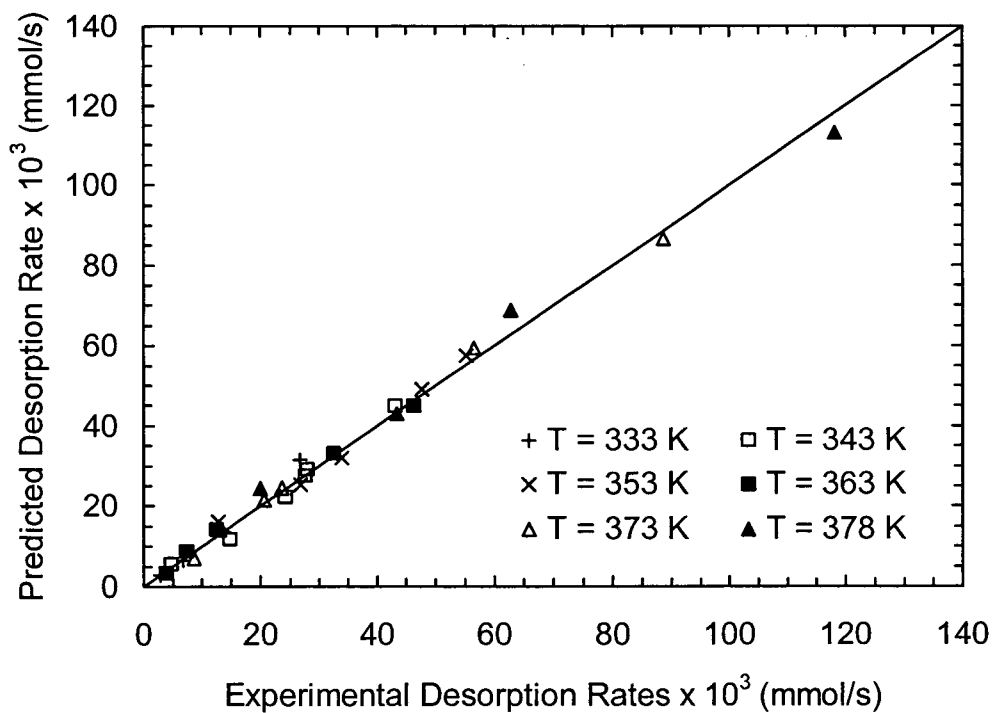


Figure 5.52: Predicted versus experimental desorption rates CO₂-MEA calculated from the correlation developed in this work

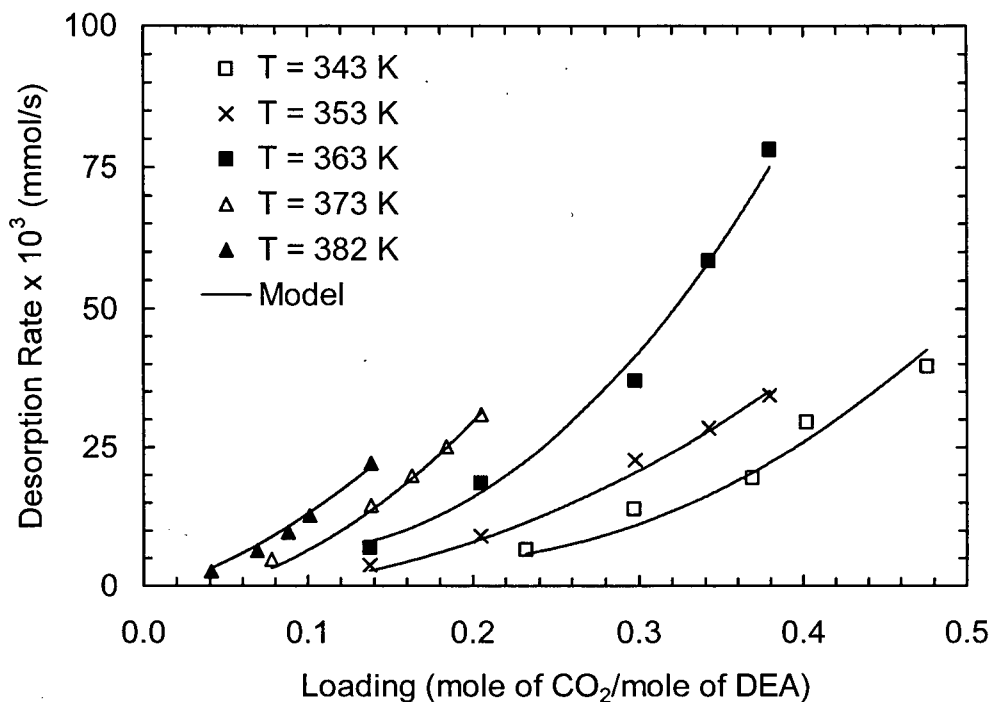


Figure 5.53: Predicted and experimental desorption rates for CO₂-DEA system as a function of temperature and CO₂ loading

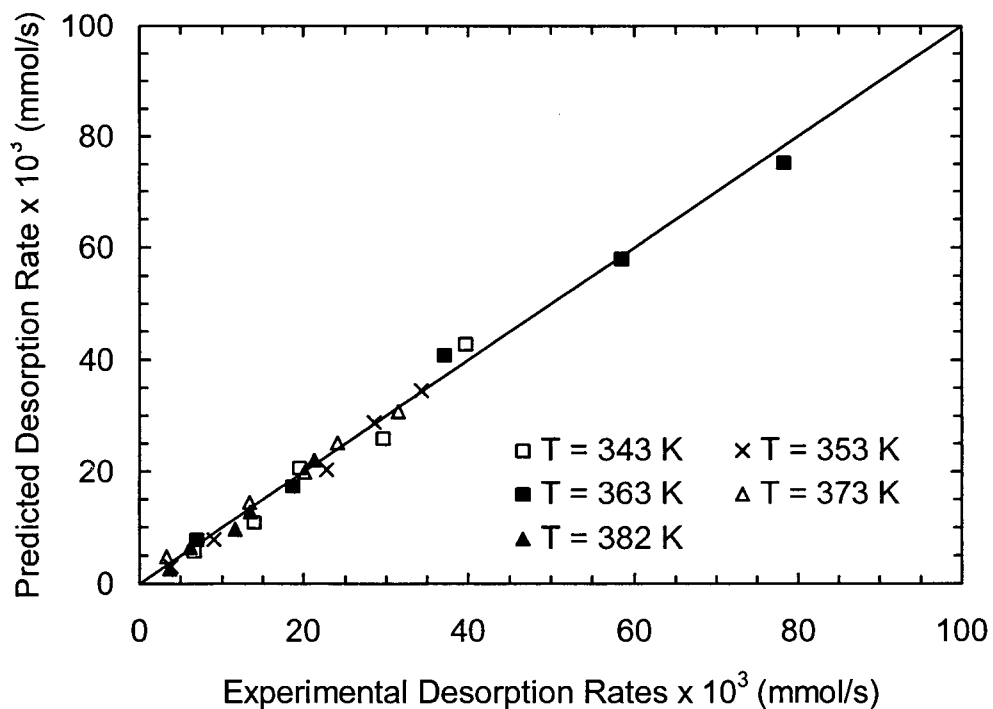


Figure 5.54: Predicted versus experimental desorption rates CO₂-DEA system calculated from the correlation developed in this work

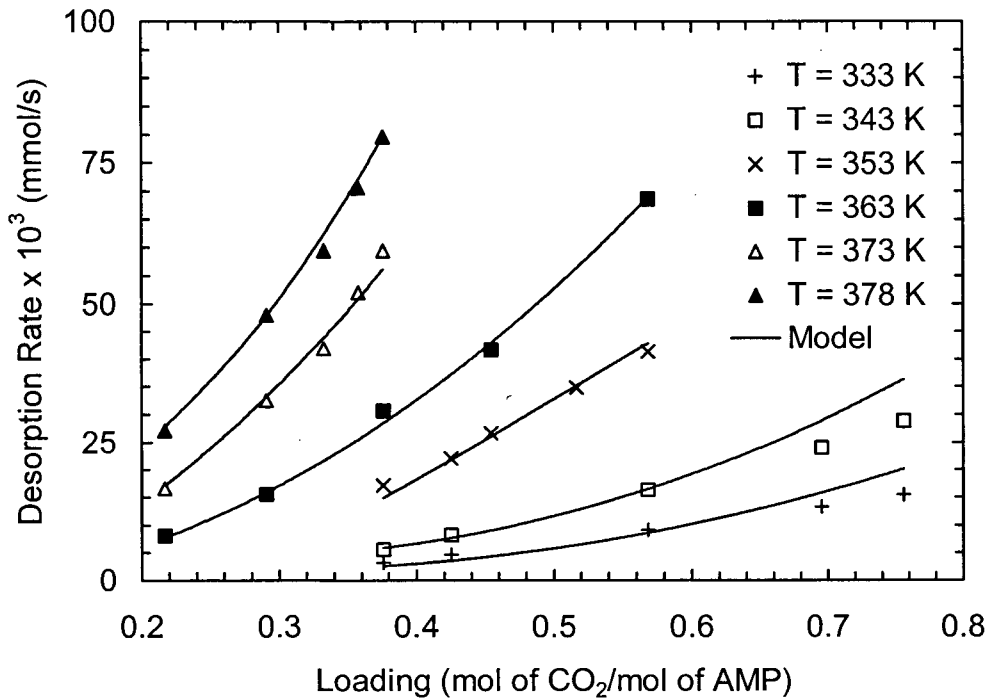


Figure 5.55: Predicted and experimental desorption rates for CO₂-AMP system as a function of temperature and CO₂ loading

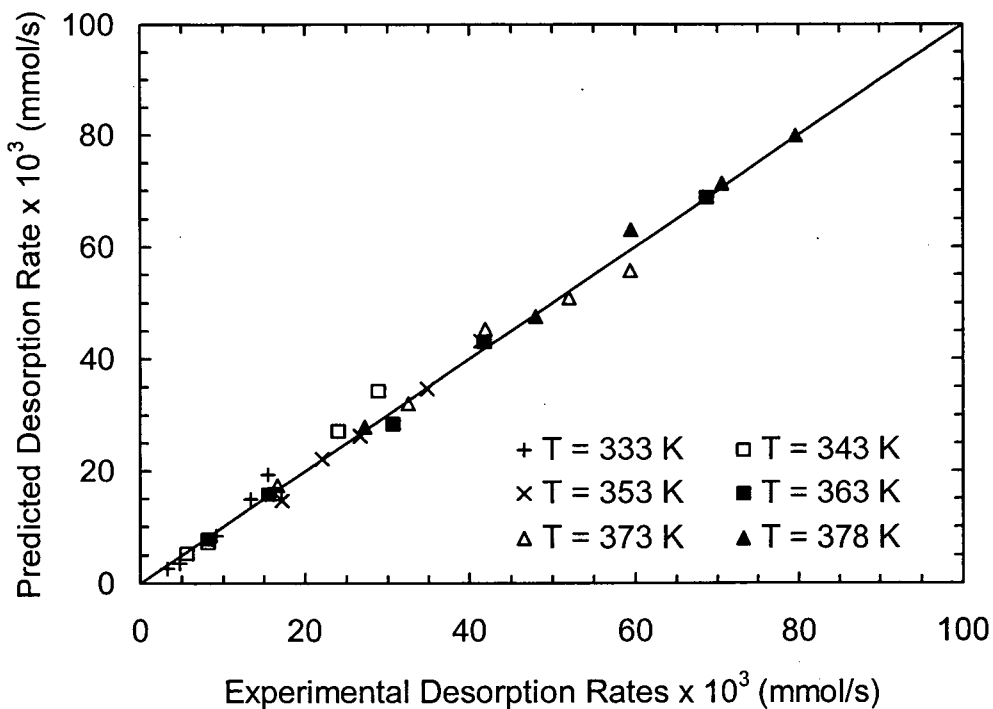


Figure 5.56: Predicted versus experimental desorption rates CO₂-AMP system calculated from the correlation developed in this work

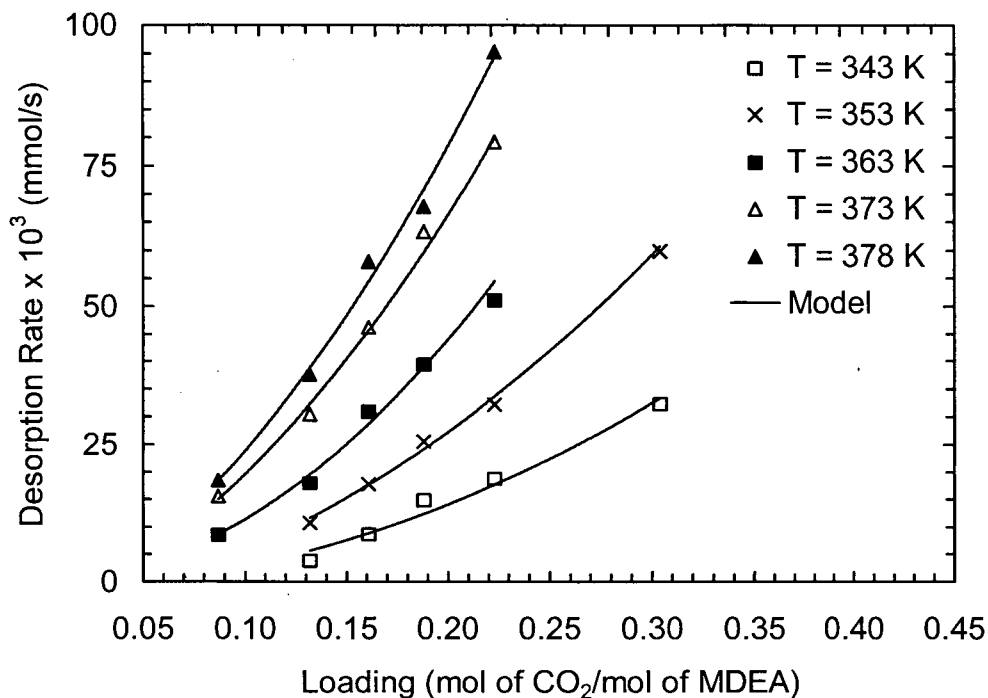


Figure 5.57: Predicted and experimental desorption rates for CO₂-MDEA system as a function of temperature and CO₂ loading

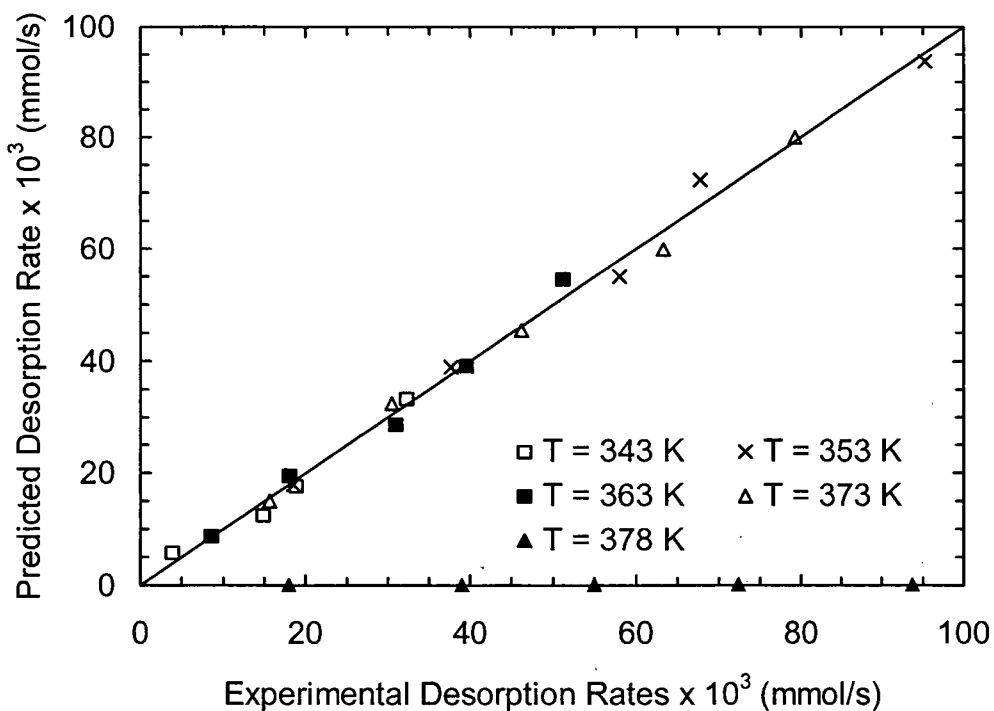


Figure 5.58: Predicted versus experimental desorption rates CO₂-MDEA system calculated from the correlation developed in this work

When the MEA concentration was 20% of the 25 wt% MEA+MDEA blend, the absorption rate increased by about a factor of 5. Similarly, when the DEA concentration was 20% of the 25 wt% DEA+MDEA blend, the absorption rate went up by about a factor of 3. Addition of MEA to 25 wt% AMP blend does improve the absorption capability of AMP, however, this improvement is nominal. No improvement in the CO₂ absorption rate was observed when DEA was added to 25 wt% AMP blends. This is reasonable because the reactivities of these amines are comparable.

The results for MEA+MDEA and DEA+MDEA mixtures are important. With the help of the model, an optimal mixture concentration could be obtained so that the desired amount of CO₂ slip could be achieved in the absorber column. This is significant in natural gas treating applications where one may not want to absorb too much CO₂ in the absorber to avoid unnecessary dilution of the acid gas going to the sulfur recovery plant.

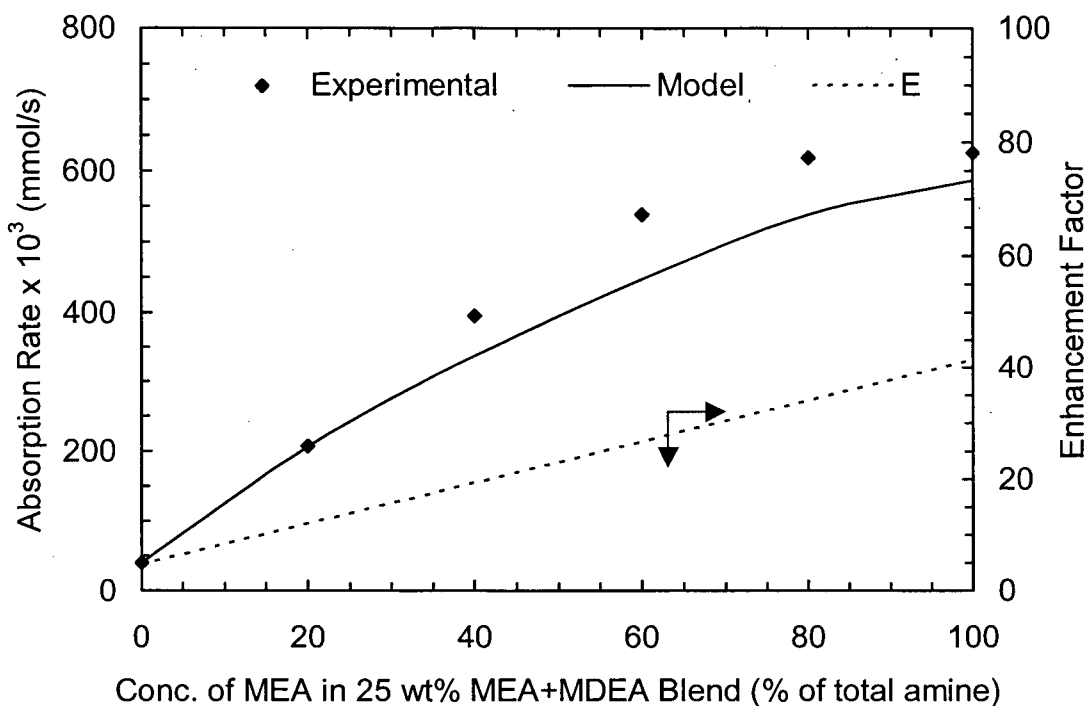


Figure 5.59: Predicted versus experimental absorption rates for CO₂-MEA+MDEA system at 303 K based on the correlation developed in this work ($p_{\text{CO}_2} = 97$ kPa)

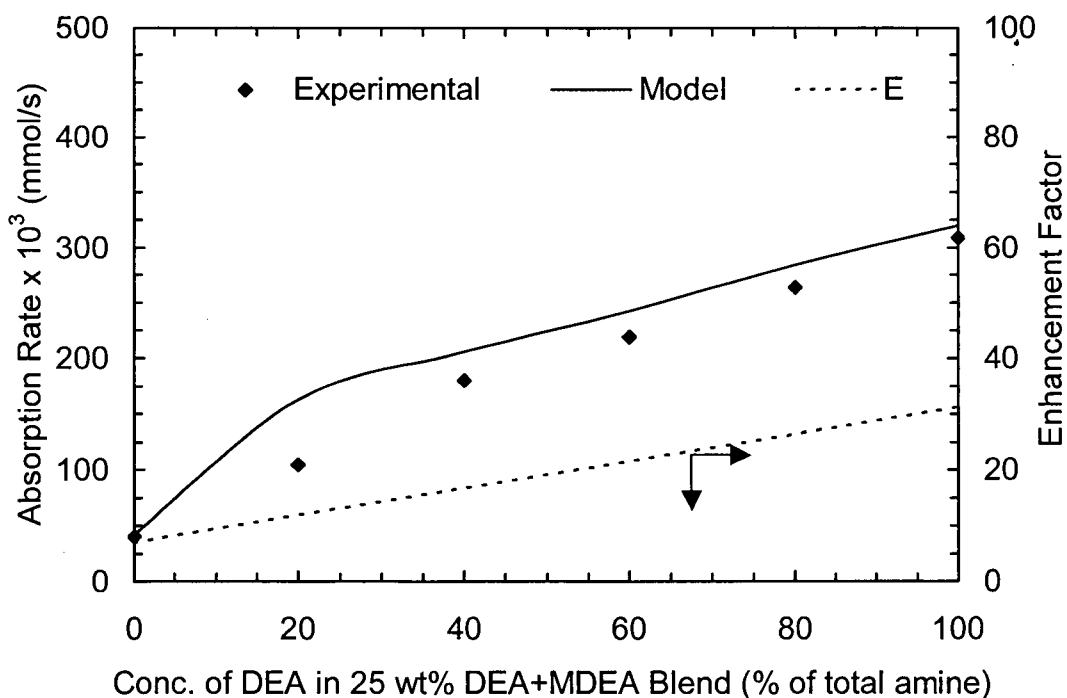


Figure 5.60: Predicted versus experimental absorption rates for CO₂-DEA+MDEA system at 303 K based on the correlation developed in this work ($p_{\text{CO}_2} = 97$ kPa)

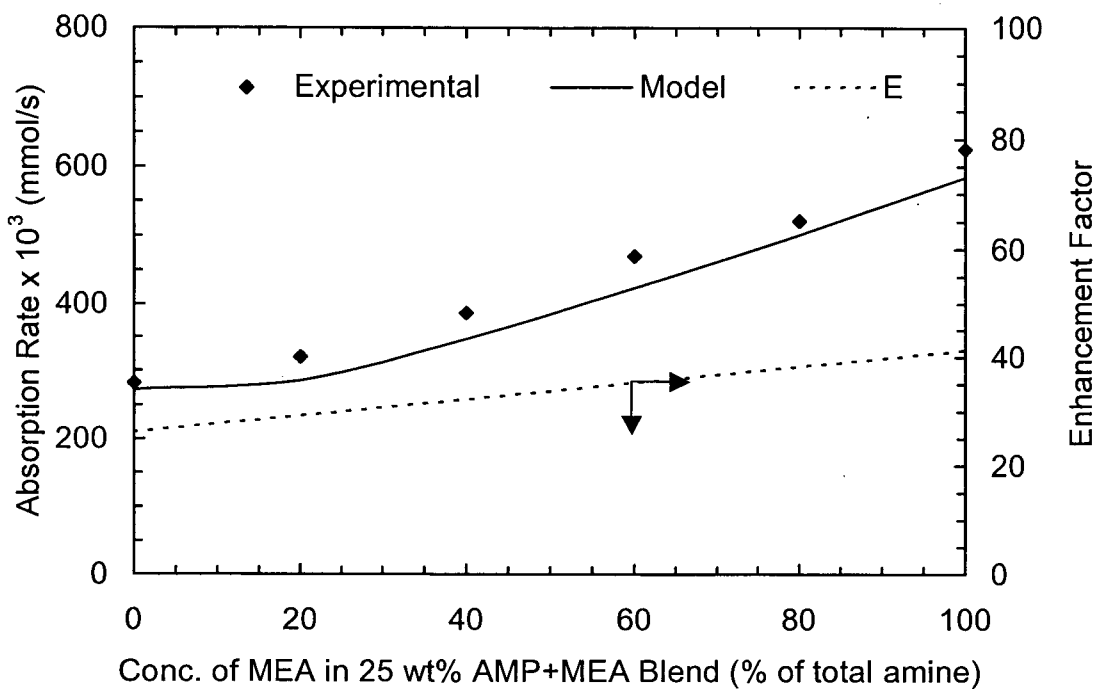


Figure 5.61: Predicted versus experimental absorption rates for CO₂-MEA+AMP system at 303 K based on the correlation developed in this work ($p_{\text{CO}_2} = 97$ kPa)

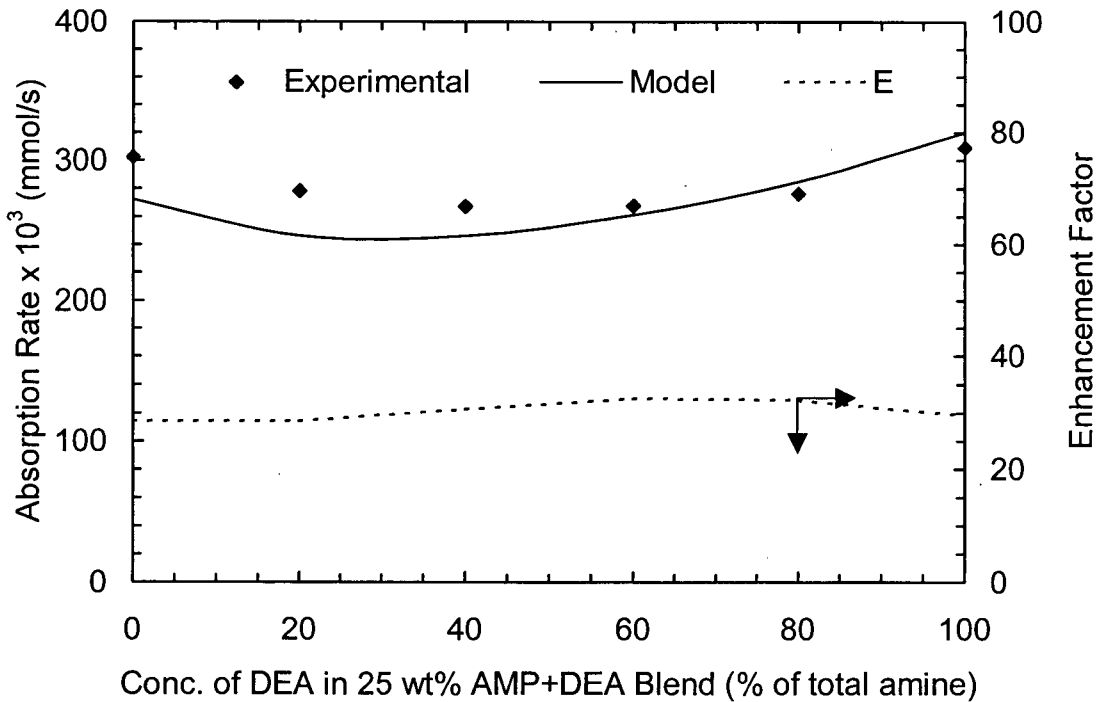


Figure 5.62: Predicted versus experimental absorption rates for CO₂-DEA+AMP system at 303 K based on the correlation developed in this work ($p_{\text{CO}_2} = 97$ kPa)

5.5 Conclusions

The parametric sensitivity analyses indicate that accurate values of CO₂ diffusivity, and the physical solubility of CO₂ given by the Henry's law constant are essential for predicting accurate absorption and desorption rates. An extensive literature search was undertaken and all available property data were compiled. It was found that the values of these parameters at stripping temperatures are not available. A series of experiments involving N₂O-water and N₂-alkanolamine systems were conducted to measure the CO₂ diffusivities and Henry's constants in water using the N₂O analogy. Using data obtained in this work and those available in the literature, correlations were developed that can be used for pure water, as well as for single and binary amine systems covering a wide range of temperatures and amine concentrations. Such correlations are not available in the literature.

The absorption and desorption rates of CO₂ in aqueous solutions of MEA, DEA, MDEA, AMP and their mixtures (MEA+MDEA, MEA+AMP, DEA+MDEA and DEA+AMP) were measured for amine concentrations in the range of 2 to 35 wt%. The absorption experiments were carried out at near atmospheric pressure using pure CO₂ saturated with water at 293 to 323 K with initially unloaded solutions. The desorption experiments were performed at 333 to 383 K for CO₂ loadings between 0.02 to 0.7 moles of CO₂ per mole of amine using humidified N₂ gas as a stripping medium. The data were analyzed using the rigorous diffusion-reaction model developed in this work. The model predicts the experimental results well for all eight different amine systems discussed above.

The results indicate that the theory of absorption with reversible chemical reaction could be applied to predict desorption rates.

The zwitterion mechanism adequately describes the reactions between CO₂ and carbamate-forming amines such as MEA, DEA and AMP under both absorption and desorption conditions. The reactions between CO₂ and aqueous MDEA solutions are best described by a base-catalyzed hydration reaction mechanism.

The kinetic data obtained show that desorption experiments can be used to determine both forward and backward rate constants accurately. The absorption experiments on the other hand could only be used to determine forward rate constants.

For MEA, DEA and AMP, the kinetic data obtained under absorption conditions do not extrapolate well to desorption temperatures. Therefore, kinetic data at higher temperatures should be obtained from desorption experiments. The existing absorption data for the CO₂-MDEA system can be extrapolated to desorption temperatures with reasonable accuracy. This is probably because MDEA is very slow reacting amine and does not form carbamate.

For the blended amine systems, it was found that small additions of MEA or DEA (< 5 wt%) significantly enhance the absorption rates of CO₂ in 25 wt% MDEA solutions. Addition of small quantity of MEA (< 5 wt%) to 25 wt% AMP blend, on the other hand, was found to have very nominal effect on the CO₂ absorption rates of AMP. No improvement in absorption rates was observed when DEA was added to 25 wt% AMP solutions.

CHAPTER 6

INTRODUCTION AND LITERATURE REVIEW

6.1 *Background*

In Part 1 of this thesis, we focused mainly on determining the kinetic parameters for fast-reacting gas-liquid systems by measuring the absorption and desorption of CO₂ in aqueous amine solutions using a novel hemispherical contactor. In Part 2, we present a novel approach to determining kinetic coefficients for extremely slow reactions. The system under consideration is carbon monoxide absorption and its subsequent reactions with aqueous diethanolamine.

The solubility of CO in pure water at 298 K and 1 bar is about 40 times less than that of CO₂ in water and its reactions with aqueous DEA at 298 K are a few orders of magnitude less than those of CO₂ with aqueous DEA. Why is it important then to study the kinetics of such slow reactions in gas treating applications? The answer to this question lies in the fact that, in gas treating units, the solvents are regenerated and reused over extended periods and are exposed to varying temperatures, about 313 K in the absorber and about 393 K in the stripper, reboiler and heat exchangers. Thus, feed gases containing appreciable quantities of CO (e.g. gas mixtures from hydrogen plants and fluid catalytic cracker units) may lead to significant absorption of CO in the amine solution at absorber temperatures that in turn may cause reactions of CO with

hydroxyl ions and DEA to form formate ions and formyl-diethanolamine (DEAF) respectively. These reactions may become particularly important at stripper and reboiler temperatures resulting in significant losses of DEA. The degradation of DEA is costly and it interferes with the proper running of gas treating units. Therefore, it is quite important to understand how CO reacts with aqueous DEA solutions and what major degradation products it forms, so that DEA losses can be quantified and preventive measures taken.

Since the reactions between CO and aqueous DEA solutions are extremely slow, a short contact time apparatus like the hemispherical contactor cannot be used to study the kinetics of these reactions. The best way to monitor the progress of these reactions is to conduct experiments in a batch autoclave reactor of the type described in Chapter 7. Although the subject matter of Part 2 is slightly different from that of Part 1, the modeling and parameter estimation approach is similar. The knowledge acquired during the CO₂ absorption/desorption study was extremely useful in approaching this second problem. This work was funded by Equilon Enterprises LLC, Westhollow Technology Center, Houston Texas and Shell Global Solutions International, Amsterdam, The Netherlands.

6.2 Literature Review

Aqueous solutions of diethanolamine (DEA) are widely used to remove acid gases, such as CO₂ and H₂S, from sour gas mixtures including natural gas, synthesis gas, flue gas and various refinery gas streams. The efficiency of these

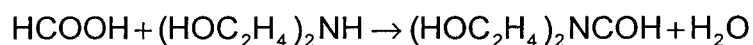
processes largely depends on the performance of the amine solution, which is continuously regenerated and used over extended periods. Although the principal acid gas-amine reactions are reversible, irreversible reactions may also occur resulting in products from which the amine cannot be regenerated under typical operating conditions. This phenomenon is called amine degradation. Numerous papers are available on the degradation of alkanolamines under the conditions typical of gas purification plants. However, most papers focus on alkanolamine degradation due to CO₂, carbon disulfide (CS₂), carbonyl sulfide (COS) and H₂S/CO₂ mixtures. Some sour gas mixtures (e.g. gas mixtures from hydrogen plants and catalytic crackers) contain significant quantities of carbon monoxide (CO) that may also cause amines degradation.

A survey of the literature reveals that CO is a strong reducing agent which is only slightly soluble in water and other physical solvents (< 0.001 mole CO/mole of water at 298 K and CO partial pressure of 101.325 kPa, Kirk Othmer, 1993; Fogg and Gerrad, 1991). An industrially significant process is the reaction of CO with secondary amines to produce formamides. For example, the industrial solvent dimethylformamide (DMF) is manufactured by reacting CO with dimethylamine at 423-428 K and CO partial pressures of 7.5-10.3 MPa in the presence of a catalyst (Duranleau and Lambert, 1985):



Similar reactions occur between alkanolamines and CO to produce formylalkanolamines. For instance, DEA is known to react with CO at high pressure ($p_{\text{CO}} = 6.2$ MPa) and temperature (423 K) over a 5 hour period to

produce $(C_2H_4OH)_2NCOH$, i.e. formyldiethanolamine or DEAF (Lambert and Duranleau, 1985). These conditions are very severe and are not likely to be met in normal refinery and gas plant operations. However, DEAF has been found in DEA solutions used to treat gases from fluid catalytic crackers (FCC units). Koike et al. (1988) have suggested that DEAF is formed by the reaction between formic acid (or formate ions) and DEA according to:



The formic acid (or formate ions) may be present in the amine solution because of the reaction between CO and OH^- ions, and by the hydrolysis of HCN generally present in the FCC dry gas. In another study, Kim et al. (1988) examined the absorption rate of CO into aqueous solutions of potassium carbonate (K_2CO_3), methyldiethanolamine (MDEA) and diethylethanolamine (DEAE) in a stirred tank reactor at 348-398 K and CO partial pressures of 0.75-3.1 MPa. There were no mass transfer limitations and the reaction between CO and hydroxyl ions (OH^-) to produce formate ions ($HCOO^-$) was found to control the rate of absorption. It was concluded that the rate of CO absorption into aqueous solutions of K_2CO_3 , DEAE and MDEA are much slower (by a factor 10^8) than the corresponding rates of CO_2 absorption. The activation energy for the $CO-OH^-$ reaction in aqueous K_2CO_3 solutions was reported to be 122.9 kJ/mol, which is significantly higher than that of 55.4 kJ/mol for the liquid phase CO_2-OH^- reaction reported by Pinsent et al. (1956). This suggests that

temperature is one of the most important parameter for the CO-OH⁻ reaction in basic solutions.

Eickmeyer (1962) gave a brief account of the deactivation of DEA promoted potassium carbonate solutions in commercial gas treating plants. The formates were claimed to result from the very slow reaction between CO and OH⁻ ions. Traces of oxygen were believed to catalyze the reaction.

From the above information it is clear that little is known about the role of CO in amine degradation. Nonetheless, there is clear evidence from refineries using DEA, which suggests that CO is the leading cause for the buildup of DEAF and formate in the gas treating system. As a result, considerable amounts of valuable DEA are lost or rendered ineffective, and efficiency and cost effectiveness are compromised. The purpose of this study was therefore to investigate the mechanism by which CO reacts with aqueous DEA and to estimate the corresponding solubility and kinetic parameters over a range of temperatures and CO partial pressures, so that one could quantify DEA losses and take preventive measures.

6.3 Objectives

The specific objectives of this part of the work were to: (a) identify the dominant DEAF formation route, (b) estimate the kinetic rate coefficients and (c) determine the physical solubility of CO in aqueous DEA solutions. To accomplish these objectives, a reaction mechanism was proposed and a mathematical model was developed. The model consists of a set of differential and algebraic

equations, which describe gas absorption with slow chemical reaction in a well-mixed batch reactor. The reason for using a batch reactor was due to the low CO solubility and its slow chemical reaction with aqueous DEA solutions observed in the series of exploratory experiments described in Chapter 7.

CHAPTER 7

EXPERIMENTAL APPARATUS AND EXPLORATORY EXPERIMENTS

This chapter describes the experimental apparatus for studying the kinetics of CO-induced degradation of aqueous diethanolamine as well as some exploratory results obtained using this equipment.

7.1 *Experimental Apparatus and Procedure*

All experiments presented in this study were carried out in a 660 mL stainless steel autoclave reactor (Model 4560, Parr Instrument Co. Moline, IL). The experimental setup, which mainly consists of a gas bomb and an autoclave, is shown in Figure 7.1. The autoclave was equipped with a variable speed magnetic stirrer with three impellers mounted at 4, 10 and 16 cm from the bottom of a common shaft (20 cm long), a heating jacket controlled by a PID temperature controller (Omega CN76000, Omega Eng. Co., Stamford, CT), gas and liquid sample lines, pressure transducer and a thermocouple inserted into the liquid phase. To ensure proper mixing of the gas and liquid phases, the liquid volume was selected such that the top impeller was always in the gas phase and the bottom two impellers were submerged in the liquid phase. The autoclave could be operated between 283-623 K and at pressures up to 13.8 MPa. The gas bomb was made of stainless steel and could be pressurized up to 20 MPa.

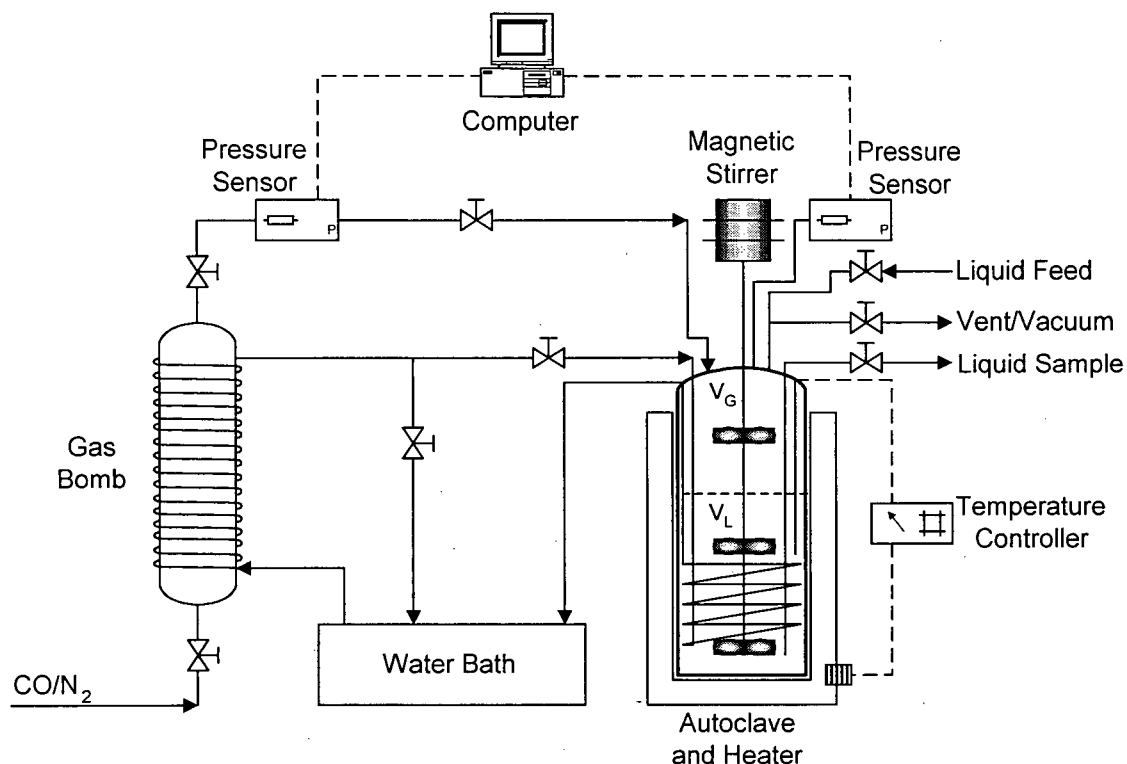


Figure 7.1: Schematic diagram of the experimental setup

For data analysis it is essential to know the precise values of the internal working volumes of the gas bomb and autoclave together with their associated piping and fittings. The volume of the gas-bomb assembly was measured by difference in weights of the assemblage when filled with water and empty. A total of 5 measurements were performed and the average volume was found to be 511.28 mL. The internal working volume of the autoclave assembly was measured by admitting a known amount of nitrogen gas from the gas bomb to the autoclave. The pressure and temperature of the autoclave were recorded and the volume was calculated by dividing the amount of gas in the autoclave by its density at that temperature and pressure. A total of 15 measurements were made and the average volume was found to be 616.7 mL.

The pressures in the autoclave and gas bomb were measured by means of pressure transducers (Omega PX303). These transducers were re-calibrated by a dead weight meter. In all experiments, the pressure changes in the autoclave and the gas bomb were recorded by a computerized data logging system.

The DEA and MDEA were obtained from Sigma-Aldrich with a lot purity greater than 99 wt%. The CO and N₂ had a purity of 99.9% and were obtained from Praxair. Aqueous solutions of DEA and MDEA were prepared by weight using distilled-deionized water.

In a typical absorption experiment, the CO was fed from a supply cylinder into the gas bomb and kept there to attain constant temperature and pressure. The autoclave was then filled with about 200-300 mL of aqueous amine solution, sealed and evacuated to a pressure of less than 7 kPa to ensure the removal of extraneous gases. While stirring the solution (at 1,380 rpm or 80% of the maximum speed), its temperature was raised and maintained at the desired value by means of the water bath or the heating jacket controlled by a PID type temperature controller. The solution pressure was noted and identified as its vapor pressure. CO was then admitted from the gas bomb and its pressure change recorded. The subsequent change in autoclave pressure was recorded continuously as a function of time. At the end of each experiment, liquid samples were taken and analyzed. In some experiments, liquid samples were also withdrawn periodically during the runs. The analytical techniques to determine

the concentration of the main reaction products (formate ions and DEAF) are given in Appendix I.

Initially, exploratory experiments were made to identify the degradation products and evaluate the trends of CO absorption at different temperatures. The primary experiments, on the other hand, were used to establish the reaction kinetics for the CO-DEA-H₂O system and estimate the kinetic and solubility parameters. The experimental procedure for both experiments was essentially the same and as described above. The main difference was that, in all primary experiments, the stirrer speed was fixed at 1,035 rpm (60% of the maximum speed) as opposed to 1,380 rpm speed used in the exploratory experiments. Also, in the primary experiments, the liquid volume was always greater than 250 mL to ensure a well-defined gas-liquid interface. It should be noted however that this is not a requirement as long as the volumetric mass transfers coefficient ($k_L a$) can be determined accurately.

7.2 Exploratory Experiments

7.2.1 CO Absorption in Aqueous DEA Solutions

To understand the effect of temperature on CO loading in aqueous DEA solutions, pure CO was absorbed in a 30 wt% DEA solutions for a period of 12 hours. The initial CO partial pressure (p_{CO}^0) was kept at 760-990 kPa and the temperature was varied from 313-403 K. The variation in CO partial pressure was due to the vapor pressure of water at different temperatures. Therefore, the lower value of p_{CO}^0 corresponded to a higher temperature and vice versa. The

results of these experiments are plotted in Figure 7.2. The CO loading represents, the total amount of CO in the solution, which includes CO in molecular form and CO that has reacted with water and DEA. The CO loading at a particular time was calculated as follow:

$$\text{CO loading (mol/mol)} = \frac{n_{\text{CO}}^{\text{total}} - n_{\text{CO}}^t}{n_{\text{DEA}}}$$

where $n_{\text{CO}}^{\text{total}}$ represents the total number of moles of CO transferred from the gas bomb to the autoclave, n_{CO}^t represents the number of moles of CO in the head space of the autoclave at any given time t and n_{DEA} represents the total number of moles of DEA in the solution. The quantities $n_{\text{CO}}^{\text{total}}$ and n_{CO}^t were calculated using the Redlich-Kwong-Soave equation of state.

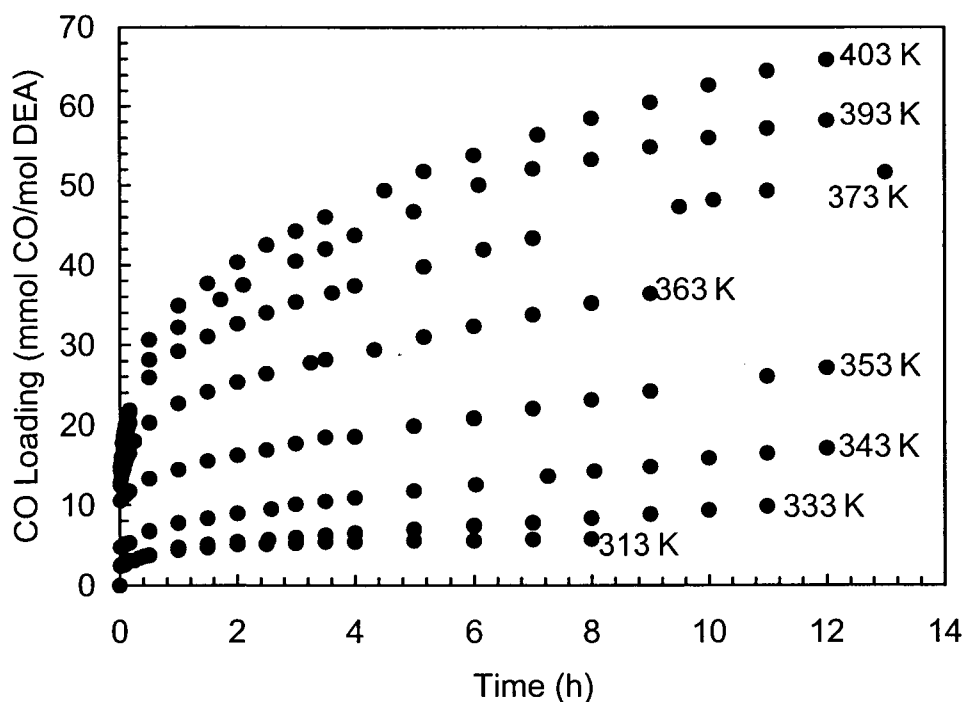


Figure 7.2: CO loading as a function of time and temperature (DEA= 30 wt%, $p_{\text{CO}}^0 = 760\text{-}990$ kPa)

As can be seen from Figure 7.2, the CO loading increases with temperature and it does not reach equilibrium even after 12 hours especially at temperatures higher than 333 K. This suggests that CO physically absorbs in and then chemically reacts with aqueous DEA solutions. The continuous increase in CO loading at higher temperatures indicates that the reactions may be irreversible. These results also show that at lower temperatures (≤ 313 K), the CO loading is mainly due to physical solubility whereas at high temperatures (≥ 333 K), chemical reactions become important and the loading is predominantly due to the reaction products.

7.2.2 Material Balance

At the end of each experiment presented in Figure 7.2, liquid samples were withdrawn and the main reaction products were identified according to the procedure given in Appendix I. The analyses showed that, in all cases where reaction was significant, DEAF and formate ions were the only reaction products. The presence of DEAF was confirmed by analyzing the liquid sample using GC/MS and comparing the results with those reported by Koike et al. (1988).

To ensure that DEAF and formate were the only principal reaction products, material balances were made for experiments in which CO was brought in contact with 30 wt% aqueous DEA solutions at 353, 393 and 413 K at initial CO partial pressures ranging from 650 to 850 kPa. The final solutions were analyzed for DEAF and formate according to the procedure given in Appendix I. Table 7.1 gives the corresponding CO material balances. The deviations

between the initial and final amounts of CO are less than 15% and fall well within the range of experimental error. No additional degradation product was observed from the analysis of liquid samples using GC and GC-MS.

Table 7.1: Overall CO balance as a function of temperature for CO absorption in 30 wt% aqueous DEA solutions

Temperature (K)		353	393	413
Initial Conditions	Solution (g)	199.16	199.14	198.99
	p_{CO} (kPa) after 5 min	852	654	711
	Initial CO introduced (g)	3.368	2.394	2.642
Final Conditions	Time (h)	48	5	23
	p_{CO} (kPa)	661	435	123
	CO loaded (g)	0.827	0.842	2.204
	Formate (wt%)	0.224	0.267	1.106
	CO in formate (g)	0.270	0.324	1.340
	DEAF (wt%)	1.061	0.811	1.292
	CO in DEAF (g)	0.445	0.340	0.541
	Molecular CO in solution ² (g)	0.132	0.091	0.026
	Final CO in all forms (g)	0.847	0.757	1.907
Deviation (%) ¹		-2.4	+10.1	+13.5

¹Defined as $100 \times (\text{CO loaded} - \text{Final CO in all forms}) / \text{CO loaded}$

²Based on Henry's constant values obtained by N₂-analogy

Table 7.2: Formate and DEAF concentrations of solutions resulting from exposing pure DEA to CO for 5 hours at $p_{CO}^{\circ} = 690$ kPa

T (K)	Formate (wt%)	DEAF (wt%)
313	0.0	0.0
393	0.0	2.4

7.2.3 CO Absorption in Pure DEA

To identify the pathways of the CO-DEA reactions, experiments were undertaken where CO was absorbed in 99.8% pure DEA solution at 313 and 393 K for 5 hours at an initial CO partial pressure of 690 kPa. At the end of each of these experiments, liquid samples were taken and analyzed by IC for DEAF and formate ions. The results of this analysis are presented in Table 7.2, which shows that at low temperature (313 K) neither DEAF nor formate ions are formed, whereas at higher temperatures (>393 K) no formate was detected although a significant amount of DEAF was formed. This suggests that CO may react directly with DEA to form DEAF similar to the industrial process for the manufacture of DMF (Duranleau and Lambert, 1985). The absence of formate ions in the sample solution also indicates that water plays an important role for the buildup of formate in the system.

7.3 Proposed Reaction Mechanism

The exploratory experiments show that CO reacts with aqueous DEA solutions to form formate ions and DEAF. These experiments also indicate that two pathways may form the DEAF: (i) via direct insertion of CO into DEA and/or (ii) via formate formation. Based on these results, we propose that the CO reacts with aqueous DEA solution according to the following reaction mechanism:

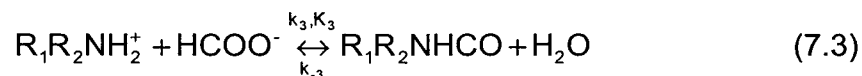
Formate Formation:



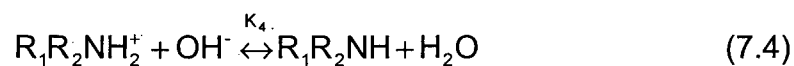
Direct Insertion:



DEA-Formate Reaction:



DEA Protonation:



Water Dissociation:



where $\text{R}_1\text{R}_2\text{NH}$ and $\text{R}_1\text{R}_2\text{NHCO}$ denote DEA and DEAF, respectively. Note that for DEA, $\text{R}_1 = \text{R}_2 = -\text{CH}_2\text{CH}_2\text{OH}$.

The validation of the proposed reaction mechanism and the determination of the unknown kinetic coefficients are presented in Chapters 8 and 9.

CHAPTER 8

MATHEMATICAL MODEL

This chapter presents the mathematical model for CO absorption in aqueous diethanolamine solution in a batch reactor. This model was used to validate the proposed reaction mechanism and to estimate the rate constants with the non-linear regression package GREG.

8.1 Reaction Mechanism

As proposed in Chapter 7, when CO is absorbed into an aqueous DEA solution, the following reactions may occur:

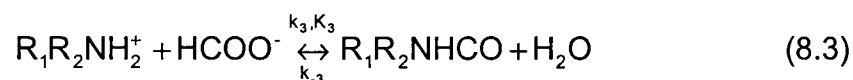
Formate Formation:



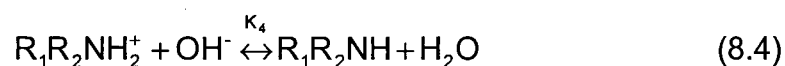
Direct Insertion:



DEA-Formate Reaction:



DEA Protonation:



Water Dissociation:



where R_1R_2NH and R_1R_2NHCO denote DEA and DEAF, respectively. Also, for DEA, $R_1 = R_2 = -CH_2CH_2OH$.

8.2 Reaction Rates

For convenience, the chemical species in reactions (8.1) to (8.5) are renamed as follows:

$$\begin{aligned} C_1 &= CO_{liq}, & C_2 &= R_1R_2NH, & C_3 &= R_1R_2NH_2^+, & C_4 &= R_1R_2NHCO \\ C_5 &= HCOO^-, & C_6 &= OH^-, & C_7 &= H_3O^+, & C_8 &= H_2O \end{aligned} \quad (8.6)$$

Reactions (8.1) and (8.2) are considered to be irreversible and to proceed at finite rates. The latter are given by the following expressions:

$$r_1 = -k_1 C_1 C_6 \quad (8.7)$$

$$r_2 = -k_2 C_1 C_2 \quad (8.8)$$

Based on the experimental evidence presented below, reaction (8.3) was considered to be reversible with the overall rate given by:

$$r_3 = -k_3 C_3 C_5 + k_{-3} C_4 \quad (8.9)$$

Reactions (8.4) and (8.5) are regarded as reversible equilibrium reactions since they involve only proton transfers.

8.3 Mathematical Model

The mathematical model is based on the concept of gas absorption with slow chemical reaction in a well-mixed batch reactor as shown in Figure 8.1. The following equations govern the mass transfer with chemical reaction in a batch autoclave (liquid volume = V_L , gas volume = V_G):

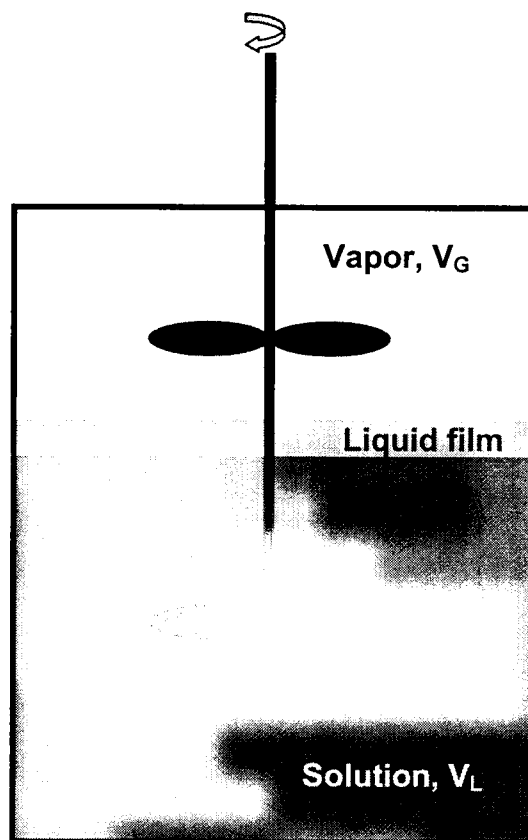


Figure 8.1: Schematic diagram of chemical reaction autoclave

Gas Phase CO Balance:

$$\frac{dp_{\text{CO}}}{dt} = -\frac{RT}{V_G} V_L E k_L a \left(\frac{p_{\text{CO}}}{H_{\text{CO-DEA}}} - C_1 \right) \quad (8.10)$$

Liquid Phase CO Balance:

$$\frac{dC_1}{dt} = E k_L a \left(\frac{p_{\text{CO}}}{H_{\text{CO-DEA}}} - C_1 \right) + r_1 + r_2 \quad (8.11)$$

DEAF Balance:

$$\frac{dC_4}{dt} = -r_3 - r_2 \quad (8.12)$$

Overall CO Balance:

$$\frac{V_G}{RT} \frac{dp_{\text{CO}}}{dt} + V_L \frac{dC_1}{dt} + V_L \frac{dC_4}{dt} + V_L \frac{dC_5}{dt} = 0 \quad (8.13)$$

Total DEA Balance:

$$\frac{dC_2}{dt} + \frac{dC_3}{dt} + \frac{dC_4}{dt} = 0 \quad (8.14)$$

Electron Neutrality Balance:

$$\frac{dC_3}{dt} + \frac{dC_7}{dt} - \frac{dC_5}{dt} - \frac{dC_6}{dt} = 0 \quad (8.15)$$

DEA Protonation:

$$K_4 = \frac{C_2}{C_3 C_6} \quad (8.16)$$

Water Dissociation:

$$K_5 = C_6 C_7 \quad (8.17)$$

The model equations (8.10)-(8.17) were derived based on the following assumptions:

- The concentration of dissolved (molecular) CO at the gas-liquid interface corresponds to the physical solubility as determined by Henry's Law (i.e., $p_{CO} = HC_1$).
- Both the gas and liquid phases are well mixed.
- The gas phase resistance to mass transfer is negligible.

The last assumption follows because pure CO was used. Also, this assumption was verified experimentally and by simulation. Consequently, there are eight ordinary differential and algebraic equations (equations 8.10-8.17) with eight unknown chemical species. The equations must be solved subject to the following initial conditions:

$$p_{CO} = p_{CO}^0 \quad \text{and} \quad C_i = C_i^0 \quad \text{for } i=1-7 \quad (8.18)$$

For the present experiments, the initial CO loading of the DEA solution is zero. Therefore, at $t=0$, $C_1^0 = C_4^0 = C_5^0 = 0$. The values of C_2^0 , C_3^0 , C_6^0 and C_7^0 can be obtained by solving the equilibrium equations shown below. When the CO loading is zero, it follows that:

Overall DEA Balance:

$$C_2^0 + C_3^0 = [R_1R_2NH]_{\text{initial}} \quad (8.19)$$

Electron Neutrality Balance:

$$C_3^0 + C_7^0 - C_6^0 = 0 \quad (8.20)$$

DEA Protonation:

$$K_4 = \frac{C_2^0}{C_3^0 C_6^0} \quad (8.21)$$

Water Dissociation:

$$K_5 = C_6^0 C_7^0 \quad (8.22)$$

For a given initial DEA concentration, the concentrations C_2^0 , C_3^0 , C_6^0 and C_7^0 can be calculated by solving equations (8.19) to (8.22) simultaneously.

8.4 Model Parameters

The parameters needed to solve the model equations (8.10) to (8.17) are listed in Table 8.1 and their determination is outlined below. Since the present reactions are very slow, one can safely assume that the enhancement factor (E) for the CO-DEA-H₂O system is unity.

Olofsson and Hepler (1975) reported the following correlation for the water dissociation constant (K_5) in the temperature range of 293-573 K:

$$\log_{10}(K_5) = 8909.483 - \frac{142613.6}{T} - 4229.195 \log_{10}(T) + 9.7384T - 0.0129638T^2 + 1.15068 \times 10^{-5} T^3 - 4.602 \times 10^{-9} T^4 \quad (8.23)$$

Bower et al. (1962) correlated their data for ($K_4 K_5$) over the temperature range of 273-323 K according to the following equation:

$$\log_{10}(K_4 K_5) = -4.0302 - \frac{1830.15}{T} + 0.0043261T \quad (8.24)$$

Table 8.1: Model parameters

Param.	Definition	Remarks
E	Enhancement factor	For slow reactions, $E = 1$
K_4	DEA protonation constant	Bower et al. (1962)
K_5	Water dissociation constant	Olofsson and Hepler(1975)
$k_L a$	Mass transfer coefficient	To be estimated
$H_{\text{CO-DEA}}$	Henry's constant for CO	To be estimated
k_1	Rate constant for Rxn. (1)	To be estimated
k_2	Rate constant for Rxn. (2)	To be estimated
k_3	Rate constant for Rxn. (3)	To be estimated
k_{-3}	Rate constant for reverse Rxn. (3)	To be estimated

The volumetric mass transfer coefficient ($k_L a$), Henry's constant of CO in aqueous DEA solution ($H_{\text{CO-DEA}}$) and the reaction rate constants (k_1 , k_2 , k_3 and k_3) were obtained as part of this work. In addition to the parameters listed in Table 8.1, the densities and viscosities of the aqueous amine solutions must also be known as a function of temperature. These properties were obtained from the correlations given by Hsu and Li (1997a, b).

8.5 Parameter Estimation

The model was solved using an algorithm called DDASAC (Caracotsios and Stewart, 1985). DDASAC is an extension of DASSL (Petzold, 1983; Brenan et al., 1989), which uses an implicit integrator for non-linear initial value problems containing ordinary differential equations with or without algebraic equations. The parameter estimation was carried out using the software package GREG (Stewart et al. 1992).

The six unknown parameters ($k_L a$, H_{CO-DEA} , k_1 , k_2 , k_3 , k_{-3}) were determined by minimizing the following objective function:

$$S(\mathbf{k}) = \sum_{i=1}^N [\hat{y}_i - y(\mathbf{k})]^T Q_i [\hat{y}_i - y(\mathbf{k})] \quad (8.25)$$

where $\mathbf{k} = (k_L a, H_{CO-DEA}, k_1, k_2, k_3, k_{-3})^T$ is the unknown parameter vector, \hat{y}_i is the measured value of the state variable (in the present case, it is the partial pressure of CO) and $y(\mathbf{k})$ is the calculated value of the state variable which is obtained by solving the model equations (8.10) to (8.17) for some assumed values of $k_L a, H_{CO-DEA}, k_1, k_2, k_3, k_{-3}$. N denotes the number of experimental data and Q is the weighting matrix. For least squares estimation, Q is taken as the identity matrix. Note that not all six parameters were estimated simultaneously. First, $k_L a$ and k_3 and k_{-3} were estimated from the data obtained in a separate series of experiments. Then using these known values $k_L a, k_3$ and k_{-3} , the rest of the unknown parameters (k_1, k_2 , and H_{CO-DEA}) were estimated. However, the same methodology was used in all three cases. The optimization was carried out using GREG (Stewart et al. 1992).

CHAPTER 9

RESULTS AND DISCUSSION

This chapter presents the results and main conclusions from the experimental and theoretical studies on the kinetics of CO-induced degradation of aqueous diethanolamine.

9.1 Absorption and Degradation in CO-DEA System

9.1.1 Determination of $k_L a$

In order to obtain accurate CO partial pressure profiles in the batch absorption experiments using the reaction model given in Chapter 8, it is essential to know the values of $k_L a$ in each case. A series of experiments were conducted where pure N₂ was absorbed into 30 wt% aqueous DEA solutions over the temperature range of 283-413 K in a batch autoclave. The experimental setup was exactly the same as that shown in Figure 6.1. In a typical experiment of this series, about 300 mL of a 30 wt% aqueous DEA solution were fed into the autoclave, a vacuum was drawn and the liquid solution along with the gas bomb containing pure N₂ was brought to the desired temperature. Once this temperature was reached, a known amount of pure N₂ was released from the gas bomb to the autoclave and the total pressure in the autoclave was recorded with time. Each experiment was run for about 105 minutes, which was found to be sufficient to completely saturate the liquid with nitrogen. To study the effect of

agitation on $k_L a$, each experiment was performed at the two stirrer speeds of 1,035 and 1,550 rpm.

Since N_2 does not react with aqueous DEA, the data can be analyzed using a physical absorption model, which is obtained by setting the reaction rates in the reaction model to zero. Physical absorption in a batch autoclave (see Figure 8.3) can then be represented by the following equations:

Gas Phase N_2 Balance

$$\frac{dp_{N_2}}{dt} = -\frac{RT}{V_G} V_L k_L a \left(\frac{p_{N_2}}{H_{N_2-DEA}} - C_{N_2} \right) \quad (9.1)$$

Liquid Phase N_2 Balance

$$\frac{dC_{N_2}}{dt} = k_L a \left(\frac{p_{N_2}}{H_{N_2-DEA}} - C_{N_2} \right) \quad (9.2)$$

Initial Conditions

$$\text{at } t=0 \quad p_{N_2} = p_{N_2}^0 \quad \text{and} \quad C_{N_2} = 0 \quad (9.3)$$

In this model, there are two ordinary differential equations and two unknown parameters ($k_L a$ and H_{N_2-DEA}), which can be determined from the partial pressure (p_{N_2}) versus time data by applying the parameter estimation technique described earlier.

Figures 9.1 and 9.2 show the experimental and predicted N_2 partial pressures using the optimized $k_L a$ and H_{N_2-DEA} values at 1,035 rpm and 283-413 K. An excellent agreement between experimental and fitted values demonstrates the accuracy of the experimental procedure. The same set of experiments was

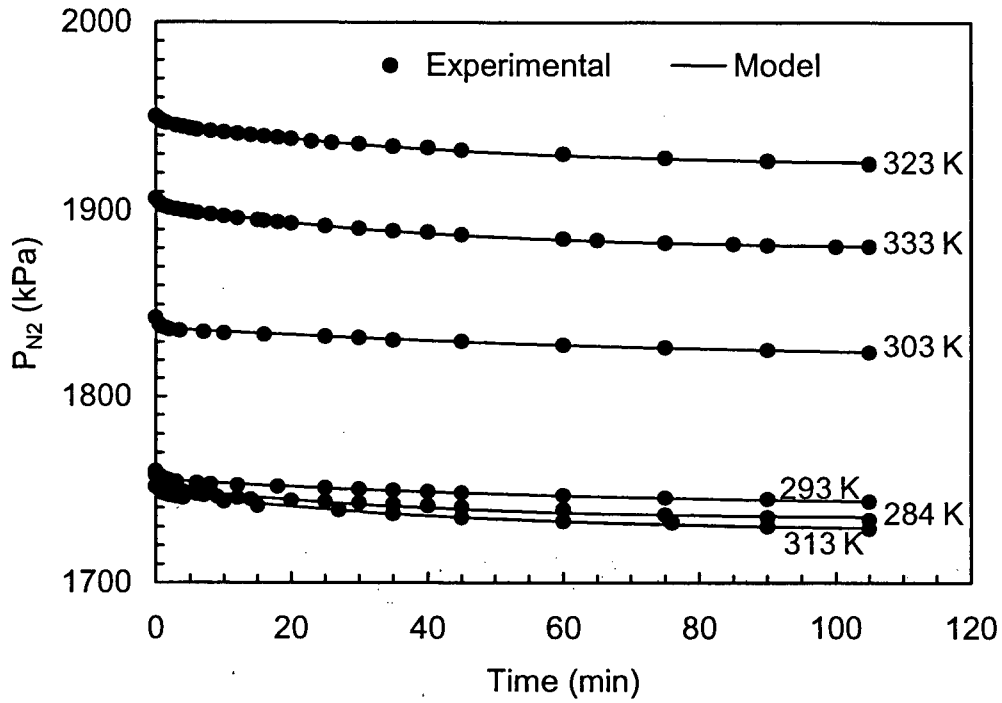


Figure 9.1: Nitrogen absorption in 30 wt% aqueous DEA solution at 1050 rpm and 284-333 K

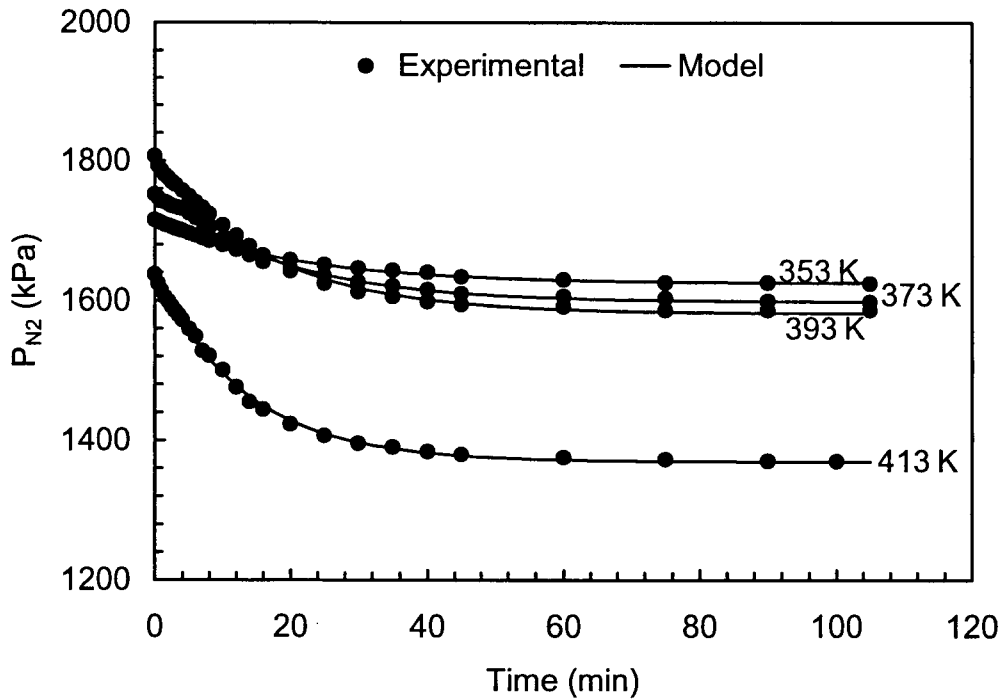


Figure 9.2: Nitrogen absorption in 30 wt% aqueous DEA solution at 1050 rpm and 353-413 K

done at 1,550 rpm and similar agreement was found. The estimates of $k_L a$ so obtained were correlated by the following equation:

$$k_L a = 0.297 \frac{D_{N_2}}{d_{imp}} Re^{0.77} Sc^{0.5} \quad (9.4)$$

where the Reynolds number (Re) and Schmidt number (Sc) are defined as follows:

$$Re = \frac{Nd_{imp}^2 \rho_L}{\mu_L} \quad \text{and} \quad Sc = \frac{\mu_L}{\rho_L D_{N_2}} \quad (9.5)$$

The impeller diameter (d_{imp}) was 3.1 cm and the diffusivity of N_2 in aqueous DEA solution (D_{N_2}) was calculated using Wilke and Chang's correlation given in Perry et al. (1963). Note that the exponent of Sc in equation (9.4) was assumed not fitted. This value is the same as reported previously (Critchfield and Rochelle, 1988; Haimour et al, 1985, Hikita et al., 1975; Danckwerts, 1970). A plot of the predicted and estimated $k_L a$ values is shown in Figure 9.3. The agreement between the measured and correlated $k_L a$ values at both stirrer speeds is within $\pm 25\%$. Consequently, equation (9.4) can be used to calculate $k_L a$ in the reaction model.

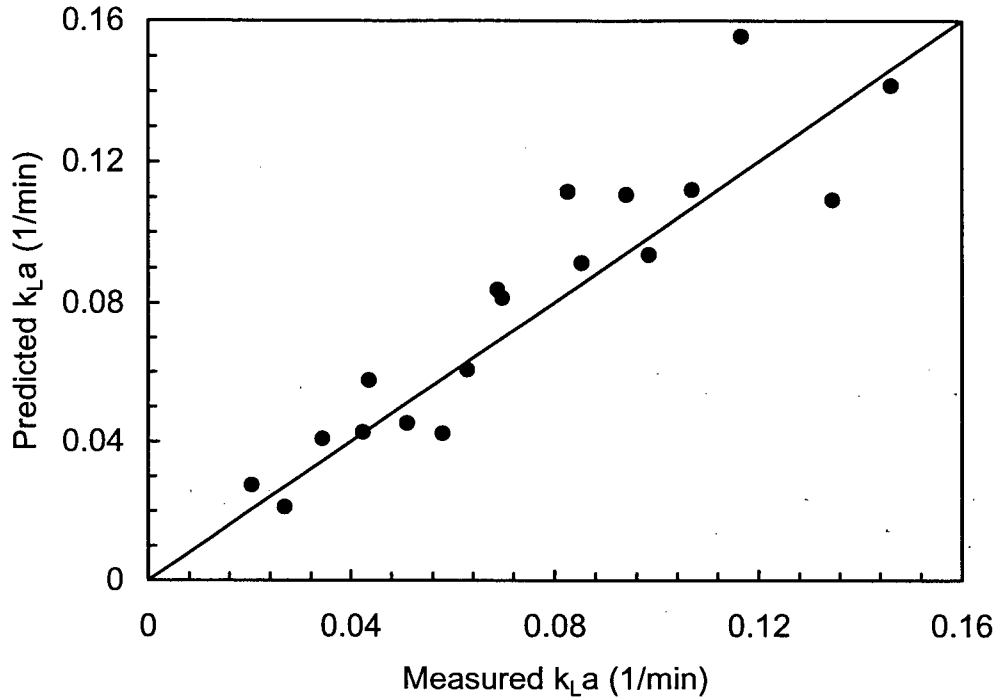


Figure 9.3: Measured and predicted volumetric mass transfer coefficient

9.1.2 Determination of $H_{\text{CO-DEA}}$ by Nitrogen Analogy

The second unknown parameter in the reaction model is the Henry's constant of CO in aqueous DEA solutions ($H_{\text{CO-DEA}}$). Since CO reacts with aqueous DEA, it is not possible to measure $H_{\text{CO-DEA}}$ by conventional techniques used for physical absorption and a new technique called the "N₂-Analogy" method was developed. This technique is based on the same principal as the "N₂O-Analogy" approach used previously for measuring the Henry's constants of CO₂ in alkanolamine solutions (Laddha et al., 1981). Like CO₂ and N₂O, the molecular masses of CO and N₂ are nearly equal and the ratio of their Henry's constants in water is about 0.70 ± 0.02 over the temperature range of 273-413 K (Fogg and Gerrard, 1991; Perry et al., 1963). If it is assumed that this ratio

remains the same even in aqueous amine solutions, then $H_{\text{CO-DEA}}$ can be calculated from the following equation:

$$\frac{H_{\text{CO-H}_2\text{O}}}{H_{\text{N}_2\text{-H}_2\text{O}}} = \frac{H_{\text{CO-DEA}}}{H_{\text{N}_2\text{-DEA}}} \quad (9.6)$$

The values of $H_{\text{CO-H}_2\text{O}}$ and $H_{\text{N}_2\text{-H}_2\text{O}}$ were obtained from the correlations given in Fogg and Gerrald (1991) and the $H_{\text{N}_2\text{-DEA}}$ data were measured in this work using the procedure described in the previous section. The $H_{\text{CO-DEA}}$ values obtained by using the N_2 -Analogy (equations 9.6) are listed in Table 9.1. A comparison of the values of Henry's constant of nitrogen in water and in aqueous DEA solution indicates that nitrogen is several times more soluble in aqueous DEA solutions than in water and its solubility increases with temperature above 313 K. This trend is not surprising because the literature data on CO and N_2 solubility (see Table 9.2) show that the solubility of these gases in pure organic solvents is 10 to 100 times higher than that in pure water, and in almost all cases, it increases with temperature above 298 K. The solubility measurements presented here were repeated at least three times and the reproducibility was within $\pm 3\%$. Due to our concern about the accuracy of the $H_{\text{CO-DEA}}$ values obtained from the N_2 -Analogy, we did not use them in the reaction model to estimate the rate constant k_1 and k_2 . Instead, we considered $H_{\text{CO-DEA}}$ as one of the unknown parameters and found it directly from the reaction model (see section on determination of k_1 , k_2 and $H_{\text{CO-DEA}}$). As indicated later, the agreement between the $H_{\text{CO-DEA}}$ values obtained

using both methods is fairly good. This suggests that our measurements of $H_{\text{CO-DEA}}$ by the N_2 -Analogy method are fairly accurate.

Table 9.1: Henry's constant of CO in 30 wt% aqueous DEA solution from N_2 -Analogy

T	$H_{\text{N}_2-\text{H}_2\text{O}}^+$	$H_{\text{CO}-\text{H}_2\text{O}}^+$	$\frac{H_{\text{CO}-\text{H}_2\text{O}}}{H_{\text{N}_2-\text{H}_2\text{O}}}$	$H_{\text{N}_2-\text{DEA}}^{++}$	$H_{\text{CO-DEA}}$
(K)	(MPa)	(MPa)	-	(MPa)	(Mpa)
313	10,133	7,072	0.70	4,519	3,154
333	11,429	8,187	0.72	2,371	1,698
353	12,048	8,613	0.72	2,047	1,463
363	11,926	8,582	0.72	1,986	1,429
373	11,683	8,400	0.72	1,834	1,319
383	11,348	8,096	0.71	1,895	1,352
393	10,943	7,701	0.70	1,976	1,390

⁺ Obtained from correlations given in Fogg and Gerrad (1991)

⁺⁺ Measured in this work

Table 9.2: Henry's constants of CO and N₂ in water and organic solvents (Fogg and Gerrad, 1991)

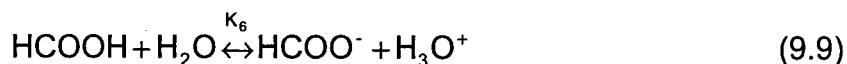
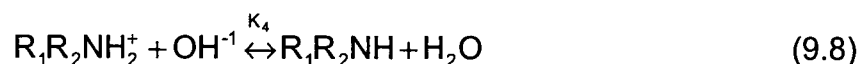
Solvent	Temp. (K)	H _{CO} (MPa)	H _{N₂} (Mpa)	$\frac{H_{CO}}{H_{N_2}}$
Water	298	5,857	8,552	0.68
	313	7,072	10,133	0.70
	333	8,187	11,429	0.72
	353	8,613	12,048	0.71
	363	8,582	11,926	0.72
	373	8,400	11,683	0.72
	383	8,096	11,348	0.71
	393	7,701	10,943	0.70
	413	6,708	9,960	0.67
Methyl acetate	298	119	173	0.69
	303	118	170	0.70
	313	116	163	0.71
2-propanone	298	130	187	0.69
	303	129	184	0.70
	313	126	177	0.71
1-1'-oxybisethane	293	60	82	0.74
	298	60	81	0.74
	303	60	80	0.75
	313	59	78	0.76
Tetrachloromethane	298	117	159	0.74
	303	116	156	0.74
	313	114	151	0.75
	323	111	146	0.76
	333	109	141	0.77
Chlorobenzene	298	161	238	0.68
	303	159	233	0.68
	313	157	225	0.70
	323	154	217	0.71
	333	150	209	0.72
	343	147	202	0.73
Benzene	298	157	228	0.69
	333	135	191	0.71
	298	58	83	0.70
Hexadecane	298	58	83	0.70
Methanol	298	308	371	0.83
Ethanol	298	220	284	0.77
1-Propanol	298	196	250	0.78

9.1.3 Determination of k_3 and k_{-3}

It was not possible to estimate k_3 and k_{-3} together with k_1 , k_2 and $H_{\text{CO-DEA}}$ by regressing the pressure versus time data obtained from CO absorption experiments. This was mainly because molecular CO is not directly involved in reaction (8.3). Consequently, the latter exerts no or little effect on the overall change in CO partial pressure due to reaction. Therefore, it was decided to estimate k_3 and k_{-3} separately by following the liquid phase reaction between formic acid and aqueous DEA. In this series of experiments, 0.5-0.65 M formic acid was added to a 30 wt% aqueous DEA solution and the mixture was allowed to react in a stirred autoclave under a nitrogen blanket for about 40-170 hours in the temperature range of 303-413 K. Liquid samples were withdrawn at regular intervals from the autoclave and analyzed for formate and DEAF using IC. The initial formate concentration was set at about 5 times the maximum concentration predicted from the CO-DEA reaction model.

9.1.3.1 DEA-Formic Acid-Water Reaction Model

To estimate k_3 and k_{-3} from the data obtained by means of the above experiments, the following liquid phase reactions can be postulated:



For convenience, we keep the same nomenclature as before except that species HCOOH is represented by C_9 . The reaction (9.7) is the same as reaction (8.3) and its rate expression is given by equation (8.9). The dissociation of formic acid represented by reaction (9.9) is an equilibrium reaction. The equilibrium constant, K_6 was estimated from the following correlation:

$$\log_{10}(K_6) = -39.06123 - \frac{173.624}{T} + 17.88348 \log_{10}(T) - 0.028039T \quad (9.11)$$

Equation (9.11) is based on the data of Harned and Embree (1934) obtained in the temperature range of 273-333 K. The equations governing the material and electronic balances in a batch reactor are:

Formate Balance:

$$\frac{dC_5}{dt} = r_3 \quad (9.12)$$

DEAF Balance:

$$\frac{dC_4}{dt} = -r_3 \quad (9.13)$$

Total DEA Balance:

$$\frac{dC_2}{dt} + \frac{dC_3}{dt} + \frac{dC_4}{dt} = 0 \quad (9.14)$$

Electron Neutrality Balances:

$$\frac{dC_3}{dt} + \frac{dC_7}{dt} - \frac{dC_5}{dt} - \frac{dC_6}{dt} = 0 \quad (9.15)$$

DEA Protonation:

$$K_4 = \frac{C_2}{C_3 C_6} \quad (9.16)$$

Formic Acid Dissociation:

$$K_6 = \frac{C_5 C_7}{C_9} \quad (9.17)$$

Water Dissociation:

$$K_5 = C_6 C_7 \quad (9.18)$$

There are seven ordinary differential and algebraic equations (equations 9.12 to 9.18) with seven unknown chemical species. The equations must be solved subject to following initial conditions:

$$C_i = C_i^0 \quad \text{for } i = 2-7,9 \quad (9.19)$$

At $t=0$, $C_4^0 = 0$. The values of C_2^0 , C_3^0 , C_5^0 , C_6^0 , C_7^0 and C_9^0 can be obtained by solving the equilibrium equations shown below. Since the DEA concentration is initially zero, it follows that:

Overall DEA Balance:

$$C_2^0 + C_3^0 = [R_1 R_2 NH]_{\text{initial}} \quad (9.20)$$

Overall Formate Balance:

$$C_5^0 + C_9^0 = [HCOOH]_{\text{initial}} \quad (9.21)$$

Electron Neutrality Balance:

$$C_3^0 + C_7^0 - C_5^0 - C_6^0 = 0 \quad (9.22)$$

DEA Protonation:

$$K_4 = \frac{C_2^0}{C_3^0 C_6^0} \quad (9.23)$$

Formic Acid Dissociation:

$$K_6 = \frac{C_5^{\circ} C_7^{\circ}}{C_9^{\circ}} \quad (9.24)$$

Water Dissociation:

$$K_5 = C_6^{\circ} C_7^{\circ} \quad (9.25)$$

For the present experiments, the initial DEA and formate concentrations are 2.85 and 0.5-0.65 mol/L respectively. Therefore, the equilibrium concentrations C_2° , C_3° , C_5° , C_6° , C_7° and C_9° can be calculated by solving equations (9.20) to (9.25) simultaneously by means of Newton's Homotopy continuation method.

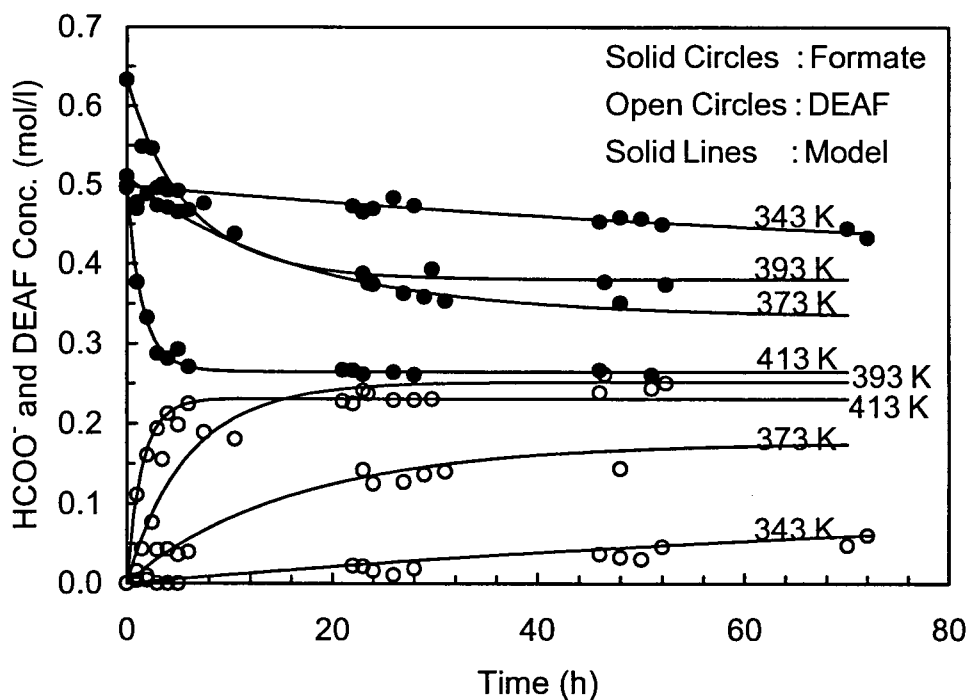


Figure 9.4: Measured and predicted formate ions and DEAF concentration

9.1.3.2 Parameter Estimation

In the above model (equations 9.12 to 9.25), there are only two unknown parameters (k_3 and k_{-3}), which can be estimated from the formate versus time data by the non-linear least squares optimization technique described earlier. The formate ion and DEAF concentrations obtained from the experiments and the model using the optimized values k_3 and k_{-3} are plotted in Figure 9.4. Good agreement between the measured and predicted formate and DEAF concentrations was obtained. Data for temperatures below 343 K are not shown in Figure 9.4 because no significant reaction was observed. In Figure 9.4, the concentration trends for Formate and DEAF clearly indicate that the reaction between formic acid and DEA is slow and reversible. The estimates for k_3 and k_{-3} at various temperatures are listed in Table 9.3 and are plotted in Figures 9.5 and 9.6 respectively. Also, these estimates could be fitted by the following Arrhenius equations:

$$k_3 = 3 \times 10^{10} \exp(-10,177/T) \quad (9.26)$$

$$k_{-3} = 2 \times 10^7 \exp(-7,637.2/T) \quad (9.27)$$

where T is in Kelvin, k_3 is in $\text{m}^3/\text{kmol h}$ and k_{-3} is in $1/\text{h}$. The activation energies, as determined from equations (9.26) and (9.27), are 84.61 kJ/mol and 63.50 kJ/mol respectively.

Table 9.3: Estimates of the rate and equilibrium constants for reaction (8.3)

T (K)	k_3 ($\text{m}^3/\text{kmol h}$)	k_{-3} ($1/\text{h}$)	K_3 (m^3/kmol)	K_3 (dimensionless)
343	4.666×10^{-3}	5.260×10^{-3}	0.887	34.91
353	6.194×10^{-3}	6.488×10^{-3}	0.955	37.42
373	4.354×10^{-2}	2.735×10^{-2}	1.592	61.93
393	1.125×10^{-1}	6.467×10^{-2}	1.740	67.15
413	6.920×10^{-1}	2.099×10^{-1}	3.297	126.27

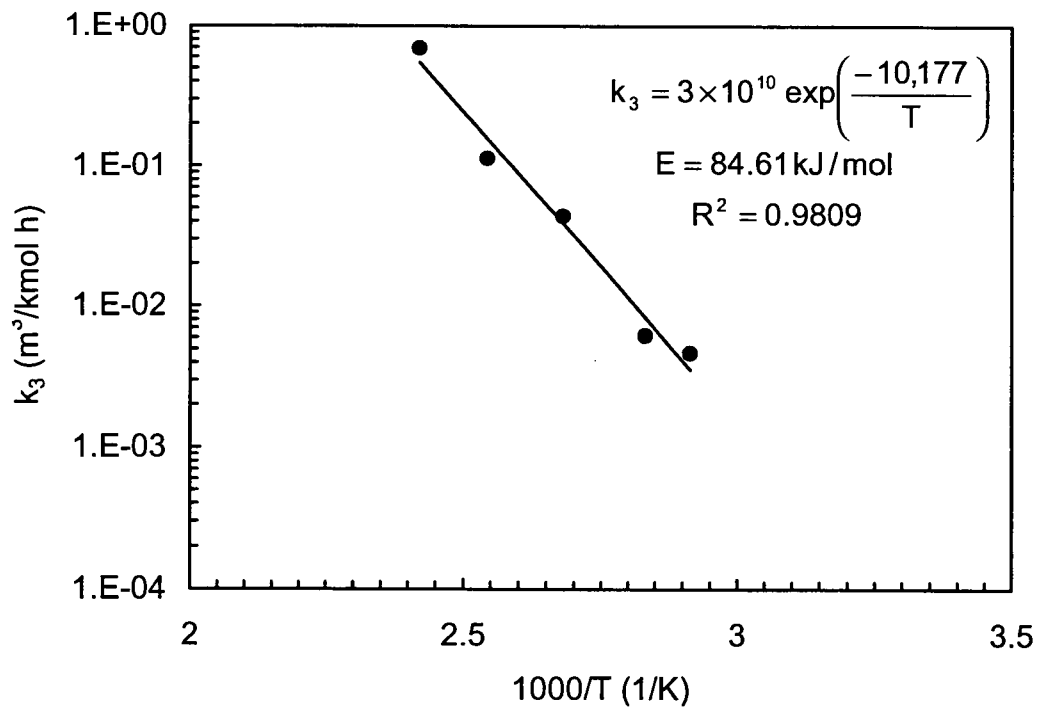


Figure 9.5: Arrhenius plot of the estimates for the forward rate constant of reaction (8.3)

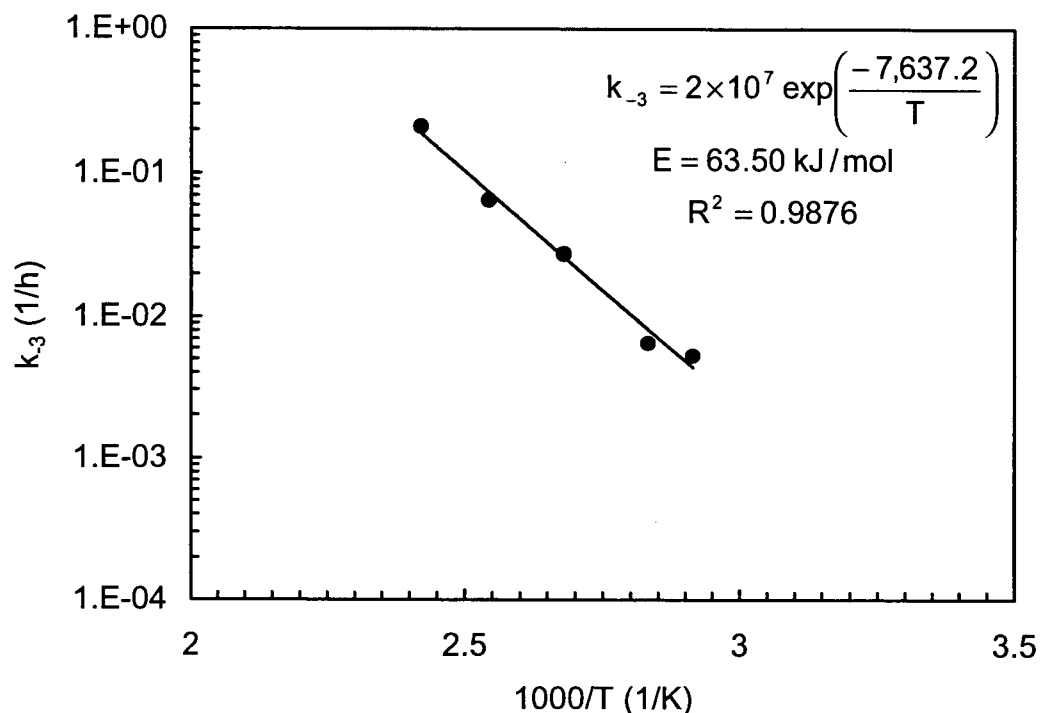


Figure 9.6: Arrhenius plot of the estimates for the reverse rate constant of reaction (8.3)

From the estimates of k_3 and k_{-3} , the equilibrium constant, K_3 , was calculated and plotted in Figure 9.7. The values of K_3 were fitted to the following Arrhenius equation:

$$K_3 = 1.355 \times 10^3 \exp(-2,540.1/T) \quad (9.28)$$

where T is in Kelvin and K_3 has units of m^3/kmol . In the literature, the temperature dependence of amine hydrolysis constants is usually reported in terms of the expressions proposed by Harned and Robinson (1940). K_3 was made dimensionless by dividing it by the concentration of water in the solution:

$$\log_{10}(K_3) = 10.339 + \frac{1199.668}{T} - 8.364 \log_{10}(T) + 0.025946T \quad (9.29)$$

The constants of equation (9.29) were estimated by the method of least squares. The literature does not contain values and correlations for k_3 , k_{-3} and K_3 and we are the first to report them.

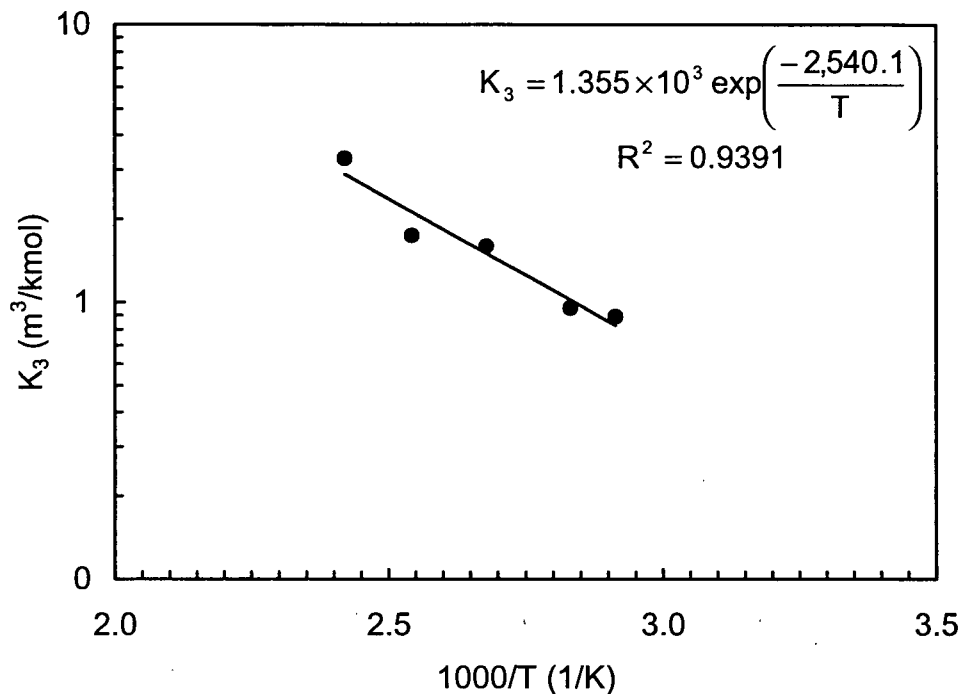


Figure 9.7: Arrhenius plot of the estimates for the equilibrium constant of reaction (8.3)

9.1.4 Determination of k_1 , k_2 and $H_{\text{CO-DEA}}$

The correlations for $k_L a$, k_3 and k_{-3} obtained above may be substituted into the reaction model (equations 8.10-8.18) to estimate the remaining unknown parameters (k_1 , k_2 and $H_{\text{CO-DEA}}$) from the pressure versus time data using the least squares minimization method discussed earlier. The experimental data were obtained from a series of batch absorption experiments, where pure CO was absorbed in 30 wt% aqueous DEA solutions in the temperature range of 313-413 K and CO partial pressure range of 800-1200 kPa. The change in total

reactor pressure due to absorption and reaction was recorded with time. The partial pressure of CO was calculated by subtracting the solution vapor pressure from the total reactor pressure at the corresponding temperature. At the end of each experiment, liquid samples were withdrawn and the concentrations of formate ions and DEAF were found.

Initially, the parameters were estimated by considering that all reactions (8.1)-(8.5) were reversible. Since, we could not estimate the values of reverse rate constants for reactions (8.1) and (8.2) the reversibility for these reactions was not considered in subsequent data analysis. The estimates for k_1 , k_2 and $H_{\text{CO-DEA}}$ are listed in Table 9.4 and a comparison of the measured and predicted CO partial pressures using these estimates is shown in Figure 9.8. Good agreement was found between the measured and predicted CO partial pressures at all temperatures. This is strong validation of the model and experimental procedure.

Table 9.4: Estimates of k_1 , k_2 and $H_{\text{CO-DEA}}$

T (K)	k_1 ($\text{m}^3/\text{kmol h}$)	k_2 ($\text{m}^3/\text{kmol h}$)	$H_{\text{CO-DEA}}$ (MPa)	$H_{\text{CO-DEA}}^+$ (MPa)
313	8.58	5.370×10^{-3}	5,928	3,161
333	27.41	1.214×10^{-2}	2,513	1,702
343	81.11	1.645×10^{-2}	2,108	-
363	130.32	2.741×10^{-2}	1,368	1,469
373	225.28	3.806×10^{-2}	1,348	1,429
383	441.47	5.591×10^{-2}	1,398	1,317
393	619.62	7.506×10^{-2}	1,297	1,348
413	813.08	1.152×10^{-1}	618	537

⁺ Calculated from N_2 -Analogy

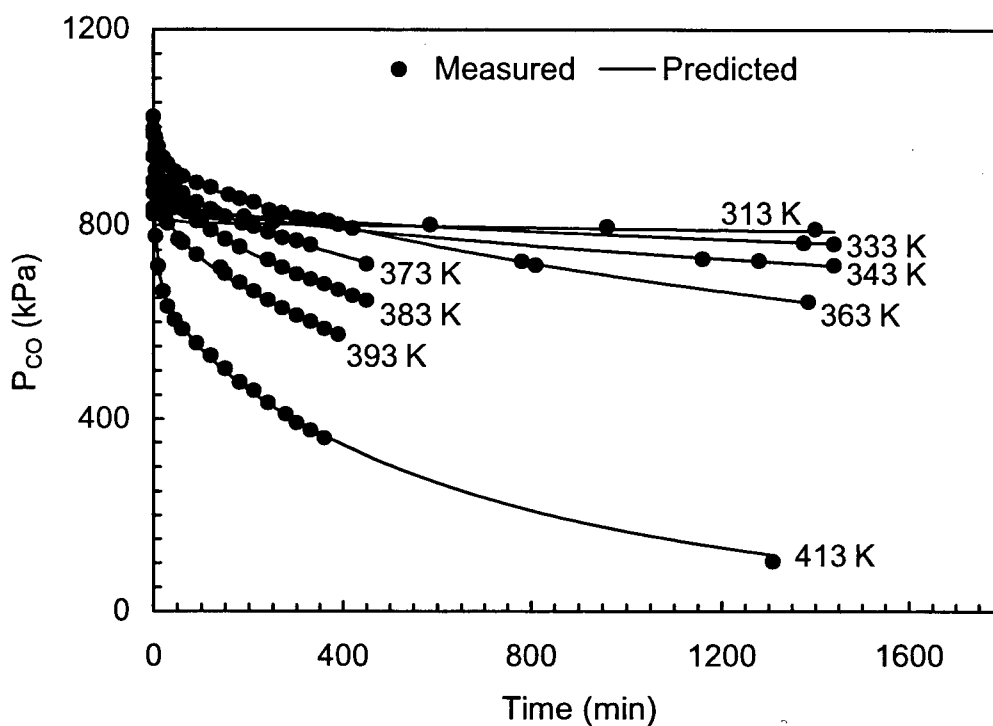


Figure 9.8: Measured and predicted partial pressures for CO absorption in 30 wt% aqueous DEA solution

We considered $H_{\text{CO-DEA}}$ as one of the unknown parameters and estimated it along with k_1 and k_2 . The values of $H_{\text{CO-DEA}}$ obtained using this approach and the N_2 -Analogy method are listed in Table 9.4. The agreement between the two sets of $H_{\text{CO-DEA}}$ values and its trend with respect to temperature is good, particularly at temperatures above 333 K. This suggests that the N_2 -Analogy is valid. The relatively large differences in the values $H_{\text{CO-DEA}}$ at temperatures lower than 333 K are probably due to the extremely slow reaction between CO and aqueous DEA solution. Consequently, the reaction model may not furnish good estimates of $H_{\text{CO-DEA}}$ at these temperatures.

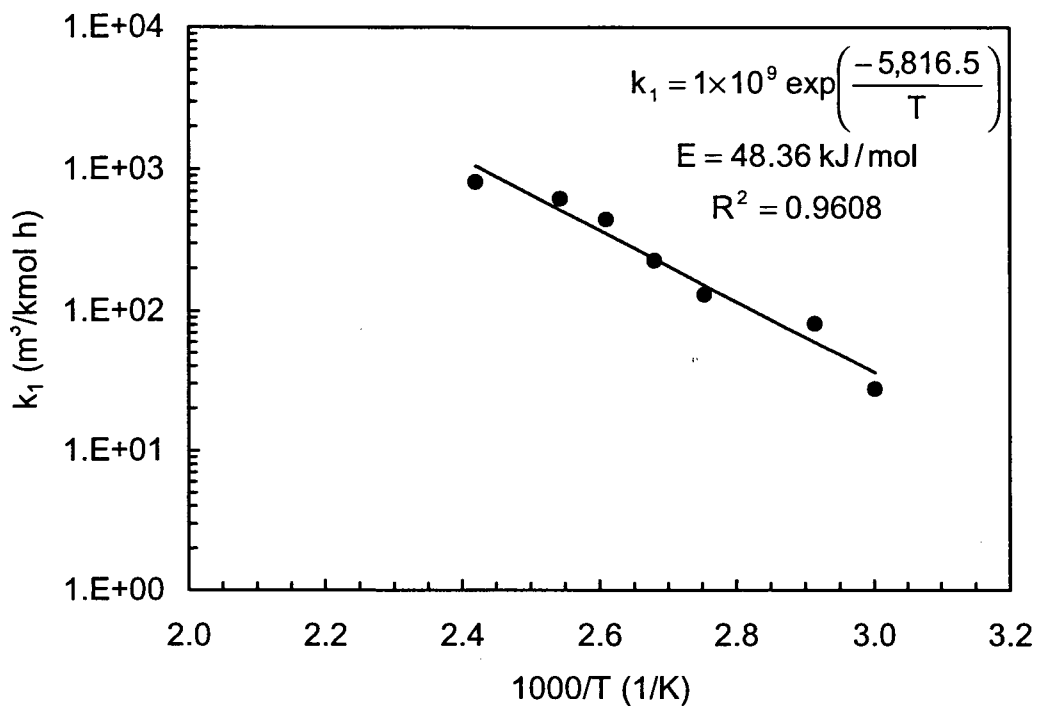


Figure 9.9: Arrhenius plot of the estimates for the second order rate constant of reaction (8.1)

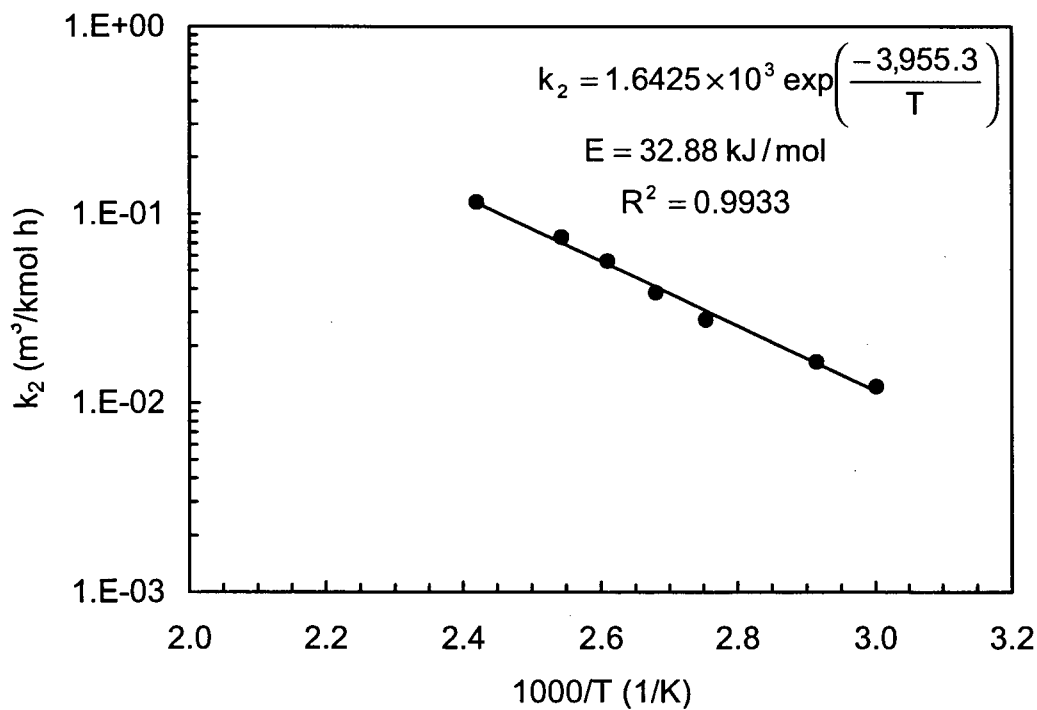


Figure 9.10: Arrhenius plot of the estimates for the second order rate constant of reaction (8.2)

The estimates for k_1 and k_2 at various temperatures are plotted in Figures 9.9 and 9.10 and are fitted to the following Arrhenius equations:

$$k_1 = 1 \times 10^9 \exp(-5,816.5/T) \quad (9.30)$$

$$k_2 = 1.6425 \times 10^3 \exp(-3,955.3/T) \quad (9.31)$$

where T has units Kelvins, while k_1 and k_2 are in units of $\text{m}^3/\text{kmol h}$. The activation energies determined from equations (9.30) and (9.31) are 48.36 kJ/mol and 32.88 kJ/mol respectively. The data for both k_1 and k_2 fall on straight lines thereby providing strong support for the validity of the present mathematical model and parameter estimation technique. McDonald (1963) studied the kinetics of the absorption of CO in basic solutions and reported a second-order rate constant (k_1) value of $93.96 \text{ m}^3/\text{kmol h}$ at 353 K. This value agrees well with the present estimates of $81.11 \text{ m}^3/\text{kmol h}$ at 343 K and $130.32 \text{ m}^3/\text{kmol h}$ at 363 K (see Table 9.4).

Comparison of the values of k_1 and k_2 in Table 9.4 suggests that the formate formation reaction (reaction 8.1) is about three orders of magnitude faster than the DEAF formation reaction (reaction 8.2). Also, a comparison of rate constants for the DEAF formation reactions via direct insertion (k_2 in Table 9.4) and formate-DEA reaction (k_3 in Table 9.3) reveals that both constants are of the same order of magnitude. However, since reaction (8.3) is reversible and since the equilibrium favors the reverse reaction, its overall effect on the net formation of DEAF is negative, particularly at temperatures higher than 343 K. This phenomenon is better illustrated in Figure 9.11, which compares the model predictions for the formation of formate ions and DEAF in a batch reactor at 393

K with and without reaction (8.3). It is clear from this figure that, under conditions when reaction (8.3) is included, the net formation of DEAF is reduced and that of formate ions is increased. However, simulation results at temperatures lower than 343 K indicate that reaction (8.3) has no effect on the buildup of formate and DEAF in the reactor. From this analysis, we conclude that the dominant DEAF formation route is via direct insertion of CO into the DEA molecule (reaction 8.2).

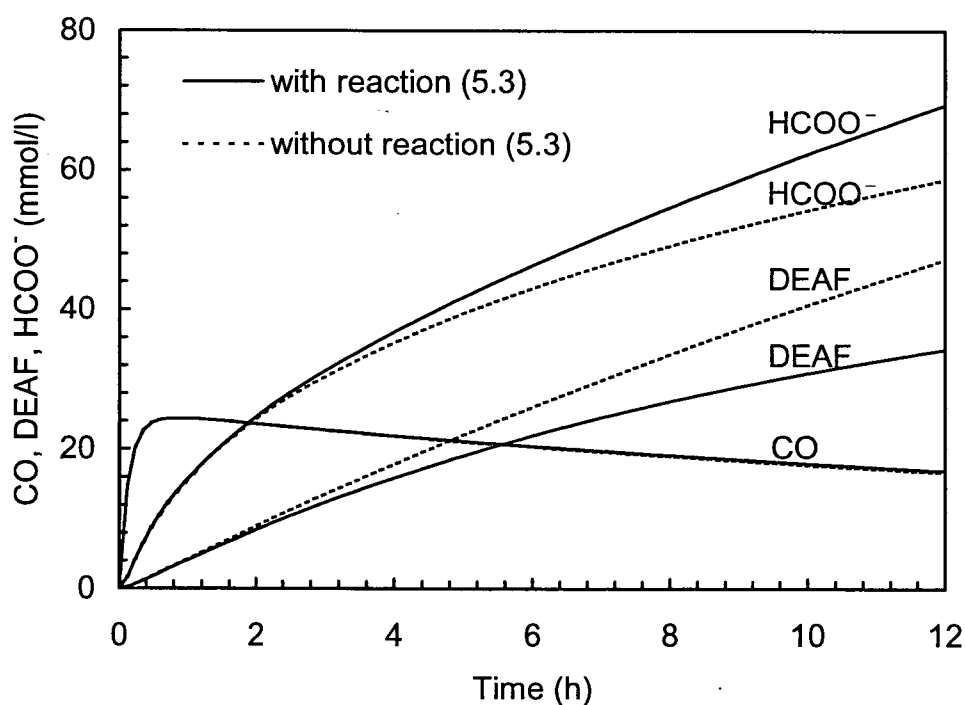
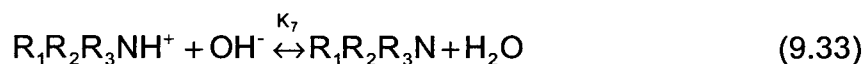


Figure 9.11: Effect of reaction (8.3) on the formation of formate and DEAF at $T = 393 \text{ K}$, $p_{\text{CO}}^{\circ} = 1000 \text{ kPa}$ and $C_{\text{DEA}} = 30 \text{ wt\%}$

9.2 Absorption and Degradation in CO-MDEA System

The reaction mechanism and the parameter estimation technique was further verified by conducting an experiment where pure CO was absorbed into 30 wt% aqueous MDEA solutions at 393 K. MDEA is a tertiary amine and is not

expected to react with CO to form diethanolacetamide (i.e. $R_1R_2NCOR_3$). Consequently, reactions (8.2) and (8.3) do not exist and the CO-MDEA- H_2O system can be represented by:



where $R_1R_2R_3N$ and $R_1R_2R_3NH^+$ denote MDEA and protonated MDEA respectively. Note that for MDEA, $R_1 = R_2 = -CH_2CH_2OH$ and $R_3 = -CH_3$. The ionic strength of a 30 wt% aqueous MDEA solution is almost the same as that of a 30 wt% aqueous DEA solution. Therefore, if the reaction mechanism is right, the same value of k_1 should be found for both systems. We therefore estimated k_1 from the batch absorption data obtained in this experiment by using the same reaction model as before (equations 9.10-9.18) and by setting r_2 and r_3 equal to zero. The value of the MDEA protonation constant (K_7) was calculated from the following correlation reported by Barth et al. (1981) over the temperature range of 298-333 K. It was extrapolated up to 393 K for this work:

$$\log_{10}(K_7K_5) = -14.01 + 0.018T \quad (9.35)$$

The parameter estimates from the experiments on CO absorption in aqueous MDEA and DEA solution at 393 K are listed in Table 9.5. As expected, the estimated values of k_1 in both cases are in excellent agreement. This once

again validates the proposed reaction mechanism and the experimental technique for parameter estimation.

Table 9.5: CO reaction with aqueous DEA and MDEA

Amine	T (K)	k_1 (m ³ /kmol h)	H_{CO-Am} (MPa)	Formyl Alkanolamine	HCOO ⁻
DEA	393	620	1,297	Yes	Yes
MDEA	393	668	841	No	Yes

9.3 Absorption and Degradation in CO-DEA+DEAF System

In order to elucidate the reversibility of reaction (8.3), an experiment was conducted where CO was absorbed in the aqueous mixture of 30 wt% DEA and 18.4 wt% DEAF at 393 K. The stock solution of DEAF had a 85% purity and was provided by the Shell Technology Center, Houston, Texas. The impurities in the stock solution were mainly water and the acetates. Purer DEAF solutions were unavailable. The experiment was conducted in a batch mode and liquid samples were withdrawn at regular intervals.

Using the parameters estimated in this work, a numerical simulation was performed to predict the rate of change of CO partial pressure and formate and DEAF concentrations in the liquid phase. These results are plotted in Figure 9.12. Clearly, the agreement between predicted and measured CO partial pressures and DEAF concentrations is excellent. However, the predicted formate ion concentrations were about 20-25% lower than those measured in our experiment. The reason for this discrepancy is not clear. One of the explanations is that the impurities in the DEAF stock solution might have converted to formate. Note that in Figure 9.12, the sudden drop in CO partial pressure at each 60-

minute interval is because the numerical simulation was done by taking into account the changes in total pressure and the gas and liquid volume due to sample withdrawal.

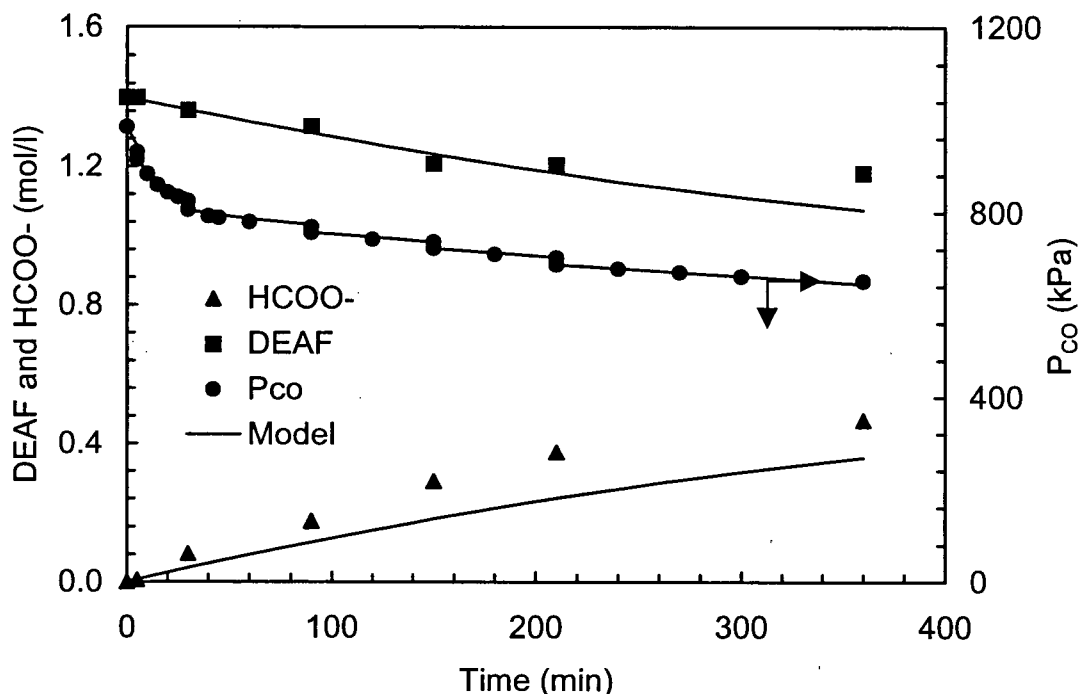


Figure 9.12: Measured and predicted concentration and partial pressure profiles for CO absorption in aqueous solution of 30 wt% DEA and 18.4 wt% DEAF at 393 K

9.4 Model Predictions

After establishing the reaction mechanism and the values of all the associated physico-chemical parameters, we are able to predict the DEAF and formate ion formation when aqueous DEA solutions are exposed to CO. We therefore measured DEAF and formate concentrations in the liquid samples withdrawn at the end of each experiment. The predicted and measured values of DEAF and formate ion concentrations in all experiments are listed in Tables 9.6 to 9.9. It can be seen from these tables that the agreement between predicted

and measured concentrations is good. In most cases, the relative error fell within $\pm 30\%$.

It should however be noted that in a few cases the error was as high as $\pm 50\%$, which could not be due to experimental error as these measurements were rechecked and same values were found. In view of the errors associated with literature correlations in calculating various physico-chemical properties and the experimental errors associated with the IC technique, this agreement can still be regarded as good.

Table 9.6: Measured and predicted Formate and DEAF concentrations for CO absorption in 30 wt% aqueous DEA solution

T (K)	Time (h)	Formate Measured (mmol/l)	Formate Predicted (mmol/l)	Error (%)	DEAF Measured (mmol/l)	DEAF Predicted (mmol/l)	Error (%)
313	62.2	5.2	5.2	0	11.0	8.2	25
333	24.0	15.4	17.2	-12	7.6	9.9	-31
343	24.0	25.4	26.0	-2	10.8	16.0	-47
363	23.1	48.0	55.1	-15	32.2	37.6	-17
373	7.5	31.6	36.2	-15	18.1	18.5	-2
383	7.5	38.7	42.3	-9	18.9	20.8	-10
393	6.5	41.9	46.7	-11	29.1	21.7	25
413	21.8	159.4	139.3	13	93.5	68.5	27

Table 9.7: Effect of amine concentration on CO reaction with aqueous DEA solution at 393 K

DEA (wt%)	Time (h)	Formate Measured (mmol/l)	Formate Predicted (mmol/l)	Error (%)	DEAF Measured (mmol/l)	DEAF Predicted (mmol/l)	Error (%)
5	7.0	30.4	32.6	-7	8.7	7.6	13
10	23.5	-	89.3	-	-	27.9	-
15	22.0	104.6	96.8	7	46.1	35.3	24
30	6.5	41.9	46.2	-10	29.1	21.8	25
50	28.0	104.2	121.8	-17	113.3	80.1	29

Table 9.8: CO absorption in aqueous solution of 30 wt% DEA and 18.4 wt% DEAF

T (K)	Time (h)	Formate Measured (mmol/l)	Formate Predicted (mmol/l)	Error (%)	DEAF Measured (mmol/l)	DEAF Predicted (mmol/l)	Error (%)
393	19.5	571.9	540.4	5	1031.5	956.3	7

Table 9.9: CO absorption in 30 wt% aqueous MDEA solution

T (K)	Time (h)	Formate Measured (mmol/l)	Formate Predicted (mmol/l)	Error (%)	DEAF Measured (mmol/l)	DEAF Predicted (mmol/l)	Error (%)
393	21.7	57.5	83.5	-45	0	0	0

9.5 *Process Implications*

Figures 9.13 and 9.14 show the predicted concentrations of various species in the liquid phase for CO absorption in 30 wt% aqueous DEA solution in a batch autoclave at temperatures of 313 K and 413 K and at initial CO partial pressure of 1,000 kPa. These temperatures are typical for absorbers and strippers in commercial plants. These figures clearly show that under identical conditions the formation of DEAF and formate is about 10-15 times higher at the stripper temperature than that at the absorber temperature. This suggests that in the absorber, where the temperature is usually low (<323 K), the physical absorption of CO is facilitated. By contrast, in the stripper and its reboiler, where the temperatures are usually high (>363 K), amine degradation will occur. Although the rates of these degradation reactions are quite slow our simulation results show that, over time, one can expect substantial DEAF and formate ion buildup in the system. For the purpose of illustration, the data shown in Figures 9.13 and 9.14 were obtained using very high initial CO partial pressures. Using the parameters estimated in this work one can easily demonstrate the implication of CO induced degradation under real plant conditions. It should, however, be noted that translating these data to real plant conditions is not straightforward. The influence of process conditions and a totally different gas composition on the various parameters must be taken into account.

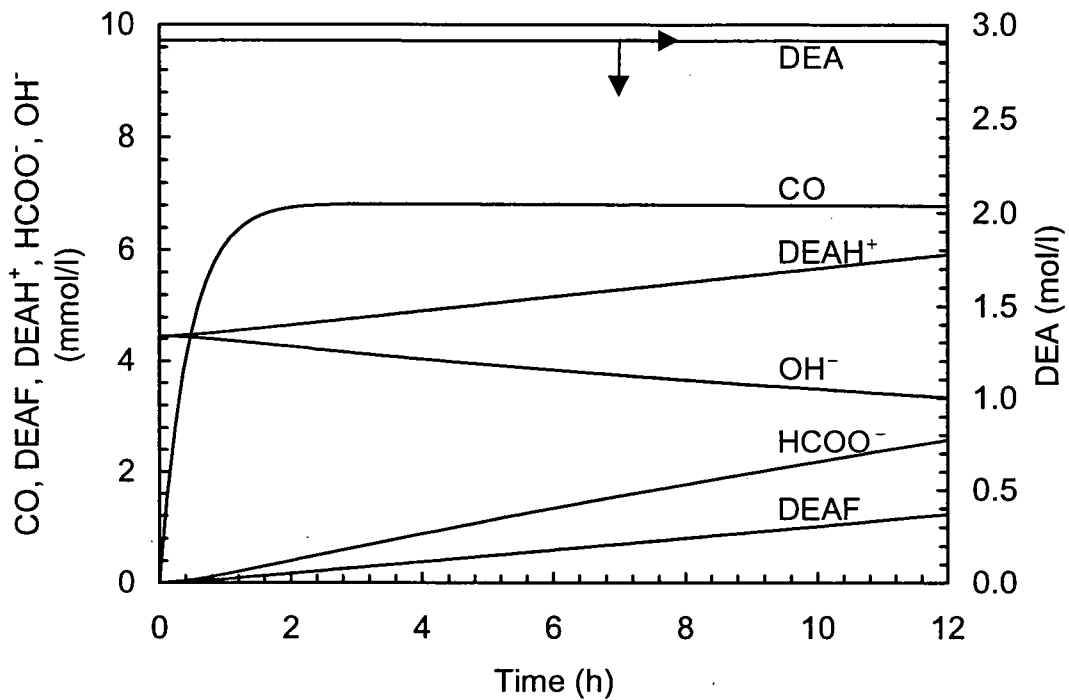


Figure 9.13: Predicted concentration profiles for CO absorption in 30 wt% aqueous DEA solution at T = 313 K and $p_{CO}^0 = 1000$ kPa

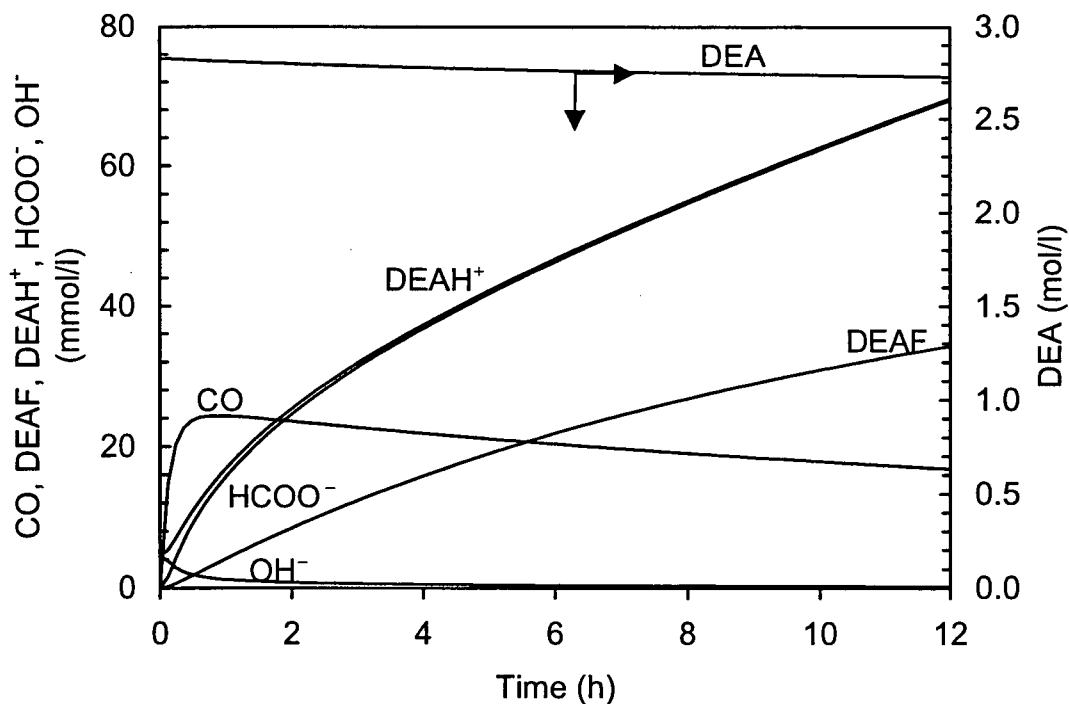


Figure 9.14: Predicted concentration profiles for CO absorption in 30 wt% aqueous DEA solution at T = 393 K and $p_{CO}^0 = 1,000$ kPa

9.6 Conclusions

The kinetics of CO-induced degradation of DEA were studied over the temperature range of 313-413 K and DEA concentrations of 5-50 wt%. A reaction mechanism was proposed and a mathematical model was developed to estimate previously unknown kinetic and solubility parameters from batch absorption experiments. The experimental data are best described by reactions (8.1) to (8.5). Numerical simulation results, based on the estimated parameters, indicate that the primary DEA degradation reaction is the direct reaction of DEA with molecular CO (reaction 8.2). The formate-DEA reaction (reaction 8.3), on the other hand, is relatively slow and reversible. Comparison of the simulation results with and without reaction (8.3) show that, at temperatures higher than 343 K, some of the DEAF formed by reaction (8.2) is hydrolyzed back to form formate ions and protonated DEA by reverse reaction (8.3). However, at temperatures lower than 343 K, reaction (8.3) seems to have no significant effect on the net formation of DEAF and formate ions in the system. The data from the experiment on CO absorption in aqueous solution containing 30 wt% DEA and 18.4 wt% DEAF, further confirms the reversibility of reaction (8.3).

Parameter estimates of the rate constants suggest that the reaction rates are quite slow but, over time, nevertheless lead to substantial DEAF and formate ion buildup in the system.

The Henry's constant of CO in aqueous DEA solution was determined by the N₂-Analogy and from the reaction model. The results are in fairly good agreement. Comparison of the values of $H_{\text{CO-DEA}}$ over the temperature range of

313-343 K shows that the value of $H_{\text{CO-DEA}}$ decreases with increasing temperature. This trend is similar to that of CO solubility in pure organic solvents reported in the literature (Fogg and Gerrard, 1991).

An experiment conducted by absorbing CO in 30 wt% aqueous MDEA solution shows that, unlike DEA, MDEA does not react with CO. There was no experimental evidence suggesting the formation of diethanolacetamide ($\text{R}_1\text{R}_2\text{NCOCH}_3$) even after 20 hours at 393 K. The rate constant for the formate ion formation reaction was found to be in excellent agreement with that obtained from CO-DEA- H_2O system. This further validates the proposed reaction mechanisms and the experimental technique used to estimate the kinetic parameters.

The DEAF and formic ion concentrations found at the end of each experiment agreed well with those predicted from the present mathematical model. In most cases the relative error was within $\pm 30\%$.

CHAPTER 10

OVERALL CONCLUSIONS AND RECOMMENDATIONS

10.1 Main Conclusions from CO₂ Absorption/Desorption Work

A comprehensive mathematical model governing the diffusion-reaction process of CO₂ absorption and desorption in aqueous amine solutions falling as a laminar liquid film over a hemispherical surface has been developed. The model applies to a general case where the aqueous solution may contain a binary mixture of amines (e.g., MEA+AMP or MEA+MDEA) and where CO₂ undergoes a series of liquid phase reversible reactions. The model readily reduces to a single aqueous amine (e.g., MEA or AMP) or physical absorbent system by setting the initial concentration of one or both amines to zero. The model can also be reduced to the well-known pseudo-first-order kinetics when all reactions are lumped into a single, overall reaction by setting the rates of all but one reaction to zero. The predicted absorption and desorption rates from the model at various amine concentrations, CO₂ partial pressures, temperatures and CO₂ loadings are consistent with the experimentally observed rates.

A numerical procedure was developed to solve the model equations and to estimate unknown model parameters using experimental data. To do this a computer code was written that performs four different tasks involving (a) calculation of physical-chemical properties for a given set of condition, (b) solution of equilibrium model for setting the initial conditions, (c) solution of

diffusion-reaction model to calculate concentration gradients at different latitudes θ , and (d) calculation of total absorption or desorption rate by integrating over the entire hemisphere. The Fortran code for tasks (a) and (d) were written as part of this study and that for tasks (b) and (c) were generated using Athena by implementing the model equations in the Athena Visual Workbench environment. These subroutines were compiled together to calculate absorption or desorption rates using the Compaq Visual-Fortran Developer Studio in Windows environment. For the purpose of parameter estimation using the present model and experimental data, the subroutines for tasks (a) to (d) were linked with an additional subroutine generated from Athena that uses weighted least squares and Bayesian estimators with single as well as multi-response data. The computer code has been successfully used to simulate a variety of different operating conditions and to estimate reaction parameters for a number of CO₂-amine-water systems.

The model was solved analytically for the simple case of physical absorption of a gas over a hemispherical liquid film and a correlation was developed for the physical mass transfer coefficient as a function of dimensionless numbers. The correlation was later used to estimate the diffusivities of CO₂ in water and N₂O in water and amine solutions. The calculated diffusivities are in good agreement with those reported in the literature. The analytical solution was also compared with the numerical solution and good agreement was found.

A novel hemispherical contactor was developed to measure absorption and desorption rates of CO_2 in aqueous amine solutions under a variety of different operating conditions encountered in actual absorption-stripping processes for gas treating. This contactor is, in principle, similar to the wetted sphere units used in many previous studies on CO_2 -alkanolamine kinetics. However, the present design offers significant improvements over the conventional designs with respect to surface rippling commonly encountered in the lower half of the full sphere unit. The unit was built in-house with a computerized data logging system and was used successfully to measure absorption and desorption rates to calculate diffusivities and kinetic parameters for both physical and chemical solvents.

The diffusion-reaction model developed in this work involves many physical chemical property parameters. A parametric sensitivity analysis indicated that accurate values of CO_2 diffusivity and CO_2 solubility given by a Henry's law constant are essential for predicting accurate absorption and desorption rates. An extensive literature search was undertaken and all available property data were compiled. It was found that the values of these parameters at stripping temperatures are not available. A series of experiments involving N_2O -water and N_2 -alkanolamine systems were conducted to measure diffusivities and Henry's constants of CO_2 in water using the N_2O analogy. Using data obtained in this work and others available in the literature, correlations were developed that can be used for pure water as well as single and binary amine systems covering

a wide range of temperatures and amine concentrations. Such correlations are not available in the literature.

The absorption and desorption rates of CO₂ in aqueous solutions of MEA, DEA, MDEA, AMP and their mixtures (MEA+MDEA, MEA+AMP, DEA+MDEA and DEA+AMP) were measured for amine concentrations in the range of 2 to 35 wt%. The absorption experiments were carried out at near atmospheric pressure using pure CO₂ saturated with water at 293 to 323 K with initially unloaded solutions. The desorption experiments were performed at 333 to 383 K for CO₂ loading between 0.02 to 0.7 moles of CO₂ per mole of amine using humidified N₂ gas as a stripping medium. The data were analyzed using the rigorous diffusion-reaction model developed in this work. The model predicts the experimental results well for all eight different amine systems studied (see Chapter 4). The results indicate that the theory of absorption with reversible chemical reaction could be applied to predict desorption rates.

A zwitterion mechanism adequately describes the reactions between CO₂ and carbamate forming amines such as MEA, DEA and AMP under both absorption and desorption conditions. The reactions between CO₂ and aqueous MDEA solutions are best described by a base-catalyzed hydration reaction mechanism.

The kinetic data obtained show that desorption experiments can be used to determine both the forward and backward rate constants accurately. The absorption experiments on the other hand could only be used to determine forward rate constants.

For MEA, DEA and AMP, the kinetic data obtained under absorption conditions do not extrapolate well to desorption temperatures. Therefore, kinetic data at higher temperatures should be obtained from desorption experiments. The existing absorption data for the CO₂-MDEA system can be extrapolated to desorption temperatures with reasonable accuracy. This is probably because MDEA is very slow reacting amine and does not form carbamate.

For the blended amine systems, it was found that small additions of MEA or DEA (< 5 wt%) significantly enhance the absorption rates of CO₂ in 25 wt% MDEA solutions. Addition of small quantity of MEA (< 5 wt%) to 25 wt% AMP blend, on the other hand, was found to have very nominal effect on the CO₂ absorption rates of AMP. No improvement in absorption rates was observed when DEA was added to 25 wt% AMP solutions.

10.2 Main Conclusions from the Work on CO-Induced Degradation of DEA

The kinetics of CO-induced degradation of DEA was studied over the temperature range of 313-413 K and DEA concentrations of 5-50 wt%. A reaction mechanism was proposed and a mathematical model was developed to estimate previously unknown kinetic and solubility parameters from batch absorption experiments.

The experimental data are best described by reactions (8.1) to (8.5). Numerical simulation results, based on the estimated parameters, indicate that the primary DEA degradation reaction is the direct reaction of DEA with

molecular CO. The formate-DEA reaction, on the other hand, is relatively slow and reversible.

Comparison of the simulation results with and without the DEA-formate reaction shows that, at temperatures higher than 343 K, some of the DEAF formed by the direct insertion reaction is hydrolyzed back to give formate ions and protonated DEA. However, at temperatures lower than 343 K, the DEA-formate reaction seems to have no significant effect on the net formation of DEAF and formate ions in the system.

The data from the experiment on CO absorption in aqueous solution containing 30 wt% DEA and 18.4 wt% DEAF confirms that the DEA-Formate reaction is reversible.

Parameter estimates of the rate constants suggest that the reaction rates are quite slow but, over time, nevertheless lead to substantial DEAF and formate ion buildup in the system.

The Henry's constant of CO in aqueous DEA solutions was determined by the N₂-Analogy and from the reaction model. The results are in fairly good agreement. Comparison of the values of $H_{\text{CO-DEA}}$ over the temperature range of 313-343 K shows that the value of $H_{\text{CO-DEA}}$ decreases with increasing temperature. This trend is similar to that of CO solubility in pure organic solvents reported in the literature.

An experiment conducted by absorbing CO in 30 wt% aqueous MDEA solution shows that, unlike DEA, MDEA does not react with CO. There was no experimental evidence suggesting the formation of diethanolacetamide

(R₁R₂NCOCH₃) even after 20 hours at 393 K. The rate constant for the formate ion formation reaction was found to be in excellent agreement with that obtained from CO-DEA-H₂O system. This further validates the proposed reaction mechanisms and the experimental technique used to estimate the kinetic parameters.

The DEAF and formic ions concentrations found at the end of each experiment agreed well with those predicted from the present mathematical model. In most cases the relative error was within $\pm 30\%$.

10.3 Recommendations for Future Work

This work provides important correlations for physical properties and kinetic parameters that cover both absorption and desorption conditions applicable to both single and blended amine systems. These correlations should be implemented in process simulators such as Aspen-Plus, TSWEET and Hysis to simulate industrial gas treating processes involving MEA, DEA, MDEA, AMP or their mixtures and the model predictions should be compared with pilot plant or industrial plant data. Further work on CO₂ absorption in partially loaded amine solutions should be carried out to obtain accurate data representing the rich end of the absorber column.

More experimental data on CO₂ absorption/desorption in mixed amine system are desirable. Special attention should be focused on the MEA+MDEA system. The presence of small amounts of MEA in aqueous MDEA solutions significantly improves the capacity of MDEA to absorb CO₂. To explore optimum

MEA concentrations, more experiments should be conducted with solutions containing less than 10 wt% MEA. Blends of MEA and MDEA could be used to economically capture CO₂ from flue gases for the purpose of sequestration or enhanced oil recovery, as the regeneration cost of such solvent systems will be significantly lower.

It will be useful to implement the kinetic mechanisms and the correlations of the kinetic parameters obtained from the work on CO-induced degradation of DEA in existing process simulators to estimate DEA losses for processes where significant amounts of CO is present in the feed gas. Innovative scheme could be developed to avoid or minimize DEA losses, which may run into millions of dollars in industry.

The hemispherical contactor could easily be used to screen new physical or chemical solvents for CO₂ and/or H₂S removal.

NOMENCLATURE

PART I.

a	Interfacial area (m^2)
C_{AM}	Concentration of amine ($kmol/m^3$)
C_i	Concentration of various ionic and non-ionic species as defined by eq. (4.30)
D_i	Diffusivity of ionic and non-ionic species in aqueous amine solution (m^2/s)
D_{CO_2}	Diffusivity of CO_2 in amine solution (m^2/s)
$D_{CO_2}^o$	Diffusivity of CO_2 in pure water (m^2/s)
D_{N_2O}	Diffusivity of N_2O in amine solution (m^2/s)
$D_{N_2O}^o$	Diffusivity of N_2O in pure water (m^2/s)
E	Enhancement factor
E_A	Absorption enhancement factor
E_D	Desorption enhancement factor
E_∞	Maximum possible enhancement factor
F_{CO_2}	Flow rate of feed CO_2 (mmol/s)
$F_{N_2}^{feed}$	Flow rate of feed N_2 (mmol/s)
$F_{N_2}^{dil}$	Flow rate of dilution N_2 (mmol/s)
g	Gravitational constant (m/s^2)
Ga	Grashof number as defined by eq. (4.77)
H_{CO_2}	Henry's constant of CO_2 in amine solution ($kPa \cdot m^3/kmol$)
$H_{CO_2}^o$	Henry's constant of CO_2 in pure water ($kPa \cdot m^3/kmol$)
H_{N_2O}	Henry's constant of N_2O in amine solution ($kPa \cdot m^3/kmol$)
$H_{N_2O}^o$	Henry's constant of CO_2 in pure water ($kPa \cdot m^3/kmol$)
k_{app}	Apparent rate constant (1/s)
k_i	Rate constant for reaction (i)
k_2^{nd}	Second order rate constant as defined by eq. (2.2) ($m^3/kmol \cdot s$)
k_g	Gas-side mass transfer coefficient ($kmol/kPa \cdot m^2 \cdot s$)
k_L^o	Physical mass transfer coefficient (m/s)
M	Hatta number as defined by eq. (2.2)
N_A	Rate of absorption (kmol/s)
N_D	Rate of desorption (kmol/s)
$p_{CO_2}^b$	Partial pressure of CO_2 in the gas bulk (kPa)
$p_{CO_2}^o$	Equilibrium partial pressure of CO_2 corresponding to its concentration in the liquid bulk (kPa)
Q	Liquid flow rate (m^3/s)
r_i	Rate of reaction number (i), ($kmol/m^3 \cdot s$)
S	Least square optimization objective function

R	Radius of the hemisphere (m)
Re	Reynolds number as defined by eq. (4.75)
Sc	Schmidt number as defined by eq. (4.76)
Sh	Sherwood number as defined by eq. (4.101)
T	Temperature (K)
V_0	Velocity at the surface of the liquid film (m/s)
V_θ	Velocity distribution in the liquid film (m/s)
x	Dimensionless distance from the gas-liquid interface
\hat{y}_i	Measured value of the state variable
y(k)	Calculated value of the state variable
z	Zwitterion

Greek Symbols

α	CO ₂ loading (mol of CO ₂ /mol amine)
Δ_θ	Liquid film thickness as a function of latitude θ (m)
Δ_0	Liquid film thickness at the equator (m)
μ	Viscosity of aqueous amine solution, (kg/m s)
ν	Kinematic viscosity (m ² /s)
ν_{AM}	Stoichiometric coefficient
ρ	Density of aqueous amine solution, (kg/m ³)
θ	Angle from the pole
τ_c	Contact time (s)

PART II.

a	Gas-liquid interfacial area, (m ⁻¹)
C_{DEA}	DEA concentration, (wt%)
C_i	Liquid phase concentrations of various chemical species as defined in Eq. (6), (kmol/m ³)
D_{N_2}	Diffusivity of nitrogen in aqueous DEA solution, (m ² /min)
d_{imp}	Impeller diameter, (m)
E	Enhancement factor in Eqs. (10) and (11)
E	Activation energy, (kcal/mol)
H	Henry's law constant, (kPa/m ³ kmol)
k_1	Rate constant for reaction (1), (m ³ /kmol h)
k_2	Rate constant for reaction (2), (m ³ /kmol h)
k_3	Rate constant of forward reaction (3), (m ³ /kmol h)
k_{-3}	Rate constant of reverse reaction (3), (1/h)
K_3	DEAF hydrolysis constant of reaction (3), (in Eq. 53 m ³ /kmol, dimensionless in Eq. 54)
K_4	DEA protonation constant as defined in Eq. (16)
K_5	Water dissociation constant as defined in Eq. (17)
K_6	Formic acid dissociation constant as defined in Eq. (42)
K_7	MDEA protonation constant as defined in Eq. (60)
k_L	Liquid side mass transfer coefficient as defined by Eq. (29), (m/min)

N	Stirrer speed, (rpm)
$n_{\text{CO}}^{\text{total}}$	Total number of moles of CO transferred from gas bomb to autoclave (mol)
n_{CO}^{t}	Number of moles of CO in the headspace of the autoclave (mol)
n_{DEA}	Number of moles of DEA in the solution (mol)
p_{CO}°	Initial partial pressure of CO, (kPa)
p_{CO}	Partial pressure of CO, (kPa)
$p_{\text{N}_2}^{\circ}$	Initial partial pressure of N ₂ , (kPa)
p_{N_2}	Partial pressure of N ₂ , (kPa)
r_i	Rate of reaction, (kmol/m ³ h)
S	Least square optimization objective function
R	Gas constant
Re	Reynolds number as defined by Eq. (30)
Sc	Schmidt number as defined by Eq. (30)
T	Temperature, K
V_{G}	Gas volume in the autoclave, (m ³)
V_{L}	Liquid volume in the autoclave, (m ³)
\hat{y}_i	Measured value of the state variable
$y(\mathbf{k})$	Calculated value of the state variable

Greek Symbols

μ_{L}	Viscosity of aqueous DEA solution, (kg/m-min)
ρ_{L}	Density of aqueous DEA solution, (kg/m ³)

Abbreviations (Part I and II)

AMP	2-amino-2-methyl-1-propanol
DEA	Diethanolamine
DEAE	Diethylethanolamine
DEAF	Formyl-diethanolamine
DMF	Dimethylformamide
FCC	Fluid catalytic cracking
HCN	Hydrogen cyanide
MDEA	Methy-diethanolamine
MEA	Monoethanolamine
R ₁	-CH ₂ CH ₂ OH
R ₂	-CH ₂ CH ₂ OH
R ₃	-CH ₃
R ₄	-C(CH ₃) ₂ CH ₂ OH
R ₁ NH ₂	MEA
R ₁ R ₂ NH	DEA
R ₁ R ₂ R ₃ N	MDEA
R ₄ NH ₂	AMP

$R_1NH_3^+$	Protonated MEA
$R_1R_2NH_2^+$	Protonated DEA
$R_1R_2R_3NH^+$	Protanated MDEA
$R_4NH_3^+$	Protanated AMP
R_1NHCOO^-	MEA carbamate
$R_1R_2NCOO^-$	DEA carbamate
R_4NHCOO^-	AMP carbamate
R_1R_2NHCO	DEAF

REFERENCES

- Al-Ghawas, H.A., Ruiz-Ibanez, G. and Sandall, O.C., 1989a, Absorption of carbonyl sulfide in aqueous methyldiethanolamine, *Chem. Eng. Sci.*, 44(3), 631.
- Al-Ghawas, H.A., Hagewiesche, D.P., Ruiz-Ibanez, G. and Sandall, O.C., 1989b, Physicochemical properties important for carbon dioxide absorption in aqueous methyldiethanolamine, *J. Chem. Eng. Data*, 34, 385.
- Alper, E., 1990, Reaction mechanism and kinetics of aqueous solutions of 2-amino-2-methyl-1-propanol and carbon dioxide, *Ind. Eng. Chem. Res.*, 29, 1725.
- Alvarez-Fuster, C., Midoux, N., Laurent, A. and Charpentier, J.C., 1980, Chemical kinetics of the reaction of carbon dioxide with amines in pseudo m-nth order conditions in aqueous and organic solutions, *Chem. Eng. Sci.*, 35, 1717.
- Aroua, M. K., Ben Amor A., and Sulaiman M. Z., 1997, Temperature dependency of the equilibrium constant for the formation of carbamate from diethanolamine. *J. Chem. Eng. Data.*, 42, 692.
- Astarita, G., 1961, Carbon dioxide absorption in aqueous monoethanolamine solutions, *Chem. Eng. Sci.*, 16, 202.
- Astarita, G., Savage, D.W. and Bisio, A., 1983, *Gas Treating with Chemical Solvents*, John Wiley and Sons, N.Y.
- Austgen, D.M., Rochelle, G.T., Peng, X. and Chen, C.C., 1989, A model of vapor-liquid equilibrium for aqueous acid gas alkanolamine systems using electrolyte NRTL equation, *Ind. Eng. Chem. Res.*, 28, 1060.
- Austgen, D.M., Rochelle, G.T. and Chen, C.C., 1991, Model of vapor-liquid equilibria for aqueous acid gas-alkanolamine systems 2. representation of H₂S and CO₂ solubility in aqueous MDEA and CO₂ solubility in aqueous mixtures of MDEA with MEA or DEA, *Ind. Eng. Chem. Res.*, 30, 1991.
- Bain, R.S. and Stewart, W.E., 1990, Application of robust nonmonotone descent criteria to the solution of nonlinear algebraic equations, *Comp. and Chem. Eng.*, 15, 203.
- Barth, D., Tondre, C., Lappai, G. and Delpuech, J.J., 1981, Kinetic study of carbon dioxide reaction with tertiary amines, *J. phys. Chem.*, 85, 3660.
- Barth, D., Tondre C. and Delpuech, J.J., 1984, Kinetics and mechanisms of the reactions of carbon dioxide with alkanolamines: a discussion concerning the cases of MDEA and DEA, *Chem. Eng. Sci.*, 39, 1753.

Barth, D., Tondre C. and Delpuech, J.J., 1986, Stopped-flow investigations of the reaction kinetics of carbon dioxide with some primary and secondary alkanolamines in aqueous solutions, *Int. J. Chem. Kinetics*, 18, 445.

Blanc, C. and Demarais, G., 1984, The reaction rate of CO₂ with diethanolamine, *Intl. Chem. Eng.*, 24, 43.

Blauwhoff, P.M.M., Versteeg, G.F. and van Swaaij, W.P.M., 1984, A study on the reaction between CO₂ and alkanolamines in aqueous solutions, *Chem. Eng. Sci.*, 39, 207.

Blauwhoff, P.M.M., Kamphuis, B., van Swaaij, W.P.M. and Westerterp, K.R., 1985, Absorber design in sour natural gas treatment plants: impact of process variables on operation and economics, *Chem. Eng. Process.*, 19, 1.

Bosch, H., Versteeg, G.F. and Van Swaaij, W.P.M., 1990a, Desorption of acid gases (CO₂ and H₂S) from loaded alkanolamine solutions, In *Gas Separation Technology*, edited by Vansant, E.F. and Dewolfs, R., Elsevier Science Publishers B.V., Amsterdam, 505-512.

Bosch, H., Versteeg, G.F. and van Swaaij, W.P.M., 1990b, Kinetics of the reaction of CO₂ with the sterically hindered amine 2-amino-2-methylpropanol at 298 K, *Chem. Eng. Sci.*, 45, 1167.

Bottoms, R.R., 1930, U.S. Patent 1,783, 901.

Bower, V.E., Robinson, R.A. and Bates, R.G., 1962, Acidic dissociation constant and related thermodynamic quantities for diethanolammonium ion in water from 0 to 50 °C, *J. Res. NBS-A. Physics and Chemistry*, 66A, 71.

Brenan, K.E., Campbell, S.L. and Petzold, L.R., 1989, *Numerical solution of initial value problems in differential-algebraic equations*, North Holland, Amsterdam.

Browning, G.J. and Weiland, R.H., 1994, Physical solubility of carbon dioxide in aqueous alkanolamines via nitrous oxide analogy, *J. Chem. Data*, 39, 817.

Caplow, M., 1968, Kinetics of carbamate formation and breakdown, *J. Am. Chem. Soc.*, 90,6795.

Caracotsios, M. and Stewart, W.E., 1985, Sensitivity analysis of initial value problems with mixed ODEs and algebraic equations, *Comp. & Chem. Eng.*, 9, 359.

Caracotsios, M. and Stewart, W.E., 1995, Sensitivity analysis of initial-boundary-value problems with mixed PDEs and algebraic equations; Applications to chemical and biochemical systems, *Comp. and Chem. Eng.*, 19, 1019.

Chakma, A, 1987, Studies on DEA and MDEA degradation, Ph.D. Thesis, University of British Columbia, Vancouver, B.C.

Chakma, A, and Meisen, A., 1988, Identification of methyldiethanolamine degradation products by gas chromatography and gas chromatography-mass spectrometry, *J. Chrom.*, 457, 287.

Clarke, J.K.A., 1964, Kinetics of absorption of carbon dioxide in monoethanolamine solutions at short contact times, *I & EC Fundamentals* 3(3),239.

Chakraborty, A.K., Astarita, G. and Bischoff, K.B., 1986, CO₂ absorption in aqueous solutions of hindered amines, *Chem. Eng. Sci.*, 41(4), 997.

Coldrey, P.W. and Harris, L., 1976, Kinetics of the liquid phase reaction between carbon dioxide and diethanolamine, *Can. J. Chem. Eng.*, 51, 566.

Critchfield, J. E. and Rochelle, G.T., 1987, CO₂ Absorption into aqueous MDEA and MDEA/MEA solutions, Presented at the AIChE National Meeting, Paper No. 43e, Houston, TX.

Critchfield, J.E., 1988, CO₂ absorption desorption in methyldiethanolamine solutions promoted with monoethanolamine and diethanolamine: mass transfer and reaction kinetics, Ph.D. dissertation, The University of Texas, Austin.

Critchfield, J.E. and Rochelle, G.T., 1988, CO₂ absorption from DEA and DEA-promoted MDEA solutions, Paper 68b, presented at AIChE spring national meeting, New Orleans, LA.

Crooks, J.E. and Donnellan, J.P., 1989, Kinetics and mechanism of the reaction between carbon dioxide and amines in aqueous solutions, *J. Chem. Soc. Perkin. Trans. II*, 331.

Danckwerts, P.V. and Sharma, M.M., 1966, The absorption of carbon dioxide into solutions of alkalis and amines (with some notes on hydrogen sulfide and carbonyl sulfide), *Chem. Engr*, Oct. CE244.

Danckwerts, P.V. and McNeil, K.M., 1967, The absorption of carbon dioxide into aqueous amine solutions and the effects of catalysis, *Trans. Inst. Chem. Eng.*, 45, T32.

Danckwerts, P.V., 1970, *Gas liquid reactions*, McGraw Hill, NY.

Danckwerts, P. V., 1970, The reaction of CO₂ with ethanolamines, *Chem. Eng. Sci.*, 34, 443.

- Danckwerts, P.V., 1979, The reaction of CO₂ with ethanolamines, Chem. Eng. Sci., 34, 443.
- Davidson, J.F. and Cullen, E.J., 1957, The determination of diffusion coefficients for sparingly soluble gas in liquids, Trans. Inst. Chem. Engrs, 35, 51.
- Davis, R.A. and Sandall, O.C., 1993, Kinetics of the reaction of carbon dioxide with secondary amines in polyethylene glycol, Chem. Eng. Sci., 48(18), 3187.
- Dawodu, O.F. and Meisen, A., 1991, Identification of products resulting from carbonyl sulfide induced degradation of diethanolamine, J. Chrom., 587, 237.
- DeCoursey, W.J., 1982, Enhancement factors for gas absorption with reversible reaction, Chem. Eng. Sci., 37, 1483.
- DeCoursey, W.J., 1992, A simpler approximation for enhancement of mass transfer by second-order reversible reaction, IChemE Symp. Ser. No. 128, 2, B269.
- Dehouche, Z. and Lieto, J., 1995, Modelling and experimental study of key parameters of absorption on wetted sphere contactor, Chem. Eng. Sci., 50, 2899.
- Deshmukh, R.D. and Mather, A.E., 1981, A mathematical model for equilibrium solubility of hydrogen sulphide and carbon dioxide in aqueous alkanolamine solutions, Chem. Engng. Sci., 36, 355.
- DiGuillo, R. M., Lee, R. J., Schaeffer, S. T., Brasher, L. L. and Teja, A. S., 1992, densities and viscosities of the ethanolamines, J. Chem. Eng. Data, 37, 239.
- Donaldson, T.L. and Y.N. Nguyen, 1980, Carbon dioxide reaction kinetics and transport in aqueous amine membranes, Ind. Eng. Chem. Fundam., 19, 260.
- Duranleau, R.G. and Lambert, C.L., 1985, Process for the preparation of formamide compounds, US patent 4529822, (TEXACO Inc).
- Duda, J.F., and Verntas, J.C., 1968, Laminar liquid jet diffusion studies, AIChE J., 14, 286.
- Edwards, T. J., Maurer, G., Newman, J., Prausnitz, J. M., 1978, Vapor-liquid equilibria in multicomponent aqueous solutions of volatile weak electrolytes. AIChE J., 24, 966.
- Eickmeyer, A.G., 1962, Catalytic removal of CO₂, Chem. Eng. Prog., 58(4), 89.

Ellis, A.J., and Golding, R.M., 1963, The solubility of carbon dioxide above 100 °C in water and in sodium chloride solutions, *Am. J. Sci.*, 261, 47.

Fogg, P.G.T. and Gerrard, W., 1991, *Solubility of gases in Liquids*, John Wiley & Sons, NY, 274.

Glasscock, D.A., 1990, Modeling and experimental study of carbon dioxide absorption into aqueous alkanolamines, Ph.D. dissertation, The University of Texas, Austin.

Glasscock, D.A., Critchfield, J.E., and Rochelle, G.T., 1991, CO₂ absorption/desorption in mixtures of methyldiethanolamine with monoethanolamine or diethanolamine, *Chem. Eng. Sci.*, 46, 2829.

Goldstein, A.M., Brown, E.C., Heinzelmann, F.J. and Say, G.R., 1986, New FLEXORB gas treating technology for acid gas removal. *Energy. Prog.*, 7, 67.

Groothius, H., 1966, *de Ingenieur*, 78, CH9.

Hagewiesche, D.P., Ashour, S.S., Al-Ghawas, H.A. and Sandall, O.C., 1995a, Absorption of carbon dioxide into aqueous blends of monoethanolamine and n-methyldiethanolamine, *Chem. Eng. Sci.*, 50, 1071.

Hagewiesche, D. P., Ashour, S. S. and Sandall, O. C., 1995b, Solubility and diffusivity of nitrous oxide in ternary mixtures of water, monoethanolamine, and N methyldiethanolamine and solution densities and viscosities, *J. Chem. Eng. Data*, 40, 627.

Haimour, N. and Sandall, O.C., 1984, Absorption of carbon dioxide into aqueous methyldiethanolamine, *Chem. Eng. Sci.*, 39, 1791-1796.

Haimour, N.M., 1990, Solubility of N₂O in aqueous solutions of diethanolamines at different temperatures, *J. Chem. Eng. Data.*, 35, 177.

Haimour, N.A. Bidarian, A. and Sandall, O.C., 1985, Absorption of CO₂ into aqueous solutions of methyldiethanolamine, Paper presented at AIChE spring national meeting, Houston.

Haimour, N., Bidarian, A. and Sandall, O.C., 1987, Kinetics of the reaction between carbon dioxide and methyldiethanolamine, *Chem. Eng. Sci.*, 42(6), 1393.

Harned, H.S. and Embree, N.D., 1934, The ionization constant of formic acid from 0 to 60 °C. *J. Amer. Chem. Soc.*, 56, 1042-1044.

Harned, H.S. and Robinson, R.A., 1940, *Trans. Faraday Soc.*, 36, 973.

- Hikita, H., Asai, S., Ishikawa, N. and Saito, Y., 1975, Kinetics of absorption of chlorine in aqueous acidic solutions of ferrous chloride, *Chem. Eng. Sci.* 30, 607.
- Hikita, H., S. Asai, H. Ishikawa, and M. Honda, 1977a, The kinetics of reactions of carbon dioxide with monoethanolamine, diethanolamine, and triethanolamine by a rapid mixing method, *Chem. Eng. J.*, 13,7.
- Hikita, H., S. Asai, H. Ishikawa, and M. Honda, 1977b, The kinetics of reactions of carbon dioxide with monoisopropanolamine, diglycolamine, and ethylenediamine by a rapid mixing method, *Chem. Eng. J.*, 14, 27.
- Hsu, C. and Li, M., 1997a, Densities of aqueous blended amines, *J. Chem. Eng. Data.* 42, 502.
- Hsu, C. and Li, M., 1997b, Viscosities of aqueous blended amines, *J. Chem. Eng. Data.* 42, 714.
- Jensen, A., Jorgensen, E., Faurholt, C., 1954a, Reactions between carbon dioxide and amino alcohols. I. monoethanolamine and diethanolamine, *Acta Chemica Scandinavica*, 8, 1137.
- Jensen, A., M.B. Jensen, and C. Faurholt, 1954b, Studies on carbamates: the carbamates of di-n-propylamine and di-iso-propylamine, *Acta Chemica Scandinavica*, 8, 1129.
- Jorgensen, E., 1956, Reactions between carbon dioxide and amino alcohols III. diethanolamine, *Acta Chemica Scandinavica*, 10,747.
- Katti, S.S., 1995, Gas-liquid-solid system: an industrial perspective. *Trans. IchemE.* 73, 595.
- Katti, S.S. and McDougal, K.A., 1986, Rate approach in the design and simulation of chemical absorbers: theory and practice, Paper presented at the annual meeting, AIChE, Miami Beach Florida.
- Kennard, M.L. and Meisen, A., 1985, Mechanisms and kinetics of diethanolamine degradation, *Ind. Eng. Chem. Fund.*, 24, 129.
- Kell, G. S., 1975, Density, thermal expansivity, and compressibility of liquid water from 0 to 150 °C: correlations and tables for atmospheric pressure and saturation reviewed and expressed on 1968 temperature scale, *J. Chem. Eng. Data*, 20, 97.
- Kent, R.L. and Eisenberg, B., 1976, Better data for amine treating, hydrocarbon process., 55, 87.

Kim, C.J., 1988, Degradation of alkanolamines in gas treating solutions: kinetics of di-2-propanolamine degradation in aqueous solutions containing carbon dioxide, *Ind. Eng. Chem. Res.* 27, 1.

Kim, C.J. and Sartori, G., 1984, Kinetics and mechanism of diethanolamine degradation in aqueous solutions containing carbon dioxide, *Int. J. Chem. Kinetics*, 16, 1257.

Kim, C.J., Palmer, A.M. and Milliman, G.E., 1988, Absorption of carbon monoxide into aqueous solutions K_2CO_3 , methyldiethanolamine and diethylethanolamine, *Ind. Eng. Chem. Res.*, 27, 324.

Kirk Othmer, 1993, *Encyclopedia of Chemical Technology*, 5, 4th edition.

Kohl, A. L. and Riesenfeld, F. C. 1985, *Gas Purification*, 4th ed.; Gulf: Houston, TX.

Ko, J.J. and Li, M.H., 2000, Kinetics of absorption of carbon dioxide into solutions of N-methyldiethanolamine + water, *Chem. Eng. Sci.*, 55, 4139.

Koike, L., Barone, J., Godinho, O.E.S., Aleixo, L.Z. and Reis, F., 1987, N-formyldiethanolamine: a new artifact in diethanolamine solutions, *Chem. Ind.*, 17, 626.

Krishnamurthy, R. and Taylor, R., 1985, A Non-equilibrium stage model of multicomponent separation processes, *AIChE J.*, 31, 449-455, *Ibid*, 1985, 456.

Laddha, S.S. and Danckwerts, P.V., 1981, Reaction of CO_2 with ethanolamines: kinetics from gas-absorption, *Chem. Eng. Sci.*, 36, 479.

Laddha, S.S., Diaz, J.M. and Danckwerts, P.V., 1981, The N_2O analogy: the solubilities of CO_2 and N_2O in aqueous solutions of organic compounds, *Chem. Eng. Sci.* 36, 228.

Laddha, S.S., and Danckwerts, P.V., 1982, The absorption of CO_2 by amine-potash solutions, *Chem. Eng. Sci.*, 37, 665.

Lambert, C.L. and Duranleau, R.G., 1985, Process for the preparation of formylalkanoalmines, US patent 4510326, (TEXACO Inc).

Leder, F., 1971, The Absorption of CO_2 into chemically reactive solutions at high temperatures, *Chem. Eng. Sci.* 26, 1381.

Levenspiel, O, 1972, *Chemical reaction engineering*, John Wiley & Sons Inc., NY.

Lewis, W.K. and Whitman, W.G., 1924, Principles of gas absorption, Ind. Eng. Chem., 16 (12), 1215.

Li, M. H. and Shen, K. P., 1992, Densities and solubilities of solutions of carbon dioxide in water + monoethanolamine + N-methyldiethanolamine, J. Chem. Eng. Data 1992, 37, 288.

Li, M. H. and Lie, Y. C., 1994, Densities and viscosities of solutions of monoethanolamine + N-methyldiethanolamine + water and monoethanolamine + 2-amino-2-methyl-1 propanol + water, J. Chem. Eng. Data, 39, 444.

Li, M.H. and Lai, M.D., 1995, Solubility and diffusivity of N₂O and CO₂ in (monoethanolamine + N-methyldiethanolamine +water) and in (monoethanolamine + 2-amino-2-methyl-1-propanol + water), J. Chem. Eng. Data, 40, 486.

Li, M.H. and Lee, W.C., 1996, Solubility and diffusivity of N₂O and CO₂ in (diethanolamine + N-methyldiethanolamine +water) and in (diethanolamine + 2-amino-2-methyl-1-propanol + water), J. Chem. Eng. Data, 41, 551.

Littel, R.J., van Swaaij, W.P.M., and Versteeg, G.F., 1990a, The kinetics of carbon dioxide with tertiary amines in aqueous solution, Presented at the AIChE Spring National Meeting, Orlando, FL.

Littel, R.J., Bos, M. Knoop, G.J., 1990b, Dissociation constants of some alkanolamines at 293, 303, 318, and 333 K, J. Chem. Eng. Data, 35, 276.

Littel, R.J., Versteeg, G.F. and van Swaaij, W.P.M., 1992a, Kinetics of CO₂ with primary and secondary amines in aqueous solutions- I. zwitterion deprotonation kinetics for DEA and DIPA in aqueous blends of alkanolamines, Chem. Eng. Sci., 47, 2027.

Littel, R.J., Versteeg, G.F. and van Swaaij, W.P.M., 1992b, Kinetics of CO₂ with primary and secondary amines in aqueous solutions- II. Influence of temperature on zwitterion formation and deprotonation rates, Chem. Eng. Sci., 47, 2037.

Little, R.J., Versteeg, G.F. and van Swaaij, W.P.M., 1992c, Solubility and diffusivity data for the absorption of COS, CO₂ and N₂O in amine solutions, J. Chem. Eng. Data, 37, 49.

Lynn, S., Straatemeier, J.R. and Kramers, H., 1955, Absorption studies in the light of the penetration theory. III. absorption by wetted spheres, singly and in columns, Chem. Eng. Sci., 4, 63.

Malinin, S.D., 1975, Thermodynamics of the H₂O-CO₂ systems, Geochem. Int., 11, 1060.

- Markham, A.E. and Kobe, K.A., 1941, *Ind. Eng. Chem.*, 63, 449.
- Messaoudi, B. and Sada, E., 1996, Absorption of carbon dioxide into loaded aqueous solutions of 2-amino-2-methyl-1propanol, *J. Chem. Eng. Japan*, 29, 534.
- McDonald, R. D., 1963, The kinetics of carbon monoxide in basic solution at elevated temperatures, MSc Thesis, The University of British Columbia, Vancouver, BC.
- Olofsson, G. and Hepler, L.G., 1975, The thermodynamics of ionization of water over wide range of temperature and pressure, *J. Soln. Chem.*, 4, 127.
- Pacheco, M.A., Kaganoi, S. and Rochelle, G.T., 2000, CO₂ absorption into aqueous mixtures of diglycolamine and methyldiethanolamine, *Chem. Eng. Sci.*, 55, 5125.
- Pani, F, Gaunand, A., Cadours, R, Bouallou, C. and Richon, D., 1997, Kinetics of absorption of CO₂ in concentrated aqueous methyldiethanolamine solutions in the range 296-343K, *J.Chem. Eng. Data*, 42, 353-359.
- Penny, D.E. and Ritter, T.J., 1983, Kinetic study of the reaction between carbon dioxide and primary amines, *J.Chem.Soc., Faraday Trans.* 79, 2103.
- Perry, J.H., Chilton, C.H. and Kirkpatrick S.D., 1963, 1984, *Chemical Engineers' Handbook*, McGraw Hill, NY, 5th and 6th Edn, 14-4.
- Petzold, L.R., 1983, A description of DASSL: a differential/algebraic system solver in scientific computing, eds. Stepleman et al., North Holland, Amsterdam, 65-68.
- Prausnitz, J.M., Lichtenthaler, R.N. and de Azevedo, E.G., 1986, *Molecular thermodynamics of fluid-phase equilibria*, 2nd edn., Prentice-Hall Englewood Cliffs, NJ.
- Pinsent, B.R.W., Pearson, W.L., Roughton, F.J.W., 1956, The kinetics of the combination of carbon dioxide with hydroxide ions. *Trans. Fraday Soc.*, 52, 1512.
- Rangwala, R.A., Morrell, B.R., Mather, A.E. and Otto, F.D., 1992, Absorption of CO₂ into aqueous tertiary amine solutions, *Can. J. Chem. Eng.*, 70, 482.
- Richard, A.D. and Sandall, O.C., 1993, Kinetics of the reaction of carbon dioxide with secondary amines in polyethylene glycol, *Chem. Eng. Sci.*, 48, 3187.

Rinker, E.B., Ashour, S.S. and Sandall, O.C., 1995a, Kinetics and modeling of carbon dioxide absorption into aqueous solutions of N-methyldiethanolamine, Chem. Eng. Sci., 50(5),755.

Rinker, E. B., Russell, J. W., Tamimi, A. and Sandall, O. C., 1995b, Diffusivity of nitrous oxide in N-methyldiethanolamine + diethanolamine + water, J. Chem. Eng. Data, 40, 630.

Rinker, E. B., Oelschlager, D. W., Colussi, A. T., Henry, K. R., and Sandall, O. C., 1994, Viscosity, density, and surface tension of binary mixtures of water and N-methyldiethanolamine and water and diethanolamine and tertiary mixtures of these amines with water over the temperature range 20-100 °C, J. Chem. Eng. Data, 39, 392.

Rinker, E.B., Ashour, S.S. and Sandall, O.C., 1996, Kinetics and modeling of carbon dioxide absorption into aqueous solutions of diethanolamine, Ind. Eng. Chem. Res., 35, 1107.

Read, A.J., 1975, The first ionization constant of carbonic acid from 25 to 250 °C and to 2000 bar, J. Soln. Chem., 4, 53.

Reid, R.C., Prausnitz, J.M. and Poling, B.E., 1987, The properties of gases and liquids, 4th Edn, McGraw Hill, NY.

Rowley, R.L., Adams, M.E., Marshall, T.L., Oscarson, J.L., Wilding, W.V. and Anderson, D.J., 1998, Measurement of the absorption rate of carbon dioxide into aqueous diethanolamine, J. Chem. Eng. Data, 43, 427.

Sada, E., Kumazawa, H. and Butt, M.A., 1977, Solubilities of gases in aqueous solutions of amine, J. Chem. Eng. Data, 22, 277.

Sada, E. and Kito, S., 1972, Kagaku Kogaku, 36, 218.

Sada, E., Kumazawa, H. and Butt, M.A., 1976, Gas Absorption with consecutive chemical reaction: absorption of carbon dioxide into aqueous amine solutions, Can. J. Chem. Eng., 54, 421.

Sada, E., Kumazawa, H. and Butt, M. A., 1978, Solubility and diffusivity of gases in aqueous solutions of amines. J. Chem. Eng. Data, 23, 161.

Sada, E., Kumazawa, H., and Han, Z.Q., 1985, Kinetics of reaction between carbon dioxide and ethylenediamine in nonaqueous solvents, Chem. Eng. J., 31,109.

Saha, A.K., Bandyopadhyay, S.S. and Biswas, A.K., 1993, Solubility and diffusivity of N₂O and CO₂ in aqueous solutions of 2-amino-2-methyl-1-propanol, J. Chem. Eng. Data, 38, 78.

Saha, A.K., Bandyopadhyay, S.S. and Biswas, A.K., 1995, Kinetics of absorption of CO₂ into aqueous solutions of 2-amino-2-methyl-1-propanol, Chem. Eng. Sci. 50(22), 3587.

Sandall, O.C., Rinker, E.B. and Ashour, S., 1993, Acid gas treating by aqueous alkanolamines, Annual report to the Gas Research Institute.

Sardar, H., 1985, Development of a non-equilibrium stage model for the design and simulation of gas processing units and verification with plant data, PhD Dissertation at Clarkson University, Potsdam, N.Y.

Sartori, G. and Savage, D.W., 1983, Sterically hindered amines for CO₂ removal from gases, Ind. Eng. Chem. Fundam., 22, 239.

Sartori G., Ho, W. S. and Savage, D.W., 1987, Sterically hindered amines for acid gas absorption, Separation and Purification Methods, 16, 171.

Savage, D.W., Astarita, G. and Joshi, S., 1980, Chemical absorption and desorption of carbon dioxide from hot carbonate solutions, Chem. Eng. Sci., 35, 1513.

Sharma, M.M., 1964, Thesis, Cambridge University.

Sharma, M.M., 1965, Kinetics of reactions of carbonyl sulphide and carbon dioxide with amines and catalysis by bronsted bases of the hydrolysis of COS, Trans. Faraday Soc., 61, 681.

Song, J. H., Park, S. B., Yoon, J. H., Lee, H. and Lee, K. H., 1996, Densities and viscosities of monoethanolamine + ethylene glycol + water, J. Chem. Eng. Data, 41, 1152.

Stewart, W.E., Caracotsios, M. and Sorenson, J.P., 1992, Parameter estimation from multi response data, AIChE J., 42, 1404.

Stewart, W.E., Henson, T.L. and Box, G.E.P., 1996, Model discrimination and criticism with single-response data, AIChE J., 42, 3055.

Supap, T., Idem, R., Veawab, A., Aroonwilas, A., Tontiwachwuthikul, P., Chakma, A. and Kybett, B. D., 2001, Kinetics of the oxidative degradation of aqueous monoethanolamine in a flue gas treating unit, Ind. Eng. Chem. Res., 40, 3445.

Takenouchi, S. and Kennedy, G.C., 1964, The binary system H₂O-CO₂ at high temperatures and pressures, Am. J. Sci., 262, 1055.

Tamimi, A. Rinker, E.B. and Sandall, O.C., 1994a, Diffusion coefficients for H₂S, CO₂ and N₂O in water over the temperature range 293 - 368 K, J. Chem. Eng. Data, 39, 330.

Tamimi, A. Rinker, E.B. and Sandall, O.C., Diffusivity of N₂O in aqueous solutions of methyldiethanolamine and diethanolamine from 293 - 368 K, J. Chem. Eng. Data, 39, 396 (1994b).

Toman, J.J. and Rochelle, G.T., 1989, Carbon dioxide absorption rates and physical solubility in 50% aqueous methyldiethanolamine partially neutralized with sulfuric acid, Presented at the AIChE Spring National Meeting, Houston, TX.

Toman, J.J. and Rochelle, G.T., 1990, CO₂ Absorption rates into aqueous solutions of 2-(tert-butylamino)ethanol, presented at the Spring National AIChE Meeting, Orlando, FL.

Tomcej, R.A. and F.D. Otto, 1989, Absorption of CO₂ and N₂O into aqueous solutions of methyldiethanolamine, AIChE., 35(5), 861.

Treybal, R.E., 1980, Mass transfer operations, McGraw-Hill, N.Y.

Tseng, P.C., W.S. Ho, D.W. Savage, 1988, Carbon dioxide absorption into promoted carbonate solutions, AIChE J., 34, 922.

Van Krevelen, D.W. and Hoftijzer, P.J., 1948, Kinetics and simultaneous absorption and chemical reaction, Chem. Eng. Prog., 44, 7, 529.

Versteeg, G.F. and van Swaaij, W.P.M., 1988, On the kinetics between CO₂ and alkanolamines both in aqueous and non-aqueous solutions- II. tertiary amines, Chem. Eng. Sci., 43, 587.

Versteeg, G.F. and van Swaaij, W.P.M., 1988, Solubility and diffusivity of acid gases (CO₂ and N₂O) in aqueous alkanolamine solutions, J. Chem. Eng. Data, 33, 29.

Versteeg, G.F. and Oyevaar, M.H., 1989, The reaction between CO₂ and diethanolamine at 298 K, Chem. Eng. Sci., 44, 1264.

Wang, Y. W., Xu, S., Otto, F. D. and Mather, A. E., 1992, Solubility of N₂O in alkanolamines and in mixed solvents. Chem. Eng. J., 48, 31.

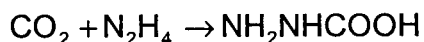
- Weiland, R.H., Chakravarty, T. and Mather, A.E., 1993, Solubility of carbon dioxide and hydrogen sulfide in aqueous alkanolamines, *Ind. Eng. Chem. Res.*, 32, 1419.
- Wild, J.D., and Potter, O.E., 1968, Gas absorption with chemical reactions into liquid flowing on a sphere, *Inst. Chem. Eng. Symp. Ser.*, 28, 30.
- Xiao, J., Li, C.W., and Li, M.H., 2000, Kinetics of absorption of carbon dioxide into aqueous solutions of 2-amino-2-methyl-1-propanol + monoethanolamine, *Chem. Eng. Sci.*, 55, 161.
- Xu, S., Wang, Y., Otto, F.D. and Mather, A.E., 1991a, Rate of absorption of CO₂ in a mixed solvent, *Ind. Eng. Chem. Res.*, 30, 1213.
- Xu, S.; Otto, F. D.; Mather, A. E., 1991b, Physical properties of aqueous AMP solutions, *J. Chem. Eng. Data*, 36, 71.
- Xu, G.W, Zhang, C.F., Qin, S.I. and Wang, Y.W., 1992a, Kinetics study on absorption of carbon dioxide into solutions of activated methyldiethanolamine, *Ind. Eng. Chem. Res.*, 31,921.
- Xu, S.; Wang, Y.; Otto, F. D.; Mather, A. E., 1992b, Physicochemical properties of 2-piperidineethanol and its aqueous solutions, *J. Chem. Eng.*, 37, 407.
- Xu, G.W., Zhang, C.F., Qin, S.J. and Zhu, B.C., 1995, Desorption of CO₂ from MDEA and activated MDEA solutions, *Ind. Eng. Chem. Res.*, 34, 874.
- Xu, S., Wang, Y.W., Otto, F.D. and Mather, A.E., 1996, Kinetics of the reaction of carbon dioxide with 2-amino-2-methyl-1-propanol solutions, *Chem. Eng. Sci.*, 51, 841.
- Yih, S. M. and Shen, K.P., 1988, Kinetics of carbon dioxide reaction with sterically hindered 2-amino-2-methyl-1-propanol aqueous solutions, *Ind. Eng. Chem. Res.*, 41, 2237.
- Yaws, C. L., Miller, J. W., Shah, P. N., Schorr, G. R. and Patel, P. M., 1976, *Chem. Eng.*, 83, 153.
- Yu, W. C., Astarita, G. and Savage, D.W., 1985, Kinetics of carbon dioxide absorption in solutions of methyldiethanolamine, *Chem. Eng. Sci.*, 40(8), 1585.
- Yu, W.C. and G. Astarita, 1987, Design of packed towers for selective chemical absorption, *Chem. Eng. Sci.*, 42, 425

APPENDIX A

DETERMINATION OF CO₂ LOADING IN AMINE SOLUTIONS

A.1 *Detection Principle*

The total CO₂ content in the liquid phase or the CO₂ loading was determined by a novel method developed by Shell Technology Center, Houston, Texas. In this method a small amount of liquid sample (0.1-1.0 gm) is injected into a solution of 30 wt% hydrochloric acid which instantly frees the CO₂ chemically combined with the amine. The nitrogen gas carries the total CO₂ to a Gastec tube filled with an indicating layer of a pale white color substance that contains hydrazine. In the Gastec tube, CO₂ reacts with hydrazine to form carbonic acid monohydrazide, which changes the color of redox indicator to a bluish-violet according to following reaction:



The length of the stain formed is directly proportional to the CO₂ concentration in the sample.

A.2 *Experimental Setup and Procedure*

Figure A.1 shows the experimental setup for determining CO₂ in amine solution. The gas analysis vessel shown in Figure A.1 was specifically designed for this type of experiments and was supplied by Shell Technology Center,

Houston, Texas. The Gastec tubes used in this work were type 2HH and were obtained from Gastec Corporation, Fukaya, Japan.

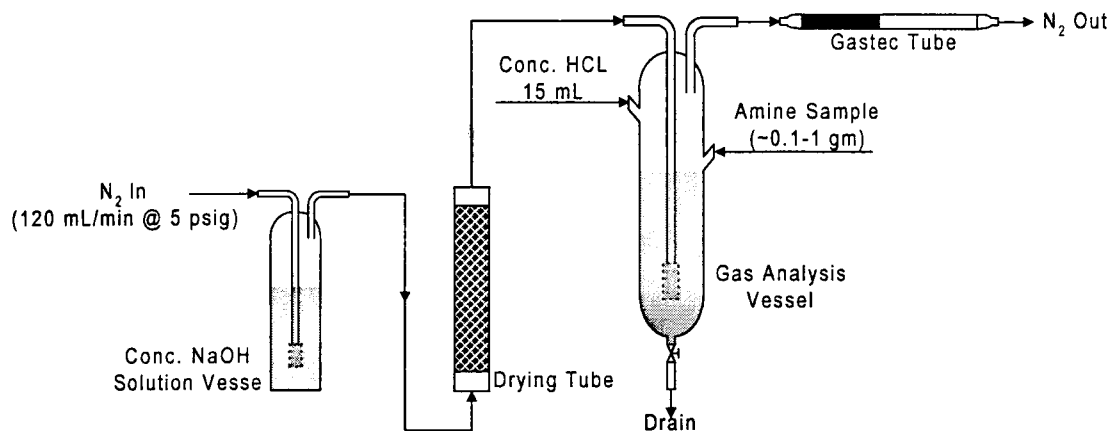


Figure A.1 Experimental setup for CO₂ measurement in Liquid Samples

In a typical run, the gas analysis vessel was thoroughly rinsed with distilled water and 15 mL of 30-wt% HCL solution was dispensed into the vessel and the cap was tightened. A low-pressure nitrogen supply line was attached to the inlet of the analysis vessel. Before entering the analysis tube, the nitrogen stream was first bubbled through a tube containing concentrated NaOH solution and then to drying tube. This was done to remove any traces of CO₂ or water vapor present in nitrogen gas from the supply cylinder. The N₂ supply was turned on and the upstream pressure was adjusted to 5 psi. The entire system was sparged for 5 minutes and checked for leaks using snoop. After breaking the tips off both ends, the Gastec tube was inserted at the outlet of the analysis vessel and kept in horizontal position by a metal stand. The nitrogen gas was allowed to sparge through the tube for 5 minutes to make sure there was no CO₂

contamination. During this period If there was any stain, the tube was discarded and a new tube was used. Once the system was CO₂ free, small amount of sample (0.1-1.0 gm, depending on CO₂ loading) was withdrawn from the air-tight sample bottle using a Hamilton gas-tight syringe, weighed in an electronic balance and injected into the sample port through the septum. At this stage nitrogen flow was adjusted to 120 mL/min and was kept at this throughout the run. The sparging was continued for exactly 40 mins. The nitrogen flow rate and the sparge time were determined by conducting a number of trial runs during the development of the procedure. In the analysis, if the stain over ranged the tube, it was repeated using smaller sample size. If there was no stain, the analysis was repeated using larger sample size. For each run, the vessel was drained and rinsed with water. Also, each analysis was repeated at least twice using a new tube every time. After each run, the Gastec tube was quickly removed from the system and the stain length was measured using a Vernier scale. If the stain length was not uniform, the maximum and minimum lengths were measured and an average was taken.

The amount of CO₂ in a liquid sample was calculated using the following equation:

$$\text{CO}_2 \text{ Loading} \left(\frac{\text{mols of CO}_2}{\text{mols of Amine}} \right) = \frac{R_f \times \text{Stain Length(cm)}/44}{\text{Amine wt\%} \times \text{Sample Size(mg)}/\text{Amine mol. wt.}}$$

The response factor, R_f, was obtained from the calibration curve prepared by injecting a liquid sample with known amount of CO₂. To do this a standard solution that contained 10,000 ppm (weight) as CO₂ stock was prepared using

sodium carbonate (24.1 gm Na_2CO_3 up to 1000 gm) in water. The relationship between the CO_2 content and the stain length was obtained by injecting standard samples ranging from 0 to 2.5 gm. Each injection was repeated at least twice and the responses were averaged. The raw data are reported in Table A.1 and the calibration curve is presented in Figure A.2. The value of the correlation coefficient ($R^2 = 0.9956$) indicates that reproducibility of the measurements is excellent.

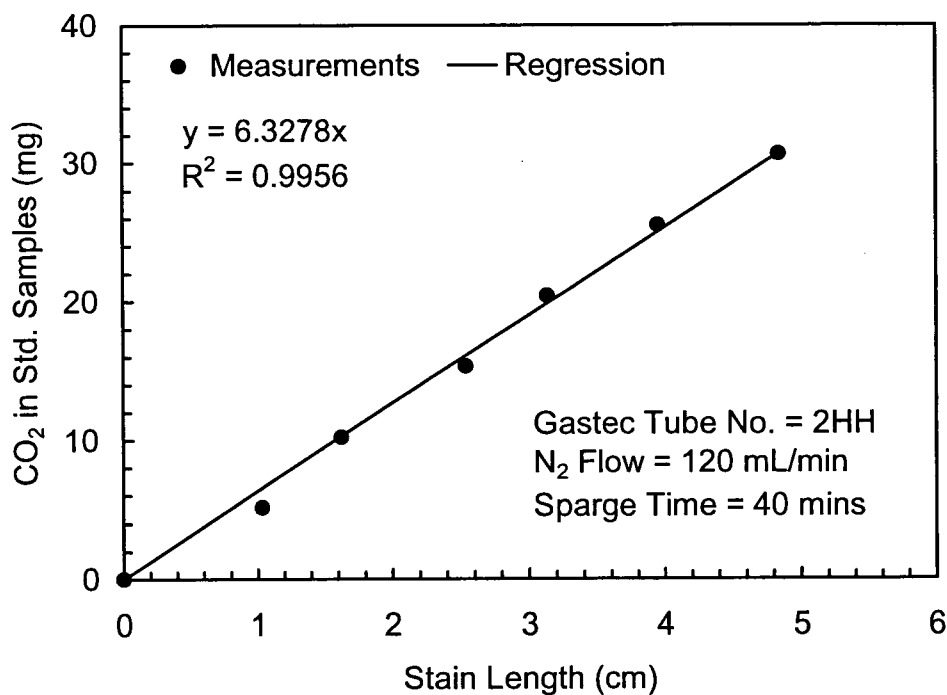


Figure A.2 Calibration Curve for Gastec Detector Tube No. 2HH for CO_2 Measurement in Liquid Samples

Table A.1: Calibration Data for Gastec Detector Tubes No. 2HH

(Standard Solution: 10, 000 ppm (by weight) Na_2CO_3 ,
 N_2 Flow = 120 ml/min, Sparge Time = 40 min)

Sample Volume	Sample Weight	CO_2 in Sample	Tube Reading (Avg. of 2 tubes)
ml	gm	mg	cm
0.0	0.00	0.00	0.00
0.5	0.51	5.10	1.03
1.0	1.02	10.20	1.63
1.5	1.53	15.30	2.54
2.0	2.04	20.40	3.14
2.5	2.55	25.50	3.95
3.0	3.06	30.60	4.84

APPENDIX B

CALIBRATION OF MEASURING INSTRUMENTS

B.1 Pressure Transducers

The calibration of pressure transducers installed on the heating tank and absorption/desorption chamber was done by pressurizing the apparatus from ambient to 20 psig and then bringing it back to ambient pressure in a stepwise manner. The calibration curve was generated using the average values. The actual pressure was measured in mm of Hg using mercury manometer and the output signal from the transducer was measured in volts using the computer data acquisition system. The calibration curves and corresponding correlations are shown in Figure B.1 and B.2.

B.2 Mass Flow Meters

The mass flow meters were calibrated for CO₂, N₂O and N₂ by means of a soap film meter. A soap film assembly as shown in Figure B.3 was set up and the ambient temperature and pressure was recorded. The time taken for a soap bubble to travel between two marks was noted using a stopwatch. For each flow at least three measurements were collected and average was used in generating the calibration curve. The output signal from the mass flow meter was measured using the computer data acquisition system. The same procedure was adopted

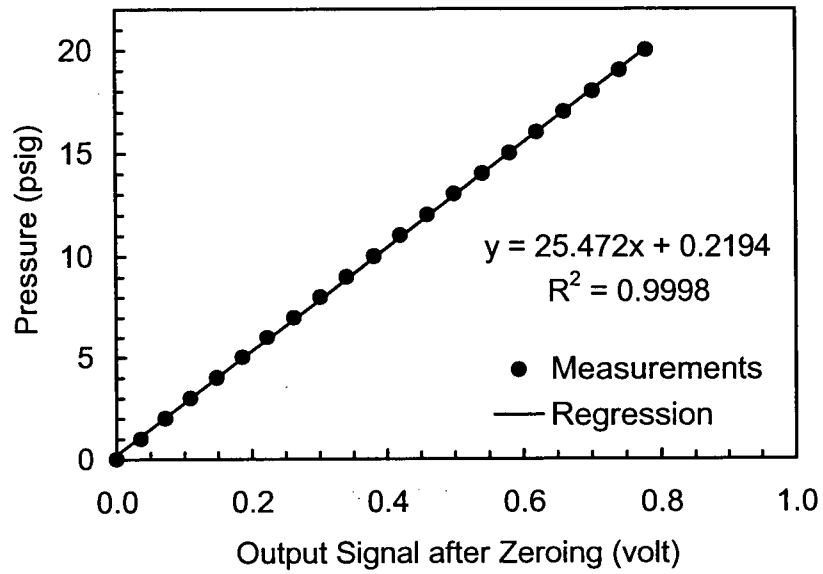


Figure B.1 Calibration Curve for Pressure Transducer on Absorption/Desorption Chamber(Omega Model PX202-030GV)

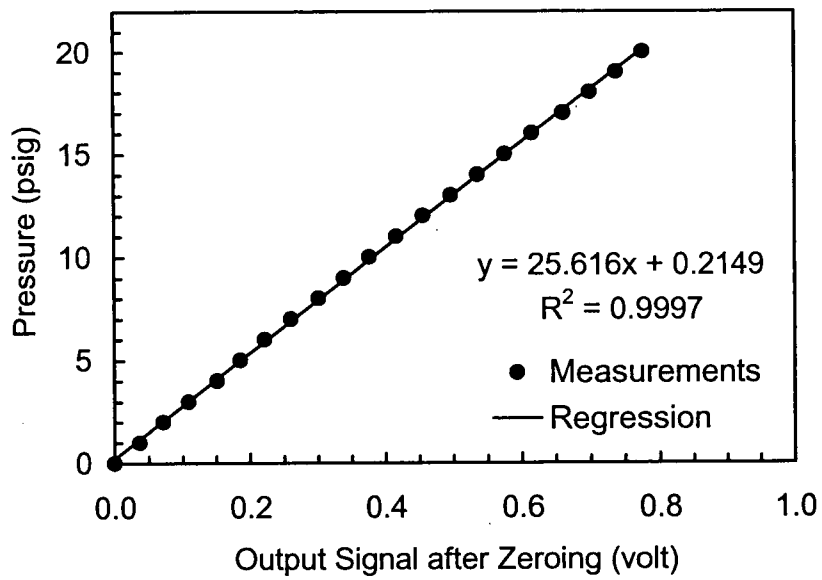


Figure B.2 Calibration Curve for Pressure Transducer on Heating Tank (Omega Model PX202-030GV)

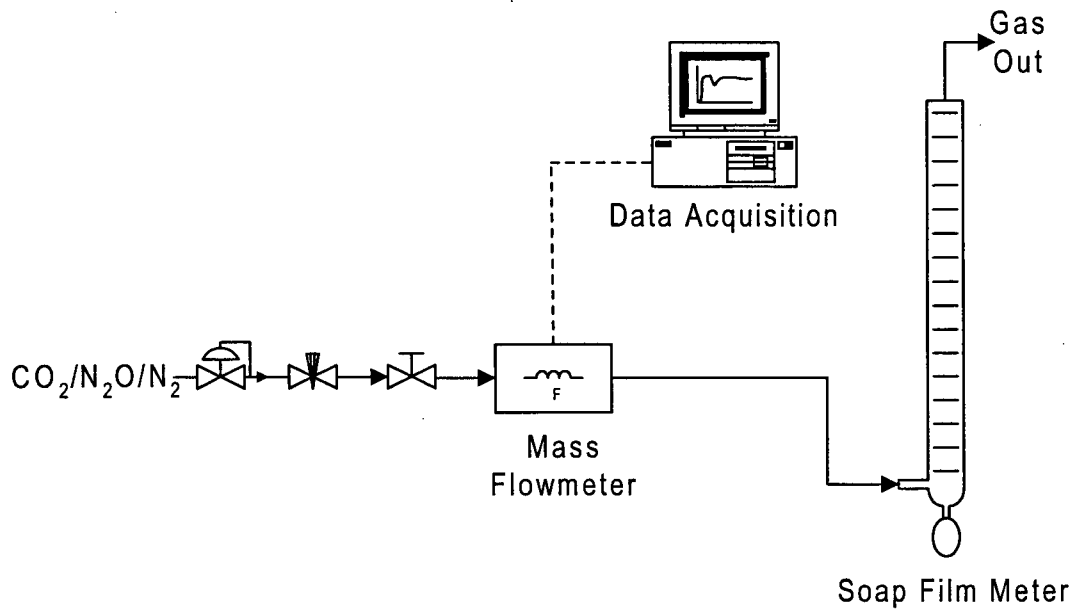


Figure B.3 Setup for Mass Flow Meter Calibration using a Soap Film Meter

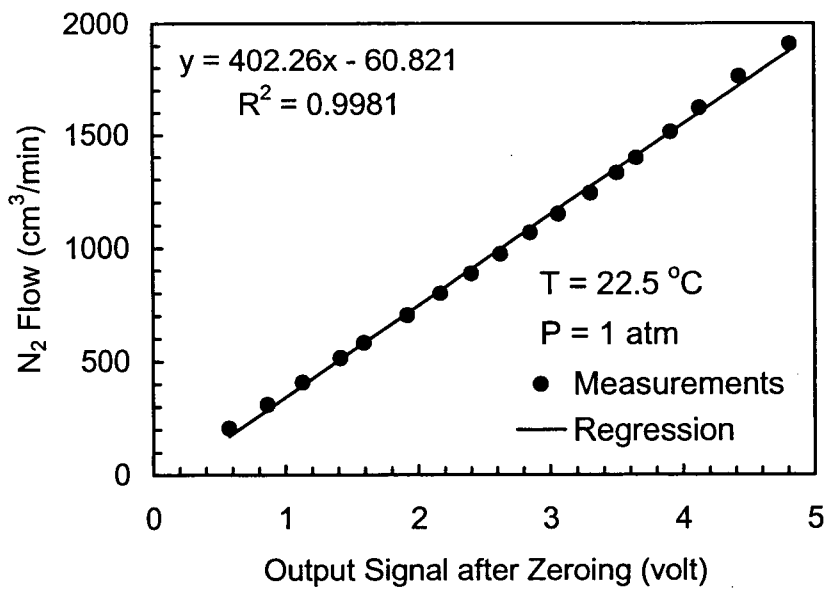


Figure B.4 Calibration Curve for Measuring Dilution N₂ Flow Rate using Mass Flow Meter (Brooks Model 5700)

for all mass flow meters. The calibration curves for the three mass flow meters used in this apparatus are plotted in Figure B.4 to B.7.

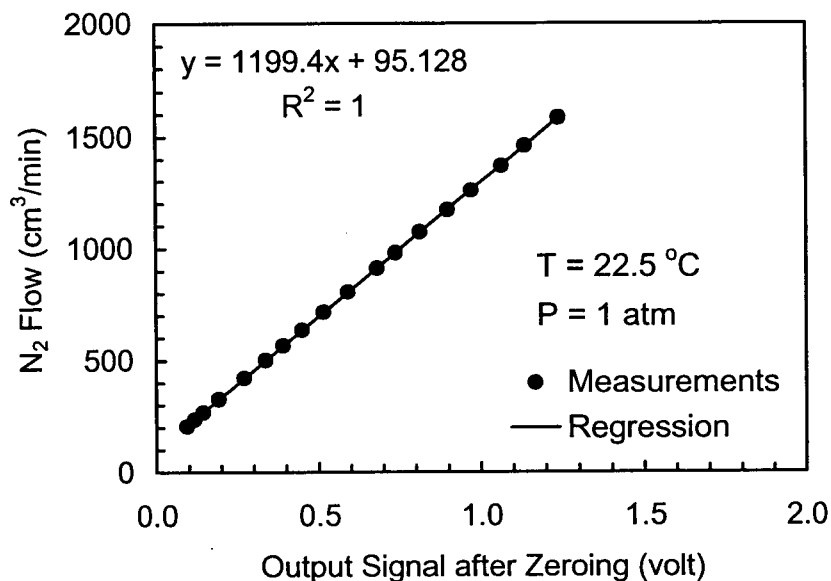


Figure B.5 Calibration Curve for Measuring Stripping N₂ Flow Rate using Mass Flow Meter (Colepalmer Model GFM171)

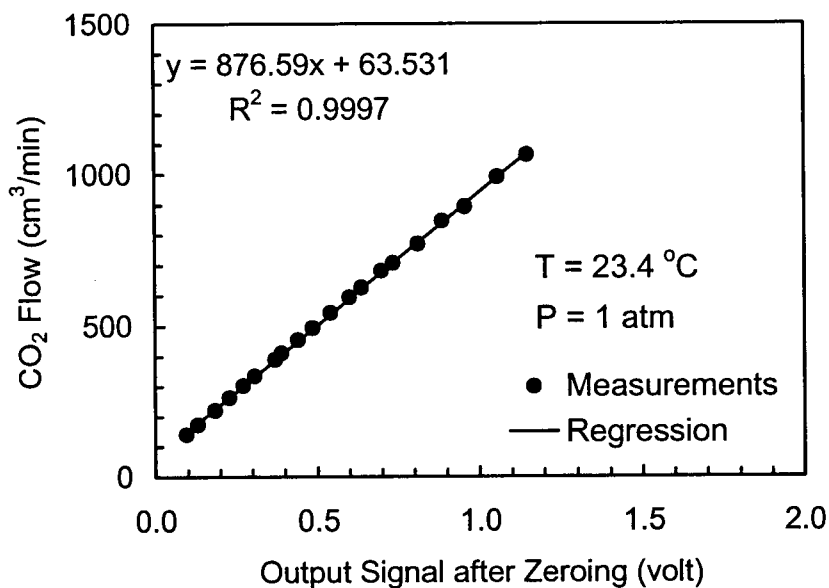


Figure B.6 Calibration Curve for Measuring CO₂ Flow Rate using Mass Flow Meter (Colepalmer Model GFM171)

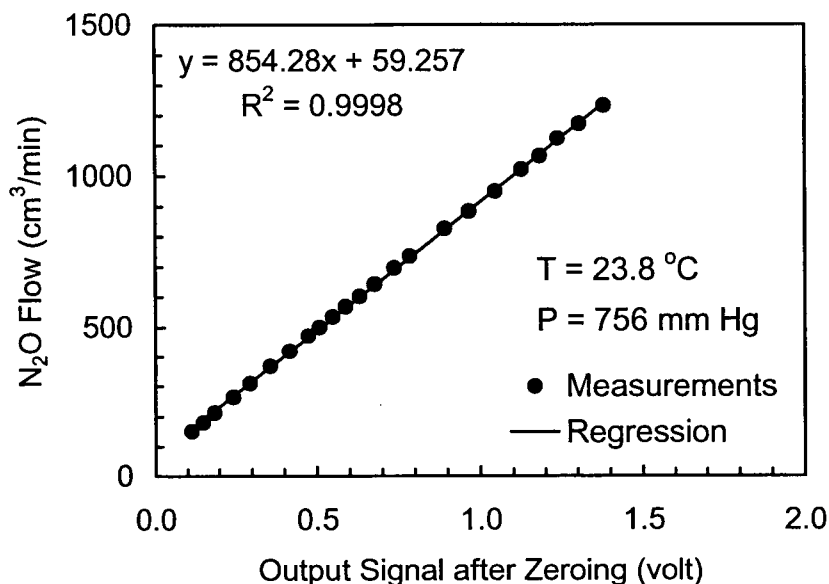


Figure B.7 Calibration Curve for Measuring N₂O Flow Rate Using Mass Flow Meter (Colepalmer Model GFM 171)

B.3 CO₂ Analyzer

The CO₂ absorption or desorption rate were determined by the difference of the CO₂ flow rate in the gas stream into and out of the hemispherical contactor. The flow rate of CO₂ into the unit were determined using the mass flow meter as described in the previous section. To determine the flow rate out of the unit a calibration of the gas analyzer was required. NOVA 300 Infrared analyzer that had a range of 0-20% (volume basis) was used in this work. The calibration was carried out in the configuration used in the actual experiment. Two mass flow meters one calibrated for N₂ and other for CO₂ were used in the setup shown in Figure B.8. To calibrate the analyzer, N₂ flow rate was fixed at a certain value and the CO₂ flow rate was varied so that a gas mixture with CO₂

composition ranging from 0 to 20% (mole basis) was sent through the analyzer. The analyzer output signal was adjusted to zero by subtracting from it the output signal value at zero CO₂ concentration. At each setting the steady state reading of the analyzer output signal and the inlet gas mixture composition were recorded by the computer. The calibration curve obtained is plotted in Figure B.9 Throughout this work, before starting an experiment the calibration was checked by sending the gas through the by pass line to the CO₂ analyzer as shown in Figure 3.2.

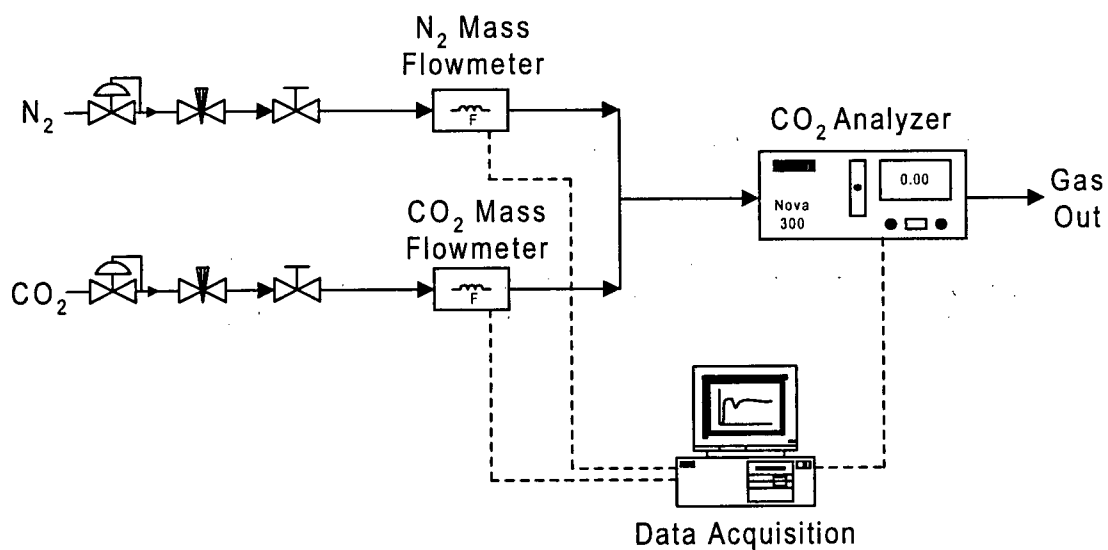


Figure B.8 Setup for CO₂ Analyzer Calibration

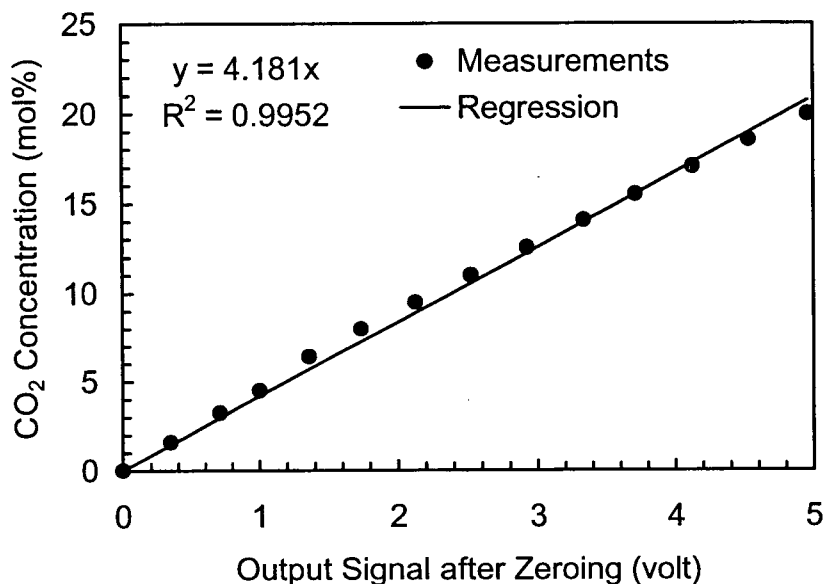


Figure B.9 Calibration Curve for Gas-Phase CO₂ Measurement using Infrared Analyzer (Model NOVA-300)

B.4 Gas Chromatograph

In absorption experiments with N₂O, the exit gas composition was determined using a gas chromatograph (Shimadzu Model GC 8A) that was equipped with a thermal conductivity detector. The principal operating conditions are summarized in Table B.1. The GC was calibrated by injecting gas mixtures of known composition. The gas mixtures were prepared by mixing N₂O and N₂ gases in various proportions using mass flow meters. The standard gas samples were stored 1-liter Tedlar sampling bags. Each sample was injected at least three times and peak areas of N₂O, N₂ and the total area were noted from the strip chart recorder. Average of the three values was used in generating the calibration curve. To compensate for error due to injection volume, the ratio of

N₂O peak area to total peak area was plotted against the N₂O mole fraction in the standard sample. The calibration data obtained are listed in Table B.2 and the calibration curve is shown in Figure B.10.

The GC method described above was also used for measuring CO₂ in the exit gas. This was done only for a few randomly selected runs to check the accuracy of the Infrared Analyzer. The column and operating conditions were identical to those used for N₂O measurement (see Table B.1). The calibration data for CO₂ are listed in Table B.3 and corresponding calibration curve is shown in Figure B.11.

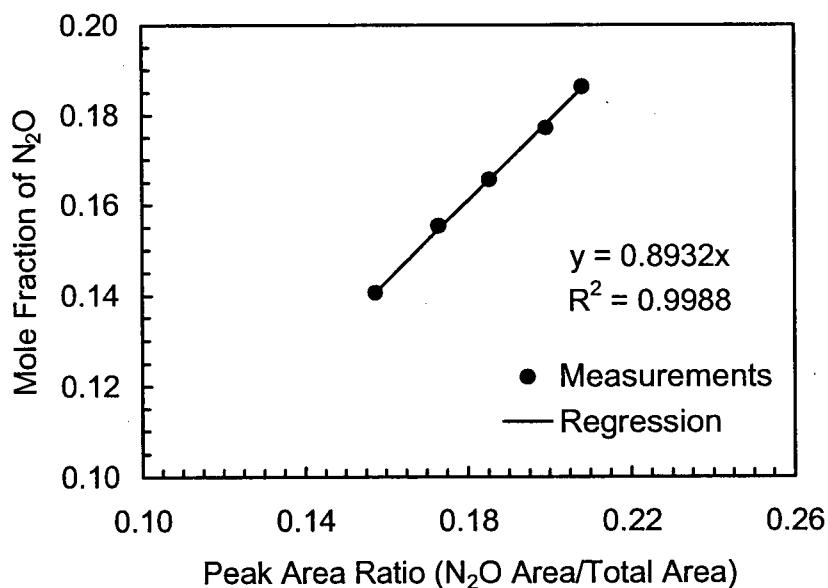


Figure B.10 Calibration Curve for Gas Phase N₂O measurement using GC (Shimadzu Model GC 8A, Column: Chromosorb 102)

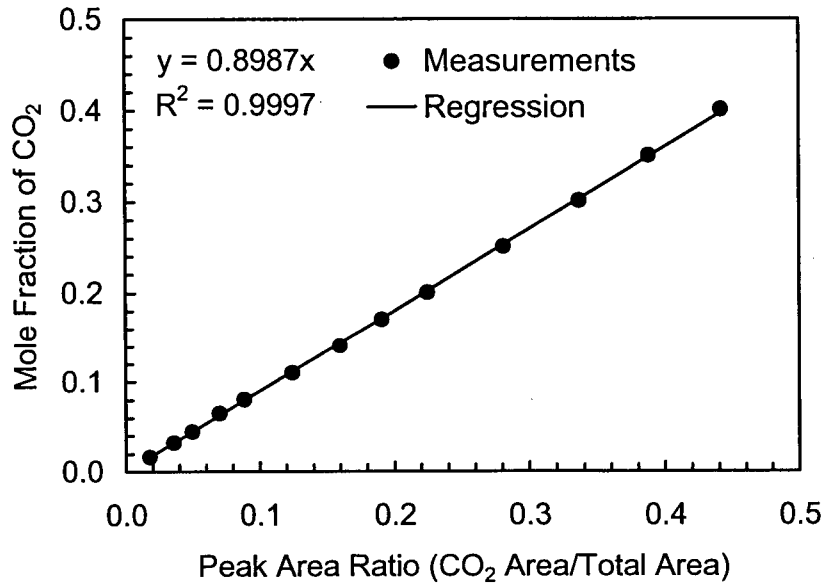


Figure B.11 Calibration Curve for Gas-Phase CO₂ Measurement using GC (Shimadzu Model GC 8A, Column: Chromosorb 102)

Table B.1 GC operating conditions for gas phase N₂O/CO₂ measurement

Item	Description
Column	Chromosorb 102, mesh size 80/100, 20'x1/8" SS packed column (supplied by Supelco Inc. Oakville, ON)
Detector	Thermal Conductivity Detector(TCD)
Column temperature	40 °C
Injector temperature	60 °C
Carrier gas	He (20 cm ³ /min)
Injection volume	0.25 cm ³

Table B.2 Calibration Data for N₂O measurement using GC

Ref. No.	N ₂ O in Std. Samples (mole fraction)	N ₂ O Peak Area	Total Peak Area	Peak Area Ratio (N ₂ O/Total)
N ₂ O Calib1	0.186	19715	94539	0.2085
		19892	95505	0.2083
		19580	94260	0.2077
N ₂ O Calib2	0.177	18795	94158	0.1996
		18946	95046	0.1993
		18943	95251	0.1989
N ₂ O Calib3	0.166	17346	93568	0.1854
		17442	94098	0.1854
		17411	94008	0.1852
N ₂ O Calib4	0.155	16160	93307	0.1732
		16140	93400	0.1728
		16055	92836	0.1729
N ₂ O Calib5	0.141	14728	93316	0.1578
		14758	93649	0.1576
		14560	92791	0.1569

Table B.3 Calibration Data for CO₂ measurement using GC

Ref. No.	CO ₂ in Std. Samples (mole fraction)	CO ₂ Peak Area	Total Peak Area	Peak Area Ratio (CO ₂ /Total)
CO ₂ Calib1	0.401	45017	102002	0.4413
		45859	103847	0.4416
		45600	103212	0.4418
CO ₂ Calib2	0.350	39432	101738	0.3876
		39647	102160	0.3881
		39638	102043	0.3884
CO ₂ Calib3	0.300	34027	100098	0.3369
		34241	101731	0.3366
		34489	102486	0.3365
CO ₂ Calib4	0.2504	28213	100217	0.2815
		28411	101089	0.2810
		28431	101124	0.2811
CO ₂ Calib5	0.200	22343	99410	0.2248
		22596	100552	0.2247
		22566	100514	0.2245
CO ₂ Calib6	0.170	18889	98872	0.1910
		18847	98828	0.1907
		18776	98279	0.1910
CO ₂ Calib7	0.140	15792	98675	0.1600
		15814	98786	0.1600
		15763	98605	0.1598
CO ₂ Calib8	0.110	12151	97658	0.1244
		12241	98647	0.1240
		12201	98512	0.1239

Table B.3 Calibration Data for CO₂ measurement using GC
(Contd.)

CO ₂ Calib9	0.0801	8601	96902	0.0887
		8670	98095	0.0884
		8637	97649	0.0885
CO ₂ Calib10	0.0651	6694	95439	0.0701
		6785	97096	0.0698
		6758	96683	0.0699
CO ₂ Calib11	0.0447	4742	95268	0.04977
		4730	95063	0.04975
		4745	95435	0.04972
CO ₂ Calib12	0.0324	3438	95411	0.03603
		3453	96065	0.03594
		3434	94917	0.03618
CO ₂ Calib13	0.0159	1698	95946	0.01769
		1713	96050	0.01783
		1692	95737	0.01767

APPENDIX C

ANALYTICAL SOLUTION FOR PHYSICAL ABSORPTION/DESORPTION MODEL

C.1 Model for Physical Gas Absorption/Desorption

The model equation for gas absorption/desorption over a hemispherical liquid film without chemical reaction is given by

$$\frac{V_{\theta}}{r} \frac{\partial C_1}{\partial \theta} = \frac{2D_1}{r} \frac{\partial C_1}{\partial r} + D_1 \frac{\partial^2 C_1}{\partial r^2} \quad (\text{C.1})$$

Initial Condition:

$$\text{at } \theta = 0 \text{ for } r \geq R \quad C_1 = C_1^0 \quad (\text{C.2})$$

Boundary Conditions:

$$\text{at } r = R \text{ for } \theta > 0 \quad \frac{\partial C_1}{\partial r} = 0 \quad (\text{C.3})$$

$$\text{at } r = R + \Delta_{\theta} \text{ for } \theta > 0 \quad C_1 = C_1^i \quad (\text{C.4})$$

C.1.1 Model Equations in Dimensionless form

Equations (C.1) to (C.4) can be written in dimensionless form by substituting the following dimensionless variables (Wild and Potter, 1968):

$$x = \frac{R + \Delta_{\theta} - r}{\Delta_{\theta}} \quad (\text{C.5})$$

$$C = \frac{C_1}{C_1^i} \quad \text{and} \quad C^o = \frac{C_1^o}{C_1^i} \quad (\text{C.6})$$

$$d\eta = \frac{RD_1}{V_o \Delta_\theta^2} d\theta = \frac{4\pi R^2 D_1}{3Q\Delta_o} (\sin^{5/3} \theta) d\theta \quad (\text{C.7})$$

and performing some algebraic manipulations

$$(1-x^2) \frac{\partial C}{\partial \eta} = \frac{\partial^2 C}{\partial x^2} \quad (\text{C.8})$$

Initial Condition:

$$\text{at } \eta = 0 \quad \text{for } x \geq 0 \quad C = C^o \quad (\text{C.9})$$

Boundary Conditions:

$$\text{at } x = 0 \quad \text{for } \eta > 0 \quad C = 1 \quad (\text{C.10})$$

$$\text{at } x = 1 \quad \text{for } \eta > 0 \quad \left(\frac{\partial C}{\partial x} \right) = 0 \quad (\text{C.11})$$

The differential equations (C.8) to (C.11) must be integrated from $\eta = 0$ (i.e. $\theta = 0$) to $\eta = \eta_2$ (i.e. $\theta = \pi/2$). The upper limit of integration is defined by the following equations:

$$\eta_2 = \frac{4\pi R^2 D_1}{3Q\Delta_o} \int_0^{\pi/2} \sin^{5/3} \theta d\theta = \frac{4\pi R^2 D_1}{3Q\Delta_o} (0.84133) \quad (\text{C.12})$$

The fraction 0.84133 in the above equation is the value of $\int_0^{\pi/2} \sin^{5/3} \theta d\theta$ and was obtained by numerical integration. The total rate of absorption/desorption of a gas over a hemispherical film can then be computed from the following equation:

$$\bar{N}_A^o = -\bar{N}_B^o = -\frac{3Q}{2} \int_0^{\eta_2} \left(\frac{\partial C_1}{\partial x} \right)_{(x=0,\eta)} d\eta \quad (C.13)$$

Note that the concentration gradient $\left(\frac{\partial C_1}{\partial x} \right)_{(x=0,\eta)}$ is positive quantity for absorption and negative for desorption. The physical mass transfer coefficient can be obtained as follows:

$$k_L^o = \frac{\bar{N}_A^o}{2\pi R^2 (C_1^i - C_1^o)} = \frac{\bar{N}_B^o}{2\pi R^2 (C_1^o - C_1^i)} \quad (C.14)$$

C.2 Analytical solution

In order to obtain an expression for physical mass transfer coefficient we need to solve the model equations (C.8) to (C.11) analytically. A quick analytical solution is possible if we assume that the penetration depth of the gas is much smaller compared to the thickness of the liquid film. Under this assumption, the liquid film can be treated as if it were infinitely deep and boundary condition at $x = 1$ (Eq. C.11) can be replaced boundary conditions at $x = \infty$ and the governing equations can be written as:

$$\frac{\partial C}{\partial \eta} = \frac{\partial^2 C}{\partial x^2} \quad (C.15)$$

Initial Condition:

$$\text{at } \eta = 0 \text{ for } x \geq 0 \quad C = C^0 \quad (\text{C.16})$$

Boundary Conditions:

$$\text{at } x = 0 \text{ for } \eta > 0 \quad C = 1 \quad (\text{C.17})$$

$$\text{at } x = \infty \text{ for } \eta > 0 \quad C = C^0 \quad (\text{C.18})$$

Equations (C.15) to (C.18) can be solved using Laplace transform. Taking the Laplace transform of Eq. (C.15) with respect to η and denoting the transform of C as \bar{C} :

$$s\bar{C} - C(0, x) = \frac{d^2\bar{C}}{dx^2} \quad (\text{C.19})$$

From the initial condition $C_1(0, x) = C^0$, which upon substitution in equation (C.19):

$$\frac{d^2\bar{C}}{dx^2} - s\bar{C} = -C^0 \quad (\text{C.20})$$

Particular solution of Eq, (C.20):

$$C_p = -\frac{C^0}{s} \quad (\text{C.21})$$

Homogenous solution of Eq. (C.20):

$$\bar{C}_h(x, s) = A_1 e^{+\sqrt{s}x} + A_2 e^{-\sqrt{s}x} \quad (\text{C.22})$$

where A_1 and A_2 are the arbitrary constants. From boundary condition at $x = 0$, $A_1 + A_2 = 1/s$ and from boundary condition at $x = \infty$, $A_1 = 0$. Therefore the general solution is:

$$\bar{C}(x,s) = \frac{e^{-\sqrt{s}x}}{s} - \frac{C^o}{s} \quad (\text{C.23})$$

or

$$C(x,\eta) = L^{-1}\left[\frac{e^{-\sqrt{s}x}}{s}\right] - L^{-1}\left[\frac{C^o}{s}\right] \quad (\text{C.24})$$

From the inverse Laplace transform table:

$$L^{-1}\left[\frac{e^{-\sqrt{s}x}}{s}\right] = 1 - \operatorname{erf}\left(\frac{x}{\sqrt{4\eta}}\right) \text{ and } L^{-1}\left[\frac{C^o}{s}\right] = C^o \quad (\text{C.25})$$

Combining equations (C.24) and (C.25):

$$C(x,\eta) = 1 - \operatorname{erf}\left(\frac{x}{\sqrt{4\eta}}\right) - C^o \quad (\text{C.26})$$

Recalling the definition of error function:

$$\operatorname{erf}(\xi) = \frac{2}{\sqrt{\pi}} \int_0^{\xi} e^{-\phi^2} d\phi \quad (\text{C.27})$$

Applying the definition of error function from equation (C.27) to equation (C.26):

$$C(x,\eta) = 1 - \frac{2}{\sqrt{\pi}} \int_0^{x/\sqrt{4\eta}} e^{-\phi^2} d\phi - C^o \quad (\text{C.28})$$

Substituting $C = \frac{C_1}{C_1^i}$ and $C^o = \frac{C_1^o}{C_1^i}$ into equation (C.28):

$$C_1(x, \eta) = C_1^i - \frac{2C_1^i}{\sqrt{\pi}} \int_0^{\frac{x}{\sqrt{4\eta}}} e^{-\phi^2} d\phi - C_1^o \quad (C.29)$$

Differentiating equation (C.29) with respect to x , obtaining $\left(\frac{\partial C_1}{\partial x}\right)_{(x=0, \eta)}$ and

substituting it into equation (C.13):

$$\bar{N}_A^o = -\bar{N}_D^o = \frac{3Q(C_1^i - C_1^o)}{2} \int_0^{\eta_2} \frac{1}{\sqrt{\pi\eta}} d\eta \quad (C.30)$$

or

$$\bar{N}_A^o = -\bar{N}_D^o = \frac{3Q(C_1^i - C_1^o)}{2} \sqrt{\frac{\eta_2}{\pi}} \quad (C.31)$$

Substituting for η_2 from equation (C.12) into equation (C.31):

$$\bar{N}_A^o = -\bar{N}_D^o = 3.1774 \sqrt{\frac{QR^2 D_1}{\Delta_o}} (C_1^i - C_1^o) \quad (C.32)$$

Substituting for \bar{N}_A^o or \bar{N}_D^o from equation (C.32) into equation (C.14):

$$k_L^o = 1.5887 \sqrt{\frac{D_1}{\pi \left(\frac{\Delta_o \pi R^2}{Q} \right)}} \quad (C.33)$$

Equation (C.33) can be written in terms dimensionless numbers as follows:

$$Sh = 1.26758 Re^{0.5} Sc^{0.5} \quad (C.34)$$

where,

$$\text{Sh} = \frac{k_L^o \sqrt{R\Delta_o}}{D_1}, \text{Re} = \frac{Q}{2\pi Rv}, \text{Sc} = \frac{v}{D_1} \quad (\text{C.35})$$

From Higbie's penetration theory the liquid phase mass transfer coefficient, k_L^o , for physical absorption is given by

$$k_L^o = 2 \sqrt{\frac{D_1}{\pi\tau_c}} \quad (\text{C.36})$$

where, τ_c is the gas-liquid contact time and can be obtained by comparing equations (C.33) and (C.36):

$$\tau_c = 1.5848\pi R^2 \left(\frac{\Delta_o}{Q} \right) \quad (\text{C.37})$$

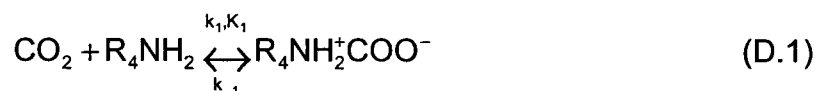
Equation (C.37) is similar to that given by Wild and Potter (1968) for complete sphere.

APPENDIX D

DERIVATION OF RATE EXPRESSION FOR ZWITTERION MECHANISM

This appendix gives the derivation for rate expression representing CO₂ reactions with a mixture of AMP and MEA in aqueous solution via zwitterion mechanism. The reactions involved are:

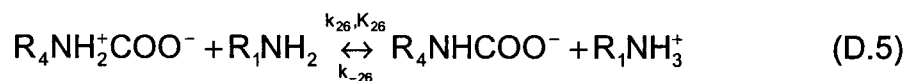
AMP- Zwitterion Formation:



AMP-Zwitterion Deprotonation:



Deprotonation of AMP-Zwitterion to MEA:



Reactions (D.1) to (D.5) are same as reactions (4.1) to (4.4) and (4.25) respectively. The nomenclature used to denote chemical species and rate constants involved in these reactions is the same as in Chapter 4. The letter Z represents the zwitterion intermediate.

Rate of Accumulation of Z = Rate of formation of Z – Rate of consumption of Z

$$\frac{dZ}{dt} = k_1 C_1 C_2 + k_{-2} C_4 C_3 + k_{-3} C_4 C_8 + k_{-4} C_4 C_9 + k_{-25} C_4 C_{11} - k_{-1} Z - k_2 Z C_2 - k_3 Z C_9 - k_4 Z C_7 - k_{25} Z C_{10} \quad (D.6)$$

Assuming a steady state exist, then $\frac{dZ}{dt} = 0$ and equation (D.6) can be solved for

Z as follows:

$$Z = \frac{k_1 C_1 C_2 + k_{-2} C_4 C_3 + k_{-3} C_4 C_8 + k_{-4} C_4 C_9 + k_{-25} C_4 C_{11}}{k_{-1} + k_2 C_2 + k_3 C_9 + k_4 C_7 + k_{25} C_{10}} \quad (D.7)$$

Rate expression for reaction (D.1) is:

$$r_1 = -k_1 C_1 C_2 + \frac{k_1}{K_1} Z \quad (D.8)$$

Substituting for Z from equation (D.7) into equation (D.8) gives:

$$r_1 = -k_1 C_1 C_2 + \frac{k_1}{K_1} \left[\frac{k_1 C_1 C_2 + k_{-2} C_4 C_3 + k_{-3} C_4 C_8 + k_{-4} C_4 C_9 + k_{-25} C_4 C_{11}}{k_{-1} + k_2 C_2 + k_3 C_9 + k_4 C_7 + k_{25} C_{10}} \right] \quad (D.9)$$

or

$$r_1 = -k_1 C_1 C_2 + \frac{k_1}{K_1 k_{-1}} \left[\frac{k_1 C_1 C_2 + k_{-2} C_4 C_3 + k_{-3} C_4 C_8 + k_{-4} C_4 C_9 + k_{-25} C_4 C_{11}}{1 + \left(\frac{k_2}{k_{-1}}\right) C_2 + \left(\frac{k_3}{k_{-1}}\right) C_9 + \left(\frac{k_4}{k_{-1}}\right) C_7 + \left(\frac{k_{25}}{k_{-1}}\right) C_{10}} \right] \quad (D.10)$$

$$\text{Let } B = \left(\frac{k_2}{k_{-1}}\right) C_2 + \left(\frac{k_3}{k_{-1}}\right) C_9 + \left(\frac{k_4}{k_{-1}}\right) C_7 + \left(\frac{k_{25}}{k_{-1}}\right) C_{10} \quad (D.11)$$

Combining equations (D.10) and (D.11) and rearranging gives:

$$r_1 = \frac{-k_1 \left[C_1 C_2 B - C_4 \left(\frac{k_{-2}}{k_1} C_3 + \frac{k_{-3}}{k_1} C_8 + \frac{k_{-4}}{k_1} C_9 + \frac{k_{-25}}{k_1} C_{11} \right) \right]}{1+B} \quad (\text{D.12})$$

or

$$r_1 = \frac{-k_1 \left[C_1 C_2 B - C_4 \left\{ \left(\frac{k_2}{k_{-1}} \right) \frac{1}{K_1 K_2} C_3 + \left(\frac{k_3}{k_{-1}} \right) \frac{1}{K_1 K_3} C_8 + \left(\frac{k_4}{k_{-1}} \right) \frac{1}{K_1 K_4} C_9 + \left(\frac{k_{25}}{k_{-1}} \right) \frac{1}{K_1 K_{25}} C_{11} \right\} \right]}{1+B} \quad (\text{D.13})$$

$$\text{Let } A = \left(\frac{k_2}{k_{-1}} \right) \frac{1}{K_1 K_2} C_3 + \left(\frac{k_3}{k_{-1}} \right) \frac{1}{K_1 K_3} C_8 + \left(\frac{k_4}{k_{-1}} \right) \frac{1}{K_1 K_4} C_9 + \left(\frac{k_{25}}{k_{-1}} \right) \frac{1}{K_1 K_{25}} C_{11} \quad (\text{D.14})$$

$$r_1 = \frac{-k_1 \left[C_1 C_2 - C_4 \left(\frac{A}{B} \right) \right]}{1 + \frac{1}{B}} \quad (\text{D.15})$$

Since r_1 is derived from reactions (4.1) to (4.4) and (4.25), in Chapter 4 r_1 is denoted as $r_{1-4,25}$. When the reaction mixture has only AMP and water then k_{25} will be zero and $r_{1-4,25}$ will reduce to r_{1-4} .

APPENDIX E

DENSITY AND VISCOSITY OF AQUEOUS AMINE SOLUTIONS

E.1 Density

The densities of binary and ternary aqueous amine mixtures were calculated using the correlation of Hsu and Li (1997a). According to this correlation the density of a liquid mixture, ρ_m can be obtained from the following equation:

$$\rho_m = \frac{\sum x_i M_i}{V_m} \quad (\text{E.1})$$

where, x_i is the mole fraction of each component in the mixture, M_i is the molar mass of pure component i , and V_m is the molar volume of the liquid mixture. The molar volume of the liquid mixture is calculated from the following equation:

$$V_m = V^E + \sum x_i V_i^0 \quad (\text{E.2})$$

where, v_i^0 is the molar volume of the pure fluid at the temperature of the system and V^E is the excess volume of the liquid mixture which for a ternary system is assumed to be:

$$V^E = V_{12}^E + V_{13}^E + V_{23}^E \quad (\text{E.3})$$

The excess volume of the binary liquid mixture, V_{12}^E can be calculated using the following Redlich-Kister type equation:

$$V_{12}^E = x_1 x_2 \sum_{i=0}^n A_i (x_1 - x_2)^i \quad (\text{E.4})$$

where, A_i are the binary interaction parameters which are assumed to have the following temperature dependence:

$$A_i = a + bT + cT^2 \quad (\text{E.5})$$

The densities of pure fluids needed to calculate v_i^o in eq. (E.2) were obtained from the correlation of the type:

$$\rho = a_1 + a_2 T + a_3 T^2 \quad (\text{E.6})$$

The correlation coefficients a , b , c , a_1 , a_2 and a_3 in eqs. (E.5) and (E.6) determined by Hsu and Li (1997a) are listed in Table E.1 and E.2. The parameter values are based on 686 data points measured in the temperature range of 303-353 K, including pure fluids, single-amine aqueous solutions, and ternary aqueous solutions of blended amines. The data include both their own density measurements and those reported in the literature. The overall average absolute percentage deviation for the density calculations was reported to be 0.041%.

To check the accuracy of this correlation, we measured the density of various aqueous amine mixtures at 303 and 323 K. These values are listed in Table E.3 and a cross plot is presented in Figure E.1. The agreement between

our measurements and the estimates using eq. (E.1) is excellent. The relative error is within $\pm 1\%$.

Table E.1 Binary Parameters of the Redlich-Kister Equation of the Excess Volume (eq. E.4 and E.5)

Param.		Binary Pair			
		MEA+H ₂ O	DEA+H ₂ O	MDEA+H ₂ O	AMP+H ₂ O
A ₀	a	-5.92024×10^{-2}	-3.31562×10	-2.88774×10	-6.51042
	b	-1.77290×10^{-4}	8.11654×10^{-2}	6.95810×10^{-2}	5.02584×10^{-3}
	c	-1.10780×10^{-6}	6.15156×10^{-6}	-5.03040×10^{-7}	1.08578×10^{-6}
A ₁	a	2.17490	-3.52516×10	-2.06623×10	5.55560
	b	1.10385×10^{-5}	9.75694×10^{-2}	6.36707×10^{-2}	-1.1325×10^{-2}
	c	0	0	0	0
		Binary Pair			
		MEA+MDEA	MEA+AMP	DEA+MDEA	DEA+AMP
A ₀	a	-2.42756×10	5.53222	-1.24706×10	1.75649×10^3
	b	1.89797×10^{-1}	1.62914×10^{-1}	1.00561×10^{-1}	-1.06202×10
	c	-2.88250×10^{-4}	-6.44380×10^{-4}	-1.62790×10^{-4}	1.59224×10^{-2}
A ₁	a	0	0	0	0
	b	-1.05682	9.86571×10^{-1}	9.63470×10^{-2}	-1.28358
	c	4.28233×10^{-3}	-2.39399×10^{-3}	1.02886×10^{-5}	4.86136×10^{-3}
A ₂	a	0	0	0	0
	b	-1.49472×10	-2.70341×10	-7.53195×10^{-3}	-6.44203×10
	c	1.52253×10^{-2}	5.68765×10^{-2}	-3.65100×10^{-3}	2.35996×10^{-1}

Based on data from: Al-Ghawas et al. (1989b), Xu et al. (1991), Xu et al. (1992), Li and Shen (1992), Rinker et al. (1994), Li and Lie (1994), Hagewiesche et al. (1995b), Hsu and Li (1997a).

Table E.2 Parameters of the Density Equation for Pure Fluids (eq. E.6)

Pure Fluid	a_1	a_2	a_3
H ₂ O	0.863559	1.21494×10^{-3}	-2.57080×10^{-6}
MEA	1.19093	-4.29990×10^{-4}	-5.66040×10^{-7}
DEA	1.20715	-1.51200×10^{-4}	-7.66530×10^{-7}
MDEA	1.22864	-5.44540×10^{-4}	-3.35930×10^{-7}
AMP	1.15632	-6.76170×10^{-4}	-2.67580×10^{-7}

Based on data from: Kell (1975), Perry and Chilton (1984), Al-Ghawas et al. (1989), Xu et al. (1991), Diguillo et al. (1992), Li and Shen (1992), Wang et al. (1994), Xu et al. (1992), Li and Lie (1994).

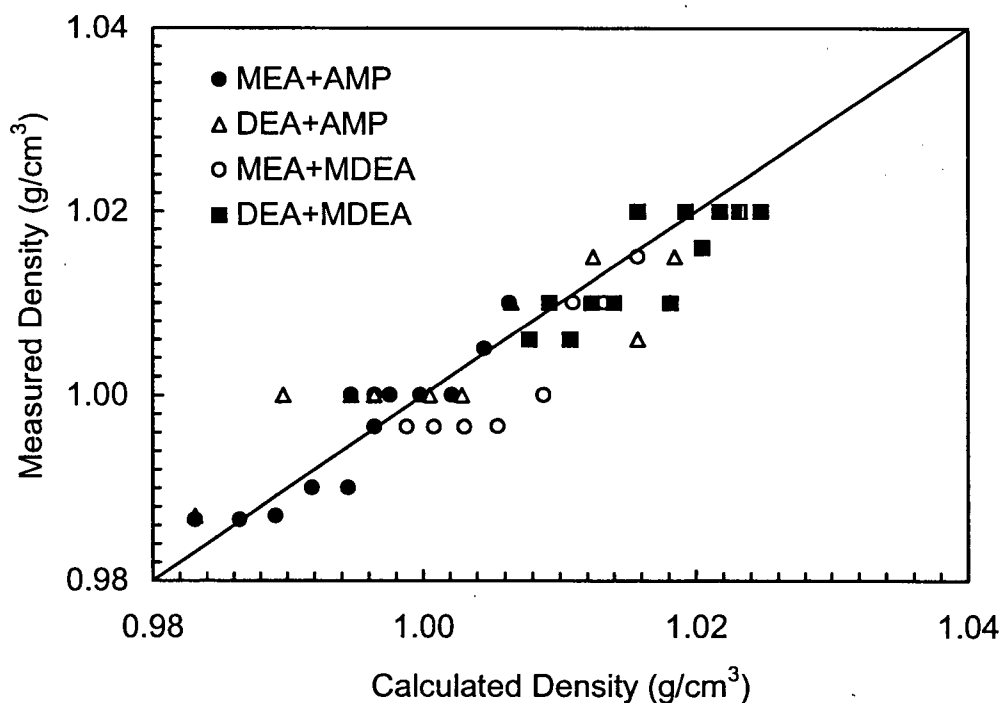


Figure E.1 Measured and calculated densities at 303 and 323 K

Table E.3 Density of Aqueous Amine Blends at 303 K and 323 K
(Total Amine = 25 wt%, Water = 75 wt%)

Blend	Density (g/cm ³)					
	T = 303 K			T = 323K		
	This work	From eq. (E.1)	Error (%)	This work	From eq. (E.1)	Error ⁺ (%)
MEA + AMP						
0 + 25	1.000	0.995	0.53	0.987	0.983	0.36
5 + 20	1.000	0.998	0.25	0.987	0.986	0.02
10 + 15	1.000	1.000	0.02	0.987	0.989	-0.22
15 + 10	1.000	1.002	-0.21	0.990	0.992	-0.18
20 + 5	1.005	1.005	0.05	0.990	0.994	-0.45
25 + 0	1.010	1.006	0.36	0.997	0.996	0.02
DEA + AMP						
0 + 25	1.000	0.995	0.53	0.987	0.983	0.40
5 + 20	1.000	1.000	-0.05	1.000	0.990	1.03
10 + 15	1.010	1.006	0.35	1.000	0.996	0.36
15 + 10	1.015	1.012	0.25	1.000	1.003	-0.29
20 + 5	1.015	1.018	-0.34	1.010	1.009	0.08
25 + 0	1.020	1.025	-0.46	1.006	1.016	-0.97
MEA + MDEA						
0 + 25	1.010	1.018	-0.80	1.006	1.008	-0.18
5 + 20	1.015	1.016	-0.07	0.997	1.005	-0.89
10 + 15	1.010	1.013	-0.32	0.997	1.003	-0.65
15 + 10	1.010	1.011	-0.09	0.997	1.001	-0.42
20 + 5	1.000	1.009	-0.88	0.997	0.999	-0.22
25 + 0	1.010	1.006	0.36	1.000	0.996	0.36
DEA + MDEA						
0 + 25	1.010	1.018	-0.80	1.006	1.008	-0.18
5 + 20	1.020	1.019	0.08	1.010	1.009	0.08
10 + 15	1.016	1.020	-0.44	1.006	1.011	-0.47
15 + 10	1.020	1.022	-0.17	1.010	1.012	-0.23
20 + 5	1.020	1.023	-0.31	1.010	1.014	-0.39
25 + 0	1.020	1.025	-0.46	1.020	1.016	0.42

⁺ Error = 100 × (measured-calculated)/measured

E.2 Viscosity

The viscosities of binary and ternary aqueous amine mixtures were calculated using the correlation of Hsu and Li (1997b). According to this correlation the kinematic viscosity of a liquid mixture, v_m , can be obtained from the following equation:

$$\ln v_m = \delta v + \sum_{i=1}^n x_i \ln v_i \quad (\text{E.7})$$

where, x_i is the mole fraction of each component in the mixture, v_i is the kinematic viscosity (μ_i/ρ_i) of pure fluid i , and δv is the deviation in kinematic viscosity, which for a ternary system is assumed to be:

$$\delta v = \delta v_{12}^E + \delta v_{13}^E + \delta v_{23}^E \quad (\text{E.8})$$

For a binary system, the δv_{12}^E is a function of temperature and mole fraction and can be calculated using the following Redlich-Kister type expression (Hsu and Li, 1997b):

$$\delta v_{12}^E = x_1 x_2 \sum_{i=0}^m A_i (x_1 - x_2)^i \quad (\text{E.8})$$

where, A_i are the binary interaction parameters which are assumed to have the following temperature dependence:

$$A_i = a + \frac{b}{T+c} \quad (\text{E.9})$$

The viscosity of pure fluids required to calculate v_i in eq. (E.7), is assumed to be the following expression:

$$\ln v = a_1 + \frac{a_2}{T + a_3} \quad (\text{E.10})$$

The correlation coefficients a , b , c , a_1 , a_2 and a_3 in eqs. (E.9) and (E.10) determined by Hsu and Li (1997b) are listed in Table E.4 and E.5. The parameter values are based on 499 data points measured in the temperature range of 303-353 K, including pure fluids, single-amine aqueous solutions, and ternary aqueous solutions of blended amines. The data include both their own viscosity measurements and those reported in the literature. The overall average absolute percentage deviation for the viscosity calculations was reported to be 1%.

To check the accuracy of eq. (E.7), we measured the viscosity of aqueous amine mixtures at 303 K using a falling ball viscometer (Colepalmer Model P-08701-00). These measurements are listed in Table E.6 and a cross plot is presented in Figure E.2. The agreement between our measurements and the estimates from eq. (E.7) is within $\pm 12\%$.

Table E.4 Binary Parameters of the Redlich-Kister Equation for the Viscosity Deviation (eqs. E.8 and E.9)

		Binary Pair			
Param.		MEA+H ₂ O	DEA+H ₂ O	MDEA+H ₂ O	AMP+H ₂ O
A ₀	a	2.58323×10^{-1}	2.76655	-6.26493	4.01239
	b	5.05207×10^2	3.64795×10^3	1.59158×10^3	2.49856×10^2
	c	-2.23155×10^2	6.78430×10	-1.79649×10^2	-2.65712×10^2
A ₁	a	-7.20106	1.71593×10	2.87926	-2.68462
	b	2.30838×10^3	-4.75487×10^3	-4.03039×10^3	0
	c	0	0	0	0
		Binary Pair			
		MEA+MDEA	MEA+AMP	DEA+MDEA	DEA+AMP
A ₀	a	2.45414×10	-1.27691×10^2	-3.71143×10	-5.71403
	b	-7.79167×10^3	4.00392×10^4	7.70451×10^3	0
	c	0	0	0	0
A ₁	a	-1.56256×10	1.10232×10^2	-1.33407×10	-6.48408×10
	b	0	0	0	0
	c	0	0	0	0

Based on data from: Al-Ghawas et al. (1989), Xu et al. (1992), Rinker et al. (1994), Li and Lie (1994), Hagewiesche et al. (1995b), Song et al. (1996), Hsu and Li (1997b).

Table E.5 Parameters of the Viscosity Equation for Pure Fluids (eq. E.10)

Pure Fluid	a_1	a_2	a_3
H ₂ O	-3.28285	4.56029×10^2	-1.54576×10^2
MEA	-3.51312	8.93173×10^2	-1.59612×10^2
DEA	-4.99689	1.58400×10^3	-1.57449×10^2
MDEA	-4.06399	1.20196×10^3	-1.54419×10^2
AMP	-4.36785	9.96598×10^2	-1.92984×10^2

Based on data from: Yaws et al. (1976), Al-Ghawas et al. (1989), Diguillo et al. (1992), Xu et al. (1992), Li and Lie (1994), Song et al. (1996).

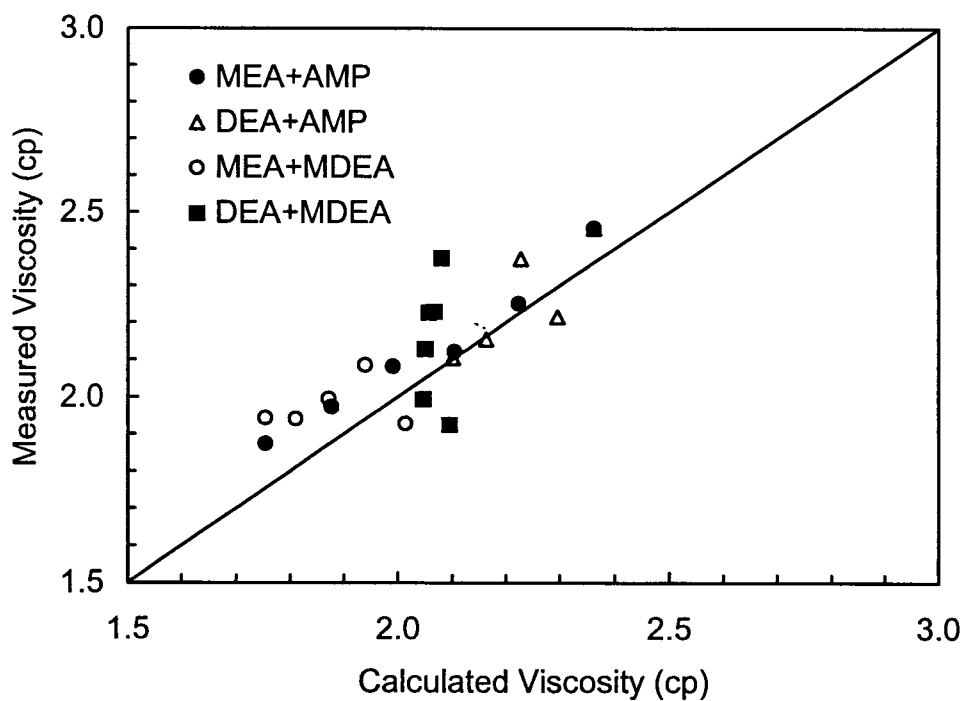


Figure E.2 Measured and calculated viscosities at 303 K.

Table E.6 Viscosity of Aqueous Amine Blends at 303 K
(Total Amine = 25 wt%, Water = 75 wt%)

Blend	Viscosity (cp) (This Work)	Viscosity (cp) (From eq. E.7)	Error ⁺ (%)
MEA + AMP			
0 + 25	2.455	2.363	3.8
5 + 20	2.250	2.224	1.2
10 + 15	2.120	2.103	0.8
15 + 10	2.081	1.991	4.3
20 + 5	1.972	1.877	4.8
25 + 0	1.872	1.754	6.3
DEA + AMP			
0 + 25	2.455	2.363	3.8
5 + 20	2.215	2.296	-3.7
10 + 15	2.372	2.228	6.1
15 + 10	2.155	2.162	-0.3
20 + 5	2.105	2.100	0.2
25 + 0	1.994	2.046	-2.6
MEA + MDEA			
0 + 25	1.924	2.094	-8.9
5 + 20	1.927	2.014	-4.5
10 + 15	2.084	1.940	6.9
15 + 10	1.993	1.872	6.1
20 + 5	1.939	1.810	6.7
25 + 0	1.942	1.754	9.7
DEA + MDEA			
0 + 25	1.924	2.094	-8.9
5 + 20	2.374	2.079	12.4
10 + 15	2.229	2.066	7.3
15 + 10	2.226	2.056	7.6
20 + 5	2.128	2.049	3.7
25 + 0	1.994	2.046	-2.6

⁺ Error = 100 × (measured-calculated)/measured

APPENDIX F

HENRY'S CONSTANT OF CO₂ AND N₂O IN AQUEOUS AMINE SOLUTIONS

F.1 N₂O Analogy

In order to predict the rate of absorption and desorption of CO₂ in aqueous amine solutions or analyze the rate measurements in terms of reaction kinetics, it is essential to estimate the physical solubility of CO₂ at various amine concentrations and temperatures. This physical solubility is calculated by multiplying the partial pressure of the gas above the solution with the inverse of the Henry's law constant. Since CO₂ reacts with aqueous amines, its physical solubility in these solutions cannot be determined by direct measurements and an indirect method based on the N₂O analogy is commonly used. The analogy is based on the assumption that the ratio of the solubilities of N₂O and CO₂ is the same in aqueous amine solutions as in water at the same temperature. In view of the similarities of N₂O and CO₂ with regard to configuration, molecular volume and electronic structure, this assumption is considered reasonable and the physical solubility represented by Henry's constant can be estimated as follows:

$$\frac{H_{\text{CO}_2}}{H_{\text{N}_2\text{O}}} = \frac{H_{\text{CO}_2}^0}{H_{\text{N}_2\text{O}}^0} \quad (\text{F.1})$$

where H_{CO_2} and $H_{\text{N}_2\text{O}}$ denote the Henry's constants of CO_2 and N_2O in aqueous amines, and $H_{\text{CO}_2}^{\circ}$ and $H_{\text{N}_2\text{O}}^{\circ}$ denote Henry's constants of CO_2 and N_2O in water.

F.2 Henry's Constant of CO_2 and N_2O in Water

The data for Henry's constant of CO_2 in water and N_2O in water from the present work and those reported in the literature are presented in Tables F.1 and F.2. These data were correlated as a function of temperature according to the following correlations:

$$\text{Log}_{10}(H_{\text{CO}_2}^{\circ}) = 69.39562 - \frac{3557.793}{T} - 22.2926 \log_{10}(T) + 0.003941096 T \quad (\text{F.2})$$

$$\text{Log}_{10}(H_{\text{N}_2\text{O}}^{\circ}) = 85.8485 - \frac{4373.35}{T} - 27.71662 \log_{10}(T) + 0.003397123 T \quad (\text{F.3})$$

where T is in Kelvin and $H_{\text{CO}_2}^{\circ}$ and $H_{\text{N}_2\text{O}}^{\circ}$ are in the units of $\text{kPa}\cdot\text{m}^3/\text{kmol}$. The correlation for CO_2 is valid over the temperature range from 273 to 523 K and the correlation for N_2O is valid from 278 to 393 K. As shown in Figures F.1 and F.2, these correlations represent the solubility data reasonably well. The average absolute percent deviation (AAD%) for $\text{CO}_2\text{-H}_2\text{O}$ and $\text{N}_2\text{O-H}_2\text{O}$ is 2.32% and 4.1% respectively. Figures F.1 and F.2 also indicate that there is a good agreement between literature results and those of the present study particularly in the temperature range of 293-350 K where historically most of the data are reported.

F.3 Henry's Constant of N₂O and CO₂ in Aqueous Amine Solutions

To estimate the Henry's constant of CO₂ in aqueous amine solutions at various amine concentrations and temperatures using N₂O analogy (eq. F.1), corresponding data for N₂O are needed. Therefore, an extensive literature survey was conducted and the data for the Henry's constant of N₂O in aqueous solutions of MEA, DEA, MDEA, AMP and their mixtures (i.e., MEA+MDEA, MEA+AMP, DEA+MDEA and DEA+AMP) were compiled. These data are listed in Tables F.3 to F.10. It can be seen from these tables that the published data are limited to absorber temperatures (i.e. 293-333 K) only. The data corresponding to stripper temperatures do not exist in the open literature and are usually obtained by extrapolating the low temperature data. However, in the present study it was found that these extrapolations might lead to inaccurate prediction of mass transfer rates as the literature correlations for $H_{N_2O}^0$ and H_{N_2O} proposed by Versteeg and van-Swaaij (1988), Li and Lai, (1995) and Li and Lee, (1996) over predict the Henry's constant value at stripper temperature by a factor of 3. Note that these correlations have been developed based on the solubility data up to 323 K. Consequently, in this work the solubility of N₂O in aqueous solutions of MEA, DEA, MDEA, AMP, MEA+MDEA, MEA+AMP, DEA+MDEA and DEA+AMP were measured in the temperature range of 293-393 K and amine concentration of 10-30 wt%. These data are presented in Tables F.3 to F.10. The experimental apparatus and procedure used was identical to that described in Chapter 6 (see Figure 6.1).

To correlate the solubility of N₂O in amine solutions, a semiempirical model proposed by Wang et al. (1992) was used. According to this method the Henry's constant of N₂O in mixed solvent system can be obtained from the following equation:

$$\ln H_{N_2O} = H^E + \sum_{i=1}^n \Phi_i \ln H_{N_2O}^i \quad (F.4)$$

where H_{N_2O} is the Henry's constant of N₂O in the mixed solvent, H^E is the excess Henry's constant, $H_{N_2O}^i$ is the Henry's constant of N₂O in pure solvent i , and Φ_i is the volume fraction of solvent i . The volume fraction is calculated as

$$\Phi_i = \frac{x_i v_i}{\sum_{i=1}^n x_i v_i} \quad (F.5)$$

where v_i is the molar volume of pure solvent i , and x_i is the mole fraction of solvent i . Wang et al. (1992) measured the Henry's constants of N₂O in pure amines such as MEA, DEA, MDEA and AMP in the temperature range of 293-355 K and correlated their data as

$$H_{N_2O}^{\text{amine}} = a_1 \exp\left(\frac{a_2}{T}\right) \quad (F.6)$$

where a_1 and a_2 are correlation coefficients and are listed in Table F.11. The densities of pure solvents were calculated according to the method described in Appendix E. The Henry's constant of N₂O in pure water was calculated using eq. (F.3). The excess Henry's constant for binary system was correlated as:

$$H_{ij}^E = \Phi_i \Phi_j \alpha_{ij} \quad (\text{F.7})$$

and that for ternary solvent systems was correlated as:

$$H_{ijk}^E = \Phi_i \Phi_j \alpha_{ij} + \Phi_i \Phi_k \alpha_{ik} + \Phi_j \Phi_k \alpha_{jk} + \Phi_i \Phi_j \Phi_k \alpha_{ijk} \quad (\text{F.9})$$

where α_{ij} , α_{ik} , α_{jk} and α_{ijk} are the interaction parameters. For ternary systems (e.g. H₂O-MEA-MDEA), the parameters α_{ij} and α_{ik} represent the water-amine interactions (e.g. H₂O-MEA and H₂O-MDEA), α_{jk} represent the amine-amine interaction (e.g. MEA-MDEA) and α_{ijk} represent the amine-amine-water interaction (e.g. H₂O-MEA-MDEA). As in the work of Wang et al. (1992), α_{ijk} was set to be constant and α_{ij} , α_{ik} , α_{jk} were assumed to have the following temperature dependence:

$$\alpha_{ij} = a_1 + a_2 / T \quad (\text{F.8})$$

where is T in Kelvin and a_1 and a_2 are constants. In this work, first the constants for binary systems (i.e. H₂O+MEA, H₂O+DEA, H₂O+MDEA and H₂O+AMP) were determined by regressing the data presented in Tables F.3 to F.6 and then using those values the constants for ternary systems (i.e. H₂O+MEA+MDEA, H₂O+MEA+AMP, H₂O+DEA+MDEA and H₂O+DEA+AMP) were estimated by regressing the data given in Tables F.6 to F.10. The regression was done using the software package GREG supplied by Stewart & Associate Engineering Software Inc. The estimates of the regression coefficients for both binary and ternary systems are presented in Table F.12. The comparisons of the calculated and experimental Henry's constants of N₂O in binary and ternary aqueous amine

solutions are shown in Figures F.3 and F.4 respectively. The estimates of the average absolute percent deviation (AAD%) for each system are reported in Table F.12. The results are satisfactory. The rather large deviation may be because the regression was performed using data from all sources. Also, the solubility data for mixed amine systems studied here are not plenty. The regression results indicate that the N₂O solubility data for H₂O+DEA+MDEA and H₂O+DEA+AMP reported by Li and Lee (1996) do not correlate well with the experimental data obtained in this work and those reported by other sources as indicated by Figures 3 and 4. Overall, the N₂O solubilities in the aqueous amine systems studied in this work are well correlated using the method of Wang et al. (1992). The correlations coefficients obtained in this study are valid over the temperature range of 293-393 K and the amine concentration of 10-30 wt%.

With all the other quantities in eq. (F.1) estimated, the Henry's constant of CO₂ in unloaded aqueous amine solutions can be calculated. For the sake of brevity the results of these calculations are not presented here.

Table F.1 Henry's constant of CO₂ in water

T (K)	H _{CO₂} ^o (kPa m ³ /kmol)	Reference	T (K)	H _{CO₂} ^o (kPa m ³ /kmol)	Reference
293	2630	This work	318	4854	Versteeg &
304	3500	"	323	5155	van Swaaij (1988)
313	4234	"	333	6135	"
323	5179	"	344	7143	"
333	6233	"	350	7576	"
343	7296	"	355	8333	"
353	8305	"	360	9259	"
363	9302	"	298	2889	Malinin (1974)
373	10056	"	308	3723	"
383	10828	"	323	5192	"
393	11225	"	348	7257	"
303	3420	Li & Lee (1996)	373	9829	"
308	3835	"	423	12485	"
313	4226	"	473	11913	"
303	3382	Li & Lai (1995)	523	9760	"
313	4227	"	383	9971	Takenouchi &
323	5136	"	423	12513	Kennedy (1964)
298	2993	Saha et al. (1993)	473	12652	"
293	2744	"	523	11984	"
313	4572	"	373	9895	Ellis & Golding
333	6476	"	423	13108	(1963)
353	8600	"	450	14362	"
303	3394	Al-Ghawas et al.	473	13496	"
313	4250	(1989)	523	12099	"
323	5167	"	273	1328	Perry et al. (1963)
291	2469	Versteeg &	278	1598	"
292	2410	van Swaaij (1988)	283	1897	"
292	2571	"	288	2225	"
293	2632	"	293	2590	"
298	2967	"	298	2991	"
298	3040	"	303	3392	"
303	3571	"	308	3812	"
308	3937	"	313	4249	"
311	4098	"	318	4687	"
313	4219	"	323	5161	"
313	4202	"	333	6219	"

Table F.2 Henry's constant of N₂O in water

T (K)	H _{N₂O} ^o (kPa m ³ /kmol)	Reference	T (K)	H _{N₂O} ^o (kPa m ³ /kmol)	Reference
293	3701	This work	291	3344	Versteeg &
304	4903	"	292	3484	van Swaaij (1988)
313	5849	"	293	3333	"
323	7117	"	293	3425	"
333	8461	"	298	4132	"
343	9780	"	299	3774	"
353	10911	"	303	4950	"
363	11845	"	308	5263	"
373	12745	"	313	5917	"
383	13534	"	313	6061	"
393	14013	"	318	6993	"
303	4465	Li & Lee (1996)	323	7143	"
308	4813	"	323	7407	"
313	5822	"	340	10309	"
303	4406	Li & Lai (1995)	353	12821	"
313	5725	"	359	14085	"
323	7264	"	298	4173	Haimour (1984)
298	4234	Browning (1994)	298	4132	Sada et al. (1977)
293	3694	Sandall et. al.	298	4154	Joosten (1972)
313	6339	(1993)	298	4171	Sada&Kito (1972)
333	9104	"	298	3906	Duda and Vrentas
353	11223	"	313	6211	(1968)
298	4176	Xu et al.	278	2134	Perry et al. (1963)
323	7254	(1991)	283	2572	"
348	12348	"	288	3029	"
293	3393	Al-Ghawas et al.	293	3617	"
298	3879	(1989)	298	4114	"
303	4321	"	303	4743	"
308	4703	"	308	5539	"
313	5009	"	298	4212	Markham & Kobe
					(1941)

Table F.3 Henry's constant of N₂O in aqueous MEA solutions

T (K)	C _{MEA} (wt%)	H _{N₂O} (kPa m ³ /kmol)	Reference	T (K)	C _{MEA} (wt%)	H _{N₂O} (kPa m ³ /kmol)	Reference
293	10.0	3944	This work	303	19.6	4920	Lttel et al.
303	10.0	5146	"	303	19.7	4901	(1992c)
313	10.0	6296	"	318	1.2	7223	"
323	10.0	7324	"	318	2.6	6976	"
333	10.0	8720	"	318	5.4	6957	"
353	10.0	11193	"	318	10.0	7013	"
373	10.0	12840	"	318	15.1	7088	"
393	10.0	13925	"	318	19.9	6921	"
293	20.0	4250	"	318	21.6	7184	"
303	20.0	4998	"	333	1.4	9107	"
313	20.0	6205	"	333	3.6	9137	"
323	20.0	7373	"	333	5.4	9018	"
333	20.0	8494	"	333	9.8	9077	"
353	20.0	10460	"	333	10.9	8817	"
373	20.0	12104	"	333	16.0	8817	"
393	20.0	12764	"	333	20.4	9167	"
293	30.0	4189	"	333	22.8	8264	"
303	30.0	5165	"	348	1.3	11001	"
313	30.0	6220	"	348	2.6	10445	"
323	30.0	7222	"	348	5.5	10755	"
333	30.0	8322	"	348	11.2	10676	"
353	30.0	10081	"	348	16.6	10715	"
373	30.0	11175	"	348	18.0	9774	"
393	30.0	12597	"	348	22.7	9807	"
303	30.0	4362	Li & Lai	348	24.3	9333	"
308	30.0	4696	(1995)	298	6.7	4132	Ladha et al.
313	30.0	5127	"	298	12.5	4202	(1981)
303	1.1	4564	Lttel et al.				
303	2.4	4910	(1992c)				
303	4.8	4780	"				
303	9.5	4717	"				
303	13.2	4863	"				

Table F.4 Henry's constant of N₂O in aqueous DEA solutions

T (K)	C _{DEA} (wt%)	H _{N₂O} (kPa m ³ /kmol)	Reference	T (K)	C _{DEA} (wt%)	H _{N₂O} (kPa m ³ /kmol)	Reference
293	10.0	3810	This work	303	2.6	5018	Littel et al.
303	10.0	4768	"	303	3.2	4872	(1992c)
313	10.0	5772	"	303	6.3	5028	"
323	10.0	6982	"	303	6.3	5120	"
333	10.0	8272	"	303	8.3	4949	"
353	10.0	10971	"	303	9.0	5079	"
373	10.0	12352	"	303	12.6	5110	"
393	10.0	12984	"	303	17.9	5226	"
293	20.0	4108	"	303	26.6	5429	"
303	20.0	5111	"	303	36.8	5699	"
313	20.0	6333	"	318	2.8	7088	"
323	20.0	7267	"	318	4.4	7050	"
333	20.0	8291	"	318	7.1	7050	"
353	20.0	10743	"	318	8.6	7204	"
373	20.0	12006	"	318	14.3	7323	"
393	20.0	13681	"	318	15.9	7145	"
293	30.0	4064	"	318	25.2	7323	"
303	30.0	5128	"	318	34.6	7685	"
313	30.0	6824	"	333	4.3	8733	"
323	30.0	7975	"	333	8.9	8545	"
333	30.0	9169	"	333	17.8	8679	"
353	30.0	11156	"	333	25.4	8733	"
373	30.0	12875	"	333	33.2	8873	"
393	30.0	14197	"	298	2.0	4235	Versteeg &
303	30.0	6890	Li & Lee	298	2.1	4206	Oyevaar
308	30.0	9613	(1996)	298	4.0	4286	(1989)
313	30.0	14377	"	298	5.5	4272	"
288	10.8	3293	Haimour	298	7.7	4362	"
288	21.3	3597	(1990)	298	11.2	4546	"
288	31.5	4205	"	298	15.4	4505	"
293	10.8	5016	"	298	29.0	4496	"
293	21.3	3577	"	298	36.0	4764	"
293	31.6	3779	"	298	37.0	4848	"
298	10.8	4499	"	298	43.8	4985	"
298	21.4	5826	"	298	56.3	5151	"
298	31.6	3972	"	298	57.3	5140	"
303	10.8	4124	"	298	75.8	6132	"
303	21.4	5076	"	298	78.3	4719	"
303	31.7	7103	"	298	80.8	4424	"
				298	80.8	4563	"

Table F.4 Henry's constant of N₂O in aqueous DEA solutions
Continued

T (K)	C _{DEA} (wt%)	H _{N₂O} (kPa m ³ /kmol)	Reference	T (K)	C _{DEA} (wt%)	H _{N₂O} (kPa m ³ /kmol)	Reference
298	4.7	4164	Versteeg & van Swaaij (1988)	298	4.7	4164	Sada et al. (1977)
298	14.5	4393		298	10.4	4213	
298	14.7	4432	"	298	20.9	4385	"
298	16.1	4324	"	298	23.7	4456	"
298	20.9	4385	"	298	31.3	4631	"
298	22.9	4571	"	298	5.2	4149	Ladha et al. (1981)
298	23.7	4456	"	298	10.4	4202	
298	24.2	4666	"	298	20.6	4367	"
298	24.5	4480	"				
298	31.3	4631	"				

Table F.5 Henry's constant of N₂O in aqueous MDEA solutions

T (K)	C _{MDEA} (wt%)	H _{N₂O} (kPa m ³ /kmol)	Reference	T (K)	C _{MDEA} (wt%)	H _{N₂O} (kPa m ³ /kmol)	Reference
293	10.0	3960	This work	298	30.0	4565	Al-Ghawas
303	10.0	5167	"	298	40.0	4840	et al.
313	10.0	6410	"	298	50.0	5229	(1989a)
323	10.0	7422	"	303	10.0	4483	"
333	10.0	8845	"	303	20.0	4892	"
353	10.0	11210	"	303	30.0	5101	"
373	10.0	13025	"	303	40.0	5429	"
393	10.0	14039	"	303	50.0	5631	"
293	20.0	4110	"	308	10.0	4940	"
303	20.0	4965	"	308	20.0	5172	"
313	20.0	6410	"	308	30.0	5376	"
323	20.0	7558	"	308	40.0	5668	"
333	20.0	8615	"	308	50.0	5970	"
353	20.0	10363	"	313	10.0	5205	"
373	20.0	11389	"	313	20.0	5630	"
393	20.0	12951	"	313	30.0	5898	"
293	30.0	4246	"	313	40.0	6206	"
303	30.0	5179	"	313	50.0	6426	"
313	30.0	6065	"	323	10.0	5563	"
323	30.0	6770	"	323	20.0	5841	"
333	30.0	8311	"	323	30.0	6074	"
353	30.0	10089	"	323	40.0	6220	"
373	30.0	11495	"	323	50.0	6370	"
393	30.0	12339	"	293	15.3	3663	Al-Ghawas
303	30.0	5169	Li & Lai	293	20.1	3800	et al.
308	30.0	5585	(1995)	293	30.2	4128	(1989b)
313	30.0	6188	"	298	15.3	4173	"
288	10.0	3103	Al-Ghawas	298	20.1	4308	"
288	20.0	3273	et al.	298	30.2	4623	"
288	30.0	3654	(1989a)	303	15.3	4638	"
288	40.0	4036	"	303	20.1	4769	"
288	50.0	4154	"	303	30.2	5070	"
293	10.0	3497	"	308	15.3	5039	"
293	20.0	3658	"	308	20.1	5167	"
293	30.0	4039	"	308	30.2	5453	"
293	40.0	4349	"	313	15.3	5363	"
293	50.0	4616	"	313	20.1	5490	"
298	10.0	3996	"	313	30.2	5762	"
298	20.0	4289	"				

Table F.5 Henry's constant of N₂O in aqueous MDEA solutions
Continued

T (K)	C _{MDEA} (wt%)	H _{N₂O} (kPa m ³ /kmol)	Reference	T (K)	C _{MDEA} (wt%)	H _{N₂O} (kPa m ³ /kmol)	Reference
293	4.1	3566	Versteeg &	318	6.0	6994	Versteeg &
293	4.9	3588	van Swaij	318	11.3	6609	van Swaij
293	8.5	3663	(1988)	318	11.9	7126	(1988)
293	9.4	3685	"	318	22.2	6994	"
293	11.8	3702	"	318	30.4	6976	"
293	13.0	3719	"	318	31.0	7364	"
293	16.3	3818	"	333	6.0	8873	"
293	17.7	3794	"	333	9.2	8624	"
293	21.9	3873	"	333	12.0	8931	"
293	30.6	4289	"	333	15.4	9167	"
298	7.3	4235	"	333	18.0	8545	"
298	10.0	4164	"	333	22.4	8733	"
298	14.6	4316	"	333	24.6	8571	"
298	14.8	4464	"	333	30.7	8733	"
298	19.3	4546	"	333	31.3	9077	"
298	19.5	4529	"	288	10.0	3207	Haimour
298	20.3	4480	"	288	15.0	3272	et al.
298	21.9	4596	"	288	20.0	3386	(1984)
298	22.2	4728	"	288	30.0	3773	"
298	28.2	4858	"	288	40.0	4162	"
298	29.3	4955	"	293	10.0	3662	"
298	31.9	6057	"	293	15.0	3737	"
308	7.4	5391	"	293	20.0	3830	"
308	9.7	5414	"	293	30.0	4218	"
308	11.8	5495	"	293	40.0	4541	"
308	14.8	5483	"	298	10.0	4273	"
308	15.6	5507	"	298	15.0	4404	"
308	17.2	5542	"	298	20.0	4561	"
308	17.8	5483	"	298	30.0	4846	"
308	19.7	5615	"	298	40.0	5126	"
308	21.0	5653	"	308	10.0	5530	"
308	21.8	5678	"	308	15.0	5602	"
308	22.1	5628	"	308	20.0	5772	"
308	30.8	5941	"	308	30.0	5984	"
318	5.8	6295	"	308	40.0	6285	"

Table F.6 Henry's constant of N₂O in aqueous AMP solutions

T (K)	C _{AMP} (wt%)	H _{N₂O} (kPa m ³ /kmol)	Reference	T (K)	C _{AMP} (wt%)	H _{N₂O} (kPa m ³ /kmol)	Reference
293	10.0	3456	This work	288	4.5	3243	Saha et al.
302	10.0	4489	"	293	4.5	3737	(1993)
313	10.0	5858	"	298	4.5	4216	"
323	10.0	7293	"	303	4.5	4751	"
334	10.0	8952	"	288	8.9	3413	"
353	10.0	10796	"	293	8.9	3941	"
373	10.0	13391	"	298	8.9	4446	"
393	10.0	14886	"	303	9.0	5006	"
294	20.0	3857	"	288	13.3	3550	"
304	20.0	4931	"	293	13.4	4098	"
312	20.0	5936	"	298	13.4	4613	"
323	20.0	7230	"	303	13.4	5179	"
333	20.0	8440	"	288	17.8	3717	"
353	20.0	10431	"	293	17.8	4293	"
373	20.0	12423	"	298	17.9	4826	"
393	20.0	13360	"	303	17.9	5405	"
294	30.0	5159	"	303	1.7	4863	"
303	30.0	6032	"	303	3.5	4910	"
313	30.0	6729	"	303	6.9	4988	"
323	30.0	7516	"	303	14.0	5038	"
333	30.0	8429	"	303	17.6	5237	"
343	30.0	9301	"	303	22.2	5383	"
353	30.0	10222	"	303	28.2	5686	"
363	30.0	10988	"	303	29.1	5712	"
373	30.0	11929	"	283	17.8	3213	Xu et al.
383	30.0	12973	"	288	17.8	3683	(1991b)
393	30.0	12861	"	298	17.9	4617	"
303	30.0	5856	Li and Lai	310	18.0	5986	"
308	30.0	6545	(1995)	283	26.6	3518	"
313	30.0	7531	"	288	26.7	4020	"
				298	26.8	4842	"
				310	27.0	6313	"

Table F.7 Henry's constant of N₂O in MEA+MDEA+H₂O

T (K)	C _{MEA} (wt%)	C _{MDEA} (wt%)	H _{N₂O} (kPa m ³ /kmol)	Reference
293	12.5	12.5	3660	This work
303	12.5	12.5	4791	"
313	12.5	12.5	5764	"
323	12.5	12.5	6645	"
333	12.5	12.5	7899	"
353	12.5	12.5	9606	"
373	12.5	12.5	10802	"
393	12.5	12.5	11697	"
303	24.0	6.0	4481	Li & Lai (1995)
303	18.0	12.0	4580	"
303	12.0	18.0	4696	"
303	6.0	24.0	4868	"
308	24.0	6.0	4860	"
308	18.0	12.0	4957	"
308	12.0	18.0	5156	"
308	6.0	24.0	5392	"
313	24.0	6.0	5277	"
313	18.0	12.0	5396	"
313	12.0	18.0	5624	"
313	6.0	24.0	5935	"
303	1.5	28.5	5140	Hagewiesche et al. (1995b)
303	3.0	27.0	5270	"
303	4.5	25.5	5360	"
303	2.0	38.0	5580	"
303	4.0	36.0	5670	"
303	6.0	34.0	5850	"
313	1.5	28.5	6100	"
313	3.0	27.0	6290	"
313	4.5	25.5	6480	"
313	2.0	38.0	6270	"
313	4.0	36.0	6340	"
313	6.0	34.0	6440	"
323	1.5	28.5	6350	"
323	3.0	27.0	6550	"
323	4.5	25.5	6590	"
323	2.0	38.0	6290	"
323	4.0	36.0	6320	"
323	6.0	34.0	6430	"
298	10.0	40.0	5680	Browning & Weiland (1994)
298	20.0	30.0	5465	

Table F.8 Henry's constant of N₂O in MEA+AMP+H₂O

T (K)	C _{MEA} (wt%)	C _{AMP} (wt%)	H _{N₂O} (kPa m ³ /kmol)	Reference
293	12.5	12.5	3919	This work
303	12.5	12.5	4920	"
313	12.5	12.5	5977	"
323	12.5	12.5	7054	"
333	12.5	12.5	8114	"
353	12.5	12.5	10049	"
373	12.5	12.5	11570	"
393	12.5	12.5	12565	"
303	24.0	6.0	4548	Li & Lai (1995)
303	18.0	12.0	4911	"
303	12.0	18.0	5415	"
303	6.0	24.0	5597	"
308	24.0	6.0	5000	"
308	18.0	12.0	5656	"
308	12.0	18.0	5961	"
308	6.0	24.0	6304	"
313	24.0	6.0	5545	"
313	18.0	12.0	6131	"
313	12.0	18.0	6813	"
313	6.0	24.0	7145	"

Table F.9 Henry's constant of N₂O in DEA+MDEA+H₂O

T (K)	C _{DEA} (wt%)	C _{MDEA} (wt%)	H _{N₂O} (kPa m ³ /kmol)	Reference
293	12.5	12.5	5106	This work
303	12.5	12.5	6313	"
313	12.5	12.5	7879	"
323	12.5	12.5	9140	"
333	12.5	12.5	10774	"
353	12.5	12.5	12927	"
373	12.5	12.5	14670	"
393	12.5	12.5	15264	"
303	24.0	6.0	6586	Li & Lee (1996)
303	18.0	12.0	6081	"
303	12.0	18.0	5938	"
303	6.0	24.0	5422	"
308	24.0	6.0	8480	"
308	18.0	12.0	7663	"
308	12.0	18.0	6797	"
308	6.0	24.0	6090	"
313	24.0	6.0	11537	"
313	18.0	12.0	9632	"
313	12.0	18.0	7979	"
313	6.0	24.0	6887	"
298	10.0	40.0	5680	Browning &
298	20.0	30.0	5465	Weiland (1994)

Table F.10 Henry's constant of N₂O in DEA+AMP+H₂O

T (K)	C _{DEA} (wt%)	C _{AMP} (wt%)	H _{N₂O} (kPa m ³ /kmol)	Reference
293	12.5	12.5	6048	This work
303	12.5	12.5	7450	"
313	12.5	12.5	8654	"
323	12.5	12.5	10008	"
333	12.5	12.5	11334	"
353	12.5	12.5	13970	"
373	12.5	12.5	15917	"
393	12.5	12.5	16543	"
303	24.0	6.0	6579	Li & Lee (1996)
303	18.0	12.0	6293	"
303	12.0	18.0	6164	"
303	6.0	24.0	6037	"
308	24.0	6.0	8580	"
308	18.0	12.0	7970	"
308	12.0	18.0	7439	"
308	6.0	24.0	7007	"
313	24.0	6.0	11520	"
313	18.0	12.0	10174	"
313	12.0	18.0	9054	"
313	6.0	24.0	8194	"

Table F.11: Parameters in eq. (F.6) for Henry's constant of N₂O in pure amines (Wang et al., 1992)

System	a ₁	a ₂	No. of data	AAD% ⁺
MEA	1.207 × 10 ⁵	-1136.5	6	1.39
DEA	1.638 × 10 ⁵	-1174.6	5	2.43
MDEA	1.524 × 10 ⁵	-1312.7	5	0.90
AMP	8.648 × 10 ⁴	-1205.2	6	1.55

⁺AAD% = average absolute percent deviation

Table F.12: Parameters in excess Henry's constant of N₂O in binary and ternary solvent systems (this work)

System	a ₁	a ₂	α ₁₂₃	No. of data	AAD% ⁺
MEA+H ₂ O	-2.14841	1034.851		59	3.95
DEA+H ₂ O	-2.697683	1263.981		97	7.73
MDEA+H ₂ O	-2.72350	1342.437		147	5.64
AMP+H ₂ O	-1.367139	1089.998		62	3.88
MEA+MDEA+H ₂ O	33.68282	-1436.122	-47.71418	40	5.18
MEA+AMP+H ₂ O	93.32045	-5199.785	-110.8438	20	4.53
DEA+MDEA+H ₂ O	-27.38076	2762.749	42.73698	22	7.63
DEA+AMP+H ₂ O	-50.12477	4131.152	72.02965	20	7.08

⁺AAD% = average absolute percent deviation

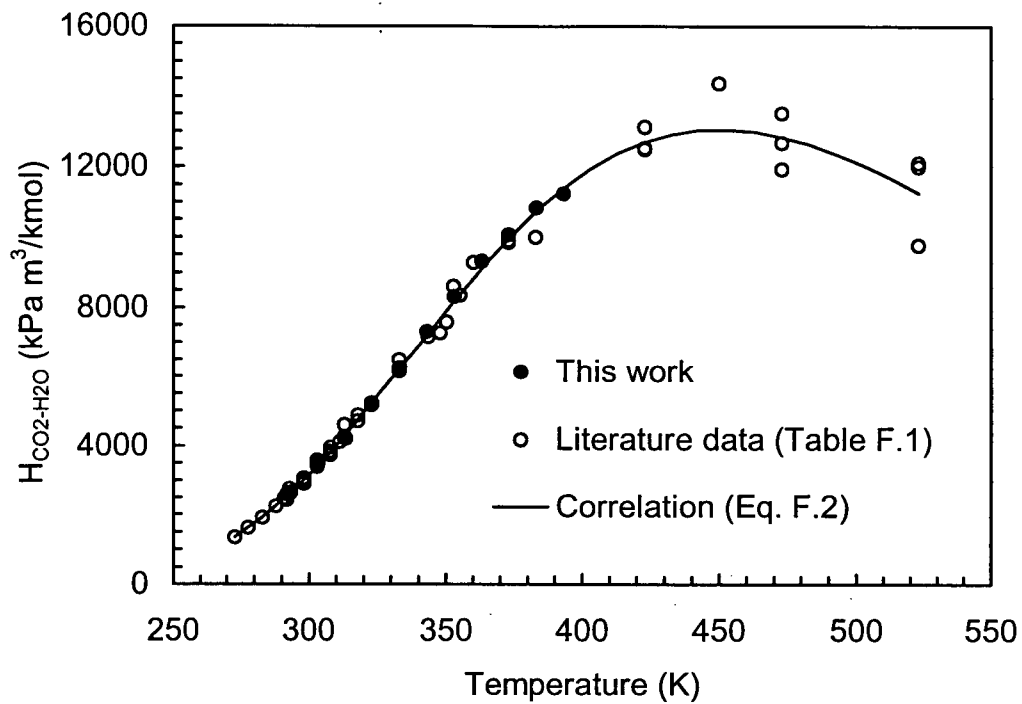


Figure F.1 Henry's constant of CO₂ in water

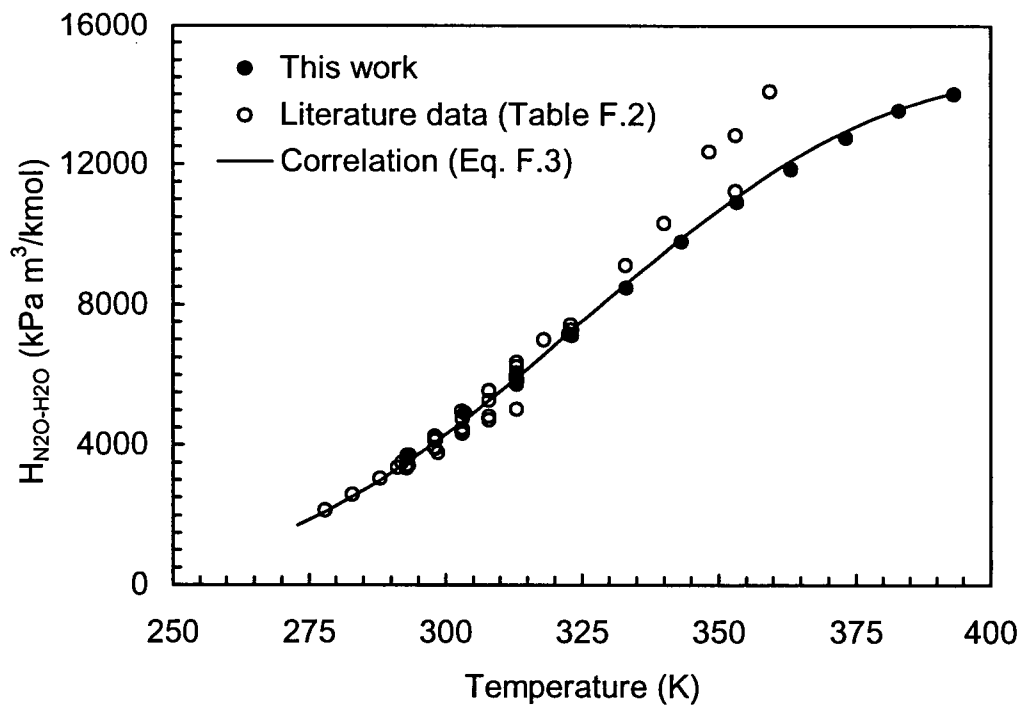


Figure F.2 Henry's constant of N₂O in water

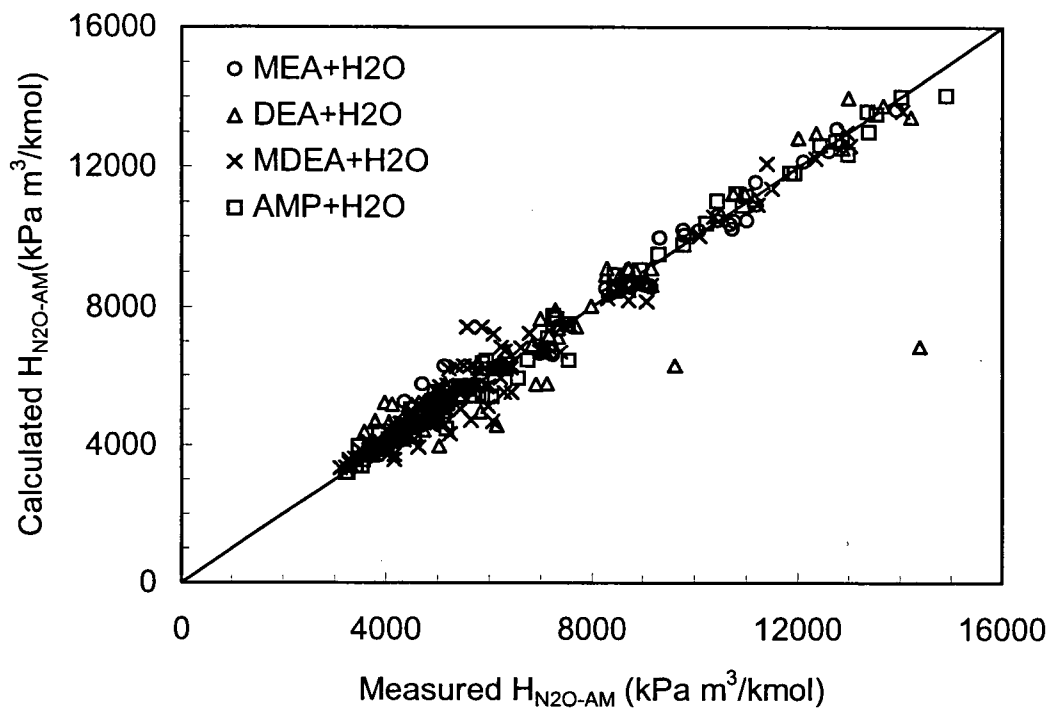


Figure F.3 Measured and calculated values of Henry's constant of N₂O in aqueous amine solutions between 288 to 393 K.

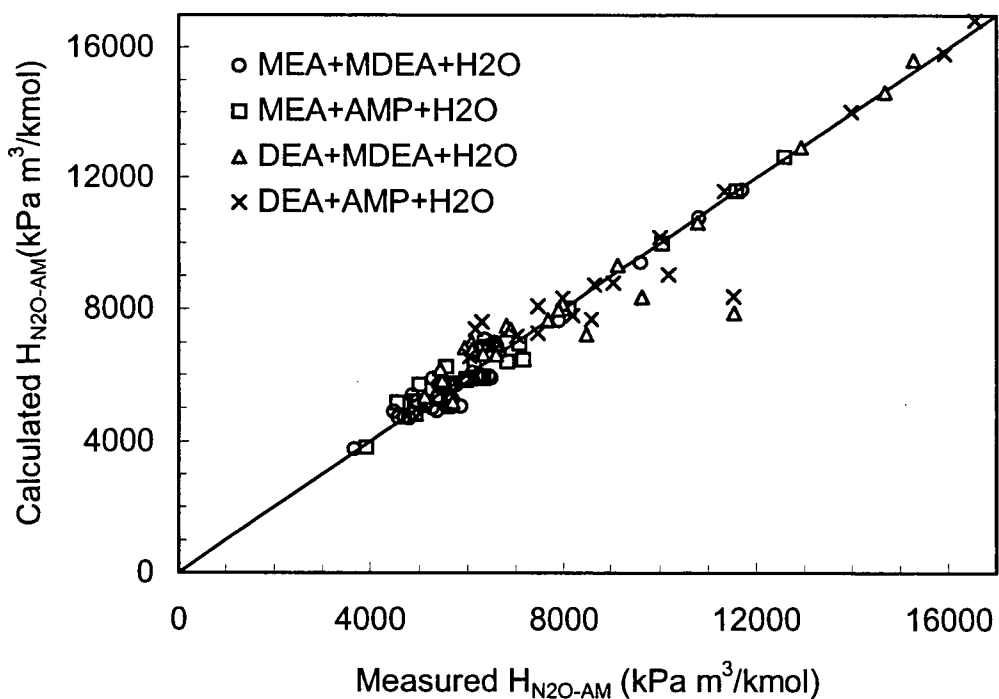


Figure F.4 Measured and calculated values of Henry's constant of N₂O in aqueous amine blends between 288 to 393 K.

APPENDIX G

DIFFUSIVITY OF CO₂ AND N₂O IN AQUEOUS AMINE SOLUTIONS

G.3 N₂O Analogy

Since CO₂ reacts with aqueous amines, its diffusivity in these solutions cannot be measured by direct absorption experiments and an indirect method based on N₂O-Analogy is frequently used. This analogy is based on the assumption that under identical conditions, the ratios of the diffusivities of CO₂ and N₂O in water and aqueous amine solutions are equal:

$$\frac{D_{\text{CO}_2}}{D_{\text{N}_2\text{O}}} = \frac{D_{\text{CO}_2}^{\circ}}{D_{\text{N}_2\text{O}}^{\circ}} \quad (\text{G.1})$$

where D_{CO_2} and $D_{\text{N}_2\text{O}}$ denote the diffusivity of CO₂ and N₂O in amine solution, and $D_{\text{CO}_2}^{\circ}$ and $D_{\text{N}_2\text{O}}^{\circ}$ denote the diffusivity of CO₂ and N₂O in water. In order to calculate D_{CO_2} using eq. (G.1), the values of $D_{\text{CO}_2}^{\circ}$, $D_{\text{N}_2\text{O}}^{\circ}$ and $D_{\text{N}_2\text{O}}$ are required which were calculated from the correlations given below.

G.2 Diffusivity of CO₂ and N₂O in Water

Diffusivities of CO₂ and N₂O in water were calculated using the following equations:

$$D_{\text{CO}_2}^{\circ} = 3.7191 \times 10^{-6} \exp\left(-\frac{2257.9}{T}\right) \quad (\text{G.2})$$

$$D_{N_2O}^o = 5.2457 \times 10^{-6} \exp\left(-\frac{2388.9}{T}\right) \quad (G.3)$$

where T is in Kelvin and $D_{CO_2}^o$ and $D_{N_2O}^o$ are in the units of m^2/s . These correlations were developed from the data acquired in this work and those reported in the literature. These data are tabulated in Tables G.1 and G.2; also, they are plotted on Figures G.1 and G.2. Evidently, the agreement between the measured and predicted values is good. The average absolute percent deviation (AAD%) for CO_2 - H_2O system is 4.1% and for N_2O - H_2O system is 10.9%. The rather large deviation for N_2O - H_2O system is because the data reported by Al-Ghawas et al. (1989a, 1989b) are about 10-70% lower than those measured in this work and those reported in other sources (see Table G.2). In general, the diffusion coefficients measured in this work are in good agreement with the literature values.

G.3 Diffusivity of N_2O and Aqueous Amine Solutions

Historically, the diffusivity of N_2O in aqueous amine solutions at various temperatures and amine concentrations is calculated using the following modified Stokes-Einstein relation:

$$D_{N_2O} \mu_{sol}^{0.8} = D_{N_2O}^o \mu_{H_2O}^{0.8} \quad (G.4)$$

In order to check the above relationship, N_2O diffusivity data for MEA, DEA, MDEA, AMP and their mixtures (MEA+MDEA, MEA+AMP, DEA+MDEA & DEA+AMP) were compiled from various literature sources. These data along with those obtained in this work are tabulated in Tables G.3 to G.10. The

corresponding Stokes-Einstein plots for single and mixed amine systems are presented in Figures G.3 and G.4 respectively. It can be seen from these plots that the Stokes-Einstein type relationship does not represent the experimental data well. The average deviation (AAD%) for single amine systems is about 20% and that for mixed amine systems is about 30%. Therefore, in this work new correlations were developed. The data for single amine systems were correlated as:

$$D_{N_2O} = \left(5.2457 \times 10^{-6} + A_{11} C_{AM} + A_{12} C_{AM}^2 \right) \exp\left(-\frac{2388.9}{T} \right) \quad (G.5)$$

and the data for mixed amine systems were correlated as:

$$D_{N_2O} = \left(5.2457 \times 10^{-6} + A_{11} C_{AM1} + A_{12} C_{AM1}^2 + A_{21} C_{AM2} + A_{22} C_{AM2}^2 + B_{12} C_{AM1} C_{AM2} \right) \exp\left(-\frac{2388.9}{T} \right) \quad (G.6)$$

where T is in Kelvin, C_{AM} is in kmol/m³ and D_{N_2O} are in the units of m²/s. The interaction parameters A_{11} , A_{12} , and B_{12} were assumed to have the following temperature dependence:

$$A_{11}, A_{12}, B_{12} = a_1 + \frac{a_2}{T} \quad (G.7)$$

where T is in Kelvin and a_1 and a_2 are constants.

In this work, first the constants for single amine systems were determined by regressing the data given in Tables G.3 to G.6 and then using these results, the constants for mixed amine systems were estimated by regressing the data given in Tables G.7 to G.10. The regression was done using the software

package GREG supplied by Stewart & Associate Engineering Software Inc. The estimates of the regression coefficients for single and mixed amine systems are presented in Table G.11 and Table G.12.

A comparison of the measured and calculated diffusion coefficients is shown in Figures G.5 and G.6. In general, the agreement is satisfactory. The overall AAD% for single amine systems is about 13% and that for mixed amine systems is about 9%. In light of the fact that different sources have used a different absorption apparatus to measure diffusivity, this much deviation is expected and the correlations can be safely used. Note that for $C_{AM} = 0$, these correlations (eqs. G.5 and G.6) reduce to the correlation for N_2O - H_2O system (eq. G.3). This unique and very important feature does not exist in other similar correlations proposed in the literature (Li and Lai, 1995 and Li and Lee, 1996).

G.4 Diffusivity of CO_2 and Aqueous Amine Solutions

Once the diffusivity of CO_2 in water, N_2O in water and N_2O in aqueous amines are known, the diffusivity CO_2 in aqueous amine solution was calculated using N_2O -analogy given by eq. (G.1).

G.5 Diffusivity of the Alkanolamines in Aqueous Solutions

The diffusion coefficients of various amines in their aqueous solutions were calculated using the correlation developed by Glasscock (1990):

$$D_{AM} = 2.5 \times 10^{-10} \left(\frac{Mw}{\rho_{AM}^{298}} \right)^{-0.54} \left(\frac{T}{298} \right) \left(\frac{\mu_{H_2O}}{\mu_{soln}} \right)^{0.6} \quad (G.8)$$

The density of pure amine at 298 K (ρ_{AM}^{298}) was calculated using eq. (E.6) and the viscosities of pure water (μ_{H_2O}) and aqueous amine solutions (μ_{sol}) were calculated from eqs. (E.10) and (E.7) respectively. The diffusion coefficients of all other ionic species were set equal to D_{AM} .

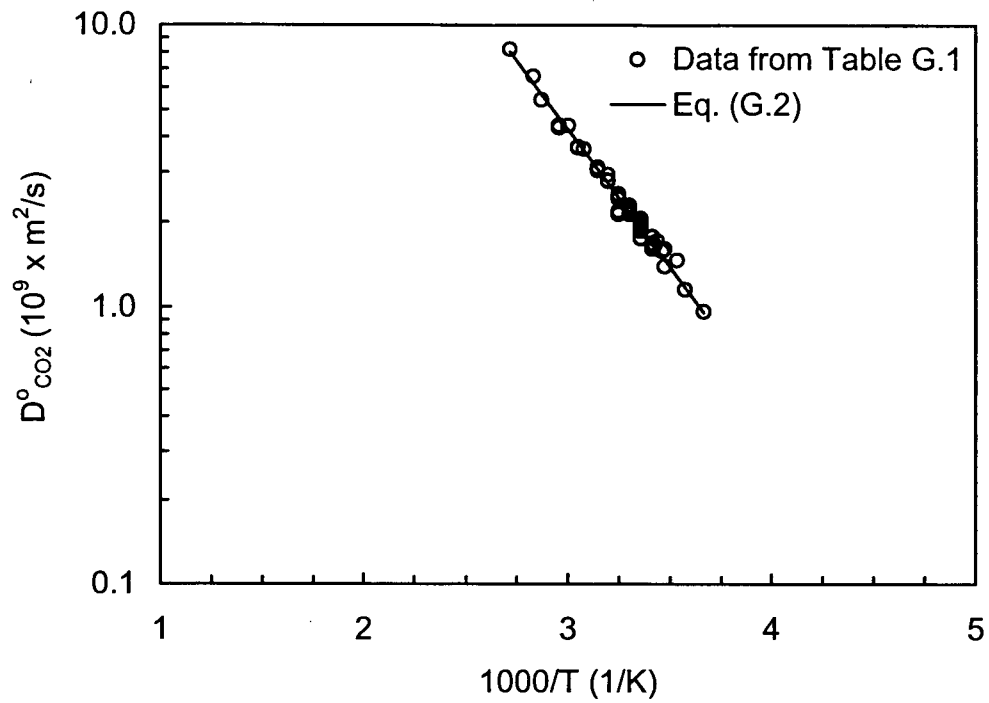


Figure G.1 Diffusivity of CO₂ in water as a function of temperature.

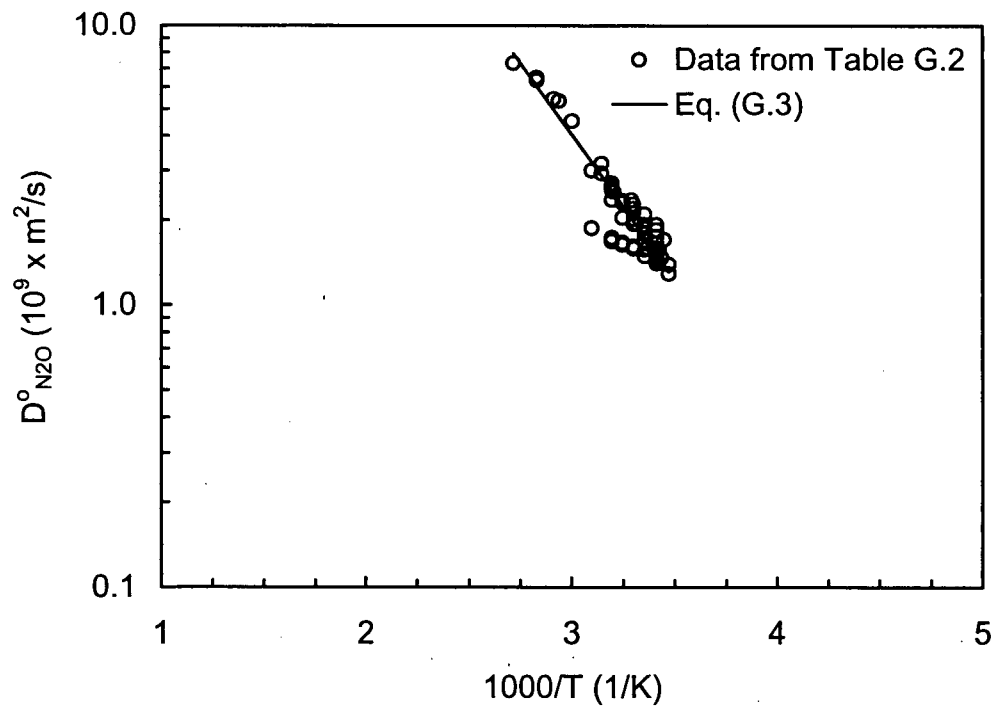


Figure G.2 Diffusivity of N₂O in water as a function of temperature.

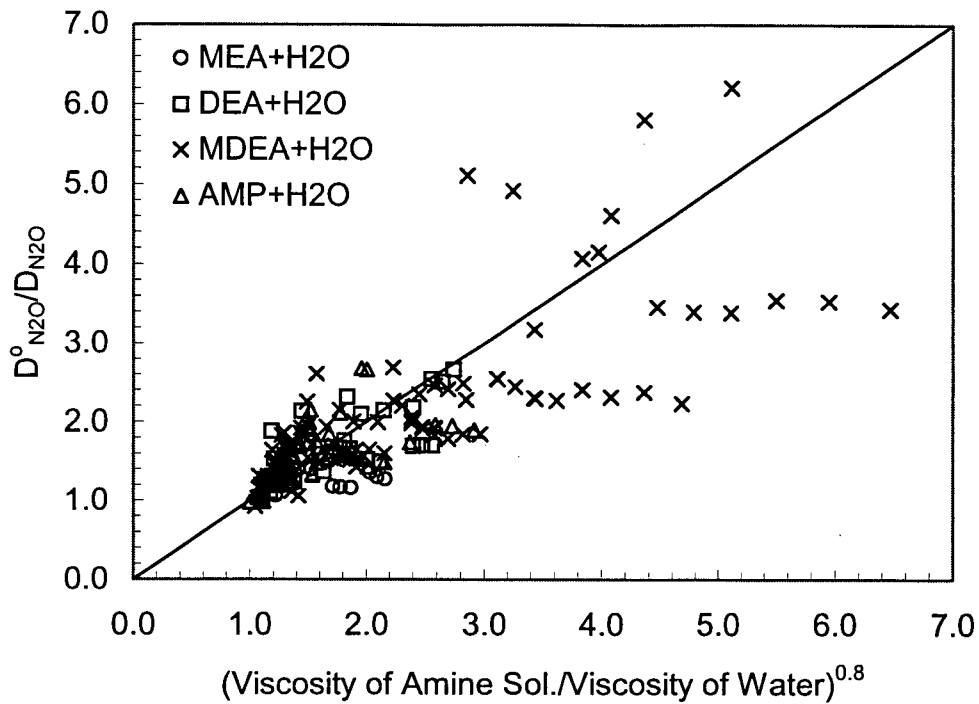


Figure G.3 Stokes-Einstein plot for diffusivity of N₂O in aqueous alkanolamine solutions.

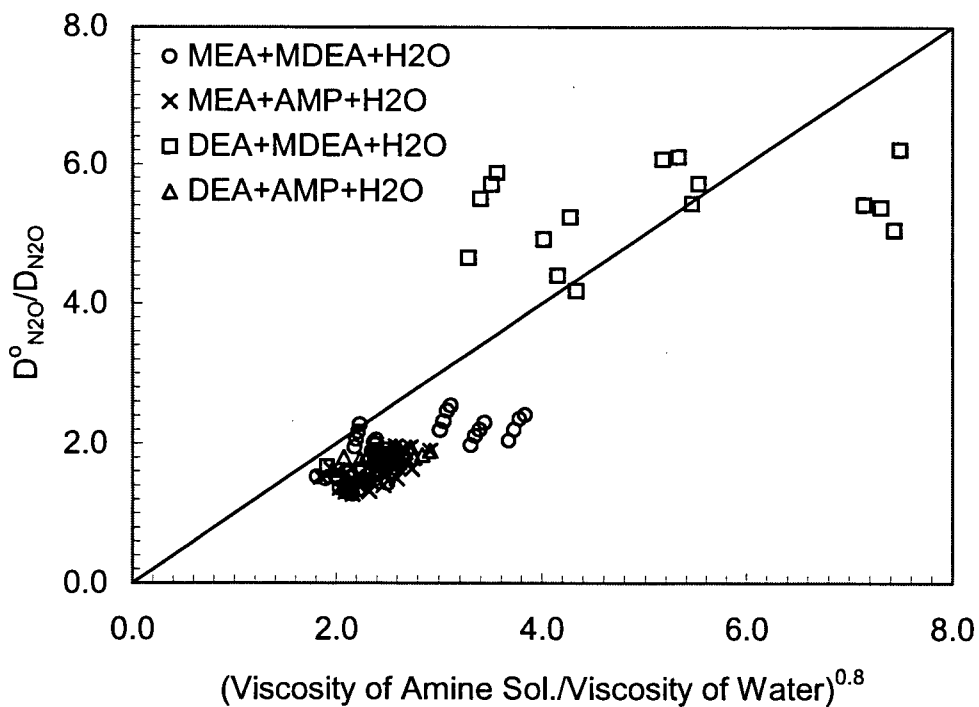


Figure G.4 Stokes-Einstein plot for diffusivity of N₂O in aqueous alkanolamine blends.

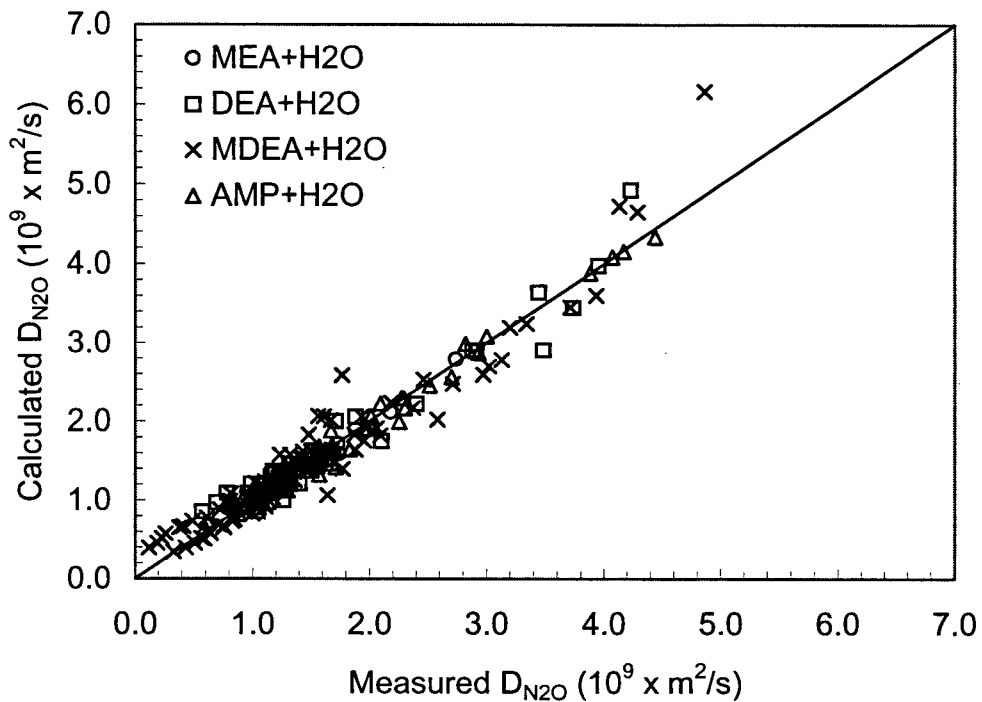


Figure G.5 Measured and calculated diffusivities of N₂O in aqueous amine solutions.

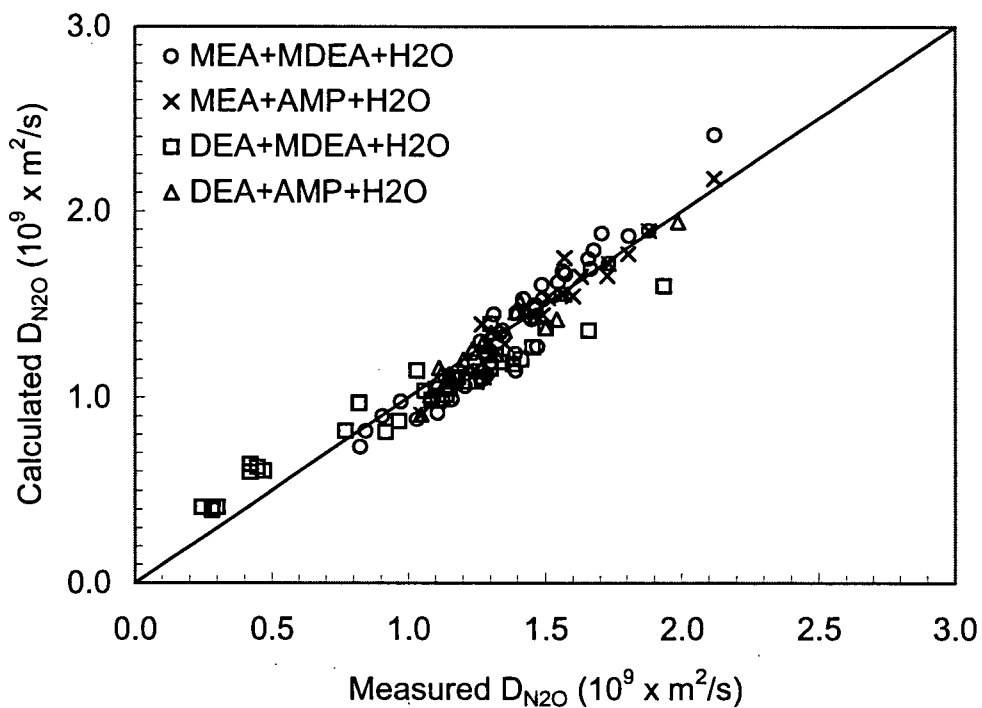


Figure G.6 Measured and calculated diffusivities of N₂O in aqueous amine blends.

Table G.1 Diffusivity of CO₂ in water

T (K)	$10^9 \times D_{\text{CO}_2}^0$ (m ² /s)	Reference	T (K)	$10^9 \times D_{\text{CO}_2}^0$ (m ² /s)	Reference
298	1.75	This work	292	1.65	Versteeg &
308	2.12	"	293	1.68	van Swaaij (1988) [†]
318	3.11	"	293	1.64	"
328	3.65	"	293	1.60	"
298	2.03	Rowley et al. (1998)	293	1.77	"
303	2.23	Li & Lee (1996)	298	1.98	"
308	2.51	"	298	1.87	"
313	2.80	"	298	1.95	"
303	2.12	Li & Lai (1995)	298	2.05	"
308	2.46	"	298	1.85	"
313	2.78	"	298	2.00	"
293	1.76	Tamimi et al. (1994a)	298	1.94	"
298	1.94	"	298	1.87	"
303	2.20	"	298	1.90	"
313	2.93	"	298	1.74	"
333	4.38	"	303	2.29	"
353	6.58	"	303	2.15	"
368	8.20	"	308	2.41	"
298	1.93	Xu et al. (1991b)	308	2.18	"
273	0.96	Versteeg &	313	2.80	"
280	1.15	van Swaaij (1988) [†]	318	3.03	"
283	1.46	"	325	3.61	"
288	1.60	"	328	3.68	"
288	1.39	"	338	4.40	"
289	1.57	"	338	4.30	"
291	1.71	"	348	5.40	"

[†]Versteeg & van Swaaij (1988) includes data from 30 different sources.

Table G.2 Diffusivity of N₂O in water

T (K)	$10^9 \times D_{N_2O}^o$ (m ² /s)	Reference	T (K)	$10^9 \times D_{N_2O}^o$ (m ² /s)	Reference
297	1.59	This work	288	1.39	Versteeg & van Swaaij (1988) ⁺
303	2.19	"	290	1.70	
313	2.61	"	291	1.47	"
323	3.00	"	292	1.56	"
303	2.11	Li & Lee (1996)	293	1.48	"
308	2.34	"	293	1.52	"
313	2.70	"	293	1.92	"
303	2.01	Li & Lai (1995)	293	1.74	"
308	2.30	"	293	1.45	"
313	2.65	"	293	1.65	"
293	1.84	Tamimi et al. (1994a)	298	2.09	"
298	1.88	"	298	1.86	"
303	1.93	"	298	1.69	"
313	2.61	"	298	1.92	"
333	4.51	"	298	1.78	"
353	6.50	"	298	1.88	"
368	7.30	"	298	1.80	"
294	1.59	Saha et al. (1993)	303	2.27	"
302	1.95	"	304	2.35	"
312	2.51	"	308	2.03	"
318	2.93	"	308	2.34	"
288	1.29	Al-Ghawas et al.	313	2.35	"
293	1.44	(1989a)	313	2.55	"
298	1.57	"	313	2.58	"
303	1.61	"	318	3.17	"
308	1.63	"	340	5.33	"
313	1.68	"	343	5.43	"
323	1.87	"	353	6.32	"
293	1.40	Al-Ghawas et al.			
298	1.49	(1989b)			
303	1.58	"			
308	1.66	"			
313	1.73	"			

⁺Versteeg & van Swaaij (1988) includes data from 30 different sources.

Table G.3 Diffusivity of N₂O in aqueous MEA solutions

T (K)	C _{MEA} (wt%)	10 ⁹ × D _{N₂O} (m ² /s)	Reference
303	25.0	1.70	This work
313	25.0	2.18	"
323	25.0	2.74	"
303	30.0	1.56	Li and Lai (1995)
308	30.0	1.73	"
313	30.0	1.88	"
298	4.5	1.74	Sada et al. (1978)
298	8.3	1.63	"
298	12.3	1.46	"
298	16.8	1.24	"
298	20.4	1.15	"

Table G.4 Diffusivity of N₂O in aqueous DEA solutions

T (K)	C _{DEA} (wt%)	10 ⁹ × D _{N₂O} (m ² /s)	Reference
303	25.0	1.32	This work
313	25.0	1.66	"
323	25.0	2.10	"
303	30.0	1.16	Li & Lee (1996)
308	30.0	1.32	"
313	30.0	1.50	"
293	10.0	1.23	Tamimi et al. (1994b)
298	10.0	1.31	"
303	10.0	1.51	"
313	10.0	1.71	"
333	10.0	2.91	"
353	10.0	3.95	"
368	10.0	4.23	"
293	20.0	0.96	"
298	20.0	0.98	"
303	20.0	1.19	"
313	20.0	1.57	"
333	20.0	2.40	"
353	20.0	3.48	"
368	20.0	3.73	"
293	30.0	0.57	"
298	30.0	0.69	"
303	30.0	0.78	"
313	30.0	1.17	"
333	30.0	1.88	"
353	30.0	2.88	"
368	30.0	3.44	"
298	3.1	1.66	Sada et al. (1978)
298	6.0	1.56	"
298	11.6	1.40	"
298	16.9	1.26	"
298	20.7	1.04	"

Table G.5 Diffusivity of N₂O in aqueous MDEA solutions

T (K)	C _{MDEA} (wt%)	10 ⁹ × D _{N₂O} (m ² /s)	Reference	T (K)	C _{MDEA} (wt%)	10 ⁹ × D _{N₂O} (m ² /s)	Reference
303	25.0	1.23	This work	293	50.0	0.12	Tamimi et al.
313	25.0	1.54	"	298	50.0	0.19	(1994b)
323	25.0	1.95	"	303	50.0	0.23	"
303	30.0	1.08	Li & Lai (1995)	313	50.0	0.41	"
308	30.0	1.18	"	333	50.0	0.97	"
313	30.0	1.29	"	353	50.0	1.23	"
303	30.0	1.03	Hagewiesche	368	50.0	1.56	"
303	40.0	0.82	et al. (1995b)	288	10.0	1.05	Al-Ghawas et al.
313	30.0	1.24	"	293	10.0	1.16	(1989)
313	40.0	1.11	"	298	10.0	1.33	"
323	30.0	1.42	"	303	10.0	1.43	"
323	40.0	1.27	"	308	10.0	1.48	"
293	10.0	1.36	Tamimi et al.	313	10.0	1.61	"
298	10.0	1.41	(1994b)	323	10.0	1.76	"
303	10.0	1.60	"	288	20.0	0.84	"
313	10.0	1.93	"	293	20.0	0.99	"
333	10.0	3.20	"	298	20.0	1.15	"
353	10.0	4.13	"	303	20.0	1.29	"
368	10.0	4.86	"	308	20.0	1.41	"
293	20.0	1.06	"	313	20.0	1.50	"
298	20.0	1.11	"	323	20.0	1.67	"
303	20.0	1.25	"	288	30.0	0.71	"
313	20.0	1.67	"	293	30.0	0.82	"
333	20.0	2.71	"	298	30.0	0.97	"
353	20.0	3.93	"	303	30.0	1.03	"
368	20.0	4.29	"	308	30.0	1.16	"
293	30.0	0.61	"	313	30.0	1.24	"
298	30.0	0.72	"	318	30.0	1.30	"
303	30.0	0.81	"	323	30.0	1.42	"
313	30.0	1.27	"	288	40.0	0.59	"
333	30.0	2.02	"	293	40.0	0.64	"
353	30.0	3.02	"	298	40.0	0.75	"
368	30.0	3.71	"	303	40.0	0.82	"
293	40.0	0.26	"	308	40.0	0.99	"
298	40.0	0.38	"	313	40.0	1.11	"
303	40.0	0.49	"	318	40.0	1.17	"
313	40.0	0.80	"	323	40.0	1.27	"
333	40.0	1.77	"	288	50.0	0.33	"
353	40.0	2.58	"	293	50.0	0.43	"
368	40.0	2.97	"	298	50.0	0.51	"

Table G.5 Diffusivity of N₂O in aqueous MDEA solutions
Continued

T (K)	C _{MDEA} (wt%)	10 ⁹ × D _{N₂O} (m ² /s)	Reference	T (K)	C _{MDEA} (wt%)	10 ⁹ × D _{N₂O} (m ² /s)	Reference
303	50.0	0.56	Al-Ghawas et al.	298	11.7	1.64	Versteeg et al.
308	50.0	0.64	(1989)	298	12.5	0.95	(1988)
313	50.0	0.75	"	298	13.3	0.77	"
318	50.0	0.84	"	308	3.9	1.98	"
323	50.0	0.93	"	308	5.0	1.87	"
293	2.1	1.46	Versteeg et al.	308	7.6	1.64	"
293	2.6	1.32	(1988)	308	8.1	1.64	"
293	4.4	1.22	"	308	8.9	1.54	"
293	4.8	1.16	"	308	10.2	1.43	"
293	6.7	1.26	"	308	10.8	1.38	"
293	8.4	0.81	"	308	11.3	1.31	"
298	1.5	1.88	"	318	3.0	2.46	"
298	2.5	1.32	"	318	5.8	2.18	"
298	3.1	1.44	"	318	9.1	2.06	"
298	4.3	1.36	"	318	12.2	1.68	"
298	5.9	1.32	"	318	15.8	1.47	"
298	6.5	1.32	"	318	17.5	1.10	"
298	6.5	1.25	"	333	4.7	3.34	"
298	7.2	1.16	"	333	8.0	3.13	"
298	8.8	1.02	"	333	12.7	2.37	"
298	9.7	1.06	"	333	15.9	2.09	"

Table G.6 Diffusivity of N₂O in aqueous AMP solutions

T (K)	C _{AMP} (wt%)	10 ⁹ × D _{N₂O} (m ² /s)	Reference	T (K)	C _{AMP} (wt%)	10 ⁹ × D _{N₂O} (m ² /s)	Reference
303	25.0	1.13	This work	298	12.2	0.81	Xu et al.
313	25.0	1.71	"	300	12.3	0.91	(1991b)
323	25.0	2.25	"	301	12.3	0.97	"
303	30.0	1.05	Li & Lai (1995)	304	12.3	1.02	"
308	30.0	1.16	"	313	12.3	1.47	"
313	30.0	1.30	"	323	12.4	2.09	"
294	3.1	1.57	Saha et al.	334	12.5	2.82	"
294	6.1	1.30	(1993)	344	12.5	3.88	"
294	9.2	1.09	"	348	12.6	4.44	"
294	12.2	0.88	"	294	18.3	0.59	"
302	3.1	1.83	"	296	18.4	0.62	"
302	6.1	1.55	"	308	18.5	1.06	"
302	9.2	1.30	"	319	18.6	1.57	"
302	12.3	1.10	"	328	18.7	2.27	"
312	3.1	2.30	"	338	18.8	3.00	"
312	6.2	1.98	"	348	18.9	4.07	"
312	9.2	1.68	"	349	18.9	4.17	"
312	12.3	1.45	"				
318	3.1	2.70	"				
318	6.2	2.29	"				
318	9.3	2.01	"				
318	12.4	1.67	"				

Table G.7 Diffusivity of N₂O in MEA+MDEA+H₂O

T (K)	C _{MEA} (wt%)	C _{MDEA} (wt%)	10 ⁹ × D _{N₂O} (m ² /s)	Reference
303	12.5	12.5	1.31	This work
313	12.5	12.5	1.71	"
323	12.5	12.5	2.12	"
303	24.0	6.0	1.49	Li and Lai (1995)
303	18.0	12.0	1.40	"
303	12.0	18.0	1.34	"
303	6.0	24.0	1.24	"
308	24.0	6.0	1.67	"
308	18.0	12.0	1.55	"
308	12.0	18.0	1.46	"
308	6.0	24.0	1.35	"
313	24.0	6.0	1.81	"
313	18.0	12.0	1.68	"
313	12.0	18.0	1.57	"
313	6.0	24.0	1.47	"
303	1.5	28.5	1.14	Hagewiesche et al. (1995)
303	3.0	27.0	1.27	"
303	4.5	25.5	1.39	"
303	2.0	38.0	0.84	"
303	4.0	36.0	0.91	"
303	6.0	34.0	0.97	"
313	1.5	28.5	1.27	"
313	3.0	27.0	1.35	"
313	4.5	25.5	1.45	"
313	2.0	38.0	1.16	"
313	4.0	36.0	1.21	"
313	6.0	34.0	1.29	"
323	1.5	28.5	1.49	"
323	3.0	27.0	1.56	"
323	4.5	25.5	1.66	"
323	2.0	38.0	1.31	"
323	4.0	36.0	1.39	"
323	6.0	34.0	1.47	"

Table G.8 Diffusivity of N₂O in MEA+AMP+H₂O

T (K)	C _{MEA} (wt%)	C _{AMP} (wt%)	10 ⁹ × D _{N₂O} (m ² /s)	Reference
303	12.5	12.5	1.27	This work
313	12.5	12.5	1.57	"
323	12.5	12.5	2.12	"
303	24.0	6.0	1.51	Li and Lai (1995)
303	18.0	12.0	1.42	"
303	12.0	18.0	1.32	"
303	6.0	24.0	1.21	"
308	24.0	6.0	1.63	"
308	18.0	12.0	1.57	"
308	12.0	18.0	1.46	"
308	6.0	24.0	1.35	"
313	24.0	6.0	1.80	"
313	18.0	12.0	1.73	"
313	12.0	18.0	1.60	"
313	6.0	24.0	1.49	"

Table G.9 Diffusivity of N₂O in DEA+MDEA+H₂O

T (K)	C _{DEA} (wt%)	C _{MDEA} (wt%)	10 ⁹ × D _{N₂O} (m ² /s)	Reference
303	12.5	12.5	1.26	This work
313	12.5	12.5	1.66	"
323	12.5	12.5	1.93	"
303	24.0	6.0	1.15	Li and Lee (1996)
303	18.0	12.0	1.14	"
303	12.0	18.0	1.12	"
303	6.0	24.0	1.11	"
308	24.0	6.0	1.30	"
308	18.0	12.0	1.27	"
308	12.0	18.0	1.25	"
308	6.0	24.0	1.22	"
313	24.0	6.0	1.45	"
313	18.0	12.0	1.41	"
313	12.0	18.0	1.38	"
313	6.0	24.0	1.34	"
293	2.1	47.9	0.28	Rinker et al. (1995b)
313	2.1	47.9	0.42	"
333	2.1	47.9	0.82	"
353	2.1	47.9	1.30	"
293	9.0	41.0	0.28	"
313	9.0	41.0	0.42	"
333	9.0	41.0	0.92	"
353	9.0	41.0	1.10	"
293	15.3	34.7	0.30	"
313	15.3	34.7	0.47	"
333	15.3	34.7	0.77	"
353	15.3	34.7	1.06	"
293	18.5	31.5	0.24	"
313	18.5	31.5	0.45	"
333	18.5	31.5	0.97	"
353	18.5	31.5	1.03	"

Table G.10 Diffusivity of N₂O in DEA+AMP+H₂O

T (K)	C _{DEA} (wt%)	C _{AMP} (wt%)	10 ⁹ × D _{N₂O} (m ² /s)	Reference
303	12.5	12.5	1.11	This work
313	12.5	12.5	1.41	"
323	12.5	12.5	1.99	"
303	24.0	6.0	1.15	Li and Lee (1996)
303	18.0	12.0	1.12	"
303	12.0	18.0	1.11	"
303	6.0	24.0	1.08	"
308	24.0	6.0	1.30	"
308	18.0	12.0	1.27	"
308	12.0	18.0	1.24	"
308	6.0	24.0	1.20	"
313	24.0	6.0	1.46	"
313	18.0	12.0	1.43	"
313	12.0	18.0	1.39	"
313	6.0	24.0	1.54	"

Table G.11: Constants in eq. (G.7) for interaction parameter B₁₂ (this work)

System	B ₁₂		No. of data	AAD% ⁺
	a ₁	a ₂		
MEA+MDEA+H ₂ O	-5.8800 × 10 ⁻⁶	1.8453 × 10 ⁻³	33	6.6
MEA+AMP+H ₂ O	-8.7465 × 10 ⁻⁶	2.7373 × 10 ⁻³	15	3.7
DEA+MDEA+H ₂ O	1.5371 × 10 ⁻⁶	-4.3411 × 10 ⁻⁴	31	17.7
DEA+AMP+H ₂ O	1.4169 × 10 ⁻⁶	-3.0807 × 10 ⁻⁴	15	4.2

⁺AAD% = average absolute percent deviation

Table G.12: Constants in eqs. (G.7) for interaction parameters A_{11} and A_{12} (this work)

System	A_{11}		A_{12}		No. of data	AAD% [†]
	a_1	a_2	a_1	a_2		
MEA+H ₂ O	1.4196×10^{-5}	-4.4209×10^{-3}	-3.2060×10^{-6}	9.8151×10^{-4}	11	5.5
DEA+H ₂ O	-1.0565×10^{-5}	2.8859×10^{-3}	3.0475×10^{-6}	-8.9853×10^{-4}	32	13.5
MDEA+H ₂ O	-3.4332×10^{-6}	6.7358×10^{-4}	5.6658×10^{-7}	-1.4950×10^{-4}	122	16.3
AMP+H ₂ O	4.3579×10^{-6}	-1.7708×10^{-3}	-5.3039×10^{-7}	2.1819×10^{-4}	43	7.2

[†]AAD% = average absolute percent deviation

APPENDIX H

EQUILIBRIUM CONSTANTS

The equilibrium constants required to calculate the absorption and desorption rates from the model presented in Chapter 4 were calculated as a function of temperature from the correlations given below.

H.1 Water Dissociation Constant

The water dissociation constant (K_9) as defined by reaction (4.9) was calculated from the correlation reported by Olofsson and Hepler (1975) for the temperature range 293-573 K:

$$\log_{10}(K_9) = 8909.483 - \frac{142613.6}{T} - 4229.195 \log_{10}(T) + 9.7384T - 0.0129638T^2 + 1.15068 \times 10^{-5}T^3 - 4.602 \times 10^{-9}T^4$$

(H.1)

H.2 Rate Constant for Bicarbonate Formation Reaction

The forward rate constant for bicarbonate formation (k_7) as defined by reaction (4.7), was calculated from the correlation reported by Pinsent et al. (1956) and corrected for ionic strength by Astarita et al. (1983) for the temperature range of 273-313 K:

$$\log_{10}(k_7) = 13.635 - \frac{2895}{T} + 0.08 I_c \quad (\text{H.2})$$

where, I_c is the ionic strength given by

$$I_c = \frac{1}{2} \sum_{i=1}^n C_i z_i^2$$

H.3 Equilibrium Constant for Bicarbonate Formation Reaction

The data for K_7K_9 were reported by read (1975) for the temperature range of 298-523 K and were correlated according to the following equation:

$$\log_{10}(K_7K_9) = 115.36 - \frac{5652.1}{T} - 41.882 \log_{10}(T) + 0.0029116T \quad (\text{H.3})$$

H.4 Equilibrium Constant for CO_3^{2-} Formation Reaction

Equilibrium constant for reaction (4.8), K_8 , was obtained from the correlation given by Edward et al. (1978) for the temperature range of 273-498 K:

$$\log_{10}(K_8K_9) = 95.5739 - \frac{5399.0187}{T} - 35.4819 \log_{10}(T) \quad (\text{H.4})$$

H.5 MEA Protonation Constant

MEA protonation constant (K_{15}) as defined by reaction (4.15) was calculated from the correlation of Bates and Pinching (1951) for the temperature range of 273-323 K:

$$\log_{10}(K_{15}K_9) = -0.3869 - \frac{2677.91}{T} - 0.0004277T \quad (\text{H.5})$$

H.6 DEA Protonation Constant

DEA protonation constant (K_{21}) as defined by reaction (4.21) was calculated from the correlation of Bower et al. (1962) for the temperature range of 273-323 K:

$$\log_{10}(K_{21}K_9) = -4.0302 - \frac{1830.15}{T} + 0.0043261T \quad (\text{H.6})$$

H.7 MDEA Protonation Constant

The MDEA protonation constant (K_{23}) as defined by reaction (4.23) was calculated from the correlation developed using the data of Little et al. (1990) in the temperature range 293-333 K:

$$\log_{10}(K_{23}K_9) = 37.956 - \frac{3684.5}{T} - 13.833\log_{10}(T) \quad (\text{H.7})$$

H.8 AMP Protonation Constant

The AMP protonation constant (K_6K_9) as defined by equation (4.6) was obtained from the correlation developed using the data of Littel et al. (1990b) in the temperature range of 293-333 K:

$$\log_{10}(K_6K_9) = -0.39147 - \frac{2629.9}{T} - 0.19958\log_{10}(T) \quad (\text{H.8})$$

H.9 MEA Carbamate Stability Constant

MEA carbamate reversion constant (K_{14}) as defined by reaction (4.14) was calculated from the correlation reported by Kent and Eisenberg (1976) for the temperature range of 298-413 K:

$$\log_{10}(1/K_{14}) = -2.8451 + \frac{1336.8}{T} - 0.01964 \log_{10}(T) \quad (\text{H.9})$$

where T is in Kelvin. Note that in the original correlation the temperature was in Rankin. To be consistent with other correlations we converted this into Kelvin.

H.10 DEA Carbamate Stability Constant

DEA carbamate reversion constant (K_{20}) as defined by reaction (4.20) was calculated from the correlation reported by Aroua et al. (1997) for the temperature range of 303-331 K:

$$\log_{10}(1/K_{20}) = -5.12 + \frac{1781}{T} \quad (\text{H.10})$$

H.11 AMP Carbamate Stability Constant

AMP carbamate reversion constant (K_5) as defined by reaction (4.5) was calculated using the correlation developed from the data of Xu et al. (1992) for the temperature range of 313-373 K:

$$\log_{10}(1/K_5) = -120.86 + \frac{6914.6}{T} + 38.991 \log_{10}(T) \quad (\text{H.11})$$

H.11 Combined Equilibrium Constants

The rate expressions for zwitterion mechanisms (e.g. eqs. 4.31-4.33) involve several combined equilibrium constants such as K_1K_2 , K_1K_3 , K_1K_4 etc. These equilibrium constants can be obtained by appropriately combining above independent equilibrium constants as follows:

$$K_1K_2 = \frac{K_7}{K_5K_6} \quad (\text{H.12})$$

$$K_1K_3 = \frac{K_7K_9}{K_5} \quad (\text{H.13})$$

$$K_1K_4 = \frac{K_7}{K_5} \quad (\text{H.14})$$

$$K_1K_{25} = \frac{K_7}{K_5K_{15}} \quad (\text{H.15})$$

$$K_1K_{28} = \frac{K_7}{K_5K_{21}} \quad (\text{H.16})$$

$$K_{10}K_{11} = \frac{K_7}{K_{14}K_{15}} \quad (\text{H.17})$$

$$K_{10}K_{12} = \frac{K_7K_9}{K_{14}} \quad (\text{H.18})$$

$$K_{10}K_{13} = \frac{K_7}{K_{14}} \quad (\text{H.19})$$

$$K_{10}K_{24} = \frac{K_7}{K_{14}K_{23}} \quad (\text{H.20})$$

$$K_{10}K_{26} = \frac{K_7}{K_{14}K_6} \quad (\text{H.21})$$

$$K_{16}K_{17} = \frac{K_7}{K_{20}K_{21}} \quad (\text{H.22})$$

$$K_{16}K_{18} = \frac{K_7K_9}{K_{20}} \quad (\text{H.23})$$

$$K_{16}K_{19} = \frac{K_7}{K_{20}} \quad (\text{H.24})$$

$$K_{16}K_{27} = \frac{K_7}{K_{20}K_{23}} \quad (\text{H.25})$$

$$K_{16}K_{29} = \frac{K_7}{K_{20}K_6} \quad (\text{H.26})$$

APPENDIX I

DETERMINATION OF GAS-SIDE MASS TRANSFER COEFFICIENT

In absorption experiments, where mostly pure CO₂ was used, gas phase resistance to mass transfer can be considered negligible. However, in desorption experiments, where CO₂ from the liquid film is stripped into humidified N₂ gas, the gas-side resistance to mass transfer may become significant and should be included in calculation for desorption rates. This appendix describes the procedure to develop a correlation for gas-side mass transfer coefficient that was used to interpret the desorption data.

1.1 Estimation of k_g

To estimate k_g , a number of absorption experiments were performed in which gas mixtures containing CO₂ and N₂ were absorbed in 25 wt% aqueous DEA solutions at 303, 313 and 323 K. The mass flow rate of the gas per unit cross-section area was varied from 0.9 to 7 g·m⁻²·s⁻¹ and the CO₂ partial pressure in the gas was varied from 5 to 60 mole%. In all these experiments, the liquid flow rate was fixed at 3.12 mL/s. The experimental conditions with measured absorption fluxes are given in Table K.13.

The primary objective of these experiments was to conduct experiments in such a way that gas-side resistance mainly controls the mass transfer. The CO₂ reaction with

25 wt% aqueous DEA solution is very fast. So if the CO₂ partial pressure in the gas phase is low, the gas-side resistance to mass transfer becomes significant and k_g can be estimated from the following equation:

$$\frac{p_{\text{CO}_2}}{N_A} = \frac{1}{k_g a} + \frac{H_{\text{CO}_2}}{a \sqrt{k_{2^{\text{nd}}} C_{\text{AM}} D_{\text{CO}_2}}} \quad (1.1)$$

Equation (1.1) was derived assuming that the liquid phase reaction is in fast pseudo-first order regime with $E = \sqrt{M}$. The second order rate constant ($k_{2^{\text{nd}}}$) for CO₂-DEA reaction was calculated from the data of Rinker et al. (1996), the Henry's constant (H_{CO_2}) was calculated from the correlation given in Appendix F. The CO₂ partial pressure in the gas-phase (p_{CO_2}) was taken as the log mean partial pressures of CO₂ at the inlet and out let of the absorption chamber.

Table 1.1 shows the measured absorption fluxes and corresponding k_g values calculated using equation (1.1). The k_g values obtained in this work agree very well with similar measurements reported by Critchfield (1988) using a stirred cell reactor. For the experimental conditions studied in this work, the values of k_g vary from 5.5 × 10⁻⁷ to 4.5 × 10⁻⁶ kmol/kPa m² s, which constitutes about 20-30% of the total resistance. This implies that under desorption conditions, where CO₂ diffuses into mixture of N₂ and water vapors, the gas-phase resistance to mass transfer should be included in the calculation.

1.2 Development of Correlation for k_g

The simplest method of representing data for k_g is to relate the Sherwood number $\left(Sh = \frac{k_g RT d p_{BM}}{D_g P_T} \right)$ to Reynolds number $\left(Re = \frac{Gd}{\mu_g} \right)$ and the Schmidt number $\left(Sc = \frac{\mu_g}{\rho_g D_g} \right)$ as follows:

$$Sh = a (Re)^b (Sc)^c \quad (1.2)$$

For wetted wall columns, Treybal (1980) has reported $a = 0.023$, $b = 0.83$ and $c = 0.44$. These values, however, may vary somewhat from one investigator to another (Treybal, 1980). The important point to note from these results is that $k_g \propto G^{0.8}$, $D_g^{.56}$ and P_T/p_{BM} . Therefore, we have correlated the k_g values measured in this work according to the following equation:

$$k_g = a G^b D_g^c \left(\frac{P_T}{RT p_{BM}} \right) \quad (1.3)$$

where a , b and c are constants which can be determined by regression. We were unable to determine the value of the constant c in equation (1.3) by regressing our data. Therefore, we set $c = 0.5$ as reported in the literature and estimated constants a and b by regression. These values were found to be 83.341 and 0.80531 respectively. The diffusivity of CO_2 in gas mixture was calculated from the correlation given by Fuller et al. (1966).

Figure I.1 shows the comparison of the measured and calculated k_g values. The agreement is satisfactory. The percent average absolute deviation (AAD%) is 28%.

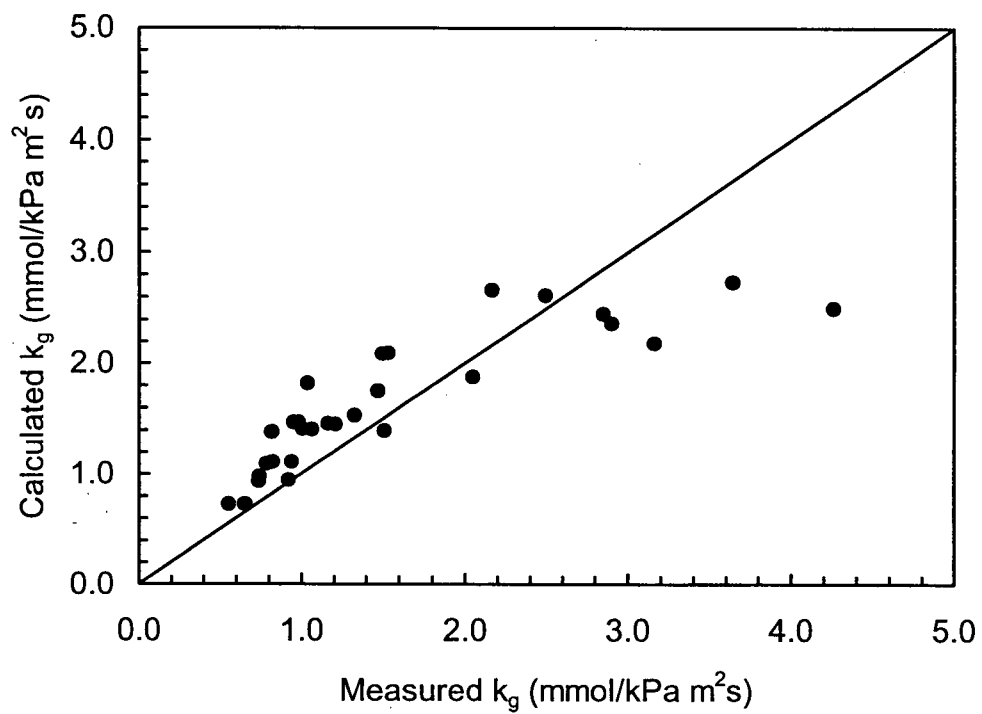


Figure I.1: Measured and calculated gas-side mass-transfer coefficients.

Table I.1: Estimates of k_g from experiments and correlation
($C_{DEA} = 25 \text{ wt}\%$)

T (K)	G_{av} (g/m ² s)	P^{total} (kPa)	$p_{CO_2}^{lm}$ (kPa)	Flux ($\frac{mmol}{m^2s}$)	k_g (mmol/kPam ² s)	
					measured	calculated from eq. (5.3)
304.8	5.87	101.3	8.36	4.30	2.90	2.36
303.2	2.88	101.4	15.90	6.04	1.01	1.41
303.1	4.63	101.4	16.14	7.04	1.53	2.09
303.3	5.99	101.4	16.89	8.30	2.49	2.61
303.0	1.57	100.5	28.34	9.49	0.74	0.97
303.5	2.30	100.5	31.82	11.14	0.82	1.38
303.1	3.16	100.5	32.27	12.39	1.04	1.81
303.4	0.96	100.7	37.72	11.91	0.65	0.72
303.4	1.45	100.7	43.67	15.04	0.79	1.09
303.3	1.97	100.7	46.64	17.36	0.95	1.47
313.2	6.14	101.3	8.23	4.27	2.85	2.45
313.2	3.00	101.3	15.22	6.24	1.16	1.46
312.7	4.61	101.3	16.01	7.09	1.50	2.08
312.7	6.09	101.3	17.29	8.44	2.17	2.66
312.8	1.50	100.4	27.38	9.30	0.74	0.93
312.8	2.37	100.4	29.85	11.82	1.07	1.41
313.2	3.03	100.4	30.39	13.46	1.47	1.75
312.9	0.97	100.4	38.16	11.28	0.56	0.73
312.9	1.51	100.4	41.51	14.83	0.82	1.11
313.3	2.02	100.4	44.31	17.08	0.98	1.47
322.6	6.31	101.3	7.71	4.38	4.26	2.50
323.1	2.99	101.3	14.76	6.31	1.21	1.45
323.0	4.87	101.3	14.83	8.08	3.16	2.18
322.6	6.37	101.3	15.50	8.61	3.64	2.73
322.7	1.54	100.4	24.87	9.52	0.92	0.94
322.5	2.37	100.4	27.62	12.61	1.51	1.39
322.8	3.33	100.4	28.57	14.22	2.05	1.87
322.8	0.99	100.4	34.59	11.34	0.65	0.72
323.2	1.53	100.4	39.25	15.21	0.94	1.11
322.7	2.16	100.4	41.27	18.14	1.33	1.53

APPENDIX J

DETERMINATION OF FORMATE AND DEAF

J.1 Formate Analysis

The concentration of formate ions in the liquid sample was determined by using ion chromatography (IC). In this method the analyte solution is carried by an eluent through a resin-packed column containing numerous ionic exchange sites. The ion chromatograph used was a Dionex 2020i system (Dionex Corporation, Sunnyvale, CA). Detailed specifications with optimized operating conditions are summarized in Table J.1. The standard solution was prepared from analytical grade formic acid obtained from Sigma-Aldrich. Both the standard solution and sample dilution were made using deionized water.

J.2 DEAF Analysis

The DEAF content of the liquid samples was first determined using a Hewlett Packard gas chromatograph (model 5830A). The principal operating conditions are summarized in Table J.2. Using this method, we were able to identify a DEAF peak at a retention time of 14 minutes. However, it was not possible to quantify DEAF because of poor reproducibility, especially at low DEAF concentrations. Therefore, a new technique, which is based on the hydrolysis of DEAF to DEA and formate ions (reaction J.1), was developed.



This method consists of three steps: (i) the liquid sample is analyzed for formate ion concentration using aforementioned IC technique, (ii) 2.0 mL of liquid sample is transferred to a 10 mL glass bottle and 0.2 mL of saturated NaOH solution are added. The bottle is closed and the mixture is kept for hydrolysis for 1 hour in a water bath at 333 K. During this time, all the DEAF is converted to DEA and formate ions, (iii) the hydrolyzed sample is analyzed for formate content by the IC technique. The DEAF content of the liquid sample is then determined from the difference in concentration of formate ions before and after hydrolysis. The accuracy and reproducibility of this method was confirmed by hydrolyzing standard DEAF solutions of various concentrations. The standard DEAF solution was prepared from 85% purity stock solution supplied by Shell Technology Center, Houston, Texas. The impurities in the stock solution were mainly water and the acetates.

Table J.1: IC operating conditions for formate analysis

Item	Description
Column	IonPac ICE-AS1
Detector	Dionex Conductivity CDM-1
Regenerator	Dionex AMMS-ICEII
Eluent	1 mM Heptafluorobutyric acid
Regenerant	5 mM Tetrabutyl ammonium hydroxide
Sample injection	Automatic
Injection volume	10 μ L
Flow	0.8 mL/min
Pressure	~6.2 MPa
Pump	Dionex gradient pump GPM-1
Peak Integrator	Peak Simple Chromatography Data System, SRI Instruments, Torrance, CA

Table J.2: GC operating conditions for DEAF analysis

Item	Description
Column	Tenax TA, 60/80 mesh packed in 6'x1/8" SS packed column (supplied by Supelco Inc. Oakville, ON)
Detector	H ₂ flame ionization (FID)
Detector temperature	310 °C
Injector temperature	280 °C
Carrier gas	N ₂ (24 mL/min)
Injection volume	5 μ L
Temperature program	180 °C hold for 2 min, ramp @ 8 °C/min to 320 °C and hold for 5 min

APPENDIX K

EXPERIMENTAL DATA

K.1 CO₂ Absorption in water

Table K.1: CO₂ absorption in pure water

Series No.	Date (m/d/y)	T (K)	Q _L (mL/s)	P ^{total} (kPa)	p _{CO2} (kPa)	Abs. Flux (mmol/m ² s)
1	5/19/98	298	1.25	100.9	97.7	1.897
	5/19/98	298	1.85	100.9	97.5	2.177
	5/19/98	298	2.50	100.9	97.5	2.484
	5/19/98	298	3.10	100.9	97.5	2.540
	5/19/98	298	3.61	100.9	97.5	2.627
2	5/20/98	308	1.25	100.9	95.1	1.532
	5/20/98	308	1.85	100.9	95.1	1.845
	5/20/98	308	2.50	100.9	95.0	2.026
	5/20/98	308	3.10	100.9	95.0	2.198
	5/20/98	308	3.61	100.9	95.0	2.551
3	5/22/98	318	1.25	100.9	91.1	1.232
	5/22/98	318	1.85	100.9	90.9	1.986
	5/22/98	318	2.50	100.9	90.9	2.201
	5/22/98	318	3.10	100.9	90.9	2.145
	5/22/98	318	3.61	101.3	91.3	2.233
4	5/21/98	328	1.25	101.3	85.2	1.107
	5/21/98	328	1.85	101.3	85.0	1.552
	5/21/98	328	2.50	101.3	85.0	1.725
	5/21/98	328	3.10	101.3	84.9	1.886
	5/21/98	328	3.61	101.3	84.8	2.134

K.2 N₂O Absorption in water

Table K.2: N₂O absorption in pure water

Series No.	Date (m/d/y)	T (K)	Q _L (mL/s)	P ^{total} (kPa)	p _{N₂O} (kPa)	Abs. Flux (mmol/m ² s)
5	6/8/98	297	1.25	100.7	97.7	1.435
	6/8/98	297	1.85	100.6	97.5	1.568
	6/8/98	297	2.50	100.6	97.5	1.682
	6/8/98	297	3.10	100.6	97.5	1.941
	6/8/98	297	3.61	100.6	97.5	1.847
6	6/2/98	303	1.25	100.6	96.3	1.169
	6/2/98	303	1.85	100.6	96.2	1.660
	6/2/98	303	2.50	100.6	96.2	1.701
	6/5/98	303	3.10	100.6	96.2	1.856
	6/5/98	303	3.61	100.6	96.2	2.056
7	6/9/98	313	1.25	100.5	92.9	1.279
	6/9/98	313	1.85	100.5	93.0	1.073
	6/9/98	313	2.50	100.5	92.9	1.678
	6/9/98	313	3.10	100.5	92.9	1.629
	6/9/98	313	3.61	100.5	92.9	1.613
8	6/14/98	323	1.25	100.9	88.3	1.151
	6/14/98	323	1.85	100.9	88.2	1.453
	6/14/98	323	2.50	100.9	88.3	1.103
	6/14/98	323	3.10	100.9	88.2	1.389
	6/14/98	323	3.61	100.9	88.2	1.213

K.3 N₂O Absorption in Aqueous Solutions of Single Amines

Table K.3: N₂O absorption in 25 wt% aqueous MEA solution

Series No.	Date (m/d/y)	T (K)	Q _L (mL/s)	P ^{total} (kPa)	p _{N₂O} (kPa)	Abs. Flux (mmol/m ² s)
9	6/16/98	303	1.65	100.9	96.5	1.084
	6/16/98	303	2.11	100.9	96.5	1.161
	6/16/98	303	2.85	100.9	96.5	1.220
	6/16/98	303	3.53	100.9	96.5	1.341
	6/16/98	303	4.12	100.9	96.5	1.418
10	6/17/98	313	1.65	100.5	93.0	1.048
	6/17/98	313	2.11	100.5	93.0	1.083
	6/17/98	313	2.85	100.5	93.0	1.139
	6/17/98	313	3.53	100.5	92.9	1.304
	6/17/98	313	4.12	100.5	92.9	1.286
11	6/18/98	323	1.65	100.7	88.2	1.037
	6/18/98	323	2.11	100.7	88.2	1.079
	6/18/98	323	2.85	100.7	88.2	1.084
	6/18/98	323	3.53	100.7	88.1	1.137
	6/18/98	323	4.12	100.7	88.1	1.185

Table K.4: N₂O absorption in 25 wt% aqueous DEA solution

Series No.	Date (m/d/y)	T (K)	Q _L (mL/s)	P ^{total} (kPa)	p _{N₂O} (kPa)	Abs. Flux (mmol/m ² s)
12	6/20/98	303	1.68	100.5	96.2	0.867
	6/20/98	303	2.15	100.5	96.2	0.928
	6/20/98	303	2.91	100.5	96.1	0.975
	6/20/98	303	3.60	100.5	96.1	1.072
	6/20/98	303	4.20	100.5	96.1	1.133
13	6/21/98	313	1.68	100.6	93.1	0.838
	6/21/98	313	2.15	100.6	93.1	0.866
	6/21/98	313	2.91	100.6	93.1	0.910
	6/21/98	313	3.60	100.6	93.1	1.042
	6/21/98	313	4.20	100.6	93.1	1.028
14	6/23/98	323	1.68	100.5	87.9	0.829
	6/23/98	323	2.15	100.5	87.9	0.863
	6/23/98	323	2.91	100.5	87.9	0.867
	6/23/98	323	3.60	100.5	87.9	0.909
	6/23/98	323	4.20	100.5	87.9	0.947

Table K.5: N₂O absorption in 25 wt% aqueous MDEA solution

Series No.	Date (m/d/y)	T (K)	Q _L (mL/s)	P ^{total} (kPa)	p _{N₂O} (kPa)	Abs. Flux (mmol/m ² s)
15	6/25/98	303	1.75	100.5	96.2	0.924
	6/25/98	303	2.24	100.5	96.1	0.994
	6/25/98	303	3.02	100.5	96.1	1.019
	6/25/98	303	3.74	100.5	96.1	1.131
	6/25/98	303	4.36	100.5	96.1	1.196
16	6/26/98	313	1.75	100.7	93.3	0.883
	6/26/98	313	2.24	100.7	93.3	0.924
	6/26/98	313	3.02	100.7	93.2	0.972
	6/26/98	313	3.74	100.7	93.2	1.089
	6/26/98	313	4.36	100.7	93.2	1.074
17	6/27/98	323	1.75	101.0	88.5	0.880
	6/27/98	323	2.24	101.0	88.5	0.922
	6/27/98	323	3.02	101.0	88.5	0.915
	6/27/98	323	3.74	101.0	88.4	0.969
	6/27/98	323	4.36	101.0	88.4	1.012

Table K.6: N₂O absorption in 25 wt% aqueous AMP solution

Series No.	Date (m/d/y)	T (K)	Q _L (mL/s)	P ^{total} (kPa)	p _{N₂O} (kPa)	Abs. Flux (mmol/m ² s)
18	7/3/98	303	1.70	101.0	96.7	0.861
	7/3/98	303	2.17	101.0	96.7	0.955
	7/3/98	303	2.93	101.0	96.7	0.843
	7/3/98	303	3.63	101.0	96.7	0.994
	7/3/98	303	4.24	101.0	96.7	1.050
19	7/4/98	313	1.70	101.0	93.5	0.863
	7/4/98	313	2.17	101.0	93.5	0.977
	7/4/98	313	2.93	101.0	93.5	1.034
	7/4/98	313	3.63	101.0	93.5	1.015
	7/4/98	313	4.24	101.0	93.5	1.002
20	7/5/98	323	1.70	100.7	88.2	0.864
	7/5/98	323	2.17	100.7	88.2	0.950
	7/5/98	323	2.93	100.7	88.2	0.872
	7/5/98	323	3.63	100.7	88.2	0.980
	7/5/98	323	4.24	100.7	88.2	1.036

K.3 N₂O Absorption in Aqueous Solutions of Mixed Amines

Table K.7: N₂O absorption in aqueous solutions of 12.5 wt% MEA plus 12.5 wt% MDEA.

Series No.	Date (m/d/y)	T (K)	Q _L (mL/s)	P ^{total} (kPa)	p _{N₂O} (kPa)	Abs. Flux (mmol/m ² s)
21	7/25/98	303	1.70	100.6	96.3	1.047
	7/25/98	303	2.01	100.6	96.3	1.136
	7/25/98	303	2.72	100.6	96.3	1.150
	7/25/98	303	3.55	100.6	96.3	1.289
	7/25/98	303	4.15	100.6	96.2	1.365
22	7/26/98	313	1.70	100.6	93.1	1.016
	7/26/98	313	2.01	100.6	93.1	1.091
	7/26/98	313	2.72	100.6	93.1	1.150
	7/26/98	313	3.55	100.6	93.1	1.233
	7/26/98	313	4.15	100.6	93.1	1.217
23	7/27/98	323	1.70	101.0	88.4	1.016
	7/27/98	323	2.01	101.0	88.4	1.076
	7/27/98	323	2.72	101.0	88.4	1.015
	7/27/98	323	3.55	101.0	88.4	1.097
	7/27/98	323	4.15	101.0	88.4	1.146

Table K.8: N₂O absorption in aqueous solutions of 12.5 wt% MEA plus 12.5 wt% AMP.

Series No.	Date (m/d/y)	T (K)	Q _L (mL/s)	P ^{total} (kPa)	p _{N₂O} (kPa)	Abs. Flux (mmol/m ² s)
24	7/29/98	303	1.87	101.3	96.9	1.029
	7/29/98	303	2.22	101.3	96.9	1.125
	7/29/98	303	2.99	101.3	96.9	1.124
	7/29/98	303	3.91	101.3	96.9	1.260
	7/29/98	303	4.56	101.3	96.9	1.337
25	8/2/98	313	1.87	101.1	93.6	0.972
	8/2/98	313	2.22	101.1	93.6	1.058
	8/2/98	313	2.99	101.1	93.6	1.116
	8/2/98	313	3.91	101.1	93.6	1.159
	8/2/98	313	4.56	101.1	93.6	1.143
26	8/3/98	323	1.87	101.0	88.4	0.956
	8/3/98	323	2.22	101.0	88.4	1.006
	8/3/98	323	2.99	101.0	88.4	1.078
	8/3/98	323	3.91	101.0	88.4	1.083
	8/3/98	323	4.56	101.0	88.4	1.131

Table K.9: N₂O absorption in aqueous solutions of 12.5 wt% DEA plus 12.5 wt% MDEA.

Series No.	Date (m/d/y)	T (K)	Q _L (mL/s)	P ^{total} (kPa)	p _{N₂O} (kPa)	Abs. Flux (mmol/m ² s)
27	8/7/98	303	1.86	100.9	96.6	0.750
	8/7/98	303	2.21	100.9	96.6	0.811
	8/7/98	303	2.98	100.9	96.6	0.811
	8/7/98	303	3.90	100.9	96.6	0.909
	8/7/98	303	4.55	100.9	96.6	0.961
28	8/8/98	313	1.86	101.1	93.7	0.736
	8/8/98	313	2.21	101.1	93.7	0.781
	8/8/98	313	2.98	101.1	93.7	0.814
	8/8/98	313	3.90	101.1	93.7	0.892
	8/8/98	313	4.55	101.1	93.7	0.881
29	8/10/98	323	1.86	101.3	88.7	0.707
	8/10/98	323	2.21	101.3	88.7	0.745
	8/10/98	323	2.98	101.3	88.7	0.721
	8/10/98	323	3.90	101.3	88.7	0.771
	8/10/98	323	4.55	101.3	88.7	0.805

Table K.10: N₂O absorption in aqueous solutions of 12.5 wt% DEA plus 12.5 wt% AMP.

Series No.	Date (m/d/y)	T (K)	Q _L (mL/s)	P ^{total} (kPa)	p _{N₂O} (kPa)	Abs. Flux (mmol/m ² s)
30	8/15/98	303	1.86	100.7	96.4	0.633
	8/15/98	303	2.21	100.7	96.4	0.685
	8/15/98	303	2.98	100.7	96.4	0.685
	8/15/98	303	3.90	100.7	96.4	0.768
	8/15/98	303	4.55	100.7	96.4	0.812
31	8/16/98	313	1.86	100.9	93.4	0.638
	8/16/98	313	2.21	100.9	93.4	0.635
	8/16/98	313	2.98	100.9	93.4	0.673
	8/16/98	313	3.90	100.9	93.4	0.703
	8/16/98	313	4.55	100.9	93.4	0.770
32	8/17/98	323	1.86	100.7	88.3	0.635
	8/17/98	323	2.21	100.7	88.2	0.669
	8/17/98	323	2.98	100.7	88.2	0.682
	8/17/98	323	3.90	100.7	88.2	0.707
	8/17/98	323	4.55	100.7	88.2	0.738

K.4 CO₂ Absorption in Aqueous Solutions of Single Amines

Table K.11: CO₂ absorption in aqueous MEA solutions

Series No.	Date (m/d/y)	T (K)	Q _L (mL/s)	C _{MEA} (wt%)	P ^{total} (kPa)	p _{CO2} (kPa)	Abs. Flux (mmol/m ² s)
33	11/11/98	303.4	2.06	4.74	101.2	96.91	21.11
	11/11/98	303.2	2.05	12.02	101.2	96.96	39.08
	11/11/98	303.2	2.10	14.26	101.2	96.96	49.24
	11/11/98	303.2	2.04	16.32	101.2	96.96	54.55
	11/11/98	303.2	2.05	19.60	101.2	96.96	59.62
	11/11/98	303.8	2.04	23.03	101.2	96.81	66.39
	11/11/98	303.8	2.09	31.41	101.2	96.81	70.79

Table K.12: CO₂ absorption in aqueous DEA solutions

Series No.	Date (m/d/y)	T (K)	Q _L (mL/s)	C _{DEA} (wt%)	P ^{total} (kPa)	p _{CO2} (kPa)	Abs. Flux (mmol/m ² s)
34	8/30/98	303.2	1.70	2.95	100.3	96.09	9.99
	9/7/98	303.5	1.70	7.05	100.3	96.02	18.29
	9/7/98	303.2	1.67	12.40	100.3	96.09	23.51
	9/7/98	303.2	1.74	20.00	101.1	96.89	30.26
	10/16/99	303.4	1.83	25.00	101.5	97.24	33.87
	9/7/98	303.2	1.65	30.01	100.3	96.09	35.86
	9/7/98	303.2	1.67	36.11	100.3	96.09	36.55

Table K.13: CO₂ absorption in aqueous DEA solutions for estimation of k_g

Series No.	Date (m/d/y)	T (K)	Q _L (mL/s)	C _{DEA} (wt%)	P ^{total} (kPa)	p _{CO₂} ^{lm} (kPa)	Abs. Flux (mmol/m ² s)
35	7/29/99	303.4	3.12	25.0	101.4	4.50	3.10
	7/30/99	304.8	3.12	25.0	101.3	8.36	4.30
	8/3/99	303.2	3.12	25.0	101.4	15.90	6.04
	8/3/99	303.1	3.12	25.0	101.4	16.14	7.04
	8/3/99	303.3	3.12	25.0	101.4	16.89	8.30
	8/5/99	303.0	3.12	25.0	100.5	28.34	9.49
	8/5/99	303.5	3.12	25.0	100.5	31.82	11.14
	8/5/99	303.1	3.12	25.0	100.5	32.27	12.39
	8/9/99	303.4	3.12	25.0	100.7	37.72	11.91
	8/9/99	303.4	3.12	25.0	100.7	43.67	15.04
	8/9/99	303.3	3.12	25.0	100.7	46.64	17.36
	7/29/99	303.7	3.12	25.0	101.3	42.43	30.51
	7/29/99	303.5	3.12	25.0	101.3	44.60	22.49
	7/29/99	303.5	3.12	25.0	101.3	52.39	15.35
	7/30/99	313.3	3.12	25.0	101.3	4.32	2.99
	8/4/99	313.2	3.12	25.0	101.3	8.23	4.27
	8/4/99	313.2	3.12	25.0	101.3	15.22	6.24
	8/4/99	312.7	3.12	25.0	101.3	16.01	7.09
	8/6/99	312.7	3.12	25.0	101.3	17.29	8.44
	8/6/99	312.8	3.12	25.0	100.4	27.38	9.30
	8/6/99	312.8	3.12	25.0	100.4	29.85	11.82
	8/10/99	313.2	3.12	25.0	100.4	30.39	13.46
	8/10/99	312.9	3.12	25.0	100.4	38.16	11.28
	8/10/99	312.9	3.12	25.0	100.4	41.51	14.83
	7/30/99	313.3	3.12	25.0	100.4	44.31	17.08
	7/30/99	313.2	3.12	25.0	101.3	46.73	16.29
	7/30/99	313.2	3.12	25.0	101.3	39.17	23.00
	7/30/99	313.2	3.12	25.0	101.3	40.15	31.07

Contd.

Table K.13: CO₂ absorption in aqueous DEA solutions for estimation of k_g
(Contd.)

Series No.	Date (m/d/y)	T (K)	Q _L (mL/s)	C _{DEA} (wt%)	P ^{total} (kPa)	p _{CO₂} ^{lm} (kPa)	Abs. Flux (mmol/m ² s)
35	7/30/99	322.6	3.12	25.0	101.3	4.14	2.66
	8/4/99	322.6	3.12	25.0	101.3	7.71	4.38
	8/4/99	323.1	3.12	25.0	101.3	14.76	6.31
	8/4/99	323.0	3.12	25.0	101.3	14.83	8.08
	8/6/99	322.6	3.12	25.0	101.3	15.50	8.61
	8/6/99	322.7	3.12	25.0	100.4	24.87	9.52
	8/6/99	322.5	3.12	25.0	100.4	27.62	12.61
	8/10/99	322.8	3.12	25.0	100.4	28.57	14.22
	8/10/99	322.8	3.12	25.0	100.4	34.59	11.34
	8/10/99	323.2	3.12	25.0	100.4	39.25	15.21
	7/30/99	322.7	3.12	25.0	100.4	41.27	18.14
	7/30/99	322.5	3.12	25.0	100.9	36.20	17.30
	7/30/99	323.1	3.12	25.0	100.9	31.64	22.67
	7/30/99	323.0	3.12	25.0	100.9	34.36	30.52

Table K.14: CO₂ absorption in aqueous MDEA solutions

Series No.	Date (m/d/y)	T (K)	Q _L (mL/s)	C _{MDEA} (wt%)	P ^{total} (kPa)	p _{CO₂} (kPa)	Abs. Flux (mmol/m ² s)
36	9/13/98	303.2	1.70	3.94	100.9	96.63	2.43
	9/13/98	303.2	1.67	11.17	100.9	96.63	3.75
	9/13/98	303.2	1.67	16.09	100.9	96.63	4.47
	9/14/98	303.4	1.67	20.10	100.6	96.31	4.63
	9/14/98	303.2	1.66	26.93	100.6	96.36	4.47
	9/13/98	303.4	1.70	32.02	100.9	96.58	4.23
	9/11/98	303.2	1.69	38.75	101.0	96.76	3.80

Table K.15: CO₂ absorption in aqueous AMP solutions

Series No.	Date (m/d/y)	T (K)	Q _L (mL/s)	C _{AMP} (wt%)	P ^{total} (kPa)	p _{CO2} (kPa)	Abs. Flux (mmol/m ² s)
37	6/4/99	296.3	1.75	2.00	100.7	97.89	3.47
	6/8/99	295.7	1.84	8.00	101.2	98.45	14.87
	6/9/99	296.5	1.70	10.00	101.4	98.53	17.49
	6/10/99	296.5	1.77	16.00	101.3	98.42	24.68
	5/30/99	295.3	1.47	29.03	100.3	97.64	27.88
	5/21/99	296.4	1.50	30.86	100.1	97.21	32.21
38	6/4/99	303.2	1.75	2.00	100.9	96.68	4.68
	6/8/99	303.4	1.84	8.00	101.2	96.90	14.18
	6/9/99	303.1	1.70	10.00	101.4	97.18	16.95
	6/10/99	304.0	1.77	16.00	101.3	96.85	25.28
	6/14/99	302.2	1.90	18.00	101.0	97.00	26.65
	6/16/99	303.4	1.70	20.00	101.1	96.85	30.73
	6/17/99	304.4	1.78	23.00	101.0	96.49	32.03
	5/11/99	303.7	2.06	23.89	101.2	96.84	32.71
	6/18/99	303.4	1.75	25.00	101.0	96.75	33.13
5/11/99	304.1	1.45	37.82	101.2	96.73	34.62	
39	6/4/99	308.4	1.99	2.00	100.7	95.05	4.50
	5/26/99	308.5	1.82	7.57	100.2	94.49	12.76
	6/8/99	308.4	1.84	8.00	101.2	95.50	14.91
	6/9/99	307.8	1.70	10.00	101.4	95.90	16.62
	6/10/99	308.3	1.77	16.00	101.3	95.65	24.97
	5/25/99	308.5	1.95	16.29	100.9	95.14	26.51
	6/14/99	308.4	1.90	18.00	101.0	95.34	26.91
	6/16/99	308.4	1.70	20.00	101.1	95.48	31.08
	6/17/99	307.8	1.78	23.00	101.0	95.55	33.64
5/21/99	308.5	1.50	30.86	100.1	94.36	36.74	
40	6/4/99	313.2	1.99	2.00	100.7	93.38	5.24
	5/26/99	313.0	1.82	7.57	100.2	92.89	13.16
	6/8/99	313.3	1.84	8.00	101.2	93.79	14.17
	6/9/99	313.2	1.70	10.00	101.4	94.01	16.24
	6/10/99	312.9	1.77	16.00	101.3	94.05	26.47
	5/25/99	313.4	1.95	16.29	100.9	93.40	27.65
	6/14/99	314.3	1.90	18.00	101.0	93.19	27.97
	6/16/99	313.0	1.70	20.00	101.1	93.85	32.79
	6/17/99	312.9	1.78	23.00	101.0	93.77	34.36
	5/30/99	313.1	1.47	29.03	100.3	93.00	36.13
5/21/99	313.3	1.50	30.86	100.1	92.65	40.95	

Table K.15 (contd.): CO₂ absorption in aqueous AMP solutions

Series No.	Date (m/d/y)	T (K)	Q _L (mL/s)	C _{AMP} (wt%)	P ^{total} (kPa)	p _{CO2} (kPa)	Abs. Flux (mmol/m ² s)
41	6/4/99	318.3	1.99	2.00	100.7	91.10	4.17
	5/26/99	318.4	1.82	7.57	100.2	90.50	15.34
	6/9/99	318.3	1.70	10.00	101.3	91.66	17.07
	6/10/99	318.3	1.77	16.00	101.3	91.66	27.45
	5/25/99	318.2	1.95	16.29	100.9	91.27	28.66
	6/14/99	317.9	1.90	18.00	101.0	91.58	30.02
	6/16/99	318.0	1.70	20.00	101.1	91.67	33.77
	6/17/99	318.3	1.78	23.00	101.0	91.43	36.49
	5/30/99	318.4	1.47	29.03	100.3	90.66	38.77
42	6/4/99	323.2	1.99	2.00	100.7	88.34	4.53
	5/26/99	323.2	1.82	7.57	100.2	87.86	16.18
	6/9/99	322.8	1.70	10.00	101.3	89.14	17.37
	6/10/99	322.6	1.77	16.00	101.3	89.31	28.55
	5/25/99	323.3	1.95	16.29	100.9	88.43	28.08
	6/14/99	322.6	1.90	18.00	100.6	88.58	30.79
	6/16/99	322.6	1.70	20.00	101.1	89.16	34.19
	6/17/99	322.6	1.78	23.00	101.0	89.03	36.72
	5/30/99	323.2	1.47	29.03	100.3	87.93	41.13

K.5 CO₂ Absorption in Aqueous Amine Blends

Table K.16: CO₂ absorption in aqueous blends of MEA+MDEA

Series No.	Date (m/d/y)	T (K)	Q _L (mL/s)	C _{MEA} (wt%)	C _{MDEA} (wt%)	P ^{total} (kPa)	p _{CO2} (kPa)	Abs. Flux (mmol/m ² s)
43	8/17/99	303.3	2.56	0.0	25.0	101.4	97.17	4.42
	8/19/99	303.4	3.04	5.0	20.0	101.3	96.98	22.78
	8/23/99	304.5	3.10	10.0	15.0	100.6	96.09	43.35
	8/24/99	303.5	2.94	15.0	10.0	100.7	96.39	59.02
	8/24/99	303.5	2.72	20.0	5.0	100.7	96.36	67.80
	6/25/99	303.5	1.95	25.0	0.0	101.2	96.87	68.58

Table K.17: CO₂ absorption in aqueous blends of MEA+AMP

Series No.	Date (m/d/y)	T (K)	Q _L (mL/s)	C _{AMP} (wt%)	C _{MEA} (wt%)	P ^{total} (kPa)	p _{CO2} (kPa)	Abs. Flux (mmol/m ² s)
44	6/18/99	303.4	1.75	0.0	25.0	101.0	96.75	30.94
	6/22/99	303.5	1.74	5.0	20.0	101.2	96.86	35.10
	6/23/99	303.5	1.68	10.0	15.0	100.8	96.47	42.31
	6/24/99	303.2	1.74	15.0	10.0	100.2	95.99	51.52
	6/25/99	303.4	1.74	20.0	5.0	100.9	96.56	57.11
	6/25/99	303.5	1.95	25.0	0.0	101.2	96.87	68.58

Table K.18: CO₂ absorption in aqueous blends of DEA+MDEA

Series No.	Date (m/d/y)	T (K)	Q _L (mL/s)	C _{MDEA} (wt%)	C _{DEA} (wt%)	P ^{total} (kPa)	p _{CO2} (kPa)	Abs. Flux (mmol/m ² s)
45	8/17/99	303.3	2.56	0.0	25.0	101.4	97.17	4.42
	8/20/99	303.2	3.01	5.0	20.0	101.1	96.87	11.50
	8/20/99	303.5	3.08	10.0	15.0	101.1	96.78	19.76
	8/20/99	303.5	3.12	15.0	10.0	101.0	96.68	24.02
	8/23/99	303.5	2.99	20.0	5.0	100.7	96.39	28.90
	10/16/99	303.4	1.83	25.0	0.0	101.5	97.24	33.87

Table K.19: CO₂ absorption in aqueous blends of DEA+AMP

Series No.	Date (m/d/y)	T (K)	Q _L (mL/s)	C _{AMP} (wt%)	C _{DEA} (wt%)	P ^{total} (kPa)	p _{CO2} (kPa)	Abs. Flux (mmol/m ² s)
46	6/18/99	303.4	1.75	0.0	25.0	101.0	96.75	33.13
	6/28/99	303.1	1.79	5.0	20.0	101.3	97.13	30.47
	6/28/99	303.6	1.75	10.0	15.0	101.4	97.05	29.27
	6/29/99	303.6	1.74	15.0	10.0	101.2	96.90	29.32
	6/29/99	303.4	1.77	20.0	5.0	101.2	96.91	30.28
	10/16/99	303.4	1.83	25.0	0.0	101.5	97.24	33.87

K.6 CO₂ Desorption from Aqueous Solutions of Single Amines

Table K.20: CO₂ desorption from aqueous MEA solutions

Series No.	Date (m/d/y)	T (K)	α (mol/mol)	Q _L (mL/s)	C _{MEA} (wt%)	P ^{total} (kPa)	p _{CO₂} ^{lm} (kPa)	Des. Flux (mmol/m ² s)
47	10/27/98	333.2	0.335	2.20	20.0	100.6	0.50	0.31
	10/31/98	333.2	0.384	2.24	20.0	100.7	0.93	0.74
	10/23/98	333.2	0.422	2.14	20.0	100.5	0.99	1.49
	11/2/98	333.2	0.487	2.14	20.0	101.0	2.47	2.92
48	10/27/98	343.2	0.335	2.20	20.0	100.6	0.74	0.51
	10/31/98	343.2	0.384	2.22	20.0	100.7	1.49	1.62
	10/23/98	343.2	0.422	2.14	20.0	100.5	1.50	2.65
	10/21/98	343.2	0.439	2.10	20.0	100.9	1.70	3.02
	10/21/98	343.2	0.443	2.22	20.0	101.3	1.73	3.05
	10/21/98	343.2	0.480	2.27	20.0	100.9	2.62	4.73
49	10/27/98	353.2	0.335	2.20	20.0	100.6	1.12	1.40
	11/2/98	353.5	0.362	2.22	20.0	101.0	1.18	2.94
	10/31/98	353.2	0.384	2.24	20.0	100.9	1.46	3.72
	11/2/98	353.5	0.421	2.27	20.0	101.0	1.60	5.23
	11/2/98	353.6	0.435	2.25	20.0	101.0	1.55	6.05
50	10/30/98	363.2	0.226	2.23	20.0	202.2	1.00	0.42
	10/30/98	363.3	0.269	2.23	20.0	201.2	1.15	0.80
	10/28/98	363.3	0.299	2.22	20.0	201.0	1.46	1.37
	10/25/98	363.4	0.370	2.27	20.0	200.8	2.99	3.56
	10/31/98	363.4	0.398	2.24	20.0	202.3	3.98	5.07
51	10/28/98	373.2	0.205	2.38	20.0	202.7	1.35	0.95
	10/24/98	373.3	0.265	2.30	20.0	201.3	1.51	2.27
	10/31/98	373.3	0.279	2.23	20.0	202.2	1.85	2.59
	10/25/98	373.2	0.360	2.27	20.0	200.8	3.42	6.20
	10/30/98	373.4	0.398	2.24	20.0	202.3	4.26	9.71
52	10/28/98	378.3	0.205	2.38	20.0	202.4	1.54	1.43
	10/31/98	378.3	0.218	2.35	20.0	202.3	0.66	2.19
	10/30/98	378.4	0.279	2.23	20.0	202.3	2.10	4.76
	10/31/98	378.5	0.319	2.29	20.0	202.3	1.84	6.88
	10/31/98	378.1	0.377	2.24	20.0	202.3	3.03	12.95

Table K.21: CO₂ desorption from aqueous DEA solutions

Series No.	Date (m/d/y)	T (K)	α (mol/mol)	Q _L (mL/s)	C _{DEA} (wt%)	P ^{total} (kPa)	p _{CO₂} ^{lm} (kPa)	Des. Flux (mmol/m ² s)
53	10/17/98	343.2	0.232	2.16	20.0	101.3	0.42	0.73
	10/17/98	343.2	0.297	2.28	20.0	101.3	0.88	1.53
	10/17/98	343.2	0.369	2.29	20.0	101.3	1.22	2.14
	10/17/98	343.2	0.402	2.34	20.0	101.3	1.84	3.25
	10/17/98	343.2	0.476	2.25	20.0	101.3	2.43	4.35
54	7/19/99	353.7	0.138	2.63	25.0	206.1	0.48	0.42
	7/14/99	353.5	0.205	2.48	25.0	196.3	1.12	0.99
	7/12/99	353.6	0.298	2.61	25.0	204.3	2.74	2.49
	10/18/98	353.5	0.342	2.52	25.0	204.3	3.85	3.13
	7/3/99	353.3	0.380	2.48	25.0	203.8	6.43	3.76
55	7/19/99	363.7	0.138	2.63	25.0	204.7	0.73	0.76
	7/14/99	363.5	0.205	2.48	25.0	204.9	2.20	2.04
	7/12/99	363.5	0.298	2.06	25.0	204.0	3.96	4.07
	10/18/98	363.3	0.342	2.52	25.0	204.3	4.80	6.41
	7/3/99	363.1	0.380	2.48	25.0	206.9	5.08	8.57
56	7/19/99	373.5	0.078	2.66	25.0	204.5	0.30	0.36
	7/19/99	373.6	0.138	2.63	25.0	204.5	1.11	1.47
	7/22/99	373.4	0.163	2.56	25.0	204.7	1.66	2.21
	7/22/99	373.4	0.184	2.56	25.0	204.7	2.18	2.64
	7/14/99	373.5	0.205	2.48	25.0	206.1	3.03	3.45
57	7/21/99	382.0	0.041	2.72	25.0	204.5	0.16	0.40
	7/21/99	381.7	0.069	2.72	25.0	204.5	0.29	0.68
	7/21/99	381.8	0.088	2.66	25.0	204.5	0.52	1.27
	7/22/99	382.4	0.101	2.66	25.0	204.7	0.58	1.47
	7/19/99	382.3	0.138	2.63	25.0	204.7	0.96	2.34

Table K.22: CO₂ desorption from aqueous MDEA solutions

Series No.	Date (m/d/y)	T (K)	α (mol/mol)	Q _L (mL/s)	C _{MDEA} (wt%)	P ^{total} (kPa)	p _{CO₂} ^{lm} (kPa)	Des. Flux (mmol/m ² s)
58	10/2/99	343.4	0.132	1.87	25.0	100.6	0.59	0.43
	10/4/99	343.5	0.161	1.88	25.0	100.7	0.90	0.95
	10/5/99	343.3	0.188	1.89	25.0	100.5	0.92	1.63
	10/7/99	343.4	0.223	1.88	25.0	101.3	1.16	2.06
	10/9/99	343.4	0.304	1.90	25.0	100.9	1.75	3.54
59	10/2/99	353.3	0.132	1.88	25.0	100.6	0.97	1.19
	10/4/99	353.2	0.161	1.88	25.0	101.0	1.24	1.95
	10/5/99	353.3	0.188	1.86	25.0	100.9	1.43	2.80
	10/7/99	353.3	0.223	1.89	25.0	101.0	1.60	3.54
	10/9/99	353.3	0.304	1.89	25.0	101.0	2.72	6.57
60	10/10/99	363.2	0.087	1.87	25.0	202.2	1.42	0.94
	10/2/99	363.3	0.132	1.87	25.0	201.2	2.70	1.98
	10/4/99	363.3	0.161	1.88	25.0	201.0	3.76	3.39
	10/5/99	363.4	0.188	1.89	25.0	200.8	4.12	4.33
	10/7/99	363.4	0.223	1.88	25.0	202.3	4.38	5.61
61	10/10/99	373.3	0.087	1.90	25.0	202.7	1.65	1.71
	10/2/99	373.2	0.132	1.87	25.0	201.3	2.48	3.35
	10/4/99	373.4	0.161	1.88	25.0	202.2	3.66	5.07
	10/5/99	373.5	0.188	1.87	25.0	200.8	4.26	6.94
	10/7/99	373.4	0.223	1.87	25.0	202.3	4.88	8.69
62	10/10/99	378.3	0.087	1.88	25.0	202.4	1.84	2.03
	10/2/99	378.3	0.132	1.91	25.0	202.3	2.51	4.12
	10/4/99	378.4	0.161	1.92	25.0	202.3	3.07	6.36
	10/5/99	378.4	0.188	1.92	25.0	202.3	2.81	7.43
	10/7/99	378.5	0.223	1.89	25.0	202.3	4.24	10.44

Table K.23: CO₂ desorption from aqueous AMP solutions

Series No.	Date (m/d/y)	T (K)	α (mol/mol)	Q _L (mL/s)	C _{AMP} (wt%)	P ^{total} (kPa)	p _{CO₂} ^{lm} (kPa)	Des. Flux (mmol/m ² s)
63	11/3/98	332.9	0.376	2.02	20.0	100.6	0.51	0.36
	11/14/98	333.3	0.425	2.01	20.0	100.6	0.67	0.52
	11/5/98	333.6	0.568	1.86	20.0	100.6	0.94	1.01
	11/16/98	333.6	0.695	2.01	20.0	100.6	1.30	1.46
	11/5/98	333.8	0.756	1.76	20.0	100.6	1.27	1.69
64	11/4/98	343.6	0.376	2.02	20.0	100.6	0.75	0.62
	11/14/98	343.5	0.425	1.92	20.0	100.6	0.95	0.90
	11/5/98	343.1	0.568	1.86	20.0	100.6	1.43	1.79
	11/16/98	343.6	0.695	1.81	20.0	100.6	1.77	2.64
	11/5/98	343.6	0.756	1.76	20.0	100.6	2.02	3.17
65	11/4/98	353.5	0.376	2.02	20.0	100.6	1.69	1.89
	11/14/98	353.6	0.425	1.92	20.0	100.6	1.18	2.42
	11/10/98	353.5	0.454	1.88	20.0	101.3	1.13	2.92
	11/16/98	353.6	0.516	1.81	20.0	101.3	1.38	3.82
	11/5/98	353.6	0.568	1.86	20.0	100.6	1.47	4.54
66	11/3/98	363.4	0.217	2.19	20.0	202.7	1.55	0.89
	11/23/98	363.6	0.291	2.01	20.0	202.7	2.10	1.70
	11/4/98	363.4	0.376	2.02	20.0	202.4	2.70	3.36
	11/16/98	363.6	0.454	1.98	20.0	202.4	3.43	4.58
	11/5/98	363.4	0.568	1.86	20.0	202.4	5.45	7.53
67	11/3/98	373.2	0.217	2.19	20.0	202.7	2.29	1.83
	11/23/98	373.4	0.291	2.01	20.0	202.7	3.20	3.57
	11/10/98	373.6	0.333	1.99	20.0	204.5	2.49	4.60
	11/19/98	373.4	0.358	1.92	20.0	204.5	3.11	5.71
	11/4/98	373.2	0.376	2.02	20.0	203.8	3.47	6.52
68	11/3/98	378.2	0.217	2.19	20.0	202.3	2.05	2.98
	11/23/98	378.5	0.291	2.01	20.0	202.7	2.98	5.26
	11/10/98	378.5	0.333	2.02	20.0	205.1	2.47	6.52
	11/19/98	378.3	0.358	1.92	20.0	204.5	2.58	7.74
	11/4/98	378.6	0.376	1.99	20.0	202.4	2.57	8.73

K.7 CO₂ Desorption from Aqueous Amine Blends

Table K.24: CO₂ desorption from aqueous blends of MEA+MDEA

Series No.	Date (m/d/y)	T (K)	α (mol/mol)	Q _L (mL/s)	C _{MEA} (wt%)	C _{MDEA} (mL/s)	P ^{total} (kPa)	p _{CO₂} ^{lm} (kPa)	Des. Flux (mmol/m ² s)
69	11/4/99	353.3	0.188	2.04	12.5	12.5	202.5	0.63	0.44
	11/5/99	353.4	0.241	2.05	12.5	12.5	201.9	1.17	0.80
	11/7/99	353.4	0.276	2.05	12.5	12.5	204.1	1.90	1.42
	11/8/99	353.5	0.335	2.08	12.5	12.5	202.6	3.00	3.37
70	11/4/99	363.2	0.188	2.05	12.5	12.5	202.5	0.94	0.95
	11/5/99	363.3	0.241	2.05	12.5	12.5	201.9	2.17	2.07
	11/7/99	363.3	0.276	2.05	12.5	12.5	204.1	2.56	2.91
	11/8/99	363.4	0.335	2.08	12.5	12.5	202.6	4.63	6.19
71	11/9/99	373.4	0.148	2.14	12.5	12.5	202.5	0.80	1.09
	11/4/99	373.3	0.188	2.08	12.5	12.5	201.9	1.35	1.91
	11/5/99	373.4	0.241	2.06	12.5	12.5	204.1	2.89	3.94
	11/7/99	373.3	0.276	2.07	12.5	12.5	202.6	3.67	6.16

Table K.25: CO₂ desorption from aqueous blends of MEA+AMP

Series No.	Date (m/d/y)	T (K)	α (mol/mol)	Q _L (mL/s)	C _{MEA} (wt%)	C _{AMP} (mL/s)	P ^{total} (kPa)	p _{CO₂} ^{lm} (kPa)	Des. Flux (mmol/m ² s)
72	11/13/99	353.3	0.226	2.11	12.5	12.5	202.5	0.76	0.30
	11/14/99	353.5	0.278	2.07	12.5	12.5	202.5	1.03	0.77
	11/16/99	353.3	0.306	2.06	12.5	12.5	202.3	1.45	1.24
	11/20/99	353.6	0.359	2.04	12.5	12.5	202.5	2.18	2.20
73	11/13/99	363.3	0.226	2.21	12.5	12.5	202.5	1.50	0.75
	11/14/99	363.4	0.278	2.12	12.5	12.5	202.5	2.20	1.66
	11/16/99	363.3	0.306	2.12	12.5	12.5	202.3	2.31	2.51
	11/20/99	363.5	0.359	2.13	12.5	12.5	202.5	3.67	4.62
74	11/13/99	373.2	0.226	2.29	12.5	12.5	202.5	2.38	1.80
	11/14/99	373.3	0.278	1.15	12.5	12.5	202.5	2.90	3.80
	11/16/99	373.4	0.306	2.11	12.5	12.5	202.3	3.21	5.33
	11/20/99	373.3	0.359	2.10	12.5	12.5	202.5	4.63	8.56

Table K.26: CO₂ desorption from aqueous blends of DEA+MDEA

Series No.	Date (m/d/y)	T (K)	α (mol/mol)	Q _L (mL/s)	C _{DEA} (wt%)	C _{MDEA} (mL/s)	P ^{total} (kPa)	p _{CO₂} ^{lm} (kPa)	Des. Flux (mmol/m ² s)
75	12/8/99	353.5	0.152	2.58	12.5	12.5	205.9	0.86	0.67
	12/19/99	353.4	0.186	2.58	12.5	12.5	209.0	1.62	1.05
	12/18/99	353.5	0.202	2.58	12.5	12.5	208.8	1.72	1.41
	12/12/99	353.2	0.267	2.58	12.5	12.5	206.7	2.41	2.62
76	12/8/99	363.4	0.152	2.58	12.5	12.5	208.0	1.35	1.23
	12/19/99	363.4	0.186	2.58	12.5	12.5	209.0	2.48	2.10
	12/18/99	363.4	0.202	2.58	12.5	12.5	208.8	2.57	2.50
	12/12/99	363.1	0.267	2.58	12.5	12.5	206.7	3.93	4.99
77	12/19/99	373.3	0.101	2.58	12.5	12.5	209.0	1.25	1.33
	12/8/99	373.2	0.152	2.58	12.5	12.5	208.0	2.25	2.77
	12/19/99	373.5	0.186	2.58	12.5	12.5	209.0	3.13	4.30
	12/18/99	373.4	0.202	2.58	12.5	12.5	208.8	3.01	4.98

Table K.27: CO₂ desorption from aqueous blends of DEA+AMP

Series No.	Date (m/d/y)	T (K)	α (mol/mol)	Q _L (mL/s)	C _{DEA} (wt%)	C _{AMP} (mL/s)	P ^{total} (kPa)	p _{CO₂} ^{lm} (kPa)	Des. Flux (mmol/m ² s)
78	12/2/99	353.4	0.169	2.38	12.5	12.5	208.0	0.66	0.38
	12/5/99	353.4	0.231	2.38	12.5	12.5	207.3	1.09	0.76
	11/29/99	354.0	0.260	2.38	12.5	12.5	206.0	1.25	1.18
	11/28/99	353.5	0.335	2.38	12.5	12.5	205.9	2.19	2.27
79	12/2/99	363.3	0.169	2.38	12.5	12.5	208.0	1.15	0.79
	12/5/99	363.3	0.231	2.38	12.5	12.5	207.3	2.07	1.71
	11/29/99	363.3	0.260	2.38	12.5	12.5	206.7	1.97	2.16
	11/28/99	364.1	0.335	2.38	12.5	12.5	207.6	3.47	4.27
80	12/2/99	373.1	0.169	2.38	12.5	12.5	208.0	2.13	1.95
	12/5/99	373.2	0.231	2.38	12.5	12.5	207.3	2.86	3.21
	11/29/99	373.1	0.260	2.38	12.5	12.5	206.7	2.76	4.07
	11/28/99	372.9	0.335	2.38	12.5	12.5	206.2	4.18	6.99